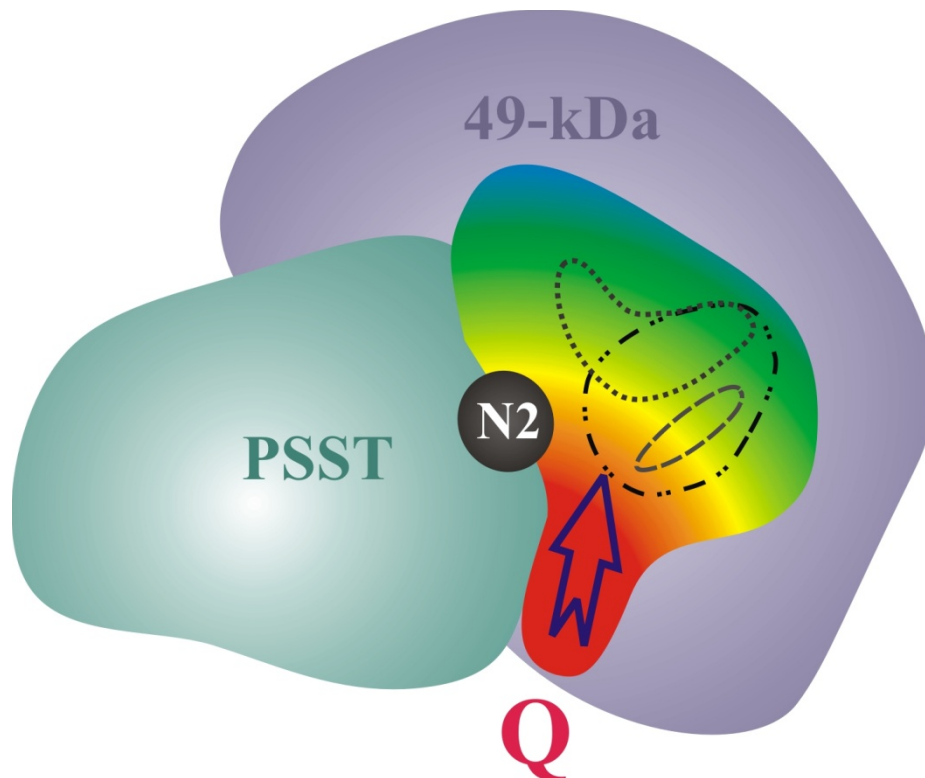


**Thesis**

**The Ubiquinone and Inhibitor Binding Pocket  
of Complex I from *Yarrowia lipolytica*:  
A Structure-based Mutagenesis Study**



by  
*Maja Aleksandra Tocilescu*  
*Molecular Bioenergetics Group*  
*Goethe-University Medical School*  
*Frankfurt am Main*

Cover picture was adapted from (Zickermann et al., 2009).  
For details see Summary Figure 5.1.

**The Ubiquinone and Inhibitor Binding Pocket  
of Complex I from *Yarrowia lipolytica*:  
A Structure-based Mutagenesis Study**

Dissertation  
zur Erlangung des Doktorgrades  
der Naturwissenschaften

vorgelegt beim Fachbereich Biowissenschaften  
der Johann Wolfgang Goethe - Universität  
in Frankfurt am Main

von  
**Maja Aleksandra Tocilescu**  
aus Belgard, Polen

Frankfurt 2009  
(D 30)

vom Fachbereich Biowissenschaften der Johann Wolfgang Goethe - Universität als  
Dissertation angenommen.

Dekan :                    Prof. Dr. Volker Müller

Gutachter :                Prof. Dr. Volker Müller

Prof. Dr. Ulrich Brandt

Datum der Disputation : 8. Mai 2009

Die vorliegende Arbeit wurde im Labor von Prof. Dr. Ulrich Brandt, Arbeitsgruppe Molekulare Bioenergetik am Zentrum der Biologischen Chemie des Fachbereichs Medizin der Johann Wolfgang Goethe-Universität, Frankfurt am Main im Zeitraum vom August 2005 bis Februar 2009 angefertigt.



## Index of Contents

<b>1</b>	<b>Introduction</b> .....	<b>1</b>
<b>1.1</b>	<b>The mitochondrial respiratory chain</b> .....	<b>1</b>
<b>1.2</b>	<b>Complex I</b> .....	<b>3</b>
1.2.1	Subunit composition .....	3
1.2.2	Structural data .....	4
1.2.3	The ubiquinone binding site .....	6
1.2.4	Complex I inhibitors .....	7
1.2.5	EPR spectroscopy of iron-sulfur clusters .....	9
1.2.6	Iron-sulfur cluster N1a .....	13
1.2.7	The mechanism of energy conversion .....	13
<b>1.3</b>	<b><i>Yarrowia lipolytica</i> as a model organism</b> .....	<b>14</b>
<b>1.4</b>	<b>Aim of this study</b> .....	<b>17</b>
1.4.1	Exploring the quinone and inhibitor binding pocket .....	17
1.4.2	Characterization of the HRGXE-motif .....	18
1.4.3	Shifting of the midpoint potential of iron-sulfur cluster N1a .....	19
1.4.4	Developing a new <i>in vivo</i> screen for complex I deficiency .....	19
<b>2</b>	<b>Materials and Methods</b> .....	<b>21</b>
<b>2.1</b>	<b>Materials</b> .....	<b>21</b>
2.1.1	Chemicals .....	21
2.1.2	Inhibitors .....	22
2.1.3	Enzymes .....	23
2.1.4	Plasmids .....	23
2.1.5	Strains .....	24
2.1.6	Instruments .....	25
2.1.7	Software .....	27
<b>2.2</b>	<b>Methods</b> .....	<b>28</b>
2.2.1	Methods of Microbiology .....	28
2.2.2	Methods of Molecular Biology .....	30
2.2.3	Methods of Protein Chemistry .....	33
2.2.4	Methods of Bioinformatics .....	38

<b>3</b>	<b>Results</b> .....	<b>41</b>
<b>3.1</b>	<b>Mutagenesis of the proposed ubiquinone and inhibitor binding cavity</b> .....	<b>41</b>
3.1.1	Assembly of mutant complex I .....	41
3.1.2	Activity of mutant complex I .....	49
3.1.3	<i>Apparent</i> $K_m$ for DBQ .....	52
3.1.4	Complex I activity with $Q_1$ and $Q_9$ as electron acceptors .....	52
3.1.5	$I_{50}$ values for DQA, rotenone and $C_{12}E_8$ .....	55
3.1.6	EIPA .....	61
<b>3.2</b>	<b><i>In vivo</i> screen for complex I deficiency</b> .....	<b>66</b>
3.2.1	The principle .....	66
3.2.2	Development of a plate assay for complex I activity .....	67
3.2.3	Screening of complex I mutants .....	69
<b>3.3</b>	<b>Tyrosine 144</b> .....	<b>71</b>
3.3.1	Assembly and activity of tyrosine 144 mutants .....	72
3.3.2	Iron-sulfur cluster N2 in tyrosine 144 mutants .....	73
3.3.3	Complex I activity at higher DBQ concentrations in mutant Y144F .....	78
3.3.4	pH dependence of residual activity of mutant Y144F .....	79
3.3.5	Reactivation of mutant Y144F .....	81
3.3.6	dNADH: $Q_1$ oxidoreductase activity in tyrosine 144 mutants .....	85
3.3.7	dNADH: $Q_2$ oxidoreductase activity of mutants Y144F and Y144W .....	87
3.3.8	Inhibitor resistance of the tyrosine 144 mutants .....	88
3.3.9	Proton pumping of complex I in mutants Y144F and Y144W .....	89
<b>3.4</b>	<b>Mutagenesis study of the HRGXE-motif</b> .....	<b>92</b>
3.4.1	The HRGXE-motif in different organisms .....	92
3.4.2	Location of the HRGXE-motif .....	93
3.4.3	Complex I assembly and activity of the HRGXE-motif mutants .....	94
3.4.4	EPR spectra from mutants of the HRGXE-motif .....	95
3.4.5	<i>Apparent</i> $K_m$ and $I_{50}$ values for mutants of the HRGXE-motif .....	97
<b>3.5</b>	<b>Mutagenesis of the 24-kDa subunit close to iron-sulfur cluster N1a</b> .....	<b>97</b>
3.5.1	Selection of targeted residues .....	97
3.5.2	Assembly and activity of complex I mutants .....	99
3.5.3	EPR spectra of the N1 signal .....	101
3.5.4	Mutagenesis of iron-sulfur cluster N1a ligands .....	103



---

<b>4</b>	<b>Discussion</b> .....	<b>105</b>
<b>4.1</b>	<b>Exploring the proposed ubiquinone and inhibitor binding cavity</b> .....	<b>105</b>
4.1.1	Mapping of mutation effects into the structure.....	105
4.1.2	Identification of functional domains.....	108
4.1.3	Role of tyrosine 144 .....	109
4.1.4	Properties of different quinone substrates .....	111
4.1.5	The inhibitor binding sites .....	112
4.1.6	Comparison to results obtained with other model organisms.....	114
4.1.7	Location of the quinone binding site(s) .....	116
4.1.8	Properties of the quinone binding site .....	119
<b>4.2</b>	<b>The HRGXE-motif</b> .....	<b>120</b>
<b>4.3</b>	<b>Iron-sulfur cluster N1a</b> .....	<b>124</b>
<b>4.4</b>	<b><i>In vivo</i> screen for complex I deficiency</b> .....	<b>126</b>
<b>5</b>	<b>Summary and Outlook</b> .....	<b>129</b>
<b>5.1</b>	<b>Summary</b> .....	<b>129</b>
<b>5.2</b>	<b>Outlook</b> .....	<b>132</b>
5.2.1	Mutagenesis of the proposed quinone and inhibitor binding cavity.....	132
5.2.2	Iron-sulfur cluster N1a.....	133
5.2.3	<i>In vivo</i> screen for complex I deficiency.....	134
<b>6</b>	<b>Zusammenfassung</b> .....	<b>135</b>
<b>7</b>	<b>References</b> .....	<b>141</b>
<b>8</b>	<b>Appendix</b> .....	<b>169</b>
<b>8.1</b>	<b>Genes and primers</b> .....	<b>169</b>
8.1.1	NUCM gene.....	169
8.1.2	NUKM gene .....	174
8.1.3	NUHM gene .....	176
<b>8.2</b>	<b>Amino acid sequences</b> .....	<b>178</b>
8.2.1	The 49-kDa subunit .....	178
8.2.2	The PSST subunit .....	180
8.2.3	The 30-kDa subunit .....	181

---

8.2.4	The 24-kDa subunit.....	182
<b>8.3</b>	<b>Structural formulas.....</b>	<b>183</b>
8.3.1	Ubiquinones.....	183
8.3.2	Inhibitors.....	185
8.3.3	Other compounds.....	188
<b>8.4</b>	<b>Abbreviations.....</b>	<b>189</b>
<b>8.5</b>	<b>List of Figures.....</b>	<b>193</b>
<b>8.6</b>	<b>List of Tables.....</b>	<b>196</b>
	<b>Danksagung.....</b>	<b>199</b>
	<b>Lebenslauf.....</b>	<b>201</b>

# 1 Introduction

## 1.1 The mitochondrial respiratory chain

The respiratory chain is located in the mitochondrial inner membrane of eukaryotic cells and catalyzes electron transfer mainly from NADH to oxygen (Hatefi, 1985). This exergonic redox reaction is coupled to proton translocation across the inner mitochondrial membrane. The proton gradient then drives the endergonic synthesis of ATP by ATP-synthase (Abrahams et al., 1994; Boyer, 1997; Nakamoto et al., 1999) and other endergonic reactions. This fundamental principle of energy conversion in cells was first proposed by Peter Mitchell (Mitchell, 1961) and is known as the chemiosmotic theory.

Electron transfer from NADH to oxygen is performed stepwise by three respiratory chain complexes (complex I, III and IV) and involves ubiquinone and cytochrome c as mobile electron carriers (Hatefi, 1985). Complex I (NADH:ubiquinone oxidoreductase) transfers electrons from matrix NADH to ubiquinone and thereby pumps two protons per electron across the inner mitochondrial membrane (Wikström, 1984; Galkin et al., 1999). Complex III (cytochrome c reductase) transfers electrons from ubiquinol to cytochrome c and pumps one proton per electron (Wikström et al., 1981; Brandt, 1996). Finally, complex IV (cytochrome c oxidase) transfers electrons from cytochrome c onto molecular oxygen, the ultimate electron acceptor, and translocates two charges per electron (Michel, 1998).

Although complex I, III and IV were isolated and studied separately, in the mitochondrial membrane they form large supercomplexes (respirasomes) supporting their stability and facilitating substrate channeling (Schägger and Pfeiffer, 2000; Schägger, 2002; Stroh et al., 2004; Schägger et al., 2004; Suthammarak et al., 2009).

Due to the ubiquinone reduction activity of the succinate dehydrogenase (complex II), the electron-transferring flavoprotein (ETF)-ubiquinone oxidoreductase and the *s,n*-glycerolphosphate dehydrogenase additional electrons are fed into the respiratory chain. However, these enzymes do not translocate protons across the mitochondrial membrane.

The respiratory chain is also the main source of reactive oxygen species (ROS) (Fridovich, 1978). ROS production occurs at the catalytic sites of complex I (Turrens and Boveris, 1980; Kushnareva et al., 2002; Galkin and Brandt, 2005; Kussmaul and Hirst, 2006) and complex III (Boveris et al., 1976; Cadenas et al., 1977; Dröse and Brandt, 2008; Borek et al., 2008) by single electrons escaping to oxygen (Brand et al., 2004). Low levels of ROS seem to be involved in cellular signaling (Bell et al., 2007; Starkov, 2008). However, higher rates lead to oxidative stress which plays a role in apoptosis, aging and several neurodegenerative diseases including Parkinson's, Huntington's and Alzheimer disease (Benzi and Moretti, 1995; Finkel and Holbrook, 2000; Emerit et al., 2004; Lin and Beal, 2006; Zhou et al., 2008).

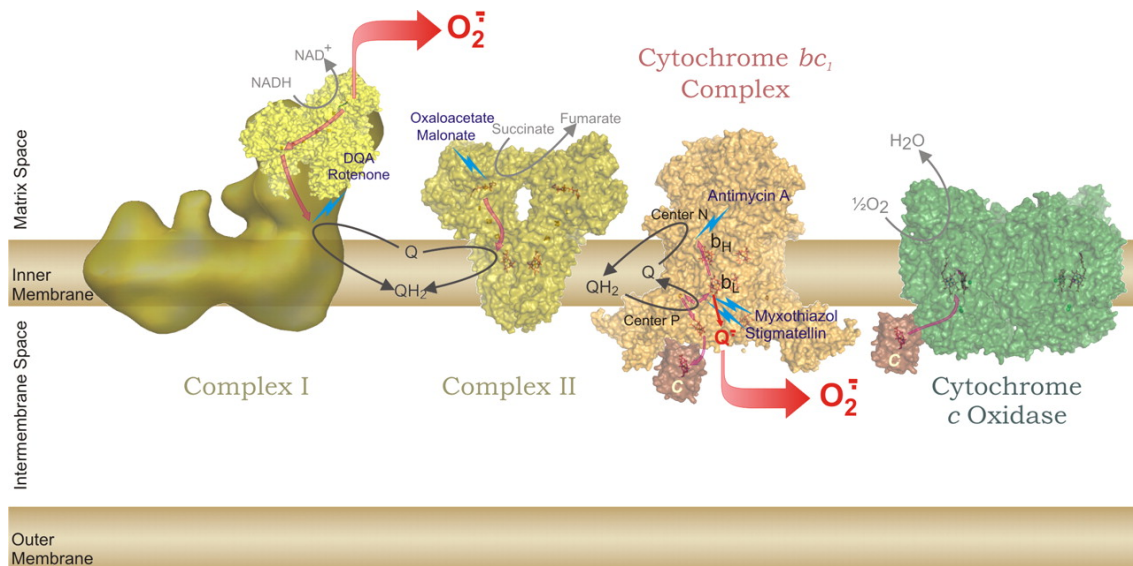


**Figure 1.1: Semi-schematic representation of the mitochondrial respiratory chain.** Complex I (NADH:ubiquinone oxidoreductase); Complex II (succinate:ubiquinone oxidoreductase); Cytochrome  $bc_1$  Complex (Complex III); Cytochrome c Oxidase (complex IV); Electron transfer (thin red arrows), sites of ROS production (thick red arrows) and sites of action of some inhibitors (blue) are indicated.  $NAD^+$  (nicotinamide adenine dinucleotide, oxidized form); NADH (nicotinamide adenine dinucleotide, reduced form); Q (ubiquinone);  $QH_2$  (ubiquinol);  $b_H$  (high potential heme b);  $b_L$  (low potential heme b); c (cytochrome c). Figure was taken from (Dröse and Brandt, 2008)

## 1.2 Complex I

### 1.2.1 Subunit composition

Mitochondrial complex I (NADH:ubiquinone oxidoreductase) is a huge multisubunit membrane protein and the least understood component of the respiratory chain (Brandt, 2006; Zickermann et al., 2008; Zickermann et al., 2009). It is composed of at least 40 protein subunits with a total mass of ~1 MDa (Carroll et al., 2006a; Morgner et al., 2008).

**Table 1.1: Central subunits of complex I**

Subunit nomenclature					Redox centers
<i>B. taurus</i>	<i>Y. lipolytica</i>	<i>H. sapiens</i>	<i>E. coli</i>	<i>T. thermophilus</i>	
hydrophilic subunits of the peripheral domain, nuclear coded in eukaryotes					
75-kDa	NUAM	NDUFS1	NuoG	Nqo3	N1b, N4 <sup>1</sup> , N5, N7 <sup>2</sup>
51-kDa	NUBM	NDUFV1	NuoF	Nqo1	FMN, N3
49-kDa	NUCM	NDUFS2	NuoD <sup>3</sup>	Nqo4	-
30-kDa	NUGM	NDUFS3	NuoC <sup>3</sup>	Nqo5	-
24-kDa	NUHM	NDUFV2	NuoE	Nqo2	N1a
TYKY	NUIM	NDUFS8	NuoI	Nqo9	N6a <sup>1</sup> , N6b <sup>1</sup>
PSST	NUKM	NDUFS7	NuoB	Nqo6	N2
hydrophobic subunits of the membrane domain, mitochondrially coded in most eukaryotes					
ND1	ND1	ND1	NuoH	Nqo8	-
ND2	ND2	ND2	NuoN	Nqo14	-
ND3	ND3	ND3	NuoA	Nqo7	-
ND4	ND4	ND4	NuoM	Nqo13	-
ND5	ND5	ND5	NuoK	Nqo12	-
ND6	ND6	ND6	NuoL	Nqo10	-
ND4L	ND4L	ND4L	NuoJ	Nqo11	-

<sup>1</sup> Iron-sulfur cluster N4 was proposed to be ligated in the TYKY instead of N6a or N6b (Yakovlev et al., 2007)

<sup>2</sup> present in some bacteria only

<sup>3</sup> in *E. coli* NuoD and NuoC are fused to NuoCD

14 subunits (see Table 1.1) are conserved between eukaryotes and prokaryotes (Yagi et al., 1998) and are sufficient to couple the redox reaction to proton translocation. These 14 subunits are usually called “central” in order to distinguish them from the remaining so called “accessory” subunits that are not directly involved in energy conversion but may have additional functions (Hirst et al., 2003). Of the 14 central subunits, 7 are rather hydrophilic and 7 are highly hydrophobic. The latter are typically encoded by mitochondrial DNA in eukaryotes (Anderson et al., 1982; Chomyn et al., 1985; Chomyn et al., 1986; Kerscher et al., 2001a).

### 1.2.2 Structural data

In contrast to other respiratory chain complexes, the crystal structure of complex I is not solved yet. However, single particle electron microscopy revealed that complex I has an L-shaped overall structure both in eukaryotes and prokaryotes (Hofhaus et al., 1991; Guenebaut et al., 1997; Guenebaut et al., 1998; Grigorieff, 1998; Djafarzadeh et al., 2000; Peng et al., 2003; Radermacher et al., 2006; Morgan and Sazanov, 2008). The hydrophobic membrane domain of the enzyme is embedded in the mitochondrial membrane, whereas the hydrophilic peripheral domain protrudes into the mitochondrial matrix. The peripheral domain contains all known redox centers, a non-covalently bound FMN and 8-9 iron-sulfur clusters (Finel et al., 1992; Ohnishi, 1998; Rasmussen et al., 2001; Hinchliffe and Sazanov, 2005; Sazanov and Hinchliffe, 2006).

In 2006 Sazanov and co-workers succeeded to solve the X-ray structure of the peripheral domain of complex I from *Thermus thermophilus* at 3.3 Å resolution (Sazanov and Hinchliffe, 2006). The Y shaped fragment revealed the spatial arrangement of the seven central hydrophilic subunits as well as the locations of all known redox centers of complex I (see Figure 1.2). Seven iron-sulfur clusters (N1b, N2, N3, N4, N5, N6a und N6b) form an approximately 95 Å long chain of redox centers. This chain starts with iron-sulfur cluster N3 next to the FMN molecule in the 51-kDa subunit, continues via the redox centers of the 75-kDa and the TYKY subunits and ends at iron-sulfur cluster N2 in the PSST subunit next to a broad cavity at the interface of the PSST and the 49-kDa subunit. In order to avoid confusion, the bovine nomenclature for homologous complex I subunits will be used throughout. Iron-sulfur cluster N1a in

the 24-kDa subunit is located at the opposite side of the FMN molecule. Iron-sulfur cluster N7 present only in some bacteria is not in electron tunneling distance to other iron-sulfur clusters and most probably serves to stabilize the 75-kDa subunit (Pohl et al., 2007).

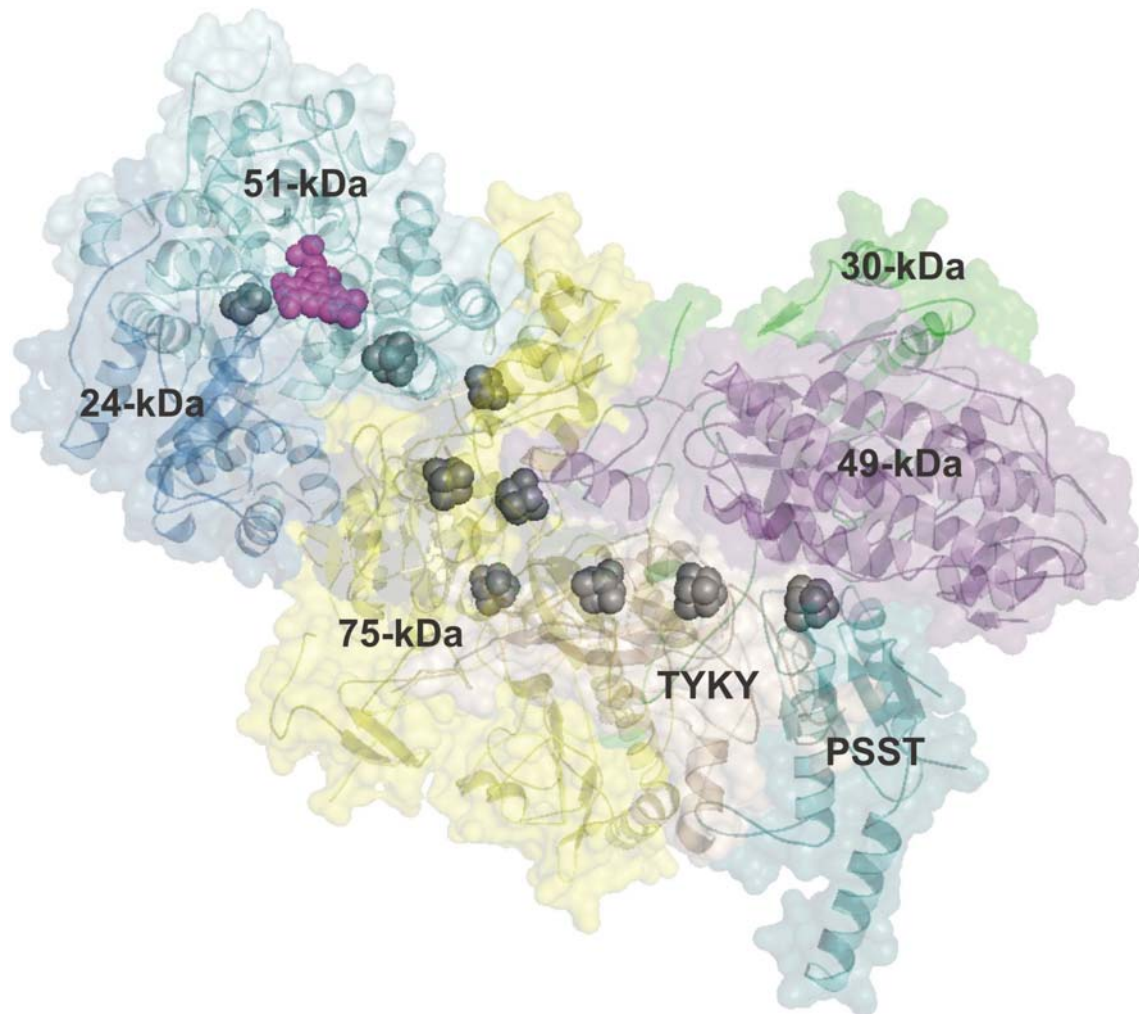


**Figure 1.2:** The crystal structure of the peripheral domain of complex I from *T. thermophilus* contains 7 out of 14 central subunits of complex I. Subunits are shown in schematic representation with transparent surface and are labeled according to the bovine nomenclature. Iron-sulfur clusters (in gray) as well as the FMN molecule (in pink) are shown as space-filled models. A chain of 7 iron-sulfur clusters connects the FMN molecule with a broad cavity assembled by the PSST and the 49-kDa subunit. The binuclear iron-sulfur cluster N1a ligated by the 24-kDa subunit is located at the opposite side of the FMN molecule. Iron-sulfur cluster N7 (lowest cluster ligated by the 75-kDa subunit) is not in electron tunnelling distance to other iron-sulfur clusters. The figure was generated from PDB ID 2FUG using the PyMOL program.

No redox centers were found in the membrane domain of complex I (Carroll et al., 2006b). However, this part of the enzyme must harbor the proton translocating device(s).

Recently, the projection map of the membrane domain from *Escherichia coli* composed of subunits ND1-ND6 and ND4L was solved from 2 D crystals (Baranova et al., 2007a). The resolution of 8 Å allowed the identification of about 60 transmembrane  $\alpha$ -helices. However, at this resolution only a tentative assignment of the densities to the subunits was possible.

The ND2, the ND4 and the ND5 subunits are homologous to  $\text{Na}^+/\text{H}^+$ -antiporters (Fearnley and Walker, 1992) and therefore were suggested to be involved in proton translocation (Friedrich and Weiss, 1997; Friedrich, 2001; Mathiesen and Hägerhäll, 2002; Mathiesen and Hägerhäll, 2003). Interestingly, the ND4 and the ND5 subunits were found to be located at the distal end of the membrane domain (Sazanov and Walker, 2000; Cardol et al., 2002; Holt et al., 2003; Baranova et al., 2007b) in considerable distance to the peripheral domain and thus to all known redox centers, suggesting long range conformational changes for driving proton translocation.

### 1.2.3 The ubiquinone binding site

It had been proposed earlier that the quinone binding pocket is formed by the PSST and the 49-kDa subunit of complex I (Kashani-Poor et al., 2001b; Kerscher et al., 2001c) that are evolutionary related to the small and large subunits of water-soluble [NiFe] hydrogenases as indicated by sequence comparison (Böhm et al., 1990; Albracht, 1993). This proposal was based on mutagenesis studies which showed that many functionally critical residues are located in this part of the enzyme and that mutations which target the former [NiFe] site conferred resistance towards complex I inhibitors which act at the quinone binding site (Darrouzet and Dupuis, 1997; Darrouzet et al., 1998; Prieur et al., 2001; Kashani-Poor et al., 2001b; Loeffen et al., 2001; Mills et al., 2004). In addition, photoaffinity labeling studies suggested that the PSST subunit forms part of the quinone and inhibitor binding pocket of complex I (Schuler et al., 1999). Further support came from more recent mutagenesis (Grgic et al., 2004; Kerscher et al., 2005) and photoaffinity labeling studies (Ichimaru et al., 2008) and the crystal structure of the



hydrophilic domain of complex I from *T. thermophilus* (Sazanov and Hinchliffe, 2006). The structure essentially shows a wire of iron-sulfur clusters which connect the FMN molecule with a broad cavity formed by the PSST and the 49 kDa subunit, which is believed to comprise the quinone binding site (see Figure 1.2).

However, from the crystal structure alone it cannot be inferred where this cavity is located relative to the membrane and the not yet crystallized membrane domain of complex I. Interestingly, single particle analysis of complex I decorated with antibodies against the 49-kDa subunit suggested that the quinone binding pocket is located at considerable distance (about 60 Å) to the membrane domain of complex I (Zickermann et al., 2003). This result was confirmed when a subcomplex of complex I (Zickermann et al., 2007) was analyzed, which allowed the fitting of the structure of the hydrophilic domain of complex I from *T. thermophilus* into the holocomplex from *Yarrowia lipolytica* (Clason et al., 2007).

#### 1.2.4 Complex I inhibitors

More than 60 families of natural and synthetic complex I inhibitors were described (Degli Esposti, 1998; Miyoshi, 1998; Lümmer, 1998; Okun et al., 1999b; Ushakova et al., 1999; Okun et al., 1999a; Okun et al., 2000). Most of these compounds are quite hydrophobic and inhibit the NADH:Q oxidoreductase activity of complex I; however, they do neither interfere with the NADH:ferricyanide oxidoreductase activity (Hatefi, 1985) nor with the reduction of EPR detectable iron-sulfur clusters (Friedrich et al., 1994). Thus it was concluded that they act at the quinone binding site of complex I.

Based on steady state kinetics, Friedrich and coworkers grouped 12 complex I inhibitors into two classes (Friedrich et al., 1994). Class I inhibitors (piericidin A, fenpyroximate and others) act in a partially competitive manner on complex I and competitively on bacterial glucose dehydrogenase, both with regard to Q<sub>2</sub>, whereas class II inhibitors (rotenone and others) act non-competitively on complex I and do not inhibit glucose dehydrogenase. After an extensive literature survey, Degli Esposti grouped complex I inhibitors into three categories (Degli Esposti and Ghelli, 1994; Degli Esposti, 1998): Type A, B and C. Thereby, type A and type B largely correspond to class I and class II, respectively. Type C inhibitors, represented by capsaicins and their synthetic analogues

like CC44 (Sato et al., 1996), form a distinct group. The n-alkyl-polyoxyethylene-ether detergent C<sub>12</sub>E<sub>9</sub> (Thesit) was proposed to be a type C inhibitor as well, since it was found to bind competitively to CC44 (Okun et al., 2000).

The establishment of various types or classes of complex I inhibitors lead to the concept that these inhibitors bind to different parts of the enzyme corresponding to multiple quinone reaction sites (Degli Esposti and Ghelli, 1994; Degli Esposti, 1998; Estornell, 2000). However, direct competition binding assays revealed that all three types of complex I inhibitors bind to partially overlapping binding sites within a large common pocket (Okun et al., 1999a). Thereby, the binding site for type A inhibitors overlaps with that for type B inhibitors, and the binding site for type C inhibitors overlaps with that for type B inhibitors but not with that for type A inhibitors (see Figure 1.3).

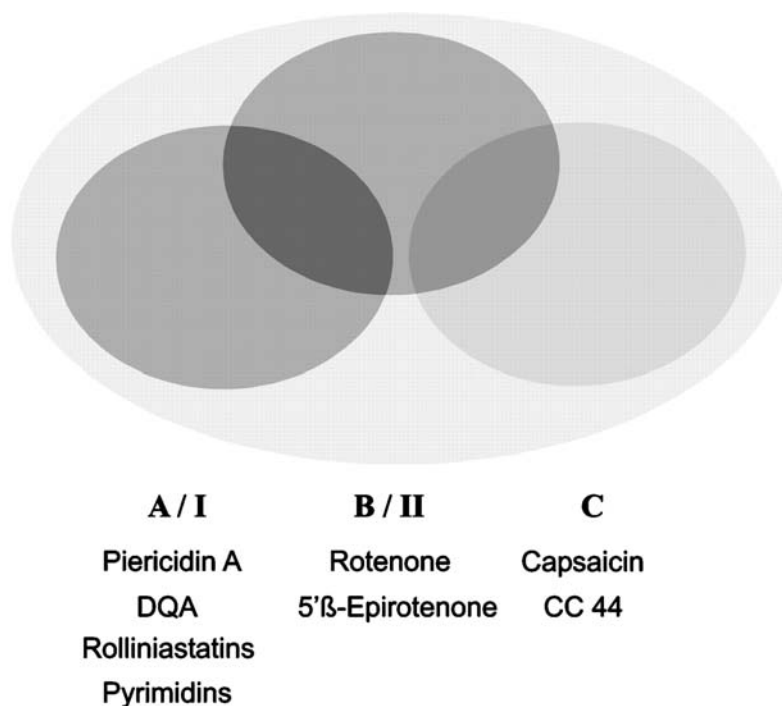


**Figure 1.3: Schematic representation of the inhibitor binding pocket of complex I.** Different types of complex I inhibitors bind to partially overlapping binding sites, represented as shadowed ovals. Figure was taken from (Okun et al., 1999a).

### 1.2.5 EPR spectroscopy of iron-sulfur clusters

Complex I contains one FMN molecule and several iron-sulfur clusters as redox centers. Only binuclear and tetranuclear iron-sulfur clusters are found in complex I; their geometry is shown in Figure 1.4. Reduced binuclear and tetranuclear iron-sulfur clusters are paramagnetic and can be detected by electron paramagnetic resonance (EPR) spectroscopy (Beinert and Albracht, 1982). The spin relaxation rates of binuclear iron-sulfur clusters are relatively slow; therefore, they give EPR signals at quite high temperature ( $\sim 70$  K). Tetranuclear iron-sulfur clusters have faster spin relaxation rates, so that their EPR signals are too broad to be detected at these temperatures. However, they can be detected at temperatures of less than 20 K. According to Ohnishi's nomenclature, signals of iron-sulfur clusters from complex I are numbered in the order of their spin relaxation rates from slow to fast (Ohnishi, 1998). Binuclear iron-sulfur clusters are named N1 (N1a or N1b), faster relaxing tetranuclear iron-sulfur clusters are named N2, N3, N4 and so forth.

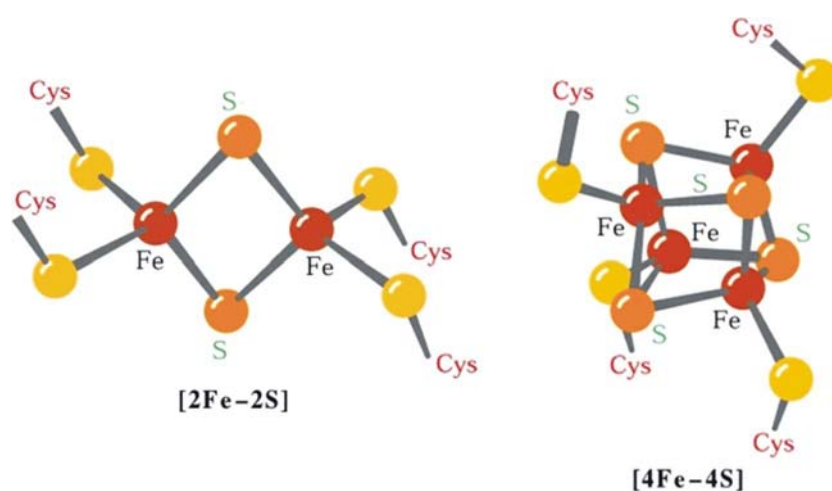


**Figure 1.4: Schematic representation of a binuclear and a tetranuclear iron-sulfur cluster.** Typically, iron-sulfur clusters are coordinated by sulfur atom from four liganding cysteine residues (in yellow). Acid-labile sulfur atoms are shown as orange spheres. Iron atoms are shown as red spheres. Figure adapted from (Voet and Voet, 1992).

In complex I from bovine heart mitochondria six iron-sulfur clusters (N1a, N1b, N2, N3, N4 and N5) are detectable by EPR (Ohnishi, 1998; Reda et al., 2008; Ohnishi and

Nakamaru-Ogiso, 2008). In complex I from *Neurospora crassa* four iron-sulfur clusters (N1, N2, N3 and N4) were detected by EPR (Wang et al., 1991) and two more (N6a and N6b) by ultraviolet-visible spectroscopy (Friedrich et al., 2000; Rasmussen et al., 2001). Bacterial complex I from *E. coli* contains six EPR detectable iron-sulfur clusters (N1a, N1b, N2, N3, N4 and N7) (Sled et al., 1993; Leif et al., 1995; Friedrich, 1998; Nakamaru-Ogiso et al., 2005; Uhlmann and Friedrich, 2005). In addition, iron-sulfur clusters N6a and N6b were detected by ultraviolet-visible spectroscopy (Friedrich et al., 2000; Rasmussen et al., 2001). Five EPR detectable iron-sulfur clusters (N1, N2, N3, N4 and N5) were described in complex I from *Y. lipolytica* (Djafarzadeh et al., 2000). Thereby, the N1 signal was shown to correspond to the N1b signal from bovine complex I (Zickermann et al., 2007). Figure 1.5 shows an EPR spectrum of purified complex I from *Y. lipolytica* in comparison to a calculated spectrum assembled from four individual simulations. The sum of simulations is very similar to the recorded spectrum, which shows that iron-sulfur clusters N1, N2, N3 and N4 are present in a 1:1:1:1 stoichiometry (Kerscher et al., 2001c). Iron-sulfur cluster N5 is not detectable at a temperature of 12 K as used here. So far, an EPR spectrum from a second binuclear iron-sulfur cluster, which would be expected from the crystal structure of the hydrophilic domain of complex I from *T. thermophilus* ((Sazanov and Hinchliffe, 2006); see also Figure 1.2) and the EPR characterization of bovine and *E. coli* complex I, could not be detected in complex I from *Y. lipolytica*.

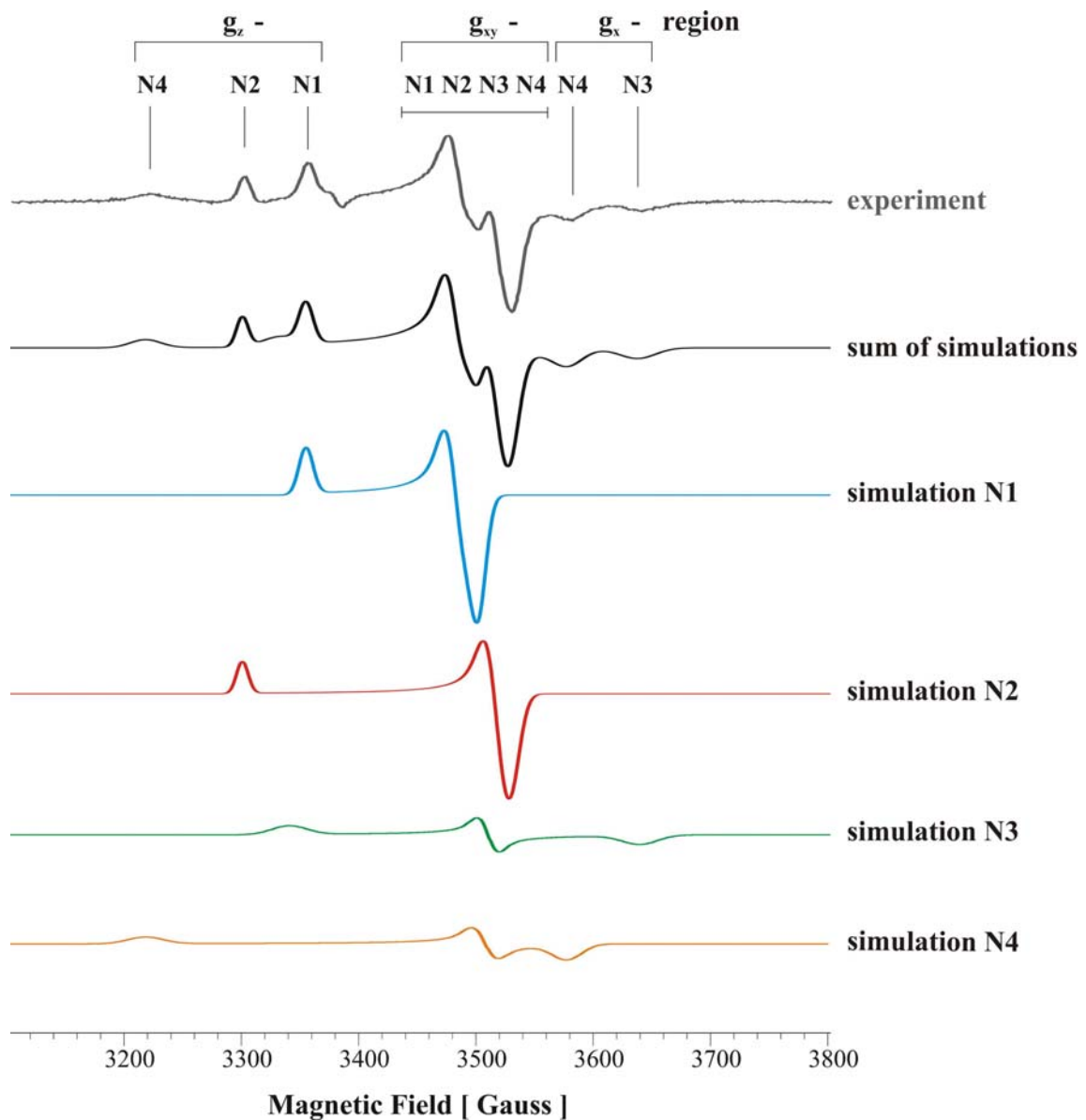


**Figure 1.5: Comparison of an EPR spectrum recorded at 12 K and 0.1 mW from purified complex I from *Y. lipolytica* to a simulated spectrum.** Contributions from iron-sulfur clusters N1, N2, N3 and N4 are labeled. The  $g_{xy}$ -signals of all iron-sulfur clusters overlap quite extensively. The experimental spectrum can be adequately simulated by the sum of simulations of iron-sulfur clusters N1, N2, N3 and N4. Iron-sulfur cluster N5 is not detectable under the experimental conditions used here. EPR parameters for the experimental spectrum: Microwave frequency 9.47 GHz, modulation frequency 100 kHz and modulation amplitude 6.4 Gauss. The experimental spectrum and the simulated spectra were kindly provided by Dr. Klaus Zwicker.

When EPR spectra are recorded from mitochondrial membranes of *Y. lipolytica*, additional signals from paramagnetic species in complex II, III and IV are detectable (see Figure 1.6).

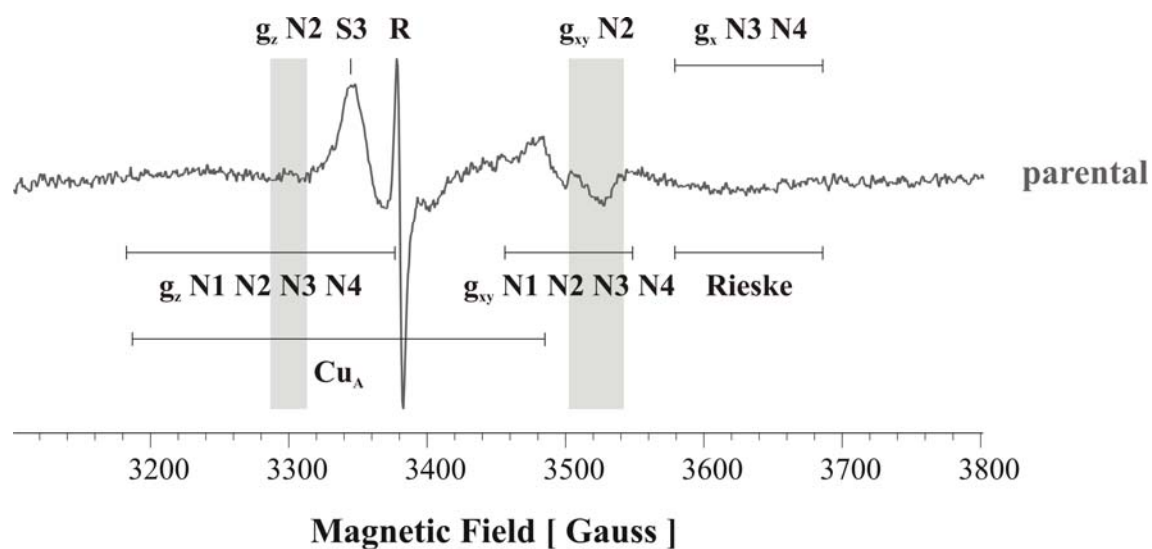


**Figure 1.6:** Example of an EPR spectrum from mitochondrial membranes from *Y. lipolytica* recorded at 12 K and 1 mW microwave power. Signals mainly arising from iron-sulfur cluster N2 are highlighted in gray. Magnetic field positions where signals from other complex I iron-sulfur clusters arise are indicated by vertical bars. In mitochondrial membranes, other paramagnetic species not related to complex I also contribute to the total EPR spectrum: S3, iron-sulfur cluster S3 from complex II; R, organic radical of unknown origin, occasionally detected in mitochondrial membranes (not a quinone radical);  $\text{Cu}_A$  from complex III. EPR parameters: Microwave frequency 9.47 GHz, modulation frequency 100 kHz and modulation amplitude 6.4 Gauss. Sample: Mitochondrial membranes from the 49-kDa parental strain (~25 mg protein per ml) were reduced with 2 mM NADH. EPR spectrum was taken from Figure 3.23 and was recorded by Dr. Klaus Zwicker.

A tentative assignment of the EPR signals to individual iron-sulfur clusters resolved in the structure of the peripheral domain of complex I from *T. thermophilus* was suggested (Sazanov and Hinchliffe, 2006). Since this is not a trivial task, the assignment of iron-sulfur clusters N4 and N5 to the binding motifs within the structure and even to the right subunits is currently debated heavily (Waletko et al., 2005; Yakovlev et al., 2007; Nakamaru-Ogiso et al., 2008; Ohnishi and Nakamaru-Ogiso, 2008).

However, it is well established that iron-sulfur clusters N1a and N2 are ligated in the 24-kDa (Yano et al., 1995; Yano et al., 1996; Yano et al., 1997; Zu et al., 2002; Barker et al., 2007) and PSST subunit (Friedrich, 1998; Duarte et al., 2002; Flemming et al., 2003), respectively, which will be important in the context of this study.

### 1.2.6 Iron-sulfur cluster N1a

Iron-sulfur cluster N1a ligated by the 24-kDa subunit (see Figure 1.8) is of particular interest, since it was suggested to prevent excessive ROS formation at the FMN site (Zu et al., 2002; Hinchliffe and Sazanov, 2005; Sazanov and Hinchliffe, 2006; Galkin and Brandt, 2005; Kussmaul and Hirst, 2006; Esterhazy et al., 2008). Like in complex I from *Neurospora crassa* (Wang et al., 1991), iron-sulfur cluster N1a is not detectable by EPR in complex I from *Y. lipolytica* (Djafarzadeh et al., 2000). However, it is detectable in complex I from *E. coli* (Leif et al., 1995; Uhlmann and Friedrich, 2005; Yakovlev et al., 2007; Euro et al., 2008b) and *Rhodothermus marinus* (Fernandes et al., 2002; Fernandes et al., 2006) and a subcomplex of complex I from *Aquifex aeolicus* (Kohlstadt et al., 2008). Interestingly, in these species iron-sulfur cluster N1a was reported to have a redox midpoint potential of around -240 mV (Uhlmann and Friedrich, 2005; Euro et al., 2008b; Fernandes et al., 2006; Kohlstadt et al., 2008), a value which is quite similar to the readily detectable so-called isopotential iron-sulfur clusters of bovine complex I (Ohnishi, 1998) and complex I from *Y. lipolytica* (Klaus Zwicker, personal communication). In contrast, a much more negative redox midpoint potential (-500 to -370 mV) was determined for N1a from *Bos taurus* (Ohnishi et al., 1981; Ohnishi, 1998; Zu et al., 2002). However, it is currently heavily debated whether iron-sulfur cluster N1a is really detectable in the bovine enzyme (Reda et al., 2008; Ohnishi and Nakamaru-Ogiso, 2008).

It seems reasonable to speculate that the iron-sulfur cluster N1a from *Y. lipolytica* is not EPR detectable due to its very low redox midpoint potential, which prevents the reduction of this cluster by commonly used reductants like NADH or dithionite.

### 1.2.7 The mechanism of energy conversion

The mechanism by which complex I couples the redox reaction to vectorial proton pumping is unknown. Several constraints must be considered: (i) two protons per electron are translocated across the bioenergetic membrane (Wikström, 1984; Galkin et al., 1999) (ii) the coupling between redox reaction and proton translocation is tight and reversible (Vinogradov, 1998) (iii) all known redox centers are located far up in the peripheral domain (Carroll et al., 2006b; Clason et al., 2007). Over the years, many

different mechanisms were proposed (Brandt, 1997; Dutton et al., 1998; Okun et al., 1999b; Brandt, 1999; Vinogradov, 2001; Friedrich, 2001; Brandt et al., 2003; Ohnishi and Salerno, 2005; Hirst, 2005b; Flemming et al., 2005; Brandt, 2006; Euro et al., 2008a; Zickermann et al., 2008; Zickermann et al., 2009), however most of them were disproven based on newer results. Since electron transfer from NADH to N<sub>2</sub> is very fast (90 μs) (Verkhovskaya et al., 2008) and close to the 100 μs predicted from electron transfer theory (Moser et al., 2006a), it is unlikely to be coupled to proton translocation. Energy transduction involving the redox-Bohr group associated with iron-sulfur cluster N<sub>2</sub> was ruled out, since a mutant which abolished pH dependency of the redox midpoint potential of N<sub>2</sub> was shown to pump protons at the same stoichiometry as the unchanged enzyme (Zwicker et al., 2006). Also, a direct mechanism analogous to the Q-cycle mechanism in complex III can be excluded, since it would require redox centers in the membrane part of the enzyme; in addition, no evidence for reductant-induced oxidation of ubiquinol was found (Sherwood and Hirst, 2006).

Taken together, the most probable mechanism involves long range conformational changes in the membrane domain coupled to and driven by quinone reduction in the peripheral domain (Brandt, 2006; Euro et al., 2008a; Zickermann et al., 2008; Zickermann et al., 2009).

### **1.3 *Yarrowia lipolytica* as a model organism**

Complex I research long time suffered from the lack of an appropriate model organism. Since *Saccharomyces cerevisiae* has no complex I (Büschges et al., 1994), mostly complex I from *Bos taurus* (Carroll et al., 2003; Hirst et al., 2003) and *Neurospora crassa* (Videira, 1998; Marques et al., 2005) were used for characterization of this enzyme. However, genetic manipulations are impossible or rather difficult in these model organisms (Schulte and Weiss, 1995). Therefore, complex I from different bacteria *E. coli* (Weidner et al., 1993), *Paracoccus denitrificans* (Yano and Yagi, 1999), *Rhodobacter capsulatus* (Dupuis et al., 1998), was studied. However, complex I from prokaryotes tends to be rather instable. In addition, the prokaryotic enzyme lacks about 30 subunits found in eukaryotes, which add additional, potentially important functions to the mitochondrial enzyme. Therefore, *Yarrowia lipolytica* was introduced as a yeast



genetic model to study mitochondrial complex I (Kerscher et al., 2001c; Kerscher et al., 2002).

*Yarrowia lipolytica* is a strictly aerobic yeast from the class of Saccharomycetes (Barth and Gaillardin, 1996). It is non pathogenic and routinely found in different food media like sausage, cheese and yogurts. At the optimal temperature of 28 °C, *Y. lipolytica* grows on different carbon sources like glucose, ethanol, sodium acetate, alkanes and fatty acids to high biomass yields (up to 100 g/l wet weight). Typical laboratory strains are not viable above a temperature of 34 °C. *Y. lipolytica* has a simple haplontic/diplontic life cycle. Under nutrient limiting conditions, sporulation within an ascus is induced. Spores have a MAT A or a MAT B mating type. Mating type switching does not occur; therefore, stable cultivation of haploid cultures is possible. The complete mitochondrial genome (Kerscher et al., 2001a) as well as the nuclear genome (Dujon et al., 2004) are sequenced. The latter is relatively small (18 Mbp) and contains only few introns. The high frequency of homologous recombination, the existence of genetic markers for positive and negative selection as well as the availability of replicative single-copy plasmids allows genetic manipulation of *Y. lipolytica* (Barth and Gaillardin, 1997).

Since *Y. lipolytica* is strictly aerobic, it contains high amounts of mitochondria with constitutively expressed respiratory chain complexes. The respiratory chain of *Y. lipolytica* contains complexes I-IV, as found in mammals. In addition, it also possesses an alternative NADH dehydrogenase (NDH2) (de Vries and Marres, 1987; Kerscher et al., 1999; Kerscher, 2000), which transfers electrons from NADH to ubiquinone, and an alternative ubiquinol oxidase (Alt. Ox.), which transfers electrons from ubiquinol to molecular oxygen (Medentsev and Akimenko, 1999; Kerscher et al., 2002) (see Figure 1.7). Both enzymes do not translocate protons across the inner mitochondrial membrane (Kerscher, 2000; Joseph-Horne et al., 2001; Henry and Nyns, 1975; de Troostembergh and Nyns, 1978; Vanlerberghe and McIntosh, 1997).

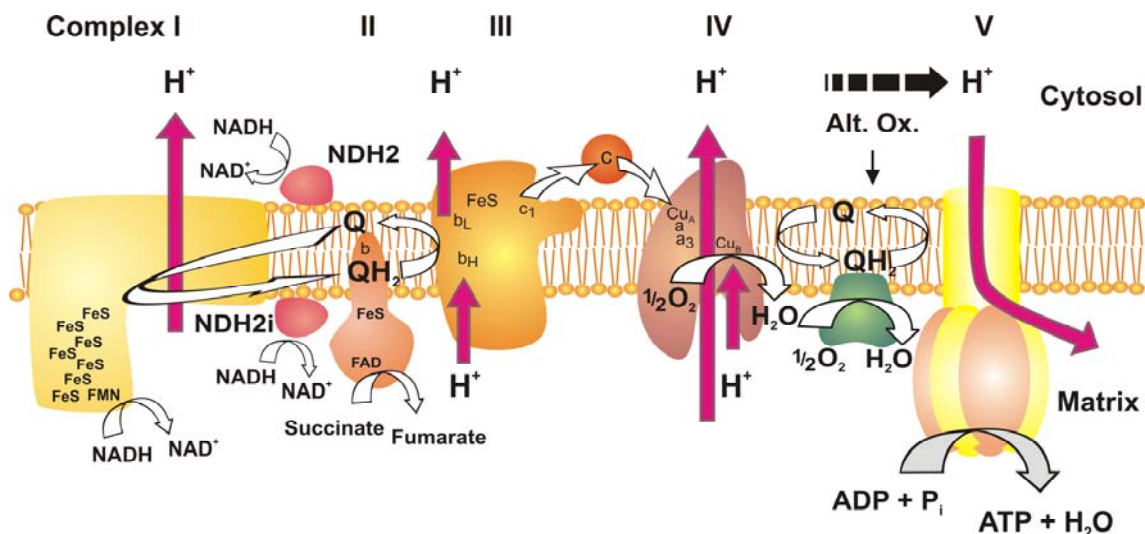


**Figure 1.7: The respiratory chain of *Y. lipolytica* strains used for mutagenesis.** White arrows indicate electron transfer, whereas red arrows indicate proton translocation. Complex V (ATP-synthase); NDH2 (alternative NADH dehydrogenase); NDH2i (internal alternative NADH dehydrogenase); Alt. Ox. (alternative ubiquinol oxidase); FeS (iron-sulfur cluster); Q (ubiquinone); QH<sub>2</sub> (ubiquinol); b (heme b); b<sub>H</sub> (high potential heme b); b<sub>L</sub> (low potential heme b); a (heme a); a<sub>3</sub> (heme a<sub>3</sub>); c (cytochrome c); c<sub>1</sub> (cytochrome c<sub>1</sub>); Cu<sub>A</sub> (copper center A); Cu<sub>B</sub> (copper center B). Figure was prepared by Prof. Dr. Ulrich Brandt and modified for this work.

Complex I deficiency is lethal in “wild type” isolates of *Y. lipolytica* (Kerscher et al., 2001b). By fusing the mitochondrial targeting signal from the 75-kDa subunit to the alternative NADH dehydrogenase, the enzyme was directed to the matrix side of the inner mitochondrial membrane (Kerscher et al., 2001b). This internal version of alternative NADH dehydrogenase (NDH2i) feeds electrons from matrix NADH into the respiratory chain, so that deletions of complex I subunits are no longer lethal in *Y. lipolytica*. In order to study the effects of point mutations, deletion strains are transformed with normal and mutant versions of the respective subunit, encoded on replicative single-copy plasmids.

The *Y. lipolytica* strains used in this study also harbor a hexahistidine affinity-tag at the C-terminus of the 30-kDa subunit. This tag allows fast isolation of highly pure complex I in high yields (several milligrams of complex I per litre of liquid culture) by affinity chromatography on a Ni<sup>2+</sup>-NTA column followed by size exclusion chromatography (Kashani-Poor et al., 2001a).

## 1.4 Aim of this study

### 1.4.1 Exploring the quinone and inhibitor binding pocket

The X-ray structure of the peripheral domain of complex I from *T. thermophilus* (Sazanov and Hinchliffe, 2006) for the first time allowed structure based mutagenesis. The focus in this study lies on the proposed quinone binding pocket assembled by the PSST and the 49-kDa subunit next to iron-sulfur cluster N2 (see Figure 1.8). This part of the enzyme not only reduces quinone to quinol but most probably couples this reaction to conformational changes which result in proton translocation across the inner mitochondrial membrane (Brandt, 2006; Euro et al., 2008a; Zickermann et al., 2008; Zickermann et al., 2009) (see chapter 1.2.7). In addition, most complex I inhibitors act on the quinone binding pocket (see chapter 1.2.4).

A large number of conservative and more drastic point mutations which alter this part of the enzyme should be generated, with the aim to delineate the location of the quinone binding site within the broad cavity and to identify residues critical for catalysis. In addition, effects of mutants on the inhibitory action of different types of complex I inhibitors (Degli Esposti, 1998), exemplified by DQA/type A (Okun et al., 1999a), rotenone/type B and C<sub>12</sub>E<sub>8</sub>/type C (Sato et al., 1996; Okun et al., 2000), were evaluated to chart their respective binding sites.

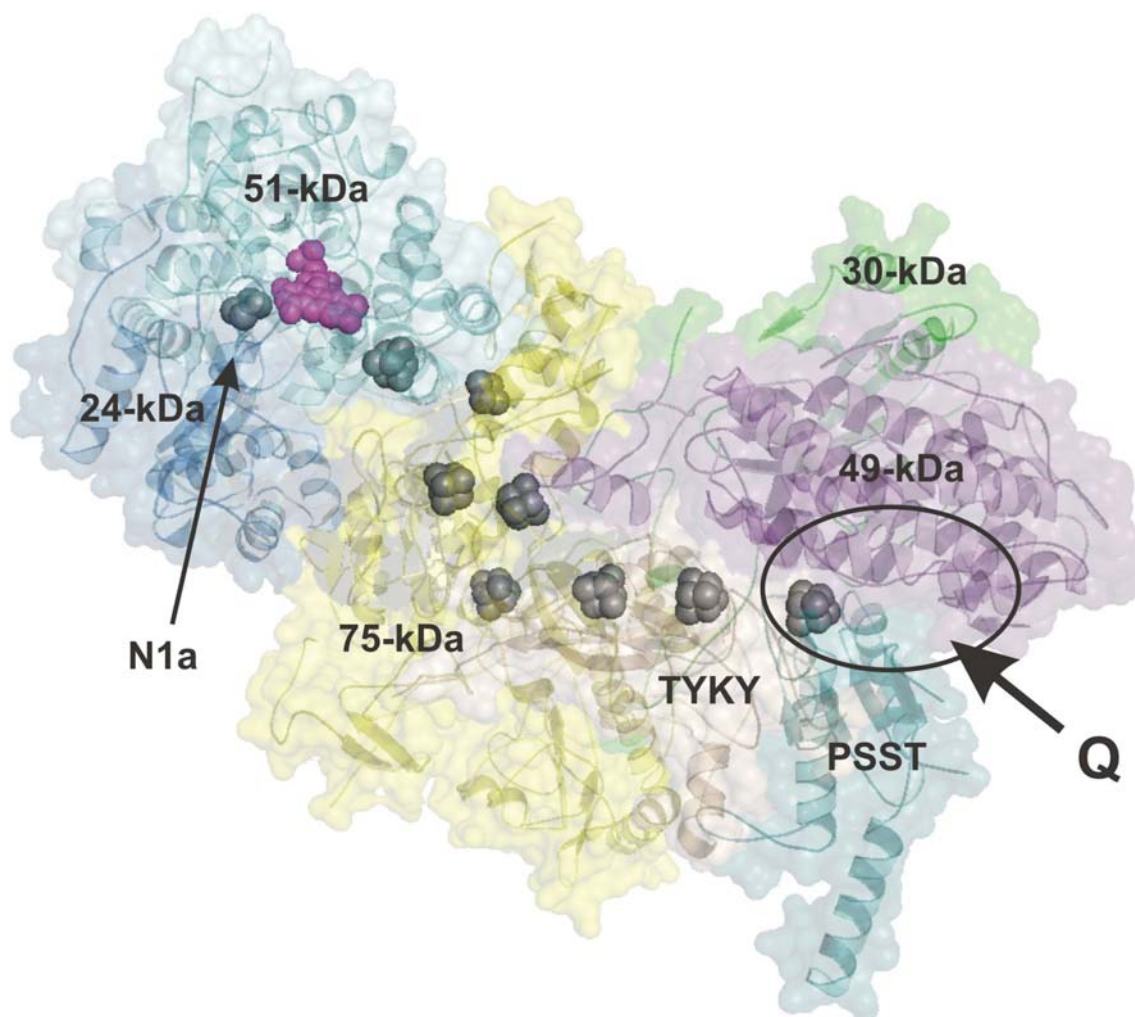


**Figure 1.8:** Regions which underwent mutagenesis in this study are highlighted in the structure of the peripheral domain of complex I from *T. thermophilus*. Subunits are shown in schematic representation with transparent surface and are labeled according to the bovine nomenclature. Iron-sulfur clusters (in gray) as well as the FMN molecule (in pink) are shown as space-filled models. The oval indicates the approximate location of the quinone and inhibitor binding pocket. The position of iron-sulfur cluster N1a ligated by the 24-kDa subunit is indicated by a thin arrow. A thick arrow indicates the putative access path for the quinone substrate (Q). The figure was generated from the crystal structure of the hydrophilic domain of complex I from *T. thermophilus* (PDB ID: 2FUG) using the PyMOL program.

### 1.4.2 Characterization of the HRGXE-motif

At the N-terminus of the 49-kDa subunit there is a strongly conserved HRGXE-motif (see chapter 3.4.1). Based on sequence comparison it had been suggested that amino acid residues from this motif form part of the quinone binding site (Prieur et al., 2001; Fisher and Rich, 2000). However, as revealed by the partial structure of complex I from *T. thermophilus* (Sazanov and Hinchliffe, 2006), amino acid residues of this motif are

not part of the quinone and inhibitor binding pocket (see chapter 3.4.2); instead they are located close to iron-sulfur cluster N2 (see chapter 4.2). Altering the HRGXE-motif by point mutations and characterization of the mutants should shed light on the function of this conserved motif.

### 1.4.3 Shifting of the midpoint potential of iron-sulfur cluster N1a

As discussed in chapter 1.2.6, iron-sulfur cluster N1a is not detectable by EPR in complex I from *Y. lipolytica*, probably due to a very low redox midpoint potential.

The redox midpoint potential of an iron-sulfur cluster seems to depend on hydrogen bonds and solvent accessibility to the iron-sulfur cluster and the presence of charged residues in its vicinity (Stephens et al., 1996). It was shown that by removing hydrogen bonds from amino acid side chains to one sulfur atom of the Rieske iron-sulfur cluster by site directed mutagenesis, the redox midpoint potential of the cluster was strongly decreased (Denke et al., 1998; Schröter et al., 1998). In addition, when a histidine located in the vicinity of iron-sulfur cluster N2 was exchanged to methionine, the redox midpoint potential of the iron-sulfur cluster was strongly decreased (Zwicker et al., 2006).

One additional project of this study was trying to increase the redox midpoint potential of iron-sulfur cluster N1a by introducing polar and positively charged amino acid residues next to iron-sulfur cluster N1a in the 24-kDa subunit from *Y. lipolytica*, and hence make iron-sulfur cluster N1a reducible and EPR detectable.

### 1.4.4 Developing a new *in vivo* screen for complex I deficiency

In order to allow for convenient testing of a large number of *Y. lipolytica* mutants for complex I deficiency, a new concept for an *in vivo* screen should be developed. An earlier screening assay (Garofano et al., 2006) was found to be not applicable to the already existing *Y. lipolytica* mutants and would require the development of a new mutagenesis strategy for all following mutagenesis projects. In addition, this assay inherently cannot screen for defects in proton pumping activity of complex I. However,

proton pumping measurements by alternative methods are very time consuming and labor intensive.

## 2 Materials and Methods

### 2.1 Materials

#### 2.1.1 Chemicals

**Acrylamide, agarose, bisacrylamide, boric acid, Coomassie blue G 250, PEG 4000, Triton X-100** (Serva, Heidelberg, Germany);

**agar** (Gibco BRL Life Technologies, Paisley, Scotland);

**Bacto™ Peptone, Bacto™ Tryptone, Bacto™ Yeast Extract** (Becton, Dickinson and Company, Le Pont de Claix, France);

**ammonium sulfate, antifoam A, BSA, ethidium bromide, dimethyl sulfoxide, dNADH, FCCP, formamide, glutaraldehyde, glycerol, hexaammineruthenium(III)-chloride, HEPES, lithium acetate, Mes, NADH, Ponceau S, PMSF, Q<sub>1</sub>, Q<sub>2</sub>, sodium chloride, TEMED, Tricine, Tris (= Trizma® Base)** (Sigma-Aldrich Inc., St. Louis, USA);

**ammonium bicarbonate, DTT, glycine, potassium chloride, potassium hydroxide, potassium sodium tartrate, Mops, sodium hydroxide, sucrose, hydrochloric acid** (Carl Roth GmbH Co, Kalsruhe, Germany);

**aminocaproic acid, digitonin, glucose, imidazole, copper(II) sulfate pentahydrate, monosodium phosphate monohydrate, silver nitrate, sodium formate** (Fluka AG, Buchs, Swiss);

**ethanol, isoamyl alcohol, methanol** (J.T. Baker, Deventer, Netherlands);

**boric acid, chloroform, isopropanol, KCN, magnesium chloride, magnesium sulfate, 2-mercaptoethanol, sodium bromide, sodium deoxycholate, sodium dithionite, sodium iodide, sodium thiosulfate pentahydrate** (Merck, Darmstadt, Germany);

**ATP** (Pharmacia, USA);

**n-dodecyl-β-D-maltoside** (Glycon, Luckenwalde, Germany);

**EDTA, sodium acetate, sodium carbonate, phenol, SDS** (AppliChem GmbH, Darmstadt, Germany);

**OG** (BIOMOL, Hamburg, Germany):

**formaldehyde** (Riedel-de Haën Laborchemikalien GmbH, Seelze, Germany); **sucrose** (Südzucker AG, Mannheim, Germany);

**acetic acid** (KMF Laborchemie Handels GmbH, Lohmar, Germany); **ACMA** (Molecular Probes Europe, Leiden, Netherlands);

**Asolectin** (Avanti Polar Lipids, Alabaster, USA);

**Chelating Sepharose™ Fast Flow** (Amersham Biosciences AB, Uppsala, Sweden);

**Bio-Beads®** (Bio-Rad Laboratories GmbH, München, Germany);

**glass beads** (diameter 0.25-0.5 mm) (Bernd Euler Biotechnologie-Mikrobiologie Geräte-Verbrauchsmaterialien, Frankfurt am Main, Germany).

### 2.1.2 Inhibitors

**Ampicillin, antimycin A, C<sub>12</sub>E<sub>8</sub>, EIPA, rotenone** (Sigma-Aldrich Inc., St. Louis, USA);

**DQA** (Aventis CropScience, Biochemical Research, Frankfurt am Main, Germany);

**hygromycin B** (PAA Laboratories Lucerna-chem, Luzern, Swiss);

**sodium azide** (Merck, Darmstadt, Germany).



### 2.1.3 Enzymes

**Table 2.1: Enzymes used**

Enzyme	Enzyme buffer	Source
T4 Polynucleotide Kinase (10.000U/ml)	10 x T4 PNK	New England BioLabs
T4 DNA Ligase (1.000U/ml)	5 x T4 DNA Ligase	Invitrogen
Phusion DNA Polymerase (2.000U/ml)	5 x Phusion HF	New England BioLabs
ClaI Endonuclease (5.000 U/ml)	10 x NEB4	New England BioLabs
DpnI Endonuclease (20.000 U/ml)	10 x NEB4	New England BioLabs
EcoRI Endonuclease (20.000 U/ml)	10 x EcoRI	New England BioLabs
NheI Endonuclease (10.000 U/ml)	10 x NEB2	New England BioLabs

### 2.1.4 Plasmids

**Table 2.2: Used plasmids**

Name	Size	Gene	Source
49k/pUB26 3	10.7 kb	NheI-fragment of NUCM in pUB26	Ljuban Grgic LG2/99
nukm pUB4	10.3 kb	EcoRI-fragment of NUKM in pUB4	Gudrun Beyer 15.03.06
24k-WT	10.8 kb	ClaI/NheI-fragment of NUHM in pUB26	Gudrun Beyer Klon 2.2 v. 31.10.01 M&N

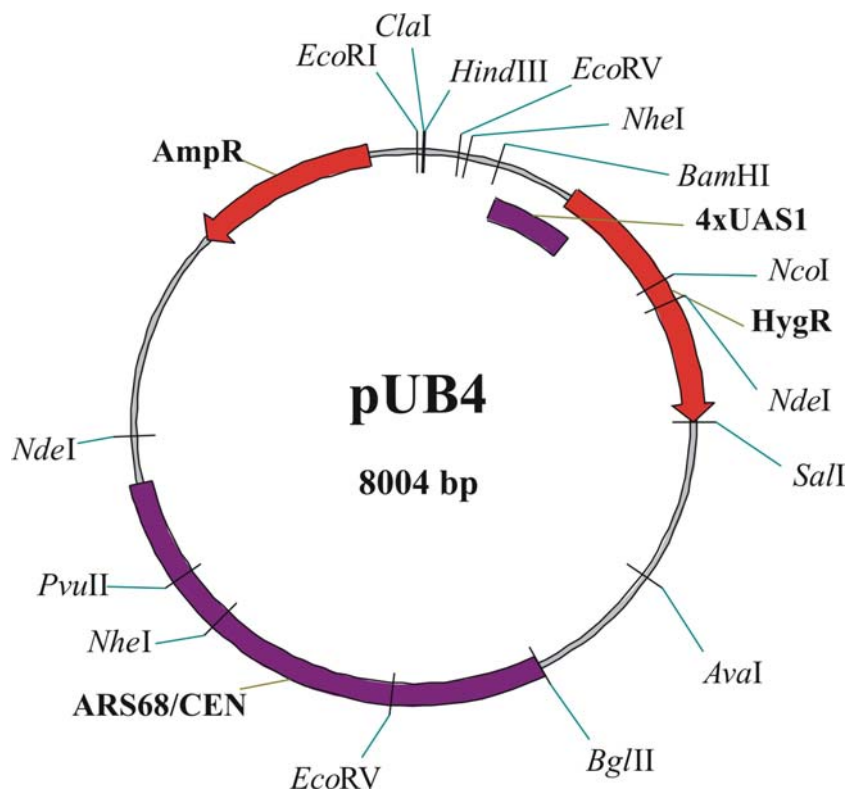


**Figure 2.1: Map of the pUB4 (and pUB26) shuttle vector:** The location of the resistance genes Amp<sup>R</sup> and Hyg<sup>R</sup>, the autonomous replication sequence ARS68/CEN, the upstream activating sequence 4xUAS1 and the restriction sites of some endonucleases are indicated. The pUB4 vector was derived from the pINA443 vector (Barth and Gaillardin, 1996) as described in (Kerscher et al., 2001b). The pUB26 vector is almost identical, but it does not contain the *NheI* restriction site in the autonomous replication sequence ARS68/CEN. Figure was prepared by Dr. Stefan Kerscher and slightly modified for this work.

## 2.1.5 Strains

**Table 2.3: *Escherichia coli* strains used**

Name	Genotype	Source
XL-10 Gold	Tetr $\Delta$ (mcrA)183 $\Delta$ (mcrCB-hsdSMR-mrr)173 endA1 supE44 thi-1 recA1 gyrA96 relA1 lac Hte [F' proAB lacIqZ $\Delta$ M15 Tn10 (Tetr) Tn5 (Kanr) Amy]	Stratagene, (Heidelberg, Germany)

**Table 2.4: *Yarrowia lipolytica* strains used**

<b>Name</b>	<b>Genotype</b>	<b>Source</b>
PIPO	30Htg Pop in Pop out, lys <sup>-</sup> , leu <sup>-</sup> , ura <sup>-</sup> , MatA,	(Kerscher et al., 2002)
GB5.2	ndh2::ura3, leu <sup>-</sup> , ac <sup>+</sup> , lys <sup>-</sup> , MatB	Gudrun Beyer
<i>Δnucm</i>	nucm::ura3, leu <sup>-</sup> , lys <sup>-</sup> , Htg2, ndh2i, spore L1 from 23.02.01	Gudrun Beyer
<i>Δnukm</i>	NUKM::leu2, Htg2, ndh2i, Sporen ura <sup>-</sup> , lys <sup>-</sup> , kL6	Gudrun Beyer
<i>Δnuhm</i>	nuhm::ura3 in GB10, leu <sup>-</sup> , lys <sup>-</sup> , MatB, Htg2, ndh2i, from 17.12.02	Gudrun Beyer
nucm parental	<i>Δnucm</i> + 49k/pUB26 3	this work
nucm mutants	<i>Δnucm</i> + 49k/pUB26 3 carrying a point mutation	Gudrun Beyer, Uta Fendel, this work
nukm parental	<i>Δnukm</i> + nukm pUB4	Gudrun Beyer
nukm mutants	<i>Δnukm</i> + nukm pUB4 carrying a point mutation	Gudrun Beyer, Uta Fendel
nuhm parental	<i>Δnuhm</i> + 24k-WT	this work
nuhm mutants	<i>Δnuhm</i> + 24k-WT carrying a point mutation	this work

## 2.1.6 Instruments

### Centrifuges:

Biofuge pico (Heraeus, Osterode, Germany)

Biofuge A (Heraeus, Osterode, Germany)

Biofuge primo R (Heraeus, Osterode, Germany)

Omnifuge 2 RS (Heraeus, Osterode, Germany)

Cryofuge 8500i (Heraeus, Osterode, Germany)

Refrigerated centrifuge J2-21 (Beckman Instruments GmbH, München, Germany)

Ultracentrifuge L7-65 and L8-70M (Beckman Instruments GmbH, München, Germany)

### Rotors:

Biofuge primo R: 7588, 7593 (Heraeus, Osterode, Germany)

Omnifuge 2 RS: 2250 (Heraeus, Osterode, Germany)

Cryofuge 8500i: F2 (Heraeus, Osterode, Germany)

Refrigerated centrifuge: JA-10, JA-20 (Beckman Instruments GmbH, München, Germany)

Ultracentrifuge: Ti 45, Ti 50.2 (Beckman Instruments GmbH, München, Germany)

TFT 50.38 (Sorvall, Hanau, Germany)

#### **Spectrophotometers:**

UV 300 (Shimadzu, Düsseldorf, Germany)

SpectraMax PLUS<sup>384</sup> (Molecular Devices GmbH, Ismaning, Germany)

SpectraMax M2<sup>°</sup> (Molecular Devices GmbH, Ismaning, Germany)

Multispec-1501 (Shimadzu, Düsseldorf, Germany)

Ultrospec II (LKB Biochrom, Cambridge, UK)

#### **Spectrofluorometers:**

Hoefer<sup>®</sup> DyNA Quant<sup>®</sup> 200 (Pharmacia Biotech, San Francisco, USA)

Shimadzu RF-5001 (Shimadzu, Düsseldorf, Germany)

#### **Thermocyclers:**

GeneAmp<sup>®</sup> PCR System 2400 (Perkin Elmer, Weiterstadt, Germany)

Cyclone<sup>®</sup> gradient, Peqlab (Biotechnologie GmbH, Erlangen, Germany)

#### **UV-Transluminators:**

BIO View (biostep GmbH, Jahnsdorf, Germany)

UV-Transluminator (Vilber Lourmat Deutschland GmbH, Eberhardzell, Germany)

#### **Chromatography systems:**

ÄKTA FPLC chromatographic system (Amersham Biosciences, Piscataway, USA)

BioLogic LP low-pressure chromatographic system (Bio-Rad Laboratories GmbH, München, Germany)

#### **Cell Disrupters:**

Fast Prep<sup>®</sup> FP 120 (Qbiogene Inc, Illkirch, France)

Cell-Desintegrator-C, (Bernd Euler Biotechnologie-Mikrobiologie Geräte-Verbrauchsmaterialien, Frankfurt am Main, Germany)

**Other instruments:**

**Electroporator:** *E. coli* Pulser (Bio-Rad, Hercules, USA)

**DNA Sequencer:** ABI PRISM<sup>TM</sup> 310 Genetic Analyzer (Perkin-Elmer, Weiterstadt, Germany)

**EPR-Spectrometer:** ESP 300 E (Bruker, Rheinstetten, Germany) equipped with a continuous flow cryostat ESR 900 (Oxford Instruments, Oxon, UK)

**EPR-tubes:** Quartz glass Nr.: 707-SQ-250M (length: 250 mm, diameter: 4 mm) (Spintec, Remshalden, Germany)

**10 l Fermenter:** Biostat E (Braun, Melsungen, Germany)

**Biological safety cabinet:** Microflow (Nunc GmbH, Wiesbaden, Germany)

**Microscope** (Leitz, Wetzlar, Germany)

**Counting chamber:** Optik Labor 0.1 mm deep, 0.0025 mm<sup>2</sup> (Neubauer, Friedrichshofen, Germany)

**Molecular Imager:** ChemiDoc XRS (Bio-Rad Laboratories GmbH, München, Germany)

**Digital camera:** COOLPIX 990 (Nikon Corporate, Japan)

**Stereoscopic glasses:** NuVision 60GX (MacNaughton, Inc., Beaverton, USA)

**Pure water system:** TKA-Pacific and TKA-GenePure (TKA Wasseraufbereitungssysteme GmbH, Niederelbert, Germany)

### 2.1.7 Software

**ABI Prism 310 Collection** (Applied Biosystems, Perkin-Elmer, Wellesley, USA)

**Sequencing Analysis** (Applied Biosystems, Perkin-Elmer, Wellesley, USA)

**AutoAssembler 2.0** (Perkin-Elmer, Wellesley, USA)

**CorelDRAW<sup>®</sup>** Graphics Suite - Version 12.0 (Corel Corporation)

**Enzfitter** Version 2.0.16.0, (Biosoft, Cambridge, UK)

**Microsoft Office 2003 Package**

**PSI-Plot** Version 5.02a (Poly Software International, Salt Lake City, USA)

**PyMOL<sup>TM</sup>** 0.99 (DeLano Scientific LLC, Palo Alto, USA)

**SOFTmax PRO** (Molecular Devices GmbH, Ismaning, Germany)

**Unicorn 5.01** (Amersham Biosciences, Piscataway, USA)

**Winepr<sup>®</sup>** (Bruker BioSpin MRI GmbH, Ettlingen, Germany)

**Simfonia<sup>®</sup>** (Bruker BioSpin MRI GmbH, Ettlingen, Germany)

## 2.2 Methods

### 2.2.1 Methods of Microbiology

#### 2.2.1.1 Cultivation of *Escherichia coli*

*E. coli* was cultivated in LB medium (0.5 % Bacto™ Yeast Extract, 1 % NaCl, 1 % Bacto™ Tryptone, pH 7.5) in the presence of Ampicillin (50 µg/ml) at 37 °C for 12-16 h. Usually, 3 ml of medium were inoculated with a single colony picked from plates after transformation of electro-competent *E. coli* cells (see 2.2.1.3).

#### 2.2.1.2 Preparation of electro-competent *Escherichia coli* cells

Electro-competent *E. coli* cells were prepared from the XL-10 Gold strain according to (Seidman et al., 1997).

#### 2.2.1.3 Transformation of electro-competent *Escherichia coli* cells

Frozen electro-competent *E. coli* cells were transformed by electroporation as described in (Seidman et al., 1997).

#### 2.2.1.4 Cultivation of *Yarrowia lipolytica*

*Y. lipolytica* cells were streaked out on YPD-agar plates (1 % Bacto™ Yeast Extract, 2 % Bacto™ Peptone, 2 % glucose, 1.5 % agar) and incubated at 28 °C. For liquid culture, YPD medium (1 % Bacto™ Yeast Extract, 2 % Bacto™ Peptone, 2 % glucose) was inoculated with a single colony of *Y. lipolytica*. Cells were grown at 27 °C under continuous shaking.

Plates and liquid medium contained hygromycin B (50-100 mg/l) as a selection marker when *Y. lipolytica* strains harboring the HygB<sup>R</sup> marker gene were cultivated.

#### 2.2.1.5 Large scale cultivation of *Yarrowia lipolytica*

In order to harvest 300-500 g of *Y. lipolytica* cells (wet weight), strains were grown in a 10 l fermenter (Biostat E, Braun, Melsungen, Germany) with airflow of 30 l/min and vigorous stirring (500 rpm) in YPD medium (1 % Bacto™ Yeast Extract, 2 % Bacto™

Peptone, 2 % glucose) for ~16 h. Temperature was kept at 28 °C and pH at 6.5. *Y. lipolytica* cells were harvested by centrifugation (10 min, 5000 x g, 4 °C) and immediately used for preparation of mitochondrial membranes (see 2.2.3.2) or shock frozen in liquid nitrogen and stored at -80°C.

#### **2.2.1.6 Transformation of *Yarrowia lipolytica***

*Y. lipolytica* cells were transformed according to (Chen et al., 1997).

#### **2.2.1.7 In vivo screen for complex I deficiency**

To screen *Y. lipolytica* strains for complex I deficiency, mutant strains were grown on fresh YPD-agar plates (1 % Bacto™ Yeast Extract, 2 % Bacto™ Peptone, 2 % glucose, 1.5 % agar) in the presence of 0.2-0.4 µM antimycin A and/or 0.4-0.6 mM sodium azide. Antimycin A was added to 20 ml warm and liquid YPD-agar plate medium. ~0.5 ml sodium-azide were evenly distributed on chilled plates using a Drigalski glass spatula. Cell numbers in fresh liquid cultures of *Y. lipolytica* strains (see 2.2.1.4) were determined with a counting chamber (for best results, liquid cultures should have optical densities of 2-5) and diluted with YPD medium (1 % Bacto™ Yeast Extract, 2 % Bacto™ Peptone, 2 % glucose) to around 3000, 300, 30 or 3 cells per 5-7 µl. From these dilutions droplets of 5-7 µl volume were applied on plates with varying inhibitor concentrations. Plates were then incubated at 28 °C for several days.

#### **2.2.1.8 Storage of *Yarrowia lipolytica* strains**

For storage, *Y. lipolytica* strains were freshly grown in YPD medium (1 % Bacto™ Yeast Extract, 2 % Bacto™ Peptone, 2 % glucose). Medium contained hygromycin B (50-100 mg/l) as a selection marker when *Y. lipolytica* strains harboring the HygB<sup>R</sup> marker gene were cultivated. Cells were sedimented by brief centrifugation and 0.6 ml of cells were added to 0.4 ml glycerol. After vortexing, strains were stored at -80 °C.

## **2.2.2 Methods of Molecular Biology**

### **2.2.2.1 Purification of plasmid DNA from *Escherichia coli***

Plasmid DNA purification was performed using the column-based-kit „NucleoSpin® Plasmid“ (Macharey & Nagel, Düren, Germany) according to the manufacturer's protocol.

### **2.2.2.2 Total DNA isolation from *Yarrowia lipolytica***

DNA was isolated according to a standard protocol (Hoffman, 1997). For plasmid DNA recovery, 1 µl of total DNA was used to transform electro-competent *E. coli* cells (see 2.2.1.3). From transformed cells, plasmid DNA was isolated as described under 2.2.2.1.

### **2.2.2.3 Determination of DNA concentration**

DNA concentration was measured using the „Hoechst 33258“ dye and standard DNA concentrations. Fluorescence was recorded on a DyNA Quant™ 200 fluorometer from Hoefer® according to the low range (A) protocol.

### **2.2.2.4 Restriction of DNA**

1 µl of DNA solution was incubated with 5 units of endonuclease and the corresponding buffer for 2 h at 37 °C in a final volume of 10 µl.

### **2.2.2.5 Agarose gel electrophoresis of DNA**

DNA-fragments were separated on 1 % agarose gels according to (Sambrook et al., 1989). Agarose gels were prepared with TAE buffer (0.4 M tris/acetate, 10 mM EDTA, pH 8.3) and contained 0.5 µg/ml ethidium bromide.

The GeneRuler™ 1kb DNA Ladder (MBI Fermentas) was used as a DNA size marker.

Electrophoresis was performed at 120 V and 90 mA.

### **2.2.2.6 Primer phosphorylation for PCR**

5' Phosphorylation of primers was performed according to (Tabor, 1987). The reaction mixture contained a primer (0.1 nmoles), ATP (0.5 mM), BSA (0.2 mg/ml) the T4 PNK



buffer and T4 polynucleotide kinase (10 units) in a final volume of 20  $\mu$ l. This mixture was incubated at 37 °C for 1 h. The reaction was stopped by incubation at 65 °C for 20 min. Phosphorylated primers were stored at -20 °C.

#### **2.2.2.7 PCR mutagenesis**

Desired point mutations were generated using appropriate primer pairs. The forward primer had a mismatch codon at the 3' end leading to the point mutation. The reverse primer ended just after the mismatch codon and contained no mismatch. Primers were ~20 bases long and were chosen to end with 1-2 guanine and/or cytosine bases (see chapter 8.1). Primers were phosphorylated prior to PCR (see 2.2.2.6). The PCR reaction mixture contained plasmid DNA harboring the target gene as template (~10 ng), both primers (0.5  $\mu$ M each), dNTP (120  $\mu$ M), Phusion HF buffer and Phusion DNA polymerase (2 units) in a final volume of 50  $\mu$ l. The reaction was started by adding the Phusion DNA polymerase (manual hot start). PCR conditions were set as follows:

- Initial denaturation: 30 sec at 98 °C
- Denaturation: 10 sec at 98 °C
- Annealing: 20 sec at 52.4 °C, 55.8 °C, 60.4 °C or 64.3 °C
- Extension: 3 min at 72 °C
- 25 cycles
- Final extension: 8 min at 72 °C

PCR products were stored at -20 °C.

#### **2.2.2.8 DNA precipitation with ethanol**

Using this method a DNA solution was concentrated and purified. Added volumes refer to the initial volume of the DNA solution. First, 3 M NaAc (0.1 x volume), 20  $\mu$ g/ $\mu$ l Dextran-Blue (1  $\mu$ l) and cold (-20 °C) ethanol (3 x volume) were added. A 30 min incubation at -20 °C was followed by a centrifugation at 11000 x g for 15 min. The blue DNA sediment was washed with cold (-20 °C) 70 % ethanol and dried at 37°C. DNA was then solubilized in TE buffer (10 mM Tris/HCl, 1 mM EDTA, pH 8) and stored at -20 °C.

### 2.2.2.9 Extraction of DNA from agarose gels

DNA bands of interest were cut out from agarose gels under weak UV light. For agarose removal, the „NucleoSpin<sup>®</sup> Extract II“ (Macharey & Nagel, Düren, Germany) was used.

### 2.2.2.10 Ligation

Ligation of PCR products was performed in the presence of 1 unit T4 DNA ligase, 1.2 µg BSA and T4 DNA ligase buffer (final volume ~7 µl) at 14 °C over night.

### 2.2.2.11 DNA sequencing

The complete open reading frames of the mutated subunit genes were sequenced to confirm the point mutations and exclude other changes. Subunit specific sequencing primers are listed in chapter 8.1.

DNA was sequenced using the dye-terminator method following the protocol of Applied Biosystems. DNA was labeled with dideoxy-nucleotide-coupled fluorophores by PCR. The PCR mixture contained 250-500 ng DNA, 640 nM primer and the „Termination Mix“ (ABI, Perkin-Elmer, Weiterstadt, Germany) in a final volume of 10 µl. PCR conditions were set as follows:

- Initial denaturation: 1 min at 96 °C
- Denaturation: 10 sec at 96 °C
- Annealing: 5 sec at 50 °C
- Elongation: 2 min at 60 °C
- 30 cycles

PCR products were precipitated with sodium acetate and ethanol and solubilized in 20 µl formamide. DNA was sequenced on a „ABI prism Genetic Analyzer 310“ (Applied Biosystems GmbH, Weiterstadt, Germany). DNA sequences were analyzed using the AutoAssembler 2.0 (ABI, Perkin-Elmer, Weiterstadt, Germany) software.

### 2.2.3 Methods of Protein Chemistry

#### 2.2.3.1 Small scale preparation of mitochondrial membranes from *Y. lipolytica*

Mitochondrial membranes were prepared from freshly harvested *Y. lipolytica* cells or cells that had been shock frozen in liquid nitrogen and stored at -80°C. Cells were harvested by centrifugation (10 min, 5300 x g, 4 °C) and washed with 50 ml H<sub>2</sub>O (10 min, 3300 x g, 4 °C). Pelleted cells (3-8 g) were resuspended in 10 ml mito buffer (600 mM sucrose, 20 mM Na-Mops, 1 mM EDTA, pH 7.2) in the presence of 2 mM PMSF. Cells were broken up in a Falcon tube by vortexing (13 x 1 min with 1 min cooling intervals on ice) in the presence of 10 g glass beads ( $\varnothing = 0.45$  mm). Unbroken cells, nuclei and glass beads were pelleted by centrifugation (45 min, 3300 x g, 4 °C). A high-speed centrifugation (120 min, 40000 x g, 4 °C) pelleted mitochondria and mitochondrial membranes. PMSF (final concentration 2 mM) was added to the homogenized pellet before mitochondrial membranes were shock frozen in liquid nitrogen and stored at -80°C.

#### 2.2.3.2 Large scale preparation of mitochondrial membranes from *Y. lipolytica*

Fresh or shock frozen *Y. lipolytica* cells (200-250 g wet weight) were resuspended in 500 ml mito buffer (600 mM sucrose, 20 mM Na-Mops, 1 mM EDTA, pH 7.2) and 2 mM PMSF were added. Cells were broken up by glass beads ( $\varnothing = 0.25$ -0.5 mm) in a cooled Cell-Desintegrator-C, (Bernd Euler Biotechnologie, Frankfurt am Main, Germany) at 1000 rpm for 2 h. After a low speed centrifugation (30 min, 4000 x g, 4 °C) to remove cell debris, mitochondrial membranes were pelleted by ultracentrifugation (60 min, 140000 x g, 4 °C). The pellet was resuspended in mito buffer (600 mM sucrose, 20 mM Na-Mops, 1 mM EDTA, pH 7.2) without EDTA, then homogenized and ultracentrifuged (60 min, 140000 x g, 4 °C) once more. Pelleted mitochondrial membranes were homogenized, supplemented with 1.5 mM PMSF, 20 mM Na-Borate and 50 mM NaCl, shock frozen in liquid nitrogen and stored at -80°C.

#### 2.2.3.3 Determination of protein concentration

Protein concentrations were determined using the DC Protein Assay-Kit (Bio-Rad, Hercules, USA) according to the manufacturer's Microplate Assay protocol.

#### 2.2.3.4 NADH:HAR oxidoreductase activity measurement

NADH:HAR oxidoreductase activity was measured as NADH oxidation at  $E_{340-400 \text{ nm}}$  ( $\epsilon = 6.22 \text{ mM}^{-1}\text{cm}^{-1}$ ) in the presence of the electron acceptor HAR on a SpectraMax PLUS<sup>384</sup> spectrophotometer. Measurements were carried out in the presence of 200  $\mu\text{M}$  NADH, 2 mM HAR, 20 mM Hepes, 250 mM sucrose, 0.2 mM EDTA and 2 mM  $\text{NaN}_3$  at pH 8.0 and 30 °C. The reaction was started by the addition of mitochondrial membranes (final concentration 25  $\mu\text{g}$  protein/ml).

The NADH:HAR oxidoreductase activity is detergent- and inhibitor-insensitive and specific for complex I (Sled and Vinogradov, 1993). The activity depends on the presence of FMN in complex I (Gavrikova et al., 1995).

#### 2.2.3.5 dNADH:DBQ oxidoreductase activity measurement

dNADH:DBQ oxidoreductase activity was determined as DQA sensitive dNADH oxidation at  $E_{340-400 \text{ nm}}$  ( $\epsilon = 6.22 \text{ mM}^{-1}\text{cm}^{-1}$ ) in the presence of the ubiquinone analogue DBQ on a SpectraMax PLUS<sup>384</sup> spectrophotometer. Measurements were carried out in the presence of 100  $\mu\text{M}$  dNADH, 20 mM Na-Mops, 50 mM NaCl, 2 mM KCN and 50  $\mu\text{g}$  protein/ml of mitochondrial membranes at pH 7.4 and 30 °C. The reaction was started by the addition of 70  $\mu\text{M}$  DBQ. To determine DQA insensitive activity, measurements were carried out in the presence of 27  $\mu\text{M}$  DQA (5 mM stock solution dissolved in DMSO). To address complex I specific activity, dNADH was used (Matsushita et al., 1987) instead of NADH, which can also be oxidized by the alternative NADH:ubiquinone oxidoreductase (NDH2) present in mitochondrial membranes from *Y. lipolytica*.

#### 2.2.3.6 Measurement of *apparent* $K_m$ for DBQ, $Q_1$ and $Q_2$

Measurements were performed as described under 2.2.3.5 with different concentrations of DBQ,  $Q_1$  or  $Q_2$ , respectively. Data were fitted using the Enzfitter software package to the Michaelis-Menten equation. However, the value for substrate concentration  $[S]$  was corrected as described earlier (Eschemann et al., 2005):

$$[S] = [S]^{added} - c$$

( $[S]$  = substrate concentration available for binding and catalysis,  $[S]^{added}$  = added substrate concentration,  $c$  = offset value)

### 2.2.3.7 Measurement of pH dependence of dNADH:DBQ oxidoreductase activity

Determination of pH dependence of dNADH:DBQ oxidoreductase activity was performed as described under 2.2.3.5 with one modification; measurements were carried out in the presence of 100  $\mu$ M dNADH, 30 mM Mes, 30 mM Mops, 30 mM sodium acetate, 30 mM Tris, 30 mM glycine, 50 mM NaCl, 2 mM KCN and 50  $\mu$ g protein/ml of mitochondrial membranes at pH 5-10 and 30 °C. pH values were adjusted using NaOH or HCl.

Data were fitted to a previously described equation (Brandt and Okun, 1997):

$$v = V_{opt} \cdot \frac{1}{1 + \frac{[H^+]}{K_A}} \cdot \frac{1}{1 + \frac{K_B}{[H^+]}}$$

( $v$  = catalytic rate under substrate saturated conditions,  $[H^+]$  = proton concentration,  $K_A$  = dissociation constant of protonable group A,  $K_B$  = dissociation constant of protonable group B,  $C$  = catalytic rate if group A was deprotonated and group B was protonated)

### 2.2.3.8 Reactivation of dNADH:DBQ oxidoreductase activity

In order to restore complex I activity in mitochondrial membranes from mutant strains, various salts and small molecules were tested; Sodium chloride (20-400 mM), sodium bromide (0-500 mM), sodium iodide (0-400 mM), sodium azide (0-500 mM), sodium formate 0-500 mM or sodium acetate (0-400 mM) were added to the assay buffer (pH was adjusted to 7.4) before NADH and mitochondrial membranes were added. Measurements were performed as described in 2.2.3.5.

### 2.2.3.9 dNADH:Q<sub>1</sub> oxidoreductase activity measurement

The dNADH:Q<sub>1</sub> oxidoreductase activity in mitochondrial membranes from *Y. lipolytica* was measured as described under 2.2.3.5 with the exception that 62  $\mu$ M Q<sub>1</sub> was used instead of DBQ.

### 2.2.3.10 dNADH oxidation measurement

dNADH oxidation was measured on a SpectraMax PLUS<sup>384</sup> spectrophotometer at E<sub>340-400 nm</sub> ( $\epsilon = 6.22 \text{ mM}^{-1}\text{cm}^{-1}$ ). Measurements were carried out in the presence of 100  $\mu\text{M}$  dNADH, 20 mM Na-Mops, 50 mM NaCl and 100  $\mu\text{g}$  protein/ml of mitochondrial membranes at pH 7.4 and 30 °C. The reaction was started by the addition of mitochondrial membranes. To determine DQA insensitive activity, measurements were carried out in the presence of 27  $\mu\text{M}$  DQA.

### 2.2.3.11 Measurement of $I_{50}$

The  $I_{50}$  value was defined as the inhibitor concentration which decreased the inhibitor sensitive dNADH:Q oxidoreductase activity by 50 %. Measurements were carried out as described under 2.2.3.5 in the presence of different concentrations of complex I inhibitors. DQA, rotenone and EIPA were provided in DMSO. C<sub>12</sub>E<sub>8</sub> was provided in 20 mM Na-Mops, 50 mM NaCl and 2 mM KCN. In contrast to other inhibitors C<sub>12</sub>E<sub>8</sub> was pre-incubated with mitochondrial membranes for at least 30-60 s at 30 °C before measurements were started.

### 2.2.3.12 Solubilization of membrane proteins for blue-native and clear-native PAGE

Sample preparation followed the principles described in (Schägger, 2003). First, mitochondrial membranes (2.8 mg total protein) from *Y. lipolytica* were resuspended in 190  $\mu\text{l}$  buffer containing 20 mM Mops and 1 mM EDTA, pH 7.2 and centrifuged (20 min, 1800 x g, 4 °C). The pellet was resuspended in 280  $\mu\text{l}$  solubilisation buffer (50 mM NaCl, 50 mM imidazole, 2 mM aminocaproic acid, 1 mM EDTA, 0.2 mM PMSF, pH 7) and 1 g n-dodecyl- $\beta$ -D-maltoside per 1 g protein or 3 g digitonin per 1 g protein was added. After centrifugation (15 min, 1800 x g, 4 °C) membranes and not solubilized proteins were pelleted.

- For blue-native PAGE, 2  $\mu\text{l}$  Coomassie blue G 250 solution (5 % in 0.5 M aminocaproic acid) were added to the supernatant.
- For clear-native and high-resolution-clear-native PAGE, Ponceau S (final concentration 0.01 % w/v) and glycerol (final concentration 5 % v/v) were added to the supernatant.

Samples were loaded on the corresponding native gels.

#### **2.2.3.13 Blue-native PAGE**

Blue-native PAGE was carried out according to the protocol of (Schägger, 2003). However, the acrylamide concentration in the sample gel was 3 % or 4 % and in the gradient separation gel 3 % or 4 % to 13 %.

#### **2.2.3.14 Complex I in-gel activity assay**

Complex I in-gel activity assay was performed according to (Zerbetto et al., 1997) with minor modifications described in (Wittig et al., 2007).

#### **2.2.3.15 2D Gels (Tricine-SDS-PAGE second dimension after Blue-native PAGE)**

Second dimension SDS-PAGE (10 %) was performed according to the standard protocol described in (Schägger, 2003).

#### **2.2.3.16 Coomassie staining of protein gels**

Coomassie staining was carried out as described in (Schägger, 2003).

#### **2.2.3.17 Silver staining of protein gels**

Prior to silver staining, coomassie stained gels had to be completely destained by an overnight incubation in a 50 % methanol, 0.1 M ammonium bicarbonate solution and washed 3 times with H<sub>2</sub>O. Silver staining of 0.7 mm gels was performed as described in (Rais et al., 2004).

#### **2.2.3.18 Complex I purification**

Complex I was purified from mitochondrial membranes (see 2.2.3.2) as described previously (Kashani-Poor et al., 2001a) with two minor modifications:

- after ultracentrifugation the supernatant was adjusted to 55 mM imidazole and pH 7.4.
- the imidazole concentration for equilibration and washing of the Ni-NTA fast flow Sepharose column was reduced from 65 mM to 55 mM.

### 2.2.3.19 Complex I proteoliposomes

Reconstitution of purified complex I into proteoliposomes was performed as described earlier (Dröse et al., 2009).

### 2.2.3.20 Measurement of proton gradient by ACMA quench

Measurements were carried out as described earlier (Dröse et al., 2005).

### 2.2.3.21 EPR spectroscopy

EPR spectroscopy of mitochondrial membranes as well as of purified complex I was performed as described in (Tocilescu et al., 2007). Standard EPR parameters were the following: Microwave frequency 9.47 GHz, modulation frequency 100 kHz and modulation amplitude 6.4 Gauss. All other parameters are given in figure legends. EPR spectra were recorded and analyzed by Dr. Klaus Zwicker.

## 2.2.4 Methods of Bioinformatics

### 2.2.4.1 Multiple sequence alignment

For multiple sequence alignment the program ClustalW was used as provided at <http://www.ebi.ac.uk/Tools/clustalw2/index.html>.

For the alignment of the 49-kDa subunit the NCBI sequences of *Y. lipolytica* (ACCESSION CAG78336), *Neurospora crassa* (ACCESSION CAA38368), *Bos taurus* (ACCESSION P17694), *Homo sapiens* (ACCESSION AAC27453), *Paracoccus denitrificans* (ACCESSION P29916), *Rhodobacter capsulatus* (ACCESSION AAC24988), *Thermus thermophilus* (ACCESSION AAA97941) and *E. coli* (ACCESSION CAA48363) were used.

For the alignment of the PSST subunit the NCBI sequences of *Y. lipolytica* (ACCESSION CAB65525), *N. crassa* (ACCESSION CAF06152), *B. taurus* (ACCESSION CAA46154), *H. sapiens* (ACCESSION AAI11518), *P. denitrificans* (ACCESSION P29918), *R. capsulatus* (ACCESSION AAC24986), *T. thermophilus* (ACCESSION AAA97939) and *E. coli* (ACCESSION BAA16121) were used.



For the alignment of the 30-kDa subunit the NCBI sequences of *Y. lipolytica* (ACCESSION XP\_504891), *N. crassa* (ACCESSION XP\_957689), *H. sapiens* (ACCESSION NP\_004542), *B. taurus* (ACCESSION NP\_777244), *R. capsulatus* (ACCESSION AAC24987), *T. thermophilus* (ACCESSION AAA97940), *P. denitrificans* (ACCESSION AAA97940) and *E. coli* (ACCESSION BAA16115) were used.

For the alignment of the 24-kDa subunit the NCBI sequences of *Y. lipolytica* (ACCESSION CAG80440), *N. crassa* (ACCESSION CAA54990), *B. taurus* (ACCESSION P04394), *H. sapiens* (ACCESSION CAG33209), *P. denitrificans* (ACCESSION AAA25588), *Rhodothermus marinus* (ACCESSION AAY42999), *T. thermophilus* (ACCESSION AAA979421) and *E. coli* (ACCESSION BAA16114) were used.

#### **2.2.4.2 Structure figure preparation**

For the interpretation of the mutagenesis results, structure figures were prepared based on the 3.3 Å resolution x-ray structure of the hydrophilic domain of respiratory complex I from *T. thermophilus* (PDB ID: 2FUG). Figures were generated using the PyMOL program version 0.99 provided at <http://pymol.sourceforge.net/>. Where the *T. thermophilus* sequence differed from that of *Y. lipolytica*, the mutagenesis wizard of the PyMOL package was used to match the *Y. lipolytica* sequence. Side chain conformations were chosen which resemble as closely as possible that of the *T. thermophilus* side chains and were sterically feasible.



## 3 Results

### 3.1 Mutagenesis of the proposed ubiquinone and inhibitor binding cavity

Taking advantage of the crystal structure of the hydrophilic part of complex I from *T. thermophilus* (Sazanov and Hinchliffe, 2006), the proposed quinone and inhibitor binding cavity was studied by structure based site-directed mutagenesis. In order to completely cover the inner surface of this cavity, 34 point mutations at 15 positions were introduced into the PSST and the 49-kDa subunits of complex I from *Y. lipolytica*. If possible, at least one rather conservative and one more drastic mutation were introduced at each position. For a comprehensive view, the obtained results will be discussed together with data from previously generated and described mutants. In total, 94 point mutations on 39 positions within the proposed quinone and inhibitor binding cavity will be described here.

#### 3.1.1 Assembly of mutant complex I

From all mutants mitochondrial membranes were isolated and complex I content was assessed as the NADH:HAR oxidoreductase activity. As shown in Table 3.1 and Table 3.2, only a few mutations (8 out of 94) decreased complex I content to less than 70 % of the parental strain. However, none of the point mutations prevented complex I assembly, with the notable exception of A84V in the PSST subunit. Since alanine 84 is only 4 Å away from iron-sulfur cluster N2 and the side chain points towards this cluster (see Figure 3.3), it seems that the addition of two methyl groups in mutant A84V sterically interfered with iron-sulfur cluster N2 and hence complex I assembly. Consistently, exchanging alanine 84 to glycine did not decrease complex I content (see Table 3.2).

**Table 3.1: Effects of point mutations introduced into the 49-kDa subunit in mitochondrial membranes from *Y. lipolytica*.**

Strain	Complex I content <sup>a</sup>	Complex I activity <sup>b</sup>	<i>app. K<sub>m</sub></i> for DBQ
	%	%	μM
parental	100±3	100±5	15
A94I <sup>i</sup>	85±3	14±2	n.d.
H95A <sup>c</sup>	130	<5	n.d.
H95M <sup>c</sup>	120	<5	n.d.
H95R <sup>c</sup>	100	<5	n.d.
V97G	56±1	72±1	n.m.
V97I	96±2	82±4	n.m.
V97W	78±2	10±2	n.d.
L98F <sup>i</sup>	101±3	22±2	n.d.
L98K <sup>i</sup>	71±2	15±2	n.d.
R99D	58±2	14±2	n.d.
R99K <sup>h</sup>	99	5	n.d.
R99Q <sup>i</sup>	75±1	n.m.	n.m.
R99T	71±1	15±2	n.d.
R141A <sup>d</sup>	130	17	10 <sup>f</sup>
R141K <sup>c</sup>	140	45	13
D143A <sup>g</sup>	118±3	30±3	18
D143C <sup>d</sup>	110	30	7 <sup>f</sup>
D143E <sup>d</sup>	170	23	9.5 <sup>f</sup>
D143N <sup>g</sup>	91±3	42±5	15
Y144F	110±2	7±2	n.d.
Y144H <sup>d</sup>	70	<5	n.d.
Y144H	86±2	<5	n.d.
Y144I	59±1	15±1	n.d.
Y144R <sup>i</sup>	58±1	9±1	n.d.
Y144S <sup>i</sup>	94±4	<5	n.d.
Y144W	129±2	8±4	n.d.
V145F	127±1	7±3	n.d.
V145K <sup>h</sup>	71	10	n.d.
V145M <sup>h</sup>	100	33	n.m.
V145T	122±4	92±8	12
S146A <sup>e</sup>	107	110	10

Strain	Complex I content <sup>a</sup>	Complex I activity <sup>b</sup>	<i>app. K<sub>m</sub></i> for DBQ
	%	%	μM
parental	100±3	100±5	15
S146C <sup>e</sup>	100	100	12
S146V <sup>g</sup>	94±4	94±6	16
M188C	98±3	104±5	18
M188L	101±2	123±5	23
M188Y	104±3	12±2	n.d.
S192I <sup>i</sup>	110±3	16±2	n.d.
S192R <sup>i</sup>	102±5	8±2	n.d.
S192Y	111±2	24±2	n.d.
M195F <sup>h</sup>	88	69	n.m.
M195K <sup>h</sup>	95	26	n.m.
D196E <sup>h</sup>	90	35	n.m.
D196N <sup>h</sup>	101	29	n.m.
L200K <sup>h</sup>	101	33	n.m.
F203E <sup>g</sup>	97±3	28±3	14
F203W <sup>g</sup>	103±3	98±6	15
F207H <sup>g</sup>	117±4	92±8	15
F207W	99±2	58±2	12
R210I	100±2	63±2	14
E211Q	124±4	83±6	16
E218Q	97±2	97±4	12
R224D	97±2	107±4	13
R224I	93±3	102±5	14
R224K	86±2	103±3	10
R224N	124±2	99±7	14
L225A	102±3	103±6	13
L225F	95±3	110±6	13
L225H	84±3	107±5	12
L225V	95±2	91±3	12
H226A <sup>d</sup>	100	20	n.d.
H226C <sup>c</sup>	122	43	5
H226M <sup>c</sup>	120	80	9

Strain	Complex I content <sup>a</sup>	Complex I activity <sup>b</sup>	<i>app. K<sub>m</sub></i> for DBQ
	%	%	μM
parental	100±3	100±5	15
H226Q <sup>c</sup>	112	56	9
P406A <sup>e</sup>	120	114	n.m.
K407A <sup>e</sup>	104	85	n.m.
K407H	80±2	78±2	13
K407R	93±3	105±4	12
K407W	66±1	12±2	n.d.
L447K <sup>h</sup>	90	10	n.d.
V451K <sup>h</sup>	87	12	n.d.
I454K <sup>h</sup>	94	7	n.d.
G455I <sup>i</sup>	71±3	16±2	n.d.
G455S <sup>i</sup>	98±1	72±4	11
D458A <sup>d</sup>	93	28	12 <sup>f</sup>
D458E <sup>g</sup>	83±1	89±3	n.m.
L459I <sup>i</sup>	92±7	92±10	16
L459K <sup>i</sup>	50±2	24±2	n.d.
V460A <sup>d</sup>	90	<5	n.d.
V460L <sup>i</sup>	83±4	21±2	n.d.
V460M <sup>h</sup>	100±2 <sup>h</sup>	16±2 <sup>h</sup>	9 <sup>f</sup>
V460S <sup>i</sup>	82±3	21±1	n.d.
F461W <sup>i</sup>	97±3	23±3	15
E463Q <sup>d</sup>	60	20	5 <sup>f</sup>
E463T <sup>i</sup>	78±1	35±2	11

Mean values ± SEM are given.

n.d., not determinable

n.m., not measured

<sup>a</sup> 100 % of complex I content corresponds to 1.25 μmol·min<sup>-1</sup>·mg<sup>-1</sup> NADH:HAR oxidoreductase activity determined for the parental strain.

<sup>b</sup> DQA sensitive complex I specific dNADH:DBQ oxidoreductase activity (0.58 μmol·min<sup>-1</sup>·mg<sup>-1</sup> was measured for the parental strain) was normalized to complex I content. The ratio of 0.58/1.25 for the parental strain was set as 100 % complex I activity.

<sup>c</sup> data from (Grgic et al., 2004)

<sup>d</sup> data from (Kashani-Poor et al., 2001b)

- <sup>e</sup> data from (Grgic, Ph.D. Thesis, University Frankfurt, 2004)  
<sup>f</sup> data from (Kashani-Poor, Ph.D. Thesis, University Frankfurt, 2000)  
<sup>g</sup> data from (Fendel et al., 2008)  
<sup>h</sup> data from (Fendel, M.D. Thesis, University Frankfurt)  
<sup>i</sup> mutations generated by U. Fendel

**Table 3.2: Effects of point mutations introduced into the PSSST subunit in mitochondrial membranes from *Y. lipolytica*.**

Strain	Complex I content <sup>a</sup>	Complex I activity <sup>b</sup>	<i>app. K<sub>m</sub></i> for DBQ
	%	%	μM
parental	100±2	100±3	14
A84G <sup>f</sup>	124	68	n.m.
A84V	26±1	n.d.	n.d.
V88F	96±2	13±1	n.d.
V88L	94±4	92±5	15
V88M	95±2	56±3	13
E89A <sup>c</sup>	145	74	19
E89C <sup>c</sup>	145	67	18
E89Q <sup>c</sup>	100	88	9
M91C <sup>e</sup>	114±2	31±4	11
M91K <sup>e</sup>	86±3	10±2	n.d.
E185Q <sup>d</sup>	110	35	18

Mean values ± SEM are given.

n.d., not determinable

n.m., not measured

<sup>a</sup> 100 % of complex I content corresponds to 1.25 μmol·min<sup>-1</sup>·mg<sup>-1</sup> NADH:HAR oxidoreductase activity determined for the parental strain.

<sup>b</sup> DQA sensitive complex I specific dNADH:DBQ oxidoreductase activity (0.6 μmol·min<sup>-1</sup>·mg<sup>-1</sup> was measured for the parental strain) was normalized to complex I content. The ratio of 0.6/1.25 for the parental strain was set as 100 % complex I activity.

<sup>c</sup> data from (Ahlers et al., 2000), NBQ was used instead of DBQ as substrate.

<sup>d</sup> data from (Garofano et al., 2003)

<sup>e</sup> data from (Fendel et al., 2008)

<sup>f</sup> data from (Fendel, M.D. Thesis, University Frankfurt)

EPR spectra recorded from mitochondrial membranes of 18 most drastic mutations indicated that complex I was properly assembled in all cases (see Figure 3.1 and Figure 3.2). Moreover, since iron-sulfur cluster N2 gives a strong and distinct EPR signal, major structural changes nearby should influence the N2 signal. However, the position in the spectrum as well as the line shape of the N2 signal was unchanged in all mutants examined. This suggests that the structural changes introduced by the mutations were rather local.

Reduced complex I content in some mutants as indicated by lower NADH:HAR oxidoreductase activity was confirmed by lower complex I specific EPR signals, i.e. a lower signal to noise ratio in the EPR spectra (see spectrum from mutant L459K in Figure 3.1).



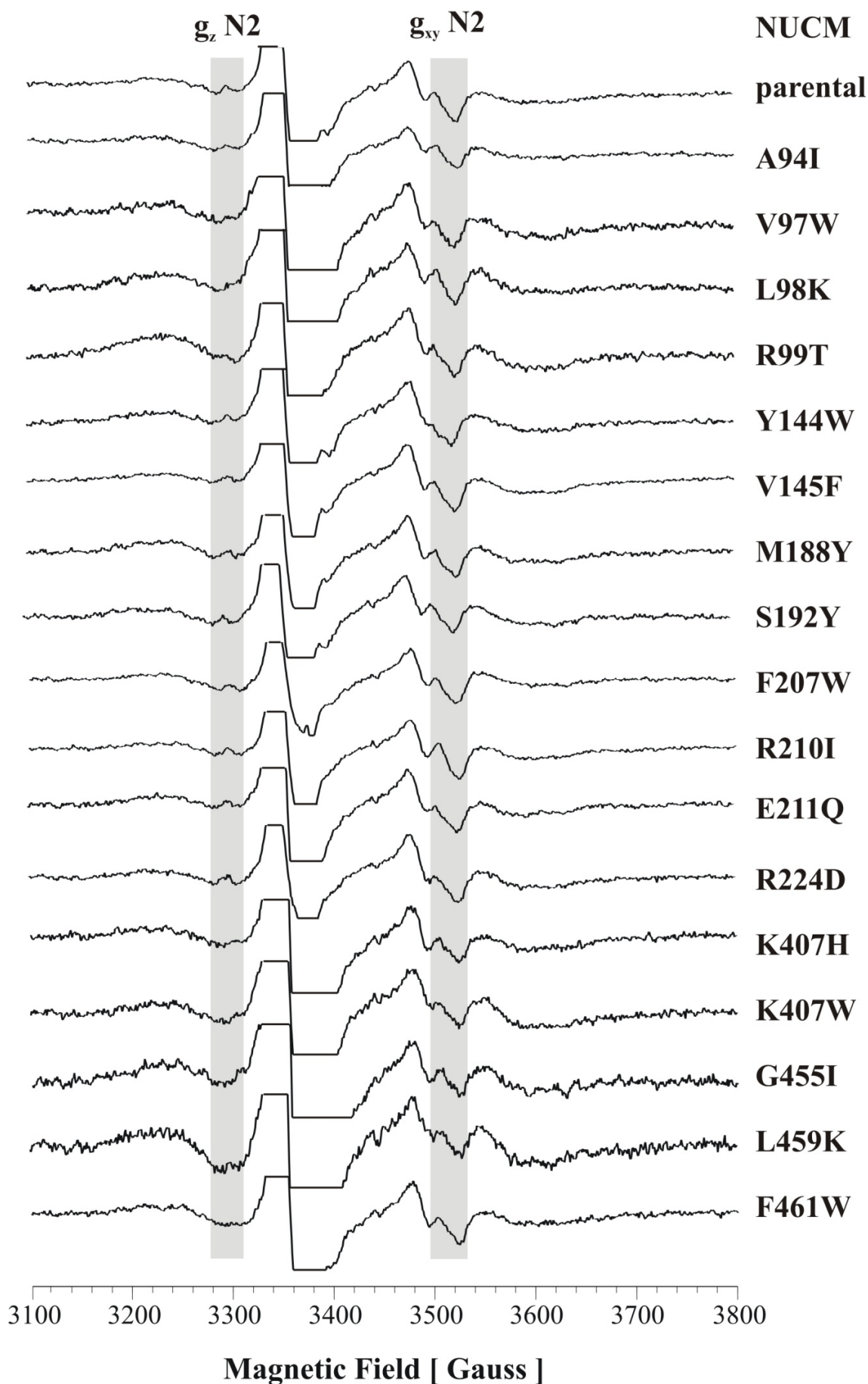


**Figure 3.1: EPR spectra of mitochondrial membranes of selected 49-kDa mutants at 12 K and 5 mW microwave power.** Field regions where mainly iron-sulfur cluster N2 gives signals are highlighted in gray. No significant differences in the spectrum of mutants compared to the parental strain could be identified. Mitochondrial membranes (10–25 mg protein per ml) were reduced with 2 mM NADH. Other EPR settings: microwave frequency 9.47 GHz, modulation amplitude 0.64 mT and modulation frequency 100 kHz. The spectra were recorded by Dr. Klaus Zwicker.

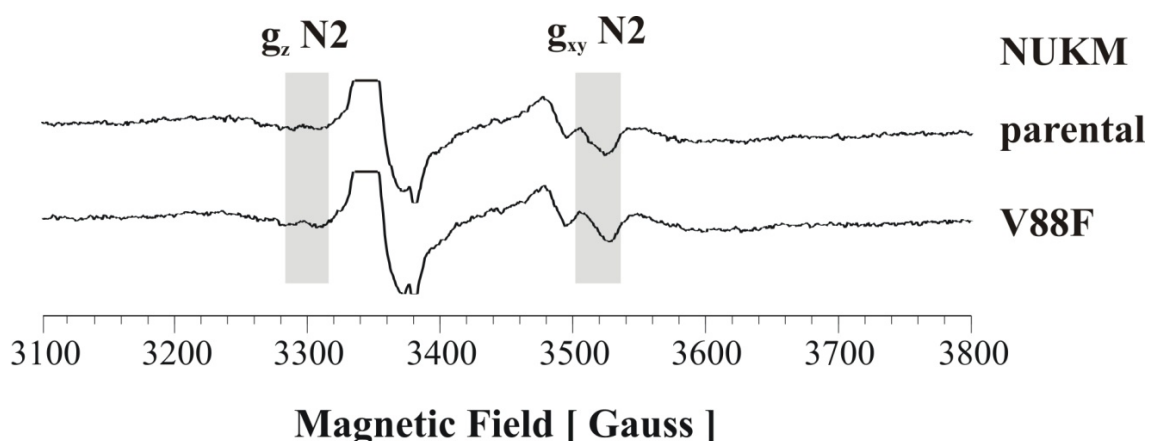


**Figure 3.2: EPR spectra of mitochondrial membranes of the PSST mutant V88F at 12 K and 5 mW microwave power.** Field regions where mainly signals from iron-sulfur cluster N2 arise are highlighted in gray. The spectrum of mutant V88F was not significantly different from the spectrum of the parental strain. Mitochondrial membranes (10–25 mg protein per ml) were reduced with 2 mM NADH. Further EPR settings: microwave frequency 9.47 GHz, modulation amplitude 0.64 mT and modulation frequency 100 kHz. The spectra were recorded by Dr. Klaus Zwicker.

For 58 mutants complex I assembly was also confirmed by blue-native PAGE from mitochondrial membranes followed by complex I in-gel activity assay. No sub-complexes of complex I were detectable, even when the incubation period for in-gel activity staining was prolonged from 5 min to 30 min (data not shown). In agreement with the results shown above, reduced complex I content in mitochondrial membranes from some mutants also gave rise to weaker complex I specific in-gel activity staining.

Taking together, the NADH:HAR oxidoreductase activities, the EPR spectra as well as the in-gel activity assays suggest that the targeted residues are not essential for proper folding and assembly of complex I.

### 3.1.2 Activity of mutant complex I

In sharp contrast to complex I assembly, many mutations severely impaired complex I activity (Table 3.1 and Table 3.2). As expected, more drastic mutations reduced complex I activity more strongly than conservative mutations. However, at some positions all introduced mutations resulted in very low activities. For example, in the case of tyrosine 144 in the 49-kDa subunit even the conservative exchange to phenylalanine, which just removes the hydroxyl group, almost completely abolished complex I activity. Similarly, all arginine 99 mutants in the 49-kDa subunit dramatically reduced complex I activity, even when this arginine was exchanged to lysine in mutant R99K. The same was true for valine 460 in the 49-kDa subunit and the conservative V460L exchange.

In contrast, at some positions none of the mutations reduced complex I activity. This was true for the highly conserved arginine 224 and leucine 225 in the 49-kDa subunit. The exchange of the large and positively charged arginine 224 to the smaller and negatively charged aspartic acid in mutant R224D as well as the exchange to the smaller and hydrophobic isoleucine in mutant R224I did not decrease complex I activity. Similarly, exchange of the hydrophobic leucine 225 to the positively charged histidine in mutant L225H did not affect complex I activity.

Since exchanges of different residues gave very different results, the effects of the introduced mutations on complex I activity must be seen in the context of their position in the quinone binding cavity according to the crystal structure from *T. thermophilus* (Sazanov and Hinchliffe, 2006) and the sequence alignment of the PSST and the 49-kDa subunits (see chapter 8.2.1 and 8.2.2). Therefore, based on the experimental results given in Tables 3.1 and 3.2, exchanged residues were grouped and color-coded according to their importance for complex I activity (Figure 3.3). When all mutations at a given position resulted in essentially normal complex I activity (>75 % of the parental strain), these positions were colored in blue. Positions where at least one exchange significantly reduced complex I activity (25-75 % of the parental strain) were colored in green. Positions where at least one exchange resulted in very low complex I activity (<25 % of the parental strain) were colored in yellow. When several mutations at a given position all resulted in very low complex I activity (<25 % of the parental strain),

these positions were colored in red. As shown in Figure 3.3, the effects of mutations strongly depended on the location of the targeted residue within the quinone binding cavity. Residues which were very critical for complex I activity (colored in red) cluster in an area in the 49-kDa subunit that begins at a loop of the N-terminal three stranded  $\beta$ -sheet, reaches down into the cavity and ends at tyrosine 144, next to iron-sulfur cluster N2. Mutations in the vicinity of this region had less pronounced effects on complex I activity (colored in yellow and green). Mutations of residues located at the distal end of the cavity where the cavity narrows to form a crevice had almost no effect on complex I activity (colored in blue), suggesting that this part of the quinone binding cavity is not critical for complex I activity.

Based on these results, the quinone binding cavity can be divided in regions critical, less critical and not critical for complex I activity.

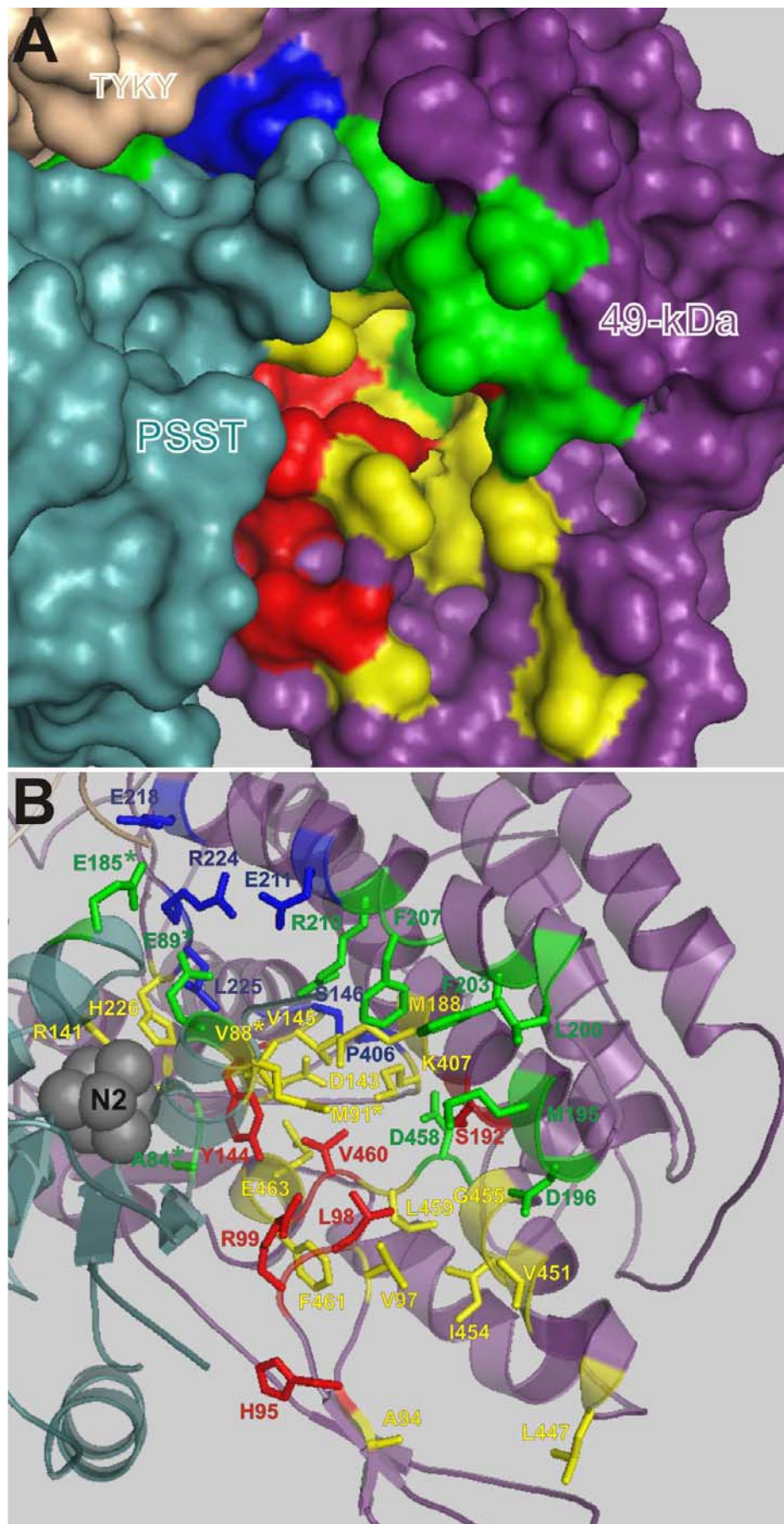


**Figure 3.3: Impact of mutations affecting the proposed ubiquinone and inhibitor binding cavity on complex I activity.** View into the quinone binding cavity assembled by the PSST and the 49-kDa subunit. A, surface representation. B, schematic representation, exchanged amino acid residues are shown in stick representation, iron-sulfur cluster N2 is shown in gray as space-filled model. Exchanged amino acid residues were colored according to their importance for complex I activity (DQA sensitive dNADH:DBQ oxidoreductase activity of mitochondrial membranes normalized to complex I content): Red, several exchanges of a given residue all resulted in very low complex I activity (<25 % of the parental strain for all exchanges). Yellow, at least one exchange of a given residue resulted in very low activity (<25 % of the parental strain for at least one exchange). Green, at least one exchange reduced complex I activity (25-75 % of the parental strain). Blue, all exchanges of a given residue had essentially no effect on complex I activity (>75 % of the parental strain for all exchanges). Amino acids are labeled according to *Y. lipolytica* numbering. Residues from the PSST subunit are marked with an asterisk. The figure was generated from coordinates from the crystal structure of the hydrophilic domain of complex I from *T. thermophilus* (PDB ID: 2FUG) by using the PyMOL program. The mutagenesis wizard from the PyMOL package was used to match the *Y. lipolytica* sequence when a residue was not conserved between *T. thermophilus* and *Y. lipolytica*.

### 3.1.3 Apparent $K_m$ for DBQ

Since point mutations within the quinone binding cavity might have changed the affinity of complex I to its substrate, *apparent*  $K_m$  values for DBQ were measured in mitochondrial membranes. However, reliable values can only be obtained from mutants with complex I activities well above 20 % of the parental strain. As shown in Table 3.1 and Table 3.2, none of the mutants with sufficient complex I activity had a markedly changed *apparent*  $K_m$  value.

### 3.1.4 Complex I activity with $Q_1$ and $Q_9$ as electron acceptors

In order to check whether the measured activity of mitochondrial membranes from mutant strains depended on the side chain of the ubiquinone used, also the activity with  $Q_1$  as electron acceptor was measured.

In addition, the activity with the endogenous ubiquinone, which is  $Q_9$  in the case of *Y. lipolytica*, was assayed. Because of the extreme hydrophobicity of  $Q_9$ , it could not be added at saturating concentrations to the assay. Therefore, omitting the addition of ubiquinone and KCN, dNADH-oxidase activity was measured to monitor electron transfer via the endogenous quinone  $Q_9$ . However, substrate saturation was most likely not achieved under these conditions resulting in overall lower rates.

As shown in Table 3.3 and Table 3.4, the relative changes in activity for most mutants measured with DBQ were also reproduced when Q<sub>1</sub> and Q<sub>9</sub> were used.

However, in mutants Y144F and F207W the activity with Q<sub>1</sub> was considerably higher, and in mutants R224I, L225A and K407H Q<sub>1</sub> activity was significantly lower than what was measured with DBQ (bold in Table 3.3). The dNADH:Q<sub>1</sub> oxidoreductase activity of mutant Y144F will be covered in more detail in chapter 3.3.

Interestingly, values measured with the endogenous Q<sub>9</sub> were very similar to those measured with DBQ, which might indicate that measurements with DBQ reflect the physiological relevant activity more closely than measurements with Q<sub>1</sub>.

**Table 3.3: Complex I activity with different ubiquinones in mitochondrial membranes from 49-kDa subunit mutants.**

Strain	Complex I activity with DBQ <sup>a</sup>	Complex I activity with Q <sub>1</sub> <sup>b</sup>	Complex I activity with Q <sub>9</sub> <sup>c</sup>
	%	%	%
parental	100±5	100±8	100±6
V97W	10±2	<5	<5
R99D	14±2	14±2	11±2
R99T	15±2	9±1	5±1
Y144F	7±2	<b>46±3</b>	11±1
Y144H	<5	<5	14±1
Y144I	15±1	<5	8±1
Y144W	8±4	5±3	8±4
V145F	7±3	<5	<5
V145T	92±8	107±8	120±12
M188Y	12±2	6±1	n.m.
S192Y	24±2	12±3	<5
F207W	58±2	<b>95±3</b>	68±4
R210I	63±2	82±3	n.m.
E211Q	83±6	61±5	n.m.
E218Q	97±4	94±3	117±6
R224D	107±4	83±3	102±5

Strain	Complex I activity with DBQ <sup>a</sup>	Complex I activity with Q <sub>1</sub> <sup>b</sup>	Complex I activity with Q <sub>9</sub> <sup>c</sup>
	%	%	%
parental	100±5	100±8	100±6
R224I	102±5	<b>70±4</b>	105±6
R224K	103±3	74±3	n.m.
R224N	99±7	83±7	156±12
L225A	103±6	<b>61±3</b>	n.m.
L225F	110±6	82±4	n.m.
L225H	107±5	78±6	109±4
L225V	91±3	106±3	94±4
K407H	78±2	<b>36±1</b>	n.m.
K407R	105±4	93±3	n.m.
K407W	12±2	36±1	11±1

Mean values ± SEM are given.

n.m., not measured

<sup>a</sup> values taken from Table 3.1: DQA sensitive complex I specific dNADH:DBQ oxidoreductase activity ( $0.58 \mu\text{mol}\cdot\text{min}^{-1}\cdot\text{mg}^{-1}$  was measured for the parental strain) was normalized to complex I content. The ratio of  $0.58/1.25$  for the parental strain was set as 100 % complex I activity.

<sup>b</sup> DQA sensitive complex I specific dNADH:Q<sub>1</sub> oxidoreductase activity ( $0.28 \mu\text{mol}\cdot\text{min}^{-1}\cdot\text{mg}^{-1}$  was measured for the parental strain) was normalized to complex I content. The ratio of  $0.28/1.25$  for the parental strain was set as 100 % complex I activity.

<sup>c</sup> DQA sensitive complex I specific dNADH oxidase activity ( $0.16 \mu\text{mol}\cdot\text{min}^{-1}\cdot\text{mg}^{-1}$  was measured for the parental strain) was normalized to complex I content. The ratio of  $0.16/1.25$  for the parental strain was set as 100 % complex I activity.



**Table 3.4: Complex I activity with different ubiquinones in mitochondrial membranes from PSST subunit mutants.**

Strain	Complex I activity with DBQ <sup>a</sup>	Complex I activity with Q <sub>1</sub> <sup>b</sup>
	%	%
parental	100±3	100±3
V88F	13±1	14±2
V88L	92±5	86±6
V88M	56±3	59±2

Mean values ± SEM are given.

n.m., not measured

<sup>a</sup> values taken from Table 3.2: DQA sensitive complex I specific dNADH:DBQ oxidoreductase activity ( $0.6 \mu\text{mol}\cdot\text{min}^{-1}\cdot\text{mg}^{-1}$  was measured for the parental strain) was normalized to complex I content. The ratio of 0.6/1.25 for the parental strain was set as 100 % complex I activity.

<sup>b</sup> DQA sensitive complex I specific dNADH:Q<sub>1</sub> oxidoreductase activity ( $0.24 \mu\text{mol}\cdot\text{min}^{-1}\cdot\text{mg}^{-1}$  was measured for the parental strain) was normalized to complex I content. The ratio of 0.24/1.25 for the parental strain was set as 100 % complex I activity.

### 3.1.5 $I_{50}$ values for DQA, rotenone and C<sub>12</sub>E<sub>8</sub>

Since many different complex I inhibitors act at or near the quinone binding site, some point mutations introduced in the broad quinone binding cavity may also influence inhibitor binding. Therefore,  $I_{50}$  values for DQA, rotenone and C<sub>12</sub>E<sub>8</sub>, each representing a class I/type A, class II/type B and type C inhibitor, respectively, were measured in mitochondrial membranes. Again, reliable values could only be obtained for mutants with complex I activities well above 20 % of the parental strain.

As shown in Table 3.5 and Table 3.6, most mutations had no effect on inhibitor sensitivity of complex I. Others like mutants K407R and E463Q in the 49-kDa subunit changed the  $I_{50}$  value for DQA only. Mutations R224I and L225F, both in the 49-kDa subunit, changed the  $I_{50}$  value for C<sub>12</sub>E<sub>8</sub> only. In contrast, mutant F207H in the 49-kDa

subunit and mutant M91C in the PSST subunit resulted in drastically changed  $I_{50}$  values for DQA and rotenone as well as for  $C_{12}E_8$ .  $I_{50}$  values which were significantly different from those of the parental strain are highlighted in bold in Table 3.5 and Table 3.6. Interestingly, most mutations which altered  $I_{50}$  values for DQA and rotenone caused resistance, whereas hypersensitivity was mostly found in mutations which altered the  $I_{50}$  value for  $C_{12}E_8$ .

**Table 3.5: Effects of 49-kDa subunit mutations on inhibitor sensitivity in mitochondrial membranes from *Y. lipolytica*.**

Strain	Complex I activity <sup>a</sup>	$I_{50}$		
		DQA	Rotenone	$C_{12}E_8$
	%		nM	
parental	100±5	16	530	3300 <sup>e</sup>
R141A <sup>c</sup>	17	21	570	n.d.
R141K <sup>b</sup>	45	<b>55</b>	<b>1500</b>	3400 <sup>e</sup>
D143A <sup>e</sup>	30±3	<b>180</b>	<b>10000</b>	2800
D143C <sup>c</sup>	30	30	580	2700 <sup>e</sup>
D143E <sup>c</sup>	23	<b>38</b>	630	3100 <sup>e</sup>
D143N <sup>e</sup>	42±5	<b>60</b>	<b>5000</b>	2500
V145M <sup>f</sup>	33	n.m.	n.m.	2400
V145T	92±8	17	550	3000 <sup>f</sup>
S146A <sup>d</sup>	110	10	300	2800 <sup>f</sup>
S146C <sup>d</sup>	100	<b>80</b>	<b>1500</b>	3400 <sup>e</sup>
S146V <sup>e</sup>	94±6	29	<b>1100</b>	3200
M188C	104±5	<b>28</b>	<b>2500</b>	3000 <sup>e</sup>
M188L	123±5	16	780	2900 <sup>e</sup>
M195F <sup>f</sup>	69	n.m.	n.m.	3200
D196E <sup>f</sup>	35	n.m.	n.m.	3000
D196N <sup>f</sup>	29	n.m.	n.m.	3200
L200K <sup>f</sup>	33	n.m.	n.m.	2600
F203E <sup>e</sup>	28±3	<b>70</b>	<b>2300</b>	2800
F203W <sup>e</sup>	98±6	14	450	<b>800</b>
F207H <sup>e</sup>	92±8	<b>45</b>	<b>3000</b>	<b>5000</b>
F207W	58±2	21	850	2600 <sup>e</sup>

Strain	Complex I activity <sup>a</sup>	<i>I</i> <sub>50</sub>		
		DQA	Rotenone	C <sub>12</sub> E <sub>8</sub>
	%	nM		
parental	100±5	16	530	3300 <sup>e</sup>
R210I	63±2	16	500	3300 <sup>e</sup>
E211Q	83±6	21	530	3200 <sup>e</sup>
E218Q	97±4	21	550	3000 <sup>e</sup>
R224D	107±4	12	550	2300 <sup>e</sup>
R224I	102±5	12	650	<b>2000</b> <sup>e</sup>
R224K	103±3	11	550	2500 <sup>e</sup>
R224N	99±7	15	700	2400 <sup>e</sup>
L225A	103±6	13	550	2500 <sup>e</sup>
L225F	110±6	11	460	<b>2000</b> <sup>e</sup>
L225H	107±5	14	700	2600 <sup>e</sup>
L225V	91±3	12	700	2300 <sup>e</sup>
H226A <sup>c</sup>	20	18	770	n.d.
H226C <sup>b</sup>	43	13	600	n.m.
H226M <sup>b</sup>	80	9	300	n.m.
H226Q <sup>b</sup>	56	13	600	n.m.
K407H	78±2	13	500	3400 <sup>e</sup>
K407R	105±4	<b>75</b>	550	3100 <sup>e</sup>
G455S <sup>g</sup>	72±4	22	700	3300 <sup>f</sup>
D458A <sup>c</sup>	28	<b>520</b>	<b>5200</b>	3300 <sup>e</sup>
D458E <sup>e</sup>	89±3	<b>30</b>	<b>2200</b>	3400
L459I <sup>g</sup>	92±10	13	620	3300 <sup>f</sup>
V460L <sup>g</sup>	21±2	<b>130</b>	<b>~9000</b>	n.d.
V460M	16±2	<b>53</b> <sup>c</sup>	760 <sup>c</sup>	n.d.
F461W <sup>g</sup>	23±3	30	800	n.d.
E463Q <sup>c</sup>	20	<b>34</b>	780	2300 <sup>e</sup>
E463T <sup>g</sup>	35±2	<b>8</b>	800	2800 <sup>e</sup>

Mean values ± SEM are given.

n.d., not determinable

n.m., not measured

<sup>a</sup> values taken from Table 3.1

<sup>b</sup> data from (Grgic et al., 2004)

<sup>c</sup> data from (Kashani-Poor et al., 2001b)

<sup>d</sup> data from (Grgic, Ph.D. Thesis, University Frankfurt, 2004)

<sup>e</sup> data from (Fendel et al., 2008)

<sup>f</sup> data from (Fendel, M.D. Thesis, University Frankfurt)

<sup>g</sup> point mutations were generated by U. Fendel

**Table 3.6: Effects of PSST subunit mutations on inhibitor sensitivity in mitochondrial membranes from *Y. lipolytica*.**

Strain	Complex I activity <sup>a</sup>	<i>I</i> <sub>50</sub>		
		DQA	Rotenone	C <sub>12</sub> E <sub>8</sub>
	%		nM	
parental	100±3	13	450	3000 <sup>d</sup>
A84G <sup>e</sup>	68	n.m.	n.m.	2900
V88L	92±5	25	500	<b>1800</b> <sup>d</sup>
V88M	56±3	<b>32</b>	330	<b>1500</b> <sup>d</sup>
E89A <sup>b</sup>	74	13	590	n.m.
E89C <sup>b</sup>	67	14	630	n.m.
E89Q <sup>b</sup>	88	11	620	n.m.
M91C <sup>d</sup>	31±4	<b>500</b>	<b>15000</b>	<b>1300</b>
E185Q <sup>c</sup>	35	20	500	2700 <sup>e</sup>

Mean values ± SEM are given.

n.d., not determinable

n.m., not measured

<sup>a</sup> values taken from Table 3.2

<sup>b</sup> data from (Ahlers et al., 2000), here NBQ was used instead of DBQ.

<sup>c</sup> data from (Garofano et al., 2003)

<sup>d</sup> data from (Fendel et al., 2008)

<sup>e</sup> data from (Fendel, M.D. Thesis, University Frankfurt)

Based on the crystal structure from *T. thermophilus* (Sazanov and Hinchliffe, 2006), the different effects of the point mutations can be discussed in the context of their location within the ubiquinone and inhibitor binding pocket for a more detailed structure/function analysis.

As evident from Figure 3.4, mutations with effects on inhibition by DQA and rotenone (highlighted in green) cluster in a subdomain of the cavity, mainly formed by the 49-kDa subunit, which corresponds to the former [NiFe] site of the homologous water soluble [NiFe] hydrogenases. Effects on DQA only (highlighted in blue) were found deeper in this pocket. In contrast, effects on C<sub>12</sub>E<sub>8</sub> only (highlighted in red) were found

in a different region, where the broad cavity narrows to form a crevice at the interface of the 49-kDa and the PSST subunit. Consistently, mutations which resulted in changed  $I_{50}$  values for all three inhibitors (highlighted in yellow) clustered at quite exposed residues between the subdomain where effects on DQA and rotenone were found and the crevice where effects on C<sub>12</sub>E<sub>8</sub> only were found.

These results confirm the view that different complex I inhibitors bind to different partially overlapping binding sites within the quinone binding pocket (Okun et al., 1999a). In addition, based on these results the binding sites of different inhibitors can be assigned to distinct domains within the broad quinone binding cavity.

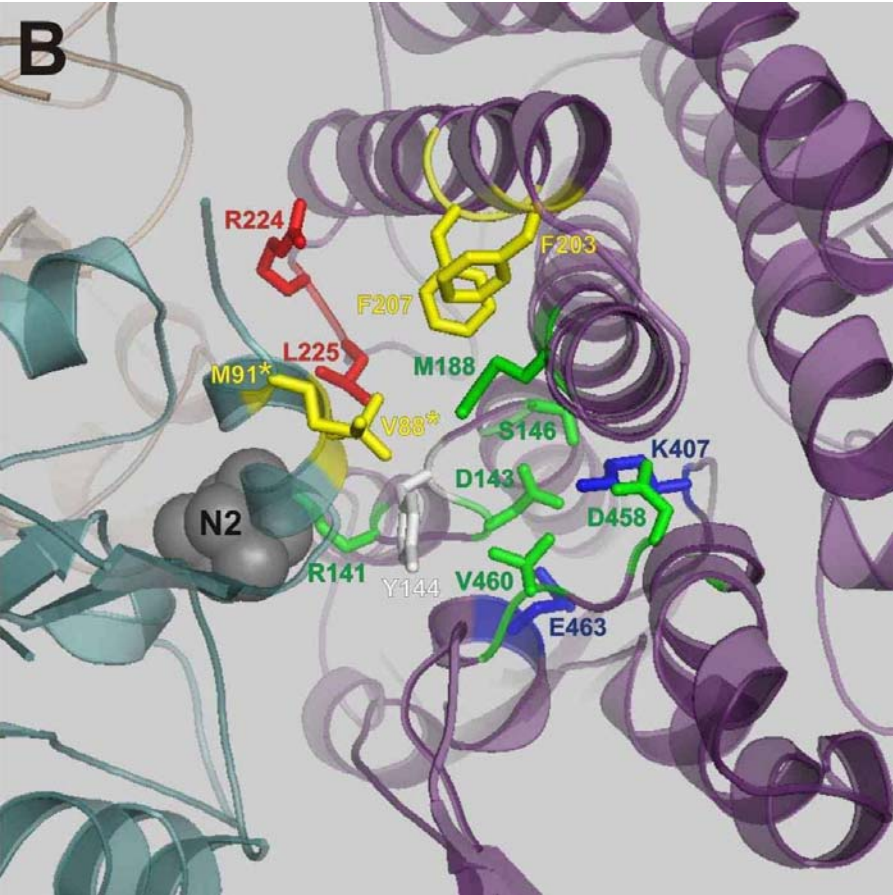
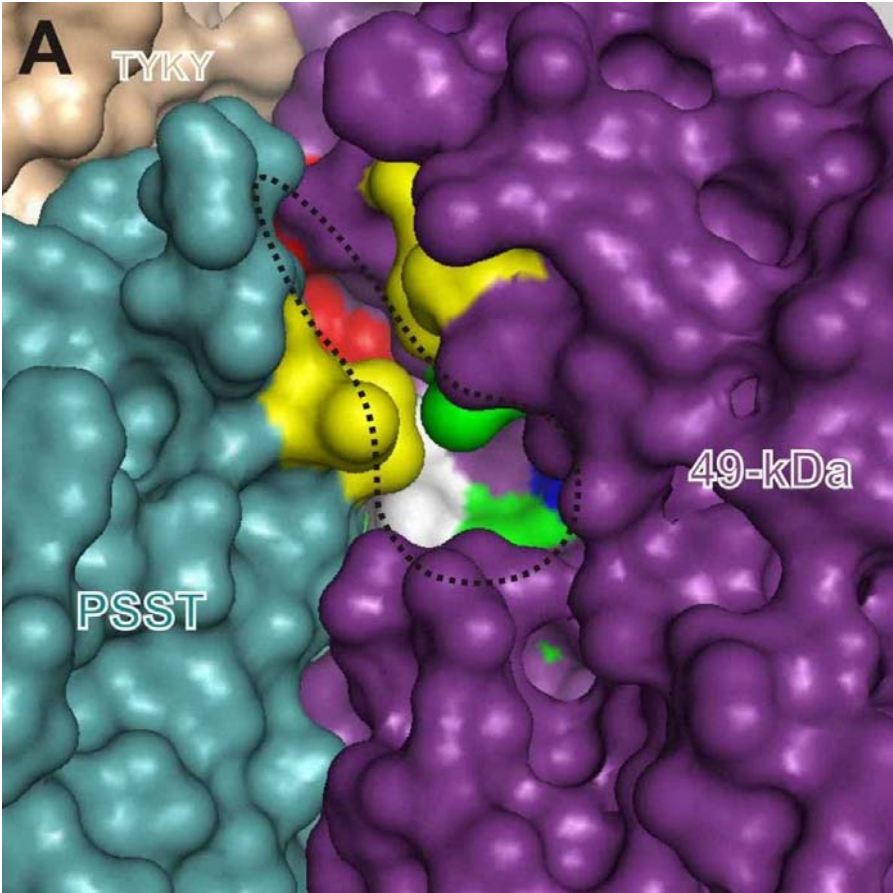


**Figure 3.4: Impact of mutations affecting the proposed ubiquinone and inhibitor binding cavity on inhibitor binding.** Similar view as in Figure 3.3. A, surface representation, the location of the former [NiFe] site in homologous [NiFe] hydrogenases and the crevice at the interface of the 49-kDa and the PSST subunit are outlined. B, schematic representation, amino acid residues which display effects on inhibitor binding when altered are shown in stick representation; for better orientation tyrosine 144 is shown in white sticks, iron-sulfur cluster N2 is shown in gray as space-filled model. Positions of mutations which changed the  $I_{50}$  value for  $C_{12}E_8$  only are highlighted in red. Positions of mutations which changed the  $I_{50}$  value for DQA only are highlighted in blue. Positions where effects on DQA and rotenone were found are colored in green. Positions where effects on DQA, rotenone and  $C_{12}E_8$  were found are colored in yellow. Amino acids are labeled according to *Y. lipolytica* numbering. Residues from the PSST subunit are marked with an asterisk. The figure was generated from the crystal structure of the hydrophilic domain of complex I from *T. thermophilus* (PDB ID: 2FUG) by using the PyMOL program. The mutagenesis wizard from the PyMOL package was used to match the *Y. lipolytica* sequence when a residue was not conserved between *T. thermophilus* and *Y. lipolytica*

### 3.1.6 EIPA

The amiloride derivative EIPA also inhibits complex I activity (Nakamaru-Ogiso et al., 2003a; Nakamaru-Ogiso et al., 2003b; Stolpe and Friedrich, 2004). It had been proposed that EIPA acts on the ND5 subunit of complex I (Nakamaru-Ogiso et al., 2003a), since it has decreased the photoaffinity labeling of presumably the ND5 subunit, which shares some sequence similarity with  $Na^+/H^+$  antiporters (Hamamoto et al., 1994; Hiramatsu et al., 1998; Mathiesen and Hägerhäll, 2002) which in turn are inhibited by amiloride (Mochizuki and Oosawa, 1985; Kleyman and Cragoe, 1988; Counillon et al., 1993; Kuroda et al., 1994; Masereel et al., 2003).

Complex I from the *Y. lipolytica* strain *nb8mΔ* lacks the ND5 subunit (Stefanie Krack, personal communication); however, the activity of this subcomplex of complex I is still inhibited by EIPA (Stefan Dröse, personal communication).

Indeed, in mitochondrial membranes from the *nb8mΔ* strain an  $I_{50}$  value of 23  $\mu$ M was determined for EIPA (Table 3.7). Strikingly, very similar  $I_{50}$  values were determined for EIPA in mitochondrial membranes from the 49-kDa subunit and the PSST subunit parental strains (Table 3.8 and Table 3.9). These results indicate that the ND4 and the ND5 subunit are not necessary for complex I inhibition by EIPA.

**Table 3.7: Characteristics of mitochondrial membranes from the *nb8mΔ* strain.**

Strain	Complex I activity <sup>a</sup>	<i>I</i> <sub>50</sub>
		EIPA
	%	μM
<i>nb8mΔ</i> <sup>b</sup>	30	23

<sup>a</sup> DQA sensitive dNADH:DBQ oxidoreductase activity normalized to complex I content determined as NADH:HAR oxidoreductase activity (determined by Stefan Kerscher).

<sup>b</sup> The strain *nb8mΔ* was generated by Stefanie Krack.

In order to identify the binding site of EIPA, *I*<sub>50</sub> values for EIPA in mitochondrial membranes from 15 point mutations within the quinone and inhibitor binding site that had been found to have effects on the binding of other inhibitors were determined.

As shown in Table 3.8 and Table 3.9, in most mutants the *I*<sub>50</sub> values for EIPA were unchanged, and only slight changes were observed in mitochondrial membranes from four mutants (highlighted in orange). However, considerably changed *I*<sub>50</sub> values were found in mutants M188C, F207H and F207W (highlighted in red). Similarly to what was observed for C<sub>12</sub>E<sub>8</sub>, usually hypersensitivity was found in mutants changing the *I*<sub>50</sub> value for EIPA. For comparison, significantly changed *I*<sub>50</sub> values for DQA, rotenone and C<sub>12</sub>E<sub>8</sub> are highlighted in bold in Table 3.8.

**Table 3.8: Effects of point mutations in the 49-kDa subunit on EIPA inhibition in mitochondrial membranes from *Y. lipolytica*.**

Strain	Complex I activity <sup>a</sup>	<i>I</i> <sub>50</sub>			
		EIPA	DQA	Rotenone	C <sub>12</sub> E <sub>8</sub>
	%	μM		nM	
parental	100±5	21	16	530	3300 <sup>b</sup>
D143C	30 <sup>c</sup>	19	30 <sup>c</sup>	580 <sup>c</sup>	2700 <sup>b</sup>
M188C	104±5	<b>14</b>	<b>28</b>	<b>2500</b>	3000 <sup>b</sup>
M188L	123±5	<b>17</b>	16	780	2900 <sup>b</sup>
F203W	98±6 <sup>b</sup>	18	14 <sup>b</sup>	450 <sup>b</sup>	<b>800<sup>b</sup></b>



Strain	Complex I activity <sup>a</sup>	<i>I</i> <sub>50</sub>			
		EIPA	DQA	Rotenone	C <sub>12</sub> E <sub>8</sub>
		%	μM	nM	
parental	100±5	21	16	530	3300 <sup>b</sup>
F207H	92±8 <sup>b</sup>	<b>13</b>	<b>45</b>	<b>3000<sup>b</sup></b>	<b>5000<sup>b</sup></b>
F207W	58±2	<b>9</b>	21	850	2600 <sup>b</sup>
R224D	107±4	24	12	550	2300 <sup>b</sup>
R224I	102±5	20	12	650	<b>2000<sup>b</sup></b>
R224N	99±7	23	15	700	2400 <sup>b</sup>
L225F	110±6	<b>26</b>	11	460	<b>2000<sup>b</sup></b>
L225H	107±5	20	14	700	2600 <sup>b</sup>
K407R	105±4	19	<b>75</b>	550	3100 <sup>b</sup>
D458A	28 <sup>c</sup>	22	<b>520<sup>c</sup></b>	<b>5200<sup>c</sup></b>	3300 <sup>b</sup>

Mean values ± SEM are given.

<sup>a</sup> values taken from Table 3.1

<sup>b</sup> data from (Fendel et al., 2008)

<sup>c</sup> data from (Kashani-Poor et al., 2001b)

**Table 3.9: Effects of point mutations in the PSST subunit on EIPA inhibition in mitochondrial membranes from *Y. lipolytica*.**

Strain	Complex I activity <sup>a</sup>	<i>I</i> <sub>50</sub>			
		EIPA	DQA	Rotenone	C <sub>12</sub> E <sub>8</sub>
		%	μM	nM	
parental	100±3	23	13	450	3000 <sup>b</sup>
V88L	92±5	<b>18</b>	25	500	<b>1800<sup>b</sup></b>
V88M	56±3	<b>18</b>	<b>32</b>	330	<b>1500<sup>b</sup></b>

Mean values ± SEM are given.

<sup>a</sup> values taken from Table 3.2

<sup>b</sup> data from (Fendel et al., 2008)

Figure 3.5 highlights the location of mutations within the structure of the quinone and inhibitor binding cavity that changed the *I*<sub>50</sub> value for EIPA considerably (colored in red) as well as mutations which only slightly affected the *I*<sub>50</sub> value (colored in orange). Amino acid side chains where mutations had no effect on the *I*<sub>50</sub> value for EIPA are shown in stick representations. Effects on EIPA binding did neither cluster in the

subdomain of the cavity corresponding to the former [NiFe] site where changes in the  $I_{50}$  values for DQA and rotenone were found, nor in the narrow crevice where changes in the  $I_{50}$  values for C<sub>12</sub>E<sub>8</sub> are found (compare Figure 3.5 to Figure 3.4). Rather, changes in the  $I_{50}$  values for EIPA marked several exposed residues in a region where mutations resulted in altered  $I_{50}$  values for DQA, rotenone and C<sub>12</sub>E<sub>8</sub>.

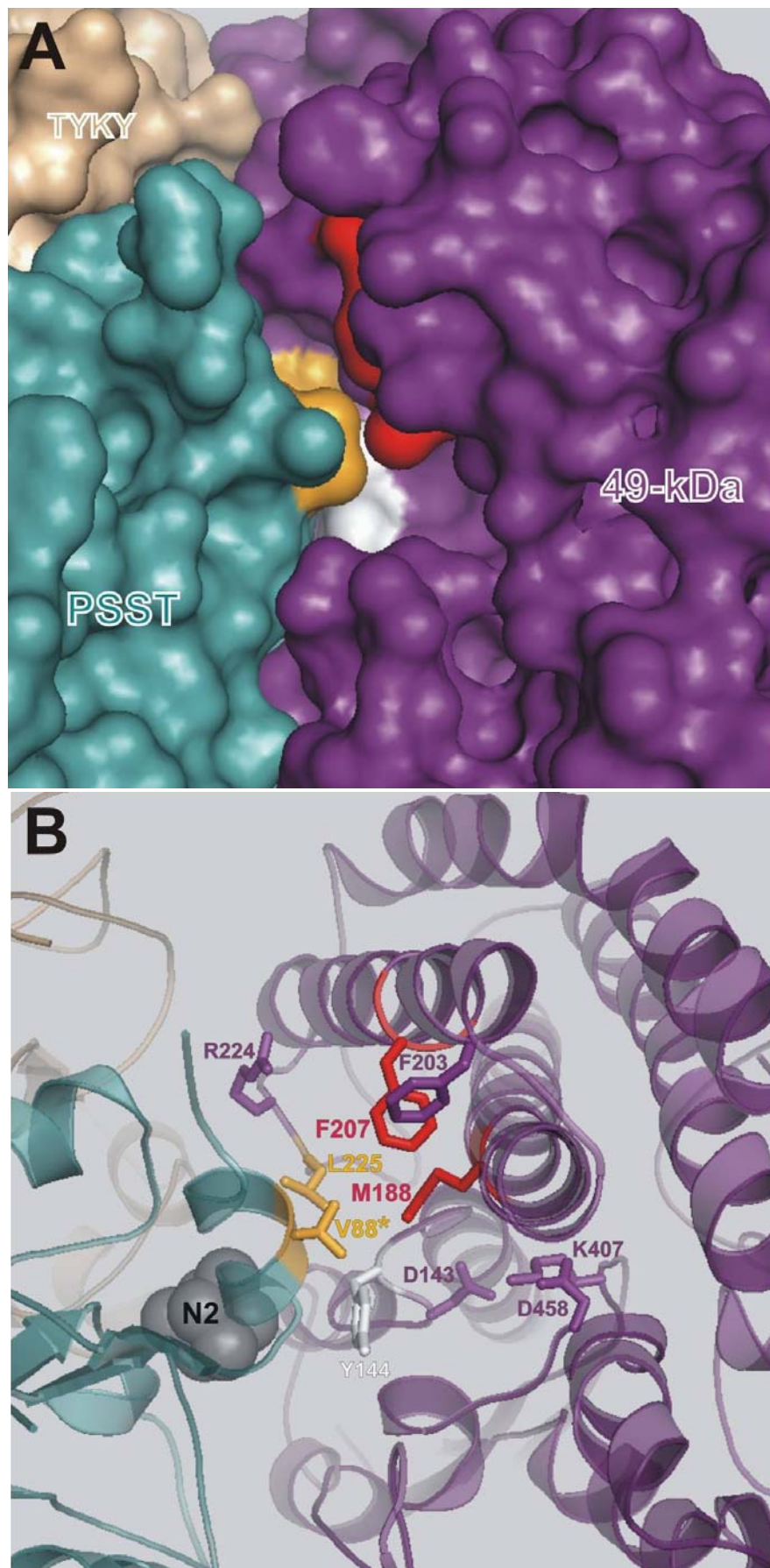


**Figure 3.5: Effects of mutants of the quinone and inhibitor binding site on the  $I_{50}$  value for EIPA.** Same view as in Figure 3.4. A, surface representation. B, schematic representation, positions of exchanges which were tested for effects on the  $I_{50}$  value for EIPA are shown in stick representation, for better orientation tyrosine 144 is shown in white sticks, iron-sulfur cluster N2 is shown in gray as space-filled model. Positions of exchanges which considerably changed the  $I_{50}$  value for EIPA are highlighted in red. Positions of exchanges which slightly changed the  $I_{50}$  value for EIPA are highlighted in orange. Amino acids are labeled according to *Y. lipolytica* numbering. Residues from the PSST subunit are marked with an asterisk. The figure was generated from the crystal structure of the hydrophilic domain of complex I from *T. thermophilus* (PDB ID: 2FUG) by using the PyMOL program. The mutagenesis wizard from the PyMOL package was used to match the *Y. lipolytica* sequence when a residue was not conserved between *T. thermophilus* and *Y. lipolytica*.

Contrary to what was proposed before (Nakamaru-Ogiso et al., 2003a), these results indicate that EIPA does not act on the ND5 subunit, but rather on the quinone binding cavity assembled by the 49-kDa and the PSST subunits.

## 3.2 *In vivo* screen for complex I deficiency

### 3.2.1 The principle

The *Y. lipolytica* strains used for mutagenesis of complex I have a matrix directed (internal) copy of the alternative NADH dehydrogenase (NDH2i) (de Vries and Marres, 1987; Kerscher et al., 2002). This membrane associated enzyme transfers electrons from NADH of the mitochondrial matrix to ubiquinone (Kerscher, 2000; Joseph-Horne et al., 2001) and therefore can compensate for the redox reaction of complex I, so that complex I deficiency is not longer lethal to this strictly aerobic yeast (Kerscher et al., 2001b). However, in contrast to complex I this protein cannot couple the redox reaction to vectorial proton translocation across the inner mitochondrial membrane. Interestingly, *Y. lipolytica* strains which lack functional complex I but have an internal copy of the NDH2 do not show any phenotypic growth deficiency (see also upper panel in Figure 3.7).

In order to screen for complex I deficiency *in vivo*, a new approach was tested. When *Y. lipolytica* is grown in the presence of a complex III and/or a complex IV inhibitor, both complexes can be bypassed due to the alternative oxidase, which transfers electrons from ubiquinol to oxygen (Henry and Nyns, 1975; de Troostembergh and Nyns, 1978;

Vanlerberghe and McIntosh, 1997; Medentsev and Akimenko, 1999; Joseph-Horne et al., 2001). Since the alternative oxidase is not capable of proton pumping, under these conditions complex I is the only enzyme of the respiratory chain which pumps protons across the inner mitochondrial membrane Figure 3.6. Hence, oxidative phosphorylation will depend on functional complex I.

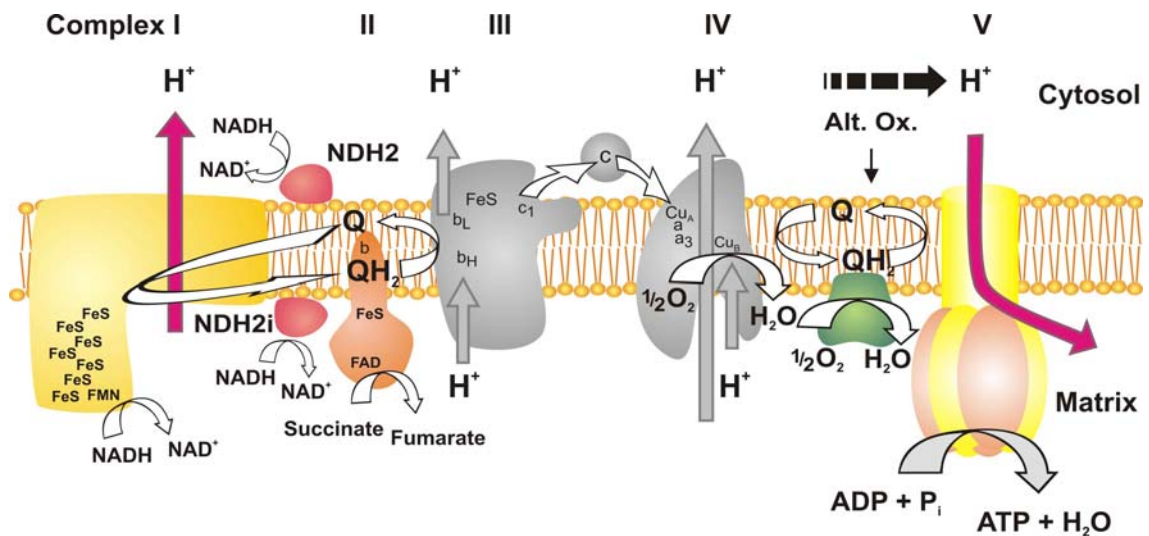


**Figure 3.6: The respiratory chain of *Y. lipolytica* strains used for mutagenesis.** In the presence of a complex III and/or a complex IV inhibitor, complex I is the only enzyme of the respiratory chain capable of proton pumping. White arrows indicate electron transfer, whereas red arrows indicate proton translocation. Complex II (succinate:ubiquinone oxidoreductase); complex III (cytochrome c reductase); complex IV (cytochrome c oxidase); complex V (ATP-synthase); NDH2 (alternative NADH dehydrogenase); NDH2i (internal alternative NADH dehydrogenase); alternative ubiquinol oxidase (Alt. Ox.); FeS (iron-sulfur cluster); FMN (flavin mononucleotide); FAD (flavin adenine dinucleotide, oxidized form); NAD<sup>+</sup> (nicotinamide adenine dinucleotide, oxidized form); NADH (nicotinamide adenine dinucleotide, reduced form); Q (ubiquinone); QH<sub>2</sub> (ubiquinol); b (heme b); b<sub>H</sub> (high potential heme b); b<sub>L</sub> (low potential heme b); a (heme a); a<sub>3</sub> (heme a<sub>3</sub>); c (cytochrome c); c<sub>1</sub> (cytochrome c<sub>1</sub>); Cu<sub>A</sub> (copper center A); Cu<sub>B</sub> (copper center B).

### 3.2.2 Development of a plate assay for complex I activity

For complex III and complex IV inhibition, antimycin A and sodium azide were tested. These inhibitors were added to YPD-agar plates (see chapter 2.2.1.7) at various concentrations (0.2-10  $\mu$ M antimycin A and 0.1-10 mM sodium azide). In order to find optimal concentrations, *Y. lipolytica* mutant Y144F and the parental strain were used as tester strains for no and full activity, respectively. Best results were achieved at

concentrations of 0.3  $\mu\text{M}$  for antimycin A and 0.5 mM for sodium azide. As shown in Figure 3.7, mutant Y144F showed weaker growth compared to the parental strain only on inhibitor containing plates.

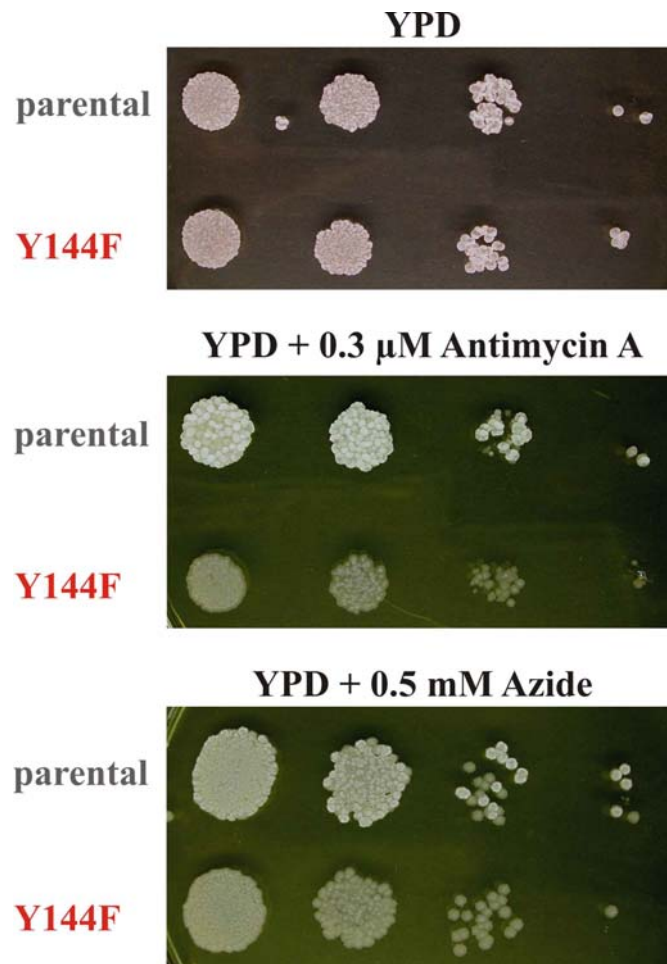


**Figure 3.7: On antimycin A and azide containing plates mutant Y144F displays diminished growth.** For both strains  $\sim 3000$ ,  $\sim 300$ ,  $\sim 30$  and  $\sim 3$  cells per droplet were placed on plates.

Antimycin A always gave better results than sodium azide. The combination of both inhibitors at various concentrations in one plate did not significantly improve the difference in growth any further (data not shown). Therefore, it seems sufficient to solely use 0.3  $\mu\text{M}$  antimycin A.

For best results, it was important that YPD liquid cultures of *Y. lipolytica* are grown in the absence of hygromycin B to similar densities until they reach late exponential phase (2-6 OD<sub>600 nm</sub>) before aliquots of the cultures were applied to plates.

### 3.2.3 Screening of complex I mutants

As shown earlier, within the quinone binding pocket there is a region where mutations had no effect on the dNADH:DBQ oxidoreductase activity of complex I (see chapter 3.1.2). This includes some charged and highly conserved residues like glutamate 218 and arginine 224. Since these residues are not critical for the redox reaction, it seemed reasonable to speculate that they might have a function in coupling the redox reaction to vectorial proton translocation. Therefore, these mutants were assayed for complex I dependent proton pumping on antimycin A containing plates. As shown in Figure 3.8, none of the mutants displayed any growth deficiency compared to the parental strain, suggesting that the affected residues are not critical for proton pumping in complex I.

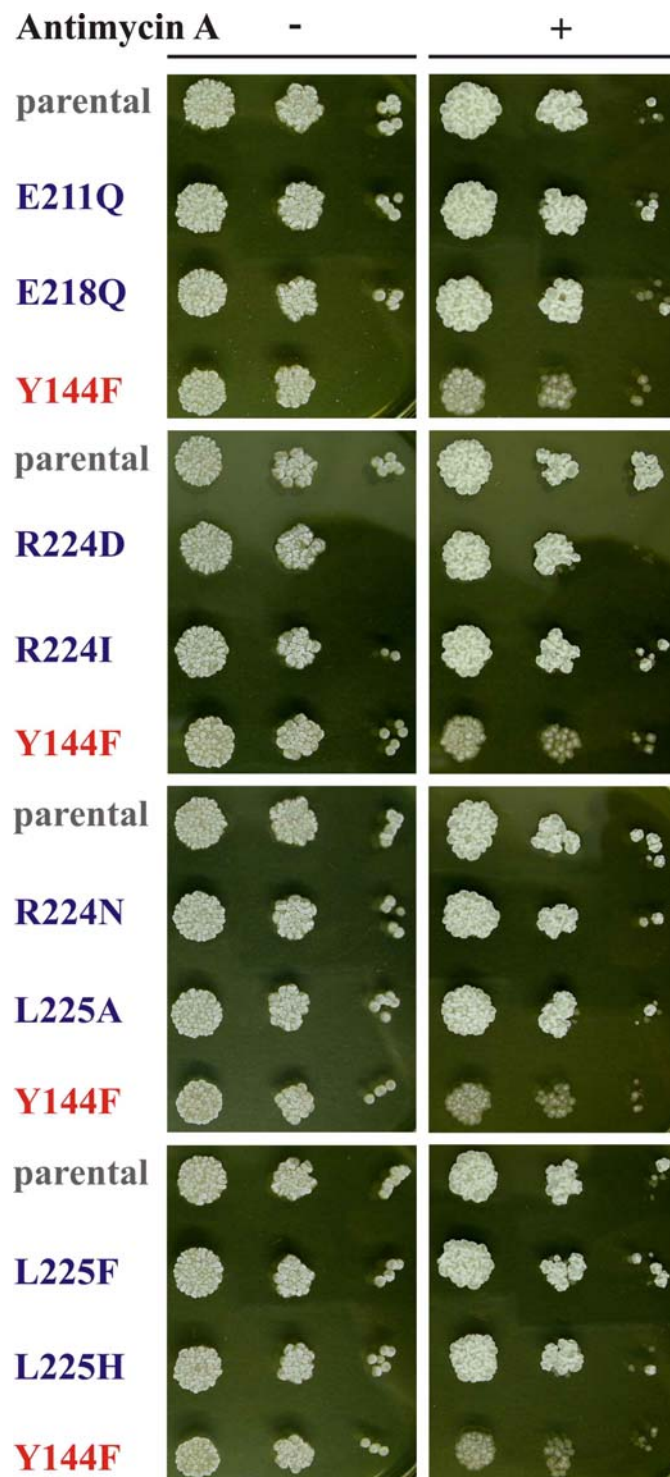


**Figure 3.8: Probing of fully redox active mutants for proton pumping defects.** Even though glutamate 218 and arginine 224 are highly conserved, none of the mutations tested here had an effect on proton pumping. The parental strain was used as positive, mutant Y144F as a negative control. For each strain ~300, ~30 and ~3 cells per droplet were placed on plates. Antimycin A was added at 0.3  $\mu$ M.



Unfortunately, the difference in growth between the parental strain and mutant Y144F, which was used as negative control, was even less pronounced when compared to the growth difference shown in Figure 3.7. This was most likely due to the fact that the liquid cultures of *Y. lipolytica* did not reach late exponential phase in this experiment (0.6-1.5 OD<sub>600nm</sub>). However, from these results it still seems clear that the tested residues are not essential for proton pumping or the coupling of the redox reaction to proton pumping.

### 3.3 Tyrosine 144

The tyrosine on position 144 in the *Y. lipolytica* sequence of the 49-kDa subunit is highly conserved from bacteria to mammals (see Figure 3.9).

<i>Y. lipolytica</i>	GTEKLI EYKTYMQALPYFDRLD <b>Y</b> VSMMTNEQVFSLAVEKL	161
<i>N. crassa</i>	GTEKLCEYRTYLQALPYFDRLD <b>Y</b> VSMMTNEQCFALAVEKL	173
<i>B. taurus</i>	GTEKLI EYKTYLQALPYFDRLD <b>Y</b> VSMMCNEQAYSLAVEKL	125
<i>H. sapiens</i>	GTEKLI EYKTYLQALPYFDRLD <b>Y</b> VSMMCNEQAYSLAVEKL	158
<i>P. denitrificans</i>	GTEKLMESRTYLQNLPLYLDRLD <b>Y</b> VAPMNQEHAWCLAIERL	105
<i>T. thermophilus</i>	GFEKTMEHRTYLQNIITYTPRMD <b>Y</b> LHSFAHDLAYALAVEKL	104
<i>E. coli</i>	GAEKMGERSWHSYIPYTDRIE <b>Y</b> LGGCVNEMPHYVLAVEKL	101
	* ** * ::: . :.* *::*: : : **:*:*	

**Figure 3.9: Sequence alignment of the 49-kDa subunit harboring the highly conserved tyrosine 144.** Tyrosine 144 of *Y. lipolytica* is highlighted in red and bold. Tyrosines from other organisms are highlighted in bold. Sequences were aligned by the multiple sequence alignment program ClustalW. Invariant (\*), highly (: ) and weakly similar ( . ) positions are labeled.

Moreover, according to the X-ray structure of the hydrophilic part of complex I from *T. thermophilus*, this tyrosine is located only 6-8 Å away from iron-sulfur cluster N2 in the proposed quinone binding pocket.

In order to gain insight into the function of tyrosine 144, this tyrosine was exchanged to phenylalanine and tryptophan retaining the aromatic character, to the hydrophobic isoleucine and to the hydrophilic residues serine, histidine and arginine. Mutant Y144H had been generated and described before (Kashani-Poor et al., 2001b); however, to avoid effects from a different genetic background when mitochondrial membranes were analyzed, this mutant was reproduced.

### 3.3.1 Assembly and activity of tyrosine 144 mutants

Mitochondrial membranes from the tyrosine mutants were isolated and complex I content and activity were measured. As listed in Table 3.10, in all mutant strains complex I assembly was possible. However, in mutants Y144I and Y144R, complex I content was reduced to ~60 %, in contrast to mutant Y144W which resulted in a slight increase in complex I content to ~130 %. Apparently, spacious hydrophobic or hydrophilic residues were less well tolerated than aromatic residues at this position.

Measurement of complex I activity revealed that all mutations resulted in an almost completely inactive complex I (Table 3.10). This was also true for mutant Y144F, whereby only a hydroxyl group was removed. Thus, the specific features of tyrosine 144 were found to be essential for complex I activity.

**Table 3.10: Effects of point mutations of Y144 in the 49-kDa subunit on complex I content, activity and N2 EPR signal in mitochondrial membranes from *Y. lipolytica*.**

Strain	Complex I content <sup>a</sup>	Complex I activity <sup>b</sup>	N2 EPR signal (see EPR spectra below)
	%	%	
parental	100±3	100±5	reference
Y144F	110±2	7±2	not altered
Y144W	129±2	8±4	N2 signal slightly shifted
Y144H <sup>c</sup>	70	<5	N2 signal slightly shifted
Y144H	86±2	<5	N2 signal slightly shifted
Y144S <sup>d</sup>	94±4	<5	reduced N2 signals
Y144I	59±1	15±1	no N2 signals
Y144R <sup>d</sup>	58±1	9±1	no N2 signals

Mean values ± SEM are given.

<sup>a</sup> 100 % of complex I content correspond to 1.25  $\mu\text{mol}\cdot\text{min}^{-1}\cdot\text{mg}^{-1}$  NADH:HAR oxidoreductase activity determined for the parental strain.

<sup>b</sup> DQA sensitive complex I specific dNADH:DBQ oxidoreductase activity ( $0.58 \mu\text{mol}\cdot\text{min}^{-1}\cdot\text{mg}^{-1}$  was measured for the parental strain) was normalized to complex I content. The ratio of 0.58/1.25 for the parental strain was set as 100 % complex I activity.

<sup>c</sup> data from (Kashani-Poor et al., 2001b)

<sup>d</sup> mutations generated by U. Fendel

### 3.3.2 Iron-sulfur cluster N2 in tyrosine 144 mutants

Since tyrosine 144 is only 6-8 Å away from iron-sulfur cluster N2 (see Figure 3.3), mutations of this tyrosine could have abolished complex I activity by interfering with iron-sulfur cluster N2. To test this hypothesis, EPR spectra of mitochondrial membranes from mutant strains were recorded. As shown in Figure 3.10, mutants Y144F, Y144W and Y144H showed no major changes in N2 EPR signals when compared to the parental strain. Mutant Y144S displayed clear changes in a region where mainly the  $g_z$  and the  $g_{xy}$  signals of iron-sulfur cluster N2 contribute to the spectrum. For mutants Y144I and Y144R no N2 signals were visible.

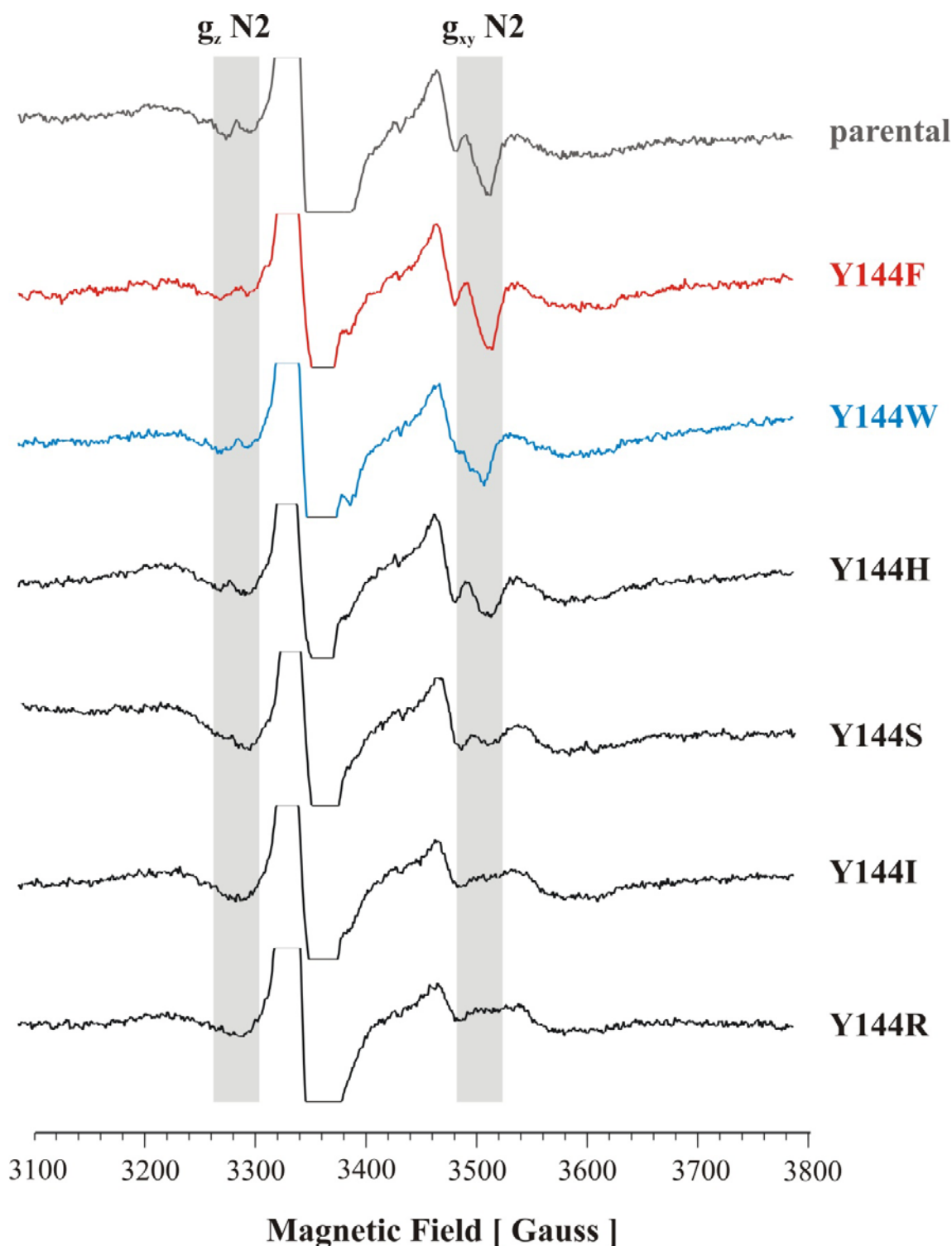


**Figure 3.10: EPR spectra of mitochondrial membranes of tyrosine 144 mutants at 12 K and 5 mW microwave power.** Field regions where mainly iron-sulfur cluster N2 gives signals are highlighted in gray. Y144F, Y144W and Y144H show essentially no difference when compared to the parental strain. In Y144S there were significant changes in N2 signals, whereas in Y144I and Y144R there were almost no signals arising from iron-sulfur cluster N2. The prominent signal at 3340 G in all spectra is due to oxidized iron-sulfur cluster S3 of complex III. Mitochondrial membranes (25 mg protein per ml) were reduced with 2 mM NADH. The EPR spectra were recorded by Dr. Klaus Zwicker.

Since small changes in the EPR signals of iron-sulfur cluster N2 cannot be detected in mitochondrial membranes, complex I from mutants Y144F and Y144W was purified for more detailed EPR analysis. Mutant Y144H had been analysed and described before (Kashani-Poor et al., 2001b). Figure 3.11 shows EPR spectra of Y144F and Y144W at 12 K. Small changes in intensity were evident in the  $g_{xy}$ -region where iron-sulfur clusters N1, N2, N3 and N4 make contributions. Changes in intensity ratios were mainly due to changes in N1 signal intensity, which was also obvious when the  $g_z$  signals from cluster N1 and N2 were compared. Variations in the intensities of iron-sulfur cluster N1 are often observed for different complex I samples even from the same *Y. lipolytica* strain (Klaus Zwicker, personal communication) and might correlate with lipid content in different complex I preparations. Therefore, the observed differences in mutant Y144F most likely reflected subtle differences during complex I preparation and were not caused by the mutation.

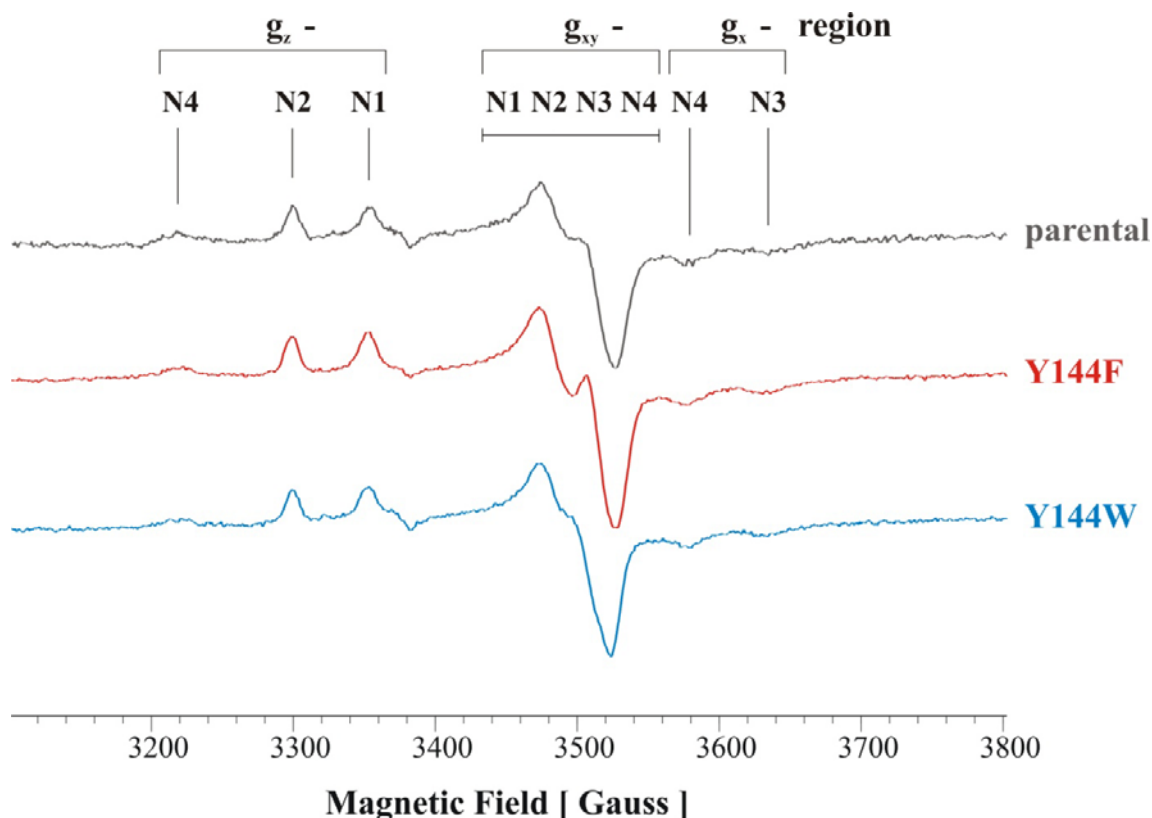


**Figure 3.11: EPR spectra of purified complex I from tyrosine mutants Y144F and Y144W at 12 K and 1 mW microwave power.** Main contributions from individual iron-sulfur clusters are indicated. Small differences in the  $g_{xy}$  region where iron-sulfur clusters N1, N2, N3 and N4 give signals are visible. Samples were reduced with 5 mM NADH. Here, purified complex I

from the PIPO strain was used as a reference. To compensate for slightly different protein concentration, spectra were normalized to equal N3 and N4 signal intensities. The EPR spectra were recorded by Dr. Klaus Zwicker.

It was not possible to directly record EPR spectra from iron-sulfur cluster N2 alone, in order to check whether the cluster was unchanged in mutants Y144F and Y144W. However, by subtracting 40 K EPR spectra (which contain only signals from iron-sulfur cluster N1) from 25 K EPR spectra (which contain signals from iron-sulfur cluster N1 and N2), spectra from iron-sulfur cluster N2 were obtained. Figure 3.12 shows such difference spectra for mutants Y144F and the Y144W. Vertical lines indicate minima and maxima from the  $g_z$  and the  $g_{yx}$  signals of iron-sulfur cluster N2. Since the difference spectrum from the parental strain was too noisy to unambiguously indicate minima and maxima, a highly concentrated complex I standard was used for this purpose. From Figure 3.12 it is obvious that the  $g_{yx}$  signal of iron-sulfur cluster N2 was shifted towards lower field in mutant Y144W. More importantly, mutant Y144F did not change the N2 signal, indicating that iron-sulfur cluster N2 was not affected by removing the hydroxyl group of tyrosine 144.

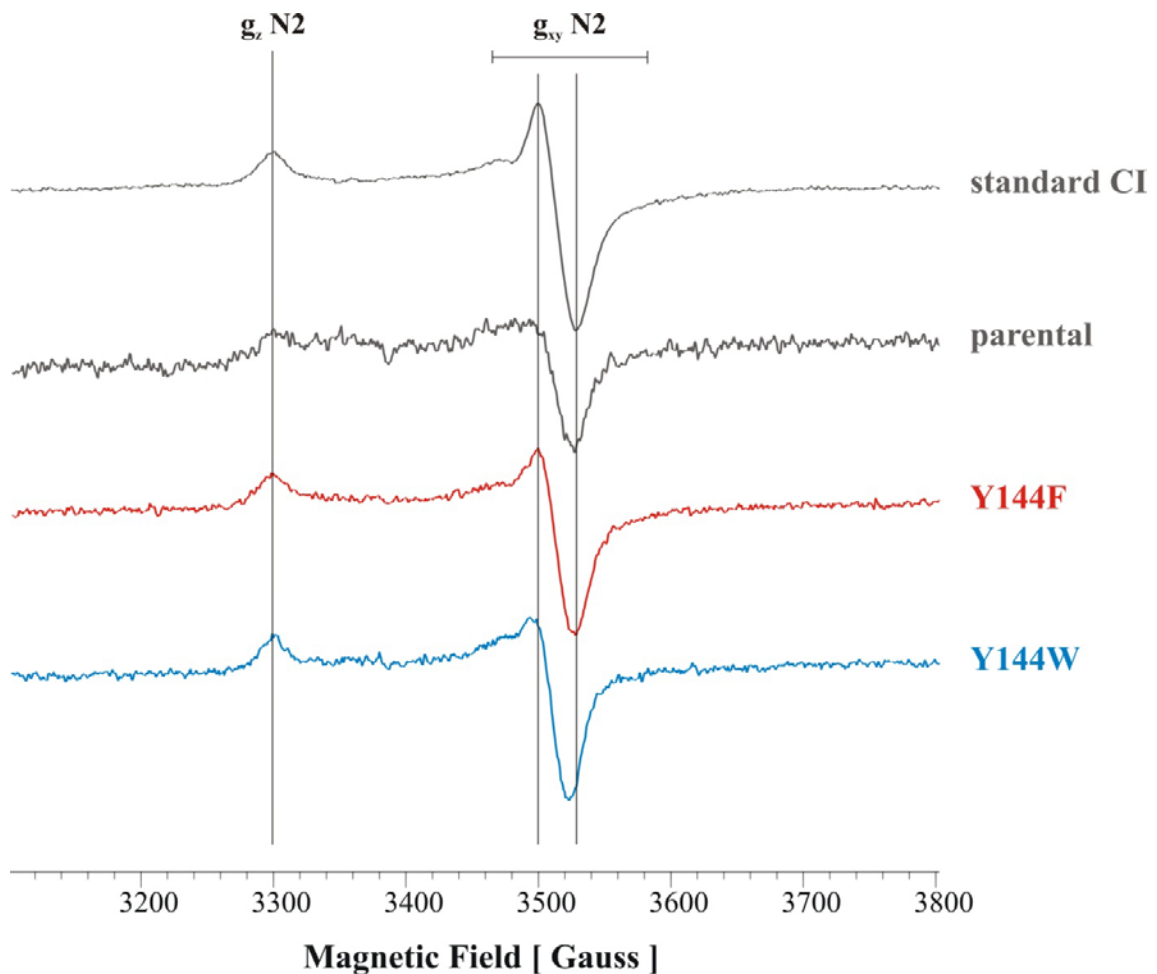


**Figure 3.12: 25 K minus 40 K difference EPR spectra from purified complex I of mutants Y144F and Y144W compared to the parental strain and to a highly concentrated complex I standard.** Main contributions from iron-sulfur clusters N2 are indicated. A small shift of the  $g_{yx}$  signal of iron-sulfur cluster N2 is evident for mutant Y144W. Mutant Y144F displayed no differences in signal N2 positions. Samples were reduced with NADH. Here, purified complex I from the PIPO strain was used as parental sample. Original 40 K and 25 K EPR spectra were recorded at 2 mW microwave power from samples reduced with 5 mM NADH. The EPR spectra were recorded by Dr. Klaus Zwicker.

Considering that even an exchange of tyrosine 144 to tryptophan, histidine or serine did not interfere with complex I assembly, it seems unlikely that by removing the hydroxyl group in mutant Y144F major conformational changes were induced which were responsible for the almost complete loss of complex I activity in mutant Y144F.

Moreover, a major impact on iron-sulfur cluster N2 is also unlikely to be responsible for the loss of activity, since EPR signals from iron-sulfur cluster N2 were unchanged in mutant Y144F.

Taking into account that tyrosine 144 is located in a central position of the proposed quinone binding pocket, very close to iron-sulfur cluster N2 which donates electrons for quinone reduction, it is reasonable to speculate that tyrosine 144 plays a critical role in quinone reduction.

### **3.3.3 Complex I activity at higher DBQ concentrations in mutant Y144F**

The very low complex I activity of mutant Y144F might have been a result of a decreased affinity for the substrate ubiquinone. Therefore, complex I activity of mitochondrial membranes from mutant Y144F was measured at higher DBQ concentrations (0-140  $\mu\text{M}$ ). However, dNADH:DBQ oxidoreductase activity was not increased by higher DBQ concentrations and was only slightly higher than with mitochondrial membranes from the  *$\Delta nucm$*  strain lacking the 49-kDa subunit and hence assembled complex I (Figure 3.13). Therefore, the loss of dNADH:DBQ oxidoreductase activity in mutant Y144F probably had not been caused by a lowered affinity of the quinone binding site to the substrate DBQ.



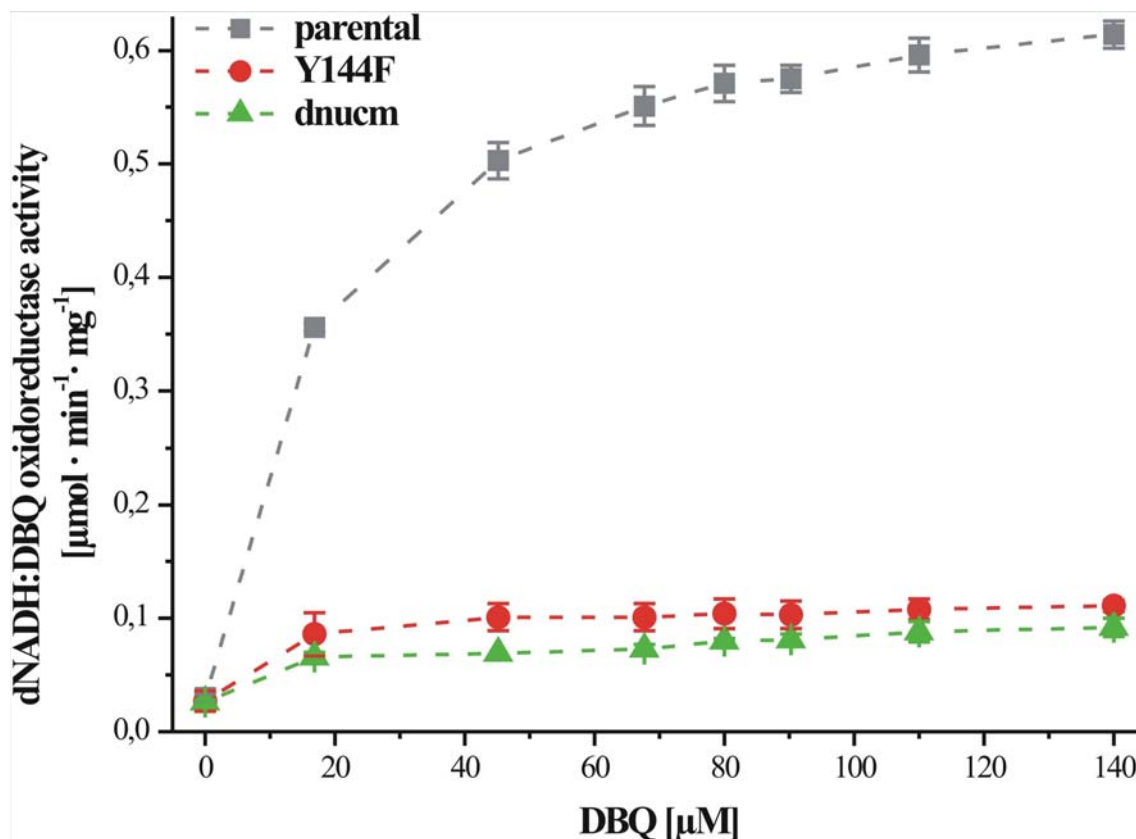


**Figure 3.13: dNADH:DBQ oxidoreductase activity of mutant Y144F at increasing DBQ concentrations.** In mitochondrial membranes from the parental strain, complex I activity was increased by higher DBQ concentrations (in gray). In contrast, no increase was observed in mitochondrial membranes from mutant Y144F strain (in red) and the *Anucm* strain (in green). The latter lacks assembled complex I and was used here as a negative control. Error bars indicate standard deviation of three measurements per data point.

### 3.3.4 pH dependence of residual activity of mutant Y144F

To check whether mutant Y144F has changed the pH optimum for quinone reduction, complex I activity in mitochondrial membranes was measured at different pH values (see Figure 3.14).

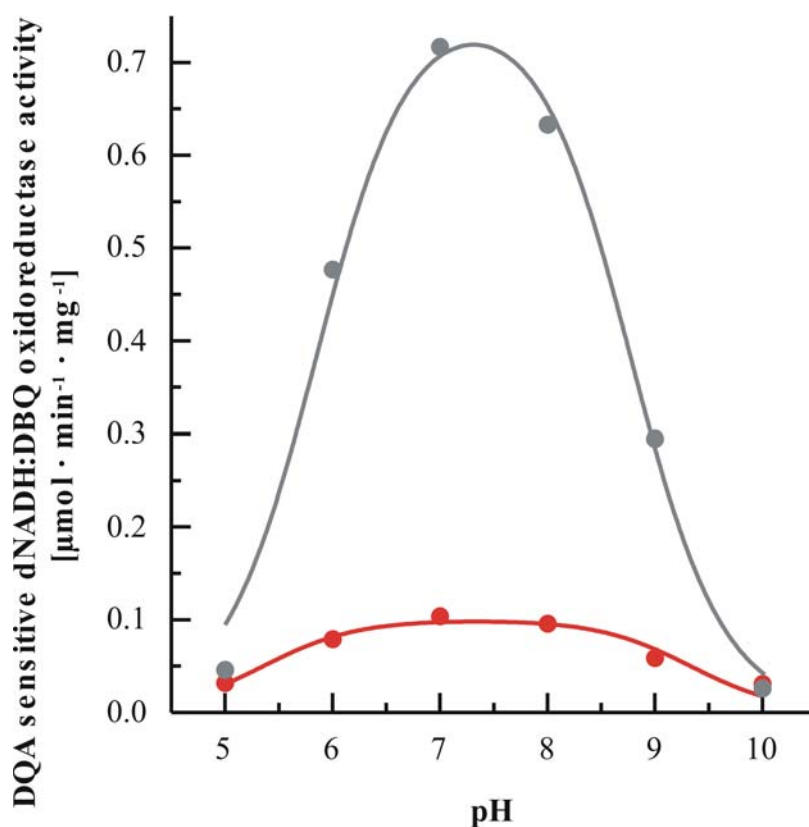


**Figure 3.14: Dependence of complex I activity on pH in mitochondrial membranes from mutant Y144F.** Values and fitted curve for mutant Y144F in red, parental strain in gray. The parameters used to fit the curve according to the equation given in chapter 2.2.3.7 are given in Table 3.11. Data points represent mean values from two to four measurements.

Values obtained for  $pK_A$ ,  $pK_B$  and  $V_{opt}$  by fitting experimental data (see chapter 2.2.3.7) are listed in Table 3.11. The differences in the  $pK_A$  and  $pK_B$  values were not highly significant, since p-values of 0.18 and 0.04, respectively, were determined by an unpaired, two-tailed t-test.

**Table 3.11: Parameters determining pH dependence of complex I activity in mitochondrial membranes from mutant Y144F and the parental strain.**

Strain	$pK_A$	$pK_B$	$V_{opt}$
parental	$5.8 \pm 0.1$	$8.8 \pm 0.1$	$0.77 \pm 0.04$
Y144F	$5.4 \pm 0.3$	$9.3 \pm 0.3$	$0.1 \pm 0.01$

Mean values  $\pm$  SEM are given.

Moreover, complex I from both the mutant Y144F and the parental strain reached maximal activity at pH 7.3.

Taken together, the pH dependence was not altered by the Y144F exchange, indicating that the hydroxyl group is not involved in protonation/deprotonation events essential for complex I activity.

### 3.3.5 Reactivation of mutant Y144F

In an attempt to restore complex I activity of the mutant Y144F, several small molecules, sodium chloride (20-400 mM), sodium bromide (0-500 mM), sodium iodide (0-400 mM), sodium azide (0-500 mM), sodium formate (0-500 mM) or sodium acetate (0-400 mM), were added to mitochondrial membranes prior to the activity measurements. Complex I activity at different additive concentrations was determined and Gaussian curves were fitted to the data. The degree of reactivation and the additive concentrations which resulted in maximal DQA sensitive complex I activity in mutant Y144F are shown in Figure 3.15. Chloride at ~280 mM, bromide at ~150 mM, iodide at ~150 mM, formate at ~330 mM and acetate at ~270 mM increased complex I activity to a different extent in mutant Y144F but decreased complex I activity in the parental strain at pH 7.4. In contrast, azide decreased complex I activity in the mutant as well as in the parental strain. The inhibitory effect of azide was seen already at the lowest concentration of 20 mM and complex I activity gradually decreased with increasing azide concentrations. An  $I_{50}$  value of 170 mM was determined for the parental strain (data not shown).

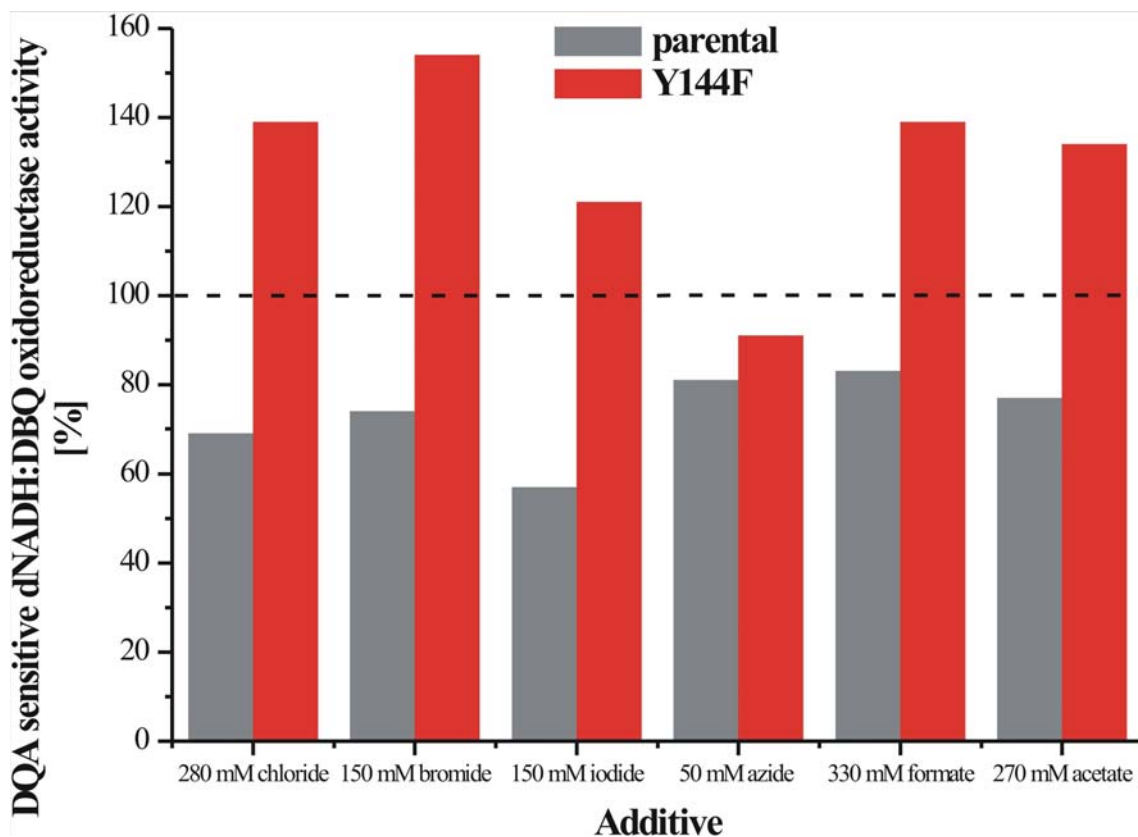


**Figure 3.15: Reactivation of DQA sensitive complex I activity by different additives at pH 7.4.** For most additives there was an optimal concentration, which increases activity in mitochondrial membranes from mutant Y144F (red bars). However, the same additive concentration decreases activity for the parental strain (gray bars). The dashed line represents activities in the absence of the respective additives (or 20 mM in the case of chloride), which were set as 100 %. For the parental strain 100 % correspond to 0.65 Units/mg protein. For mutant Y144 100 % correspond to 0.08 Units/mg protein.

As shown in Figure 3.16, the increase in total (DQA sensitive plus DQA insensitive) activity in mutant Y144F was less pronounced than that of DQA sensitive complex I activity shown in Figure 3.15. This discrepancy results from the inhibition of DQA insensitive activity by the additives.

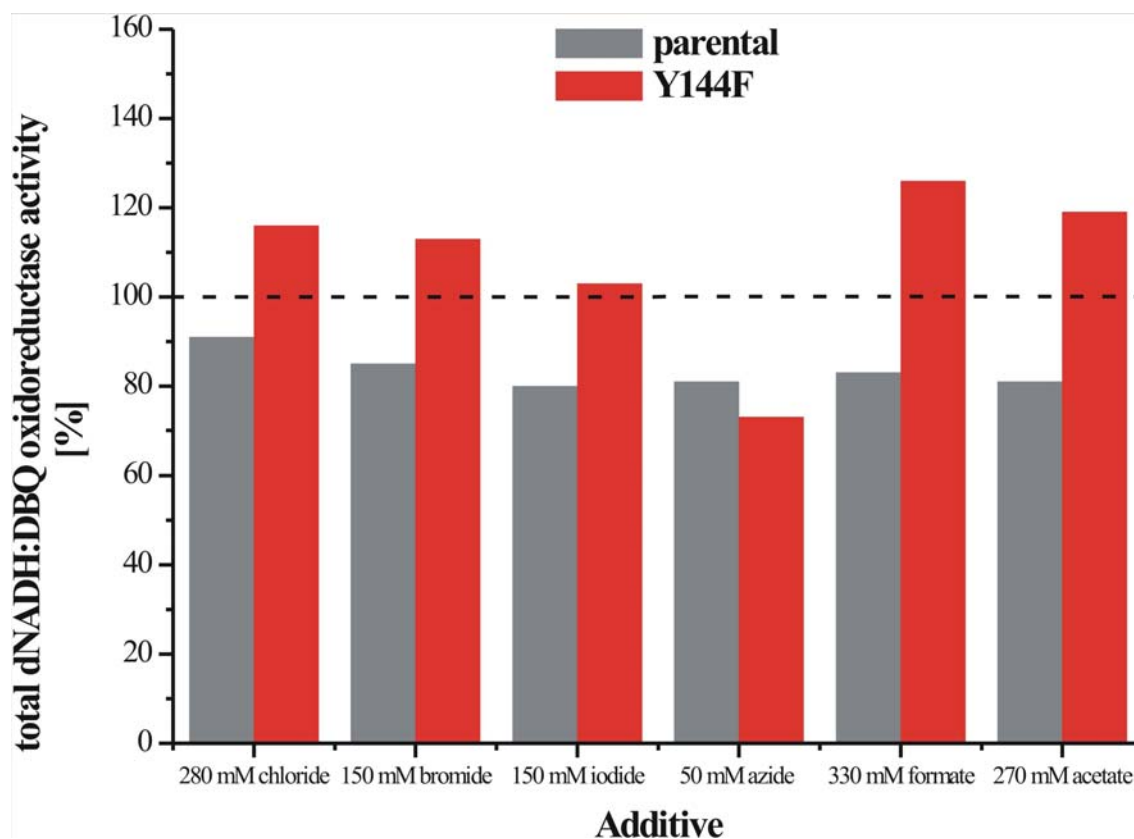


**Figure 3.16: Reactivation of total dNADH:DBQ activity by different additives.** There was an optimal concentration for most additives which increase activity in mitochondrial membranes from mutant Y144F (red bars). However, the same additive concentration decreases activity for the parental strain (gray bars). Activities measured in the absence of additives (or 20 mM in the case of chloride was studied) were set at 100 % and are indicated by the dashed line. For parental strain 100 % correspond to 0.71 Units/mg protein. For mutant Y144 100 % correspond to 0.14 Units/mg protein.

As shown in Figure 3.15 and Figure 3.16, the strongest reactivation was observed for formate and acetate. Formic acid and acetic acid are weak acids, therefore it is reasonable to speculate that donation or abstraction of a proton is partially restoring complex I activity in mutant Y144F. Since acetate has a  $pK_a$  value of 4.75, which is closer to the optimal pH for complex I activity than that of formate (3.77), the effect of pH in the presence of 300 mM acetate was examined (see Figure 3.17). According to the Henderson-Hasselbalch equation, at pH 6.2 the concentration of acetic acid is 10.3 mM, at pH 6.6 it is 4.2 mM, at pH 7.0 it is ~1.7 mM and at pH 7.4 it is ~0.7 mM. As shown in Figure 3.17, there was no qualitative difference between mutant Y144F and the parental strain in the dependence of complex I activity on acetic acid concentration.

This result argues against the hypothesis that the acids substitute for the hydroxyl group in mutant Y144F by facilitating protonation (or deprotonation) events.

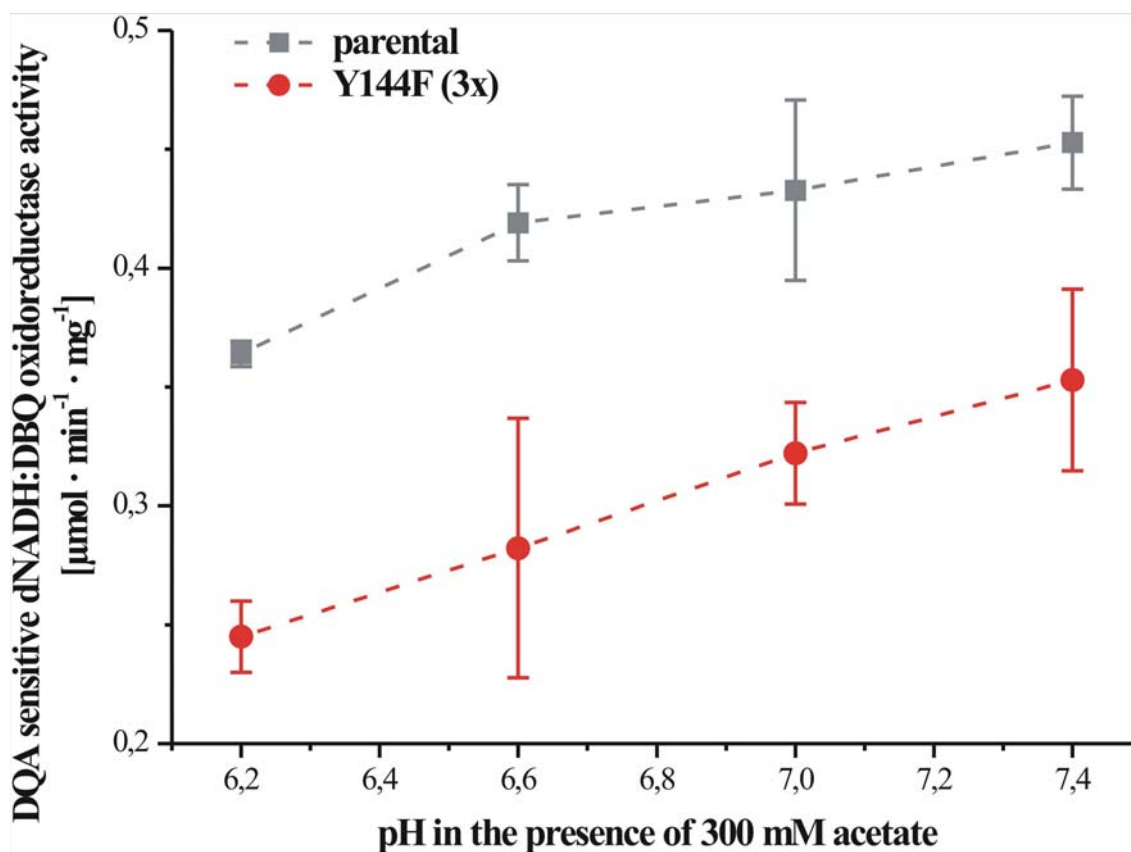


**Figure 3.17: Reactivation of DQA sensitive complex I activity by acetic acid.** The increase of complex I activity in mutant Y144F (in red) was not different from that of the parental strain (in gray). The activity values for the mutant were multiplied by 3, in order to make them graphically comparable to the parental strain. A pH of 6.2 corresponds to 10.3 mM acetic acid, pH 6.6 corresponds to 4.2 mM acetic acid, pH 7.0 corresponds to ~1.7 mM acetic acid and pH 7.4 corresponds to ~0.7 mM acetic acid according to the Henderson–Hasselbalch equation. Error bars indicate standard deviation of at least two measurements per data point.

Taken together, the highest increases in complex I activity, by 30-55 %, were observed with acetate, formate and bromide. However, it should be emphasized that for the almost inactive Y144F mutant this corresponds to an absolute increase from 7 % to 9-11 % activity compared to the parental strain without additives. The finding that it was not possible to markedly restore complex I activity by the addition of different small molecules in mutant Y144F further highlights the essential role of tyrosine 144 and its hydroxyl group for ubiquinone reduction.

### 3.3.6 dNADH:Q<sub>1</sub> oxidoreductase activity in tyrosine 144 mutants

To assay complex I activity, different hydrophilic quinones are used (Di Virgilio and Azzone, 1982; Estornell et al., 1993; Fato et al., 1996; Degli Esposti et al., 1996; Lenaz, 1998; Hano et al., 2003). DBQ is used predominantly because it gives the highest catalytic rates, which – importantly – are almost completely sensitive to complex I specific inhibitors. However, often the more hydrophilic Q<sub>1</sub> is used as electron acceptor.

Since tyrosine 144 is predicted to reside close to or to even form part of the quinone binding site, and since all mutants displayed almost no ubiquinone-reductase activity when DBQ was used, it was tested whether the tyrosine 144 mutants show any ubiquinone-reductase activity with Q<sub>1</sub>. Indeed, when tyrosine 144 was exchanged to other aromatic residues, complex I displayed considerable dNADH:Q<sub>1</sub> oxidoreductase activity. The dependence of the normalized dNADH:Q<sub>1</sub> activity on Q<sub>1</sub> concentration is visualized in Figure 3.18. From these data *apparent*  $K_m$  values and  $V_{max}$  values were determined.

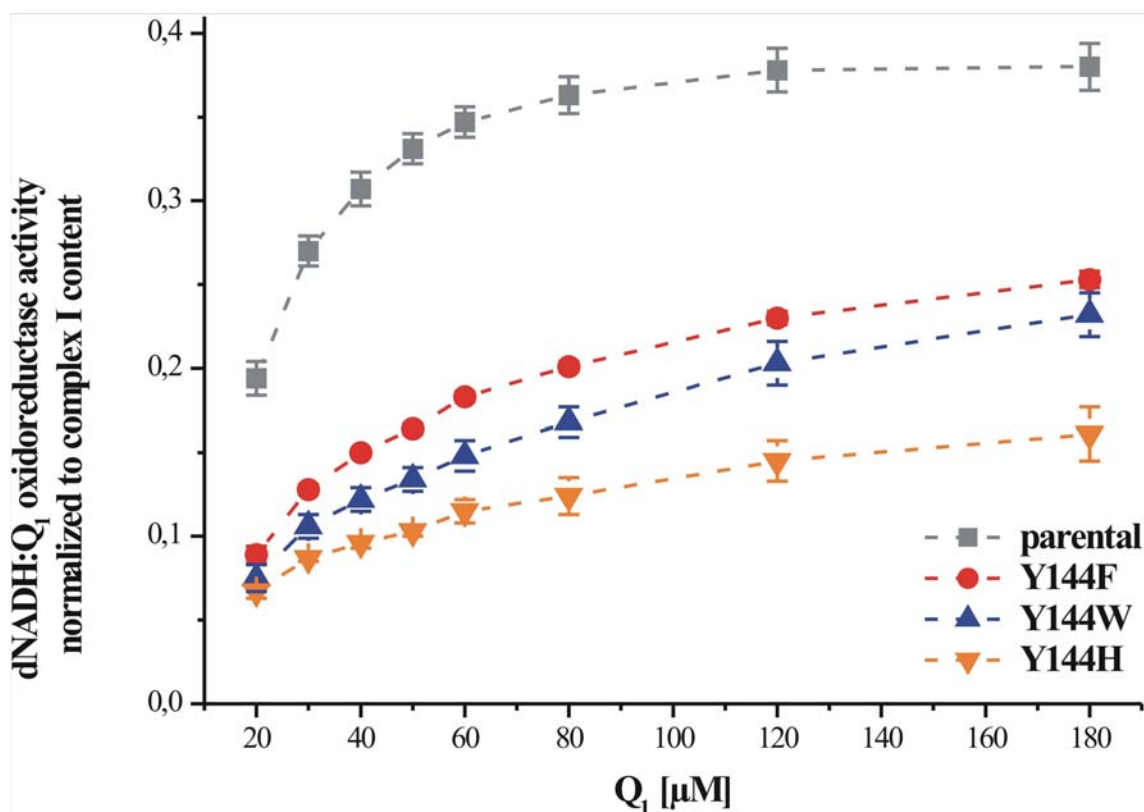


**Figure 3.18: Normalized dNADH:Q<sub>1</sub> oxidoreductase activity in mitochondrial membranes of tyrosine 144 mutants at different concentrations of Q<sub>1</sub>.** The parental strain displayed the highest dNADH:Q<sub>1</sub> activity. However, the tyrosine 144 mutants did not reach maximal activity even at a Q<sub>1</sub> concentration of 180 µM, which reflects the increased *apparent K<sub>m</sub>* value for the mutant enzyme. The dNADH:Q<sub>1</sub> oxidoreductase activity was normalized to complex I content in the mitochondrial membranes determined as NADH:HAR oxidoreductase activity. The ratio is a dimensionless quantity. Error bars indicate the standard error of mean of at least three measurements per data point.

As shown in Table 3.12 the *apparent K<sub>m</sub>* value for Q<sub>1</sub> was four times higher in mutants Y144F and Y144H and even six times higher when tyrosine 144 was exchanged to the bulkier tryptophan in mutant Y144W. In order to allow comparison of maximal activities from different strains the pseudo  $V_{max}$  value from the *Δnucm* strain, which lacks complex I, was subtracted and the  $V_{max}$  values were normalized to complex I content of the respective mitochondrial membrane preparations. Mutants Y144F and Y144W reached more than 70 % of maximal dNADH:Q<sub>1</sub> oxidoreductase activities of the parental strain, whereas mutant Y144H reached only 32 % of parental strain activity. Interestingly, when the tyrosine was exchanged with non-aromatic residues, dNADH:Q<sub>1</sub> oxidoreductase activity in the respective mitochondrial membranes was very low and comparable to the background activity measured in mitochondrial membranes from the



*Anucm* strain. These findings indicate that an aromatic ring at position 144 is essential for dNADH:Q<sub>1</sub> oxidoreductase activity.

**Table 3.12: Apparent  $K_m$  values and  $V_{max}$  values for tyrosine 144 mutants when Q<sub>1</sub> was used as electron acceptor.**

Strain	<i>app. K<sub>m</sub></i> for Q <sub>1</sub>	$V_{max}$ with Q <sub>1</sub>	$V_{max}$ normalized to CI content <sup>a</sup>
	μM	Units/mg protein	%
parental	10±1	0.43±0.01	100±2
Y144F	39±3	0.38±0.01	71±3
Y144W	62±4	0.47±0.01	77±7
Y144H	40±3	0.24±0.01	32±1
Y144S	n.d.	n.d.	n.d.
Y144I	n.d.	n.d.	n.d.
Y144R	n.d.	n.d.	n.d.

n.d., not determinable

Mean values ± SEM are given.

<sup>a</sup> for mitochondrial membranes of the *Anucm* strain a pseudo  $V_{max}$  value of 0.12 was determined. Since this strain does not contain complex I, this value was considered as a complex I unspecific background rate and was subtracted from all  $V_{max}$  values. Complex I content in mitochondrial membranes was estimated as NADH:HAR oxidoreductase activity (1.03±0.02 μmol·min<sup>-1</sup>·mg<sup>-1</sup> was measured for the parental strain). The ratio of 0.31/1.03 for the parental strain was set as 100 %.

### 3.3.7 dNADH:Q<sub>2</sub> oxidoreductase activity of mutants Y144F and Y144W

In mitochondrial membranes from all tyrosine 144 mutants there was almost no dNADH:ubiquinone oxidoreductase activity when DBQ or the endogenous ubiquinone (Q<sub>9</sub> in *Y. lipolytica*, see chapter 3.1.4) were used, while for mutants Y144F, Y144W and the Y144H there was considerable ubiquinone-reductase activity with Q<sub>1</sub>. In addition, especially for mutant Y144W a drastically changed *apparent K<sub>m</sub>* value for Q<sub>1</sub> was observed. Therefore, *apparent K<sub>m</sub>* and  $V_{max}$  values were also determined with Q<sub>2</sub> for mutants Y144F and Y144W. As shown in Table 3.13, for both mutants the *apparent K<sub>m</sub>* values were significantly increased but the  $V_{max}$  values were quite similar to the parental

strain after normalizing to complex I content. In comparison to the values determined for Q<sub>1</sub>, the effect on the *apparent*  $K_m$  value for Q<sub>2</sub> was less pronounced, especially in the mutant Y144W, and the  $V_{max}$  value with Q<sub>2</sub> was much closer to that of the parental strain. Therefore, in mitochondrial membranes from the tyrosine 144 mutants Q<sub>2</sub> seemed to be an even better electron acceptor than Q<sub>1</sub>.

**Table 3.13: Apparent  $K_m$  values and  $V_{max}$  values for the Y144F and Y144W mutants when Q<sub>2</sub> was used as electron acceptor.**

Strain	<i>app. K<sub>m</sub></i> for Q <sub>2</sub>	$V_{max}$ with Q <sub>2</sub>	$V_{max}$ normalized to CI content <sup>a</sup>
	μM	Units/mg protein	%
parental	8±1	0.46±0.02	100±5
Y144F	14±2	0.4±0.02	118±4
Y144W	14±2	0.62±0.03	92±11

Mean values ± SEM are given.

<sup>a</sup> complex I content in mitochondrial membranes was determined as NADH:HAR oxidoreductase activity (1.03±0.02 μmol·min<sup>-1</sup>·mg<sup>-1</sup> was measured for the parental strain). The ratio of 0.46/1.03 for the parental strain was set as 100 %.

In summary, the dNADH:ubiquinone oxidoreductase activities in mitochondrial membranes from the tyrosine 144 mutants strongly depended on the structure of the side chain of the ubiquinone-derivative used.

### 3.3.8 Inhibitor resistance of the tyrosine 144 mutants

In order to find out whether tyrosine 144 is also part of the inhibitor binding site,  $I_{50}$  values for DQA, rotenone, C<sub>12</sub>E<sub>8</sub> and EIPA in the presence of 150 μM Q<sub>1</sub> were measured. As shown in Table 3.14, the removal of the hydroxyl group of tyrosine 144 by the Y144F exchange was sufficient to dramatically increase resistance towards DQA and rotenone. Even higher resistance was observed when the tyrosine was exchanged for the more spacious tryptophan. Interestingly, in both mutants the  $I_{50}$  values for DQA were much more strongly increased than the  $I_{50}$  values for rotenone. This might indicate that DQA interacts with tyrosine 144 more directly than rotenone. In contrast, the  $I_{50}$

values for  $C_{12}E_8$  and EIPA were only moderately changed in these mutants. This result is in line with the finding that  $C_{12}E_8$  and EIPA interact with a different region in the quinone binding pocket.

For the 49-kDa subunit mutants V145T, F207W, E218Q R224D, R224I, R224N, L225H and L225V the inhibition of the dNADH:Q<sub>1</sub> oxidoreductase activity by DQA and rotenone was also tested (at 62  $\mu$ M Q<sub>1</sub>). In agreement with what was found when DBQ was used as an electron acceptor (Table 3.5), the  $I_{50}$  values for DQA and rotenone were not changed in any of the mutants (data not shown).

**Table 3.14:  $I_{50}$  values for DQA, rotenone,  $C_{12}E_8$  and EIPA determined in mitochondrial membranes from tyrosine mutants in the presence of 150  $\mu$ M Q<sub>1</sub>.**

Strain	$I_{50}$			
	DQA	Rotenone	$C_{12}E_8$	EIPA
		nM		$\mu$ M
parental	10	900	3000	40
Y144F	5000	2500	1500	35
Y144W	7500	4500	1500	33

Taken together, the findings that even conservative mutations of tyrosine 144 almost completely abolished dNADH:DBQ oxidoreductase activity, drastically increased the *apparent*  $K_m$  value for Q<sub>1</sub> and caused marked resistance against hydrophobic inhibitors suggest that tyrosine 144 is part of the quinone binding site as well as the inhibitor binding site of complex I.

### 3.3.9 Proton pumping of complex I in mutants Y144F and Y144W

Since mutants Y144F and Y144W displayed high dNADH:Q<sub>1</sub> oxidoreductase activities, it was interesting to test whether this redox reaction was connected to vectorial proton pumping by complex I. For this purpose, isolated complex I from mutants Y144F and Y144W was reconstituted into liposomes and proton pumping was monitored as quench in ACMA fluorescence. As shown in Figure 3.19 and Figure 3.20, both mutants were

able to pump protons as indicated by the fluorescence quench upon NADH addition. Moreover, the pumping rates of the mutants seemed to be similar to the rate of complex I from the parental strain, since a coupling factor of 1.9 was determined for proteoliposomes from the parental strain and a factor of 2.6 and 2.5 was determined for mutants Y144F and Y144W, respectively. In order to verify that the observed quench in ACMA fluorescence was indeed caused by a proton gradient, the protonophore FCCP was added at the end of each measurement. As expected, the fluorescence quench was abolished by addition of FCCP and fluorescence returned to the level before or immediately after NADH addition.

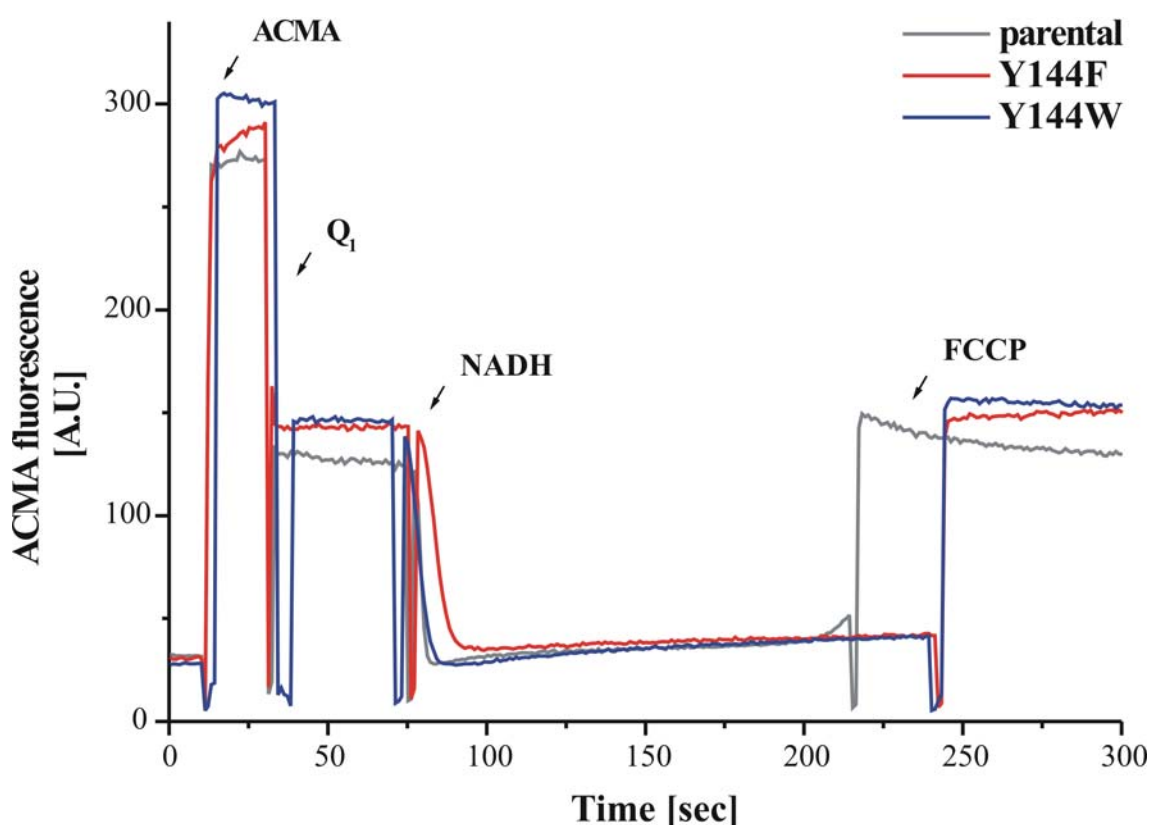


**Figure 3.19: Proton pumping by mutants Y144F and Y144W assayed as quench in ACMA fluorescence.** Following the addition of Q<sub>1</sub> and NADH, the buildup of a proton gradient across proteoliposomes was monitored as a quench in ACMA fluorescence. The line shapes of the ACMA fluorescence signal for both mutants were comparable to that of the parental strain, indicating that both mutations did not interfere with proton pumping. Arrows indicate time points for the additions of 0.5  $\mu$ M ACMA, 150  $\mu$ M Q<sub>1</sub>, 100  $\mu$ M NADH and 1  $\mu$ M FCCP. Proteoliposomes and 0.5  $\mu$ M valinomycin were added before measurements were started.

Figure 3.20 shows that proton pumping by complex I from the parental strain was inhibited by rotenone; therefore, ACMA fluorescence reached initial levels after the proton gradient was dissipated by proton leakage. In contrast, the quench in ACMA fluorescence with mutant Y144F and especially mutant Y144W were much less severely affected by the addition of 20  $\mu\text{M}$  of rotenone. This observation may at least partially be explained by the higher resistance of the mutants against rotenone.

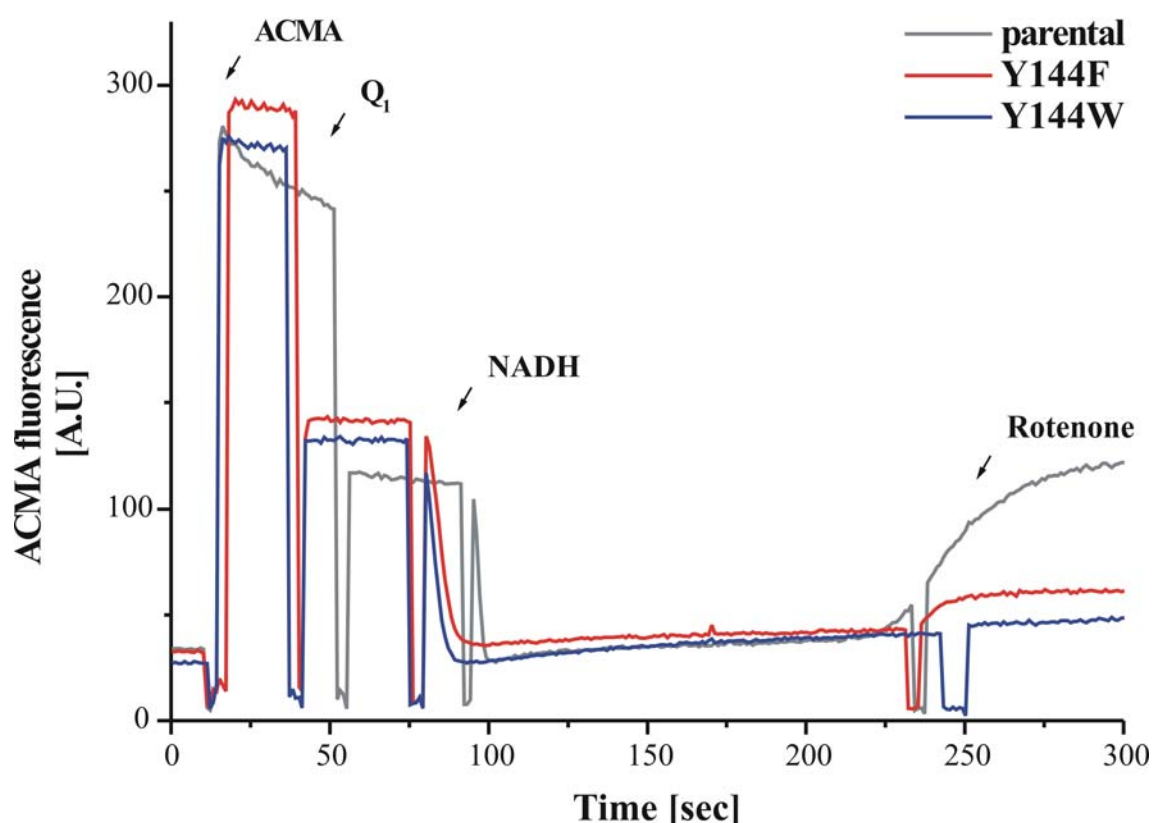


**Figure 3.20: Rotenone resistance of proton pumping by mutants Y144F and Y144W.** The quench in ACMA fluorescence after NADH addition indicated proton pumping, which in the case of the parental strain was sensitive towards rotenone. Proton pumping by mutants Y144F and Y144W was almost insensitive towards rotenone. Arrows indicate time points for the additions of 0.5  $\mu\text{M}$  ACMA, 150  $\mu\text{M}$   $\text{Q}_1$ , 100  $\mu\text{M}$  NADH and 20  $\mu\text{M}$  rotenone. Proteoliposomes and 0.5  $\mu\text{M}$  valinomycin were added before measurements were started.

As detailed in Table 3.10, the tyrosine 144 mutants show some residual dNADH:DBQ oxidoreductase activity. Therefore, proton pumping by mutants Y144F and Y144W was assayed when DBQ was used as an electron acceptor. Both mutants show small but

significant proton pumping as indicated by a quench in ACMA fluorescence, which again was sensitive to FCCP but largely resistant against rotenone (data not shown).

The finding that both the high dNADH:Q<sub>1</sub> oxidoreductase activity and the marginal dNADH:DBQ oxidoreductase activity of the tyrosine mutants resulted in proton pumping indicates that both activities reflected the physiological reaction. Moreover, these results highlight the tight coupling between redox reaction and vectorial proton pumping in complex I.

### 3.4 Mutagenesis study of the HRGXE-motif

#### 3.4.1 The HRGXE-motif in different organisms

At the N-terminus of the 49-kDa subunit there is a charged and highly conserved HRGXE-motif (see Figure 3.21), which is also partially present in most sequences of homologous [NiFe] hydrogenases (Albracht, 1993). It is composed of a highly conserved histidine, a conserved arginine, an invariant glycine, a variable amino acid residue (usually a small and polar one) and a highly conserved glutamate. Interestingly, this motif is not conserved in *T. thermophilus* because the arginine is replaced by the much smaller and uncharged threonine.

<i>Y. lipolytica</i>	E I I R S D P H V G L L <b>HRGTE</b> K L I E Y K T Y M Q A L P Y F D R L D Y V S M	147
<i>N. crassa</i>	E I V R A D P H V G L L <b>HRGTE</b> K L C E Y R T Y L Q A L P Y F D R L D Y V S M	159
<i>B. taurus</i>	M V R K C D P H I G L L <b>HRGTE</b> K L I E Y K T Y L Q A L P Y F D R L D Y V S M	111
<i>H. sapiens</i>	M V R K C D P H I G L L <b>HRGTE</b> K L I E Y K T Y L Q A L P Y F D R L D Y V S M	144
<i>P. denitrificans</i>	I V E R A D P H I G L L <b>HRGTE</b> K L M E S R T Y L Q N L P Y L D R L D Y V A P	91
<i>R. capsulatus</i>	I V E R A D P H I G L L <b>HRGTE</b> K L M E S R T Y L Q N T P Y F D R L D Y V A P	91
<i>T. thermophilus</i>	E V L E V V P H I G Y L <b>HTGFE</b> K T M E H R T Y L Q N I T Y T P R M D Y L H S	90
<i>E. coli</i>	E I V D C V P D I G Y H <b>HRGAE</b> K M G E R Q S W H S Y I P Y T D R I E Y L G G	87
	: * . : * * * * * * : : : . . * * : : * :	

**Figure 3.21: Sequence alignment of the N-terminal part of the 49-kDa subunit harboring the HRGXE-motif.** The HRGXE-motif of *Y. lipolytica* is shaded in pink. Conserved residues within the motif are shown in bold. Sequences were aligned with the multiple sequence alignment program ClustalW. Invariant (\*), highly (:), and weakly similar (.) positions are labeled. For the complete alignment see Figure 8.1.

### 3.4.2 Location of the HRGXE-motif

As shown in Figure 3.22, the residues of the HRGXE-motif are not located at the surface of the proposed ubiquinone and inhibitor binding pocket of complex I. The HRGXE-motif is rather buried in the 49-kDa subunit and spans a distance of  $\sim 13$  Å from iron-sulfur cluster N2 to the 30-kDa subunit, which is adjacent to the 49-kDa subunit.

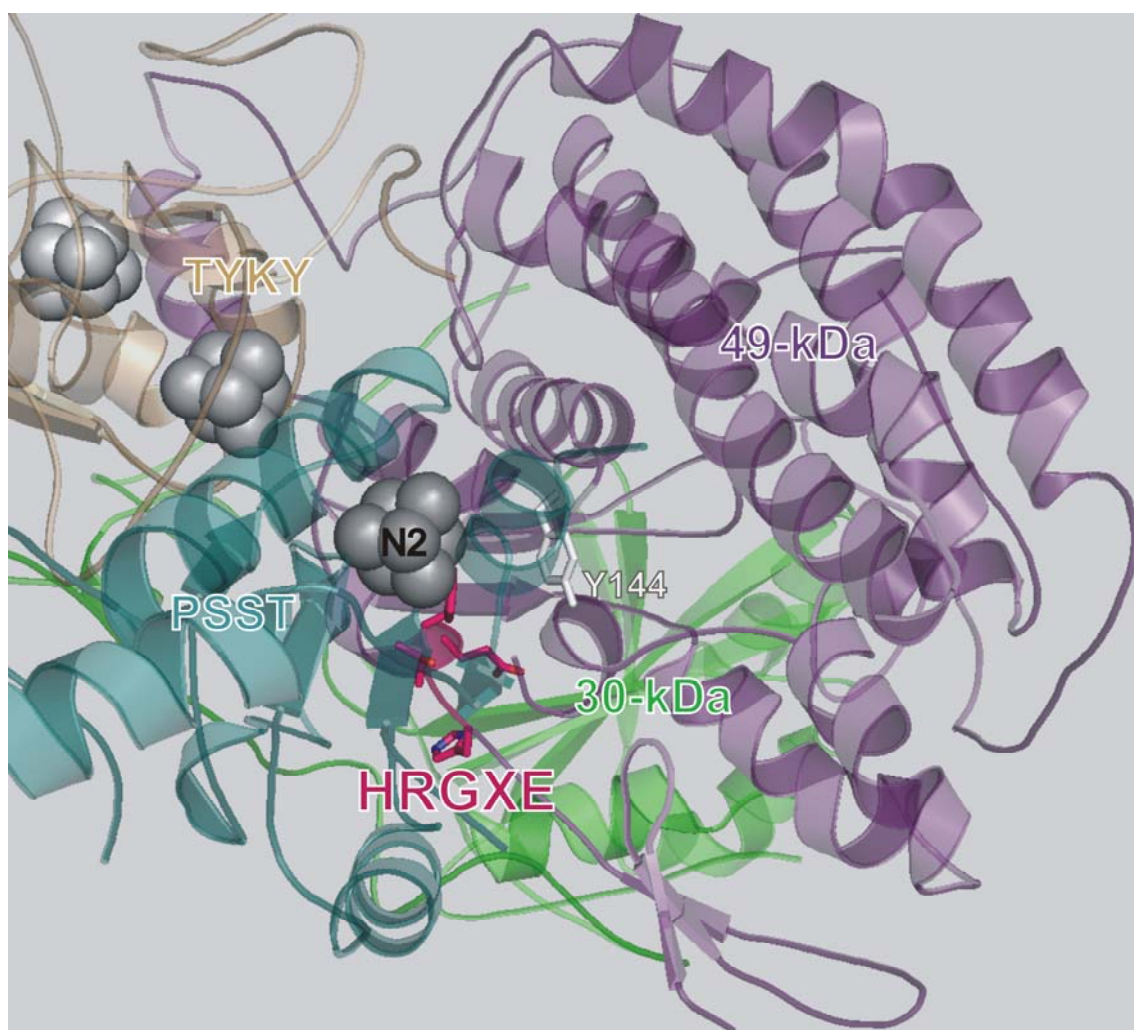


**Figure 3.22: Location of the HRGXE-motif close to iron-sulfur cluster N2 but at some distance from the ubiquinone and inhibitor binding pocket.** Amino acid residues of the HRGXE-motif are shown in stick representation and are highlighted in pink. Iron-sulfur cluster N2 is shown in gray as space-filled model. The 49-kDa, PSST, 30-kDa and TYKY subunits are shown in schematic representation. For better orientation, a view into the ubiquinone and inhibitor binding pocket similar to that in Figure 3.3 was chosen. Tyrosine 144, which delimits the left border of the ubiquinone binding pocket in this view, is shown in white sticks. The figure was generated from the crystal structure of the hydrophilic domain of complex I from *T. thermophilus* (PDB ID: 2FUG) by using the PyMOL program.

### 3.4.3 Complex I assembly and activity of the HRGXE-motif mutants

In order to gain insights into the function of the HRGXE-motif, histidine 120, arginine 121, glycine 122 and glutamate 124 in the 49-kDa subunit of *Y. lipolytica* were exchanged by mutation. The effects of the mutations on complex I content, complex I activity and the EPR signal of iron-sulfur cluster N2 in mitochondrial membranes as compared to the parental strain are summarized in Table 3.15. The exchange of histidine 120 to arginine or tryptophan impeded complex I assembly. The histidine to alanine exchange introduced earlier (Kashani-Poor et al., 2001b) interfered with complex I activity only. The conservative exchange of arginine 121 to lysine resulted in a strong decrease in complex I content and activity, indicating that this arginine is crucial for complex I from *Y. lipolytica*. The exchange of glycine 122 to the small alanine residue did not alter complex I content and activity. However, when the larger valine residue was introduced into this position, complex I content was dramatically decreased. The same was true when glutamate 124 was exchanged with the slightly smaller aspartate or arginine. Interestingly, exchanging glutamate 124 with the similar sized but uncharged glutamine resulted in decreased complex I content; however, specific complex I activity was not changed. These results suggest that size and charge of the residue at position 124 are important for proper folding of the 49-kDa subunit and the assembly of complex I, but not for complex I activity.

**Table 3.15: Effects of mutations introduced into the HRGXE-motif of the 49-kDa subunit on complex I content, activity and N2 EPR signal in mitochondrial membranes from *Y. lipolytica*.**

Strain	Complex I content <sup>a</sup>	Complex I activity <sup>b</sup>	N2 EPR signal (see Figure 3.23)
	%	%	
parental	100±3	100±5	reference
H120A <sup>c</sup>	93	39	not altered
H120R	20±1	n.d.	n.d.
H120W	22±1	n.d.	n.d.
R121K	38±2	24±1	no complex I signals
G122A	120±3	96±8	not altered
G122V	25±1	n.d.	n.d.



Strain	Complex I content <sup>a</sup>	Complex I activity <sup>b</sup>	N2 EPR signal (see Figure 3.23)
	%	%	
parental	100±3	100±5	reference
E124D	29±1	n.d.	n.d.
E124R <sup>d</sup>	31	12	n.d.
E124Q	55±1	98±2	weaker signal intensities

Mean values ± SEM are given.

n.d., not determinable

<sup>a</sup> 100 % of complex I content corresponds to 1.25  $\mu\text{mol}\cdot\text{min}^{-1}\cdot\text{mg}^{-1}$  NADH:HAR oxidoreductase activity determined for the parental strain.

<sup>b</sup> DQA sensitive complex I specific dNADH:DBQ oxidoreductase activity ( $0.58 \mu\text{mol}\cdot\text{min}^{-1}\cdot\text{mg}^{-1}$  was measured for the parental strain) was normalized to complex I content. The ratio of  $0.58/1.25$  for the parental strain was set as 100 % complex I activity.

<sup>c</sup> data from (Kashani-Poor et al., 2001b)

<sup>d</sup> data from (Grgic, Ph.D. Thesis, University Frankfurt, 2004)

#### 3.4.4 EPR spectra from mutants of the HRGXE-motif

For mutants having a complex I content of at least 35 %, also EPR spectra from mitochondrial membranes were recorded. Iron-sulfur clusters were reduced with 2 mM NADH and EPR spectra were recorded at 12 K and 5 mW microwave power. Unfortunately, hardly any complex I specific EPR signals could be detected for mutant R121K (see Figure 3.23), probably due to low complex I content. The EPR spectrum from mutant G122A was not significantly different from that of the parental strain (see Figure 3.23). In mutant E124Q lower complex I specific EPR signal intensities reflected lower content of assembled complex I (see Figure 3.23). Aside from this, EPR signals for iron-sulfur cluster N2 were not significantly altered.

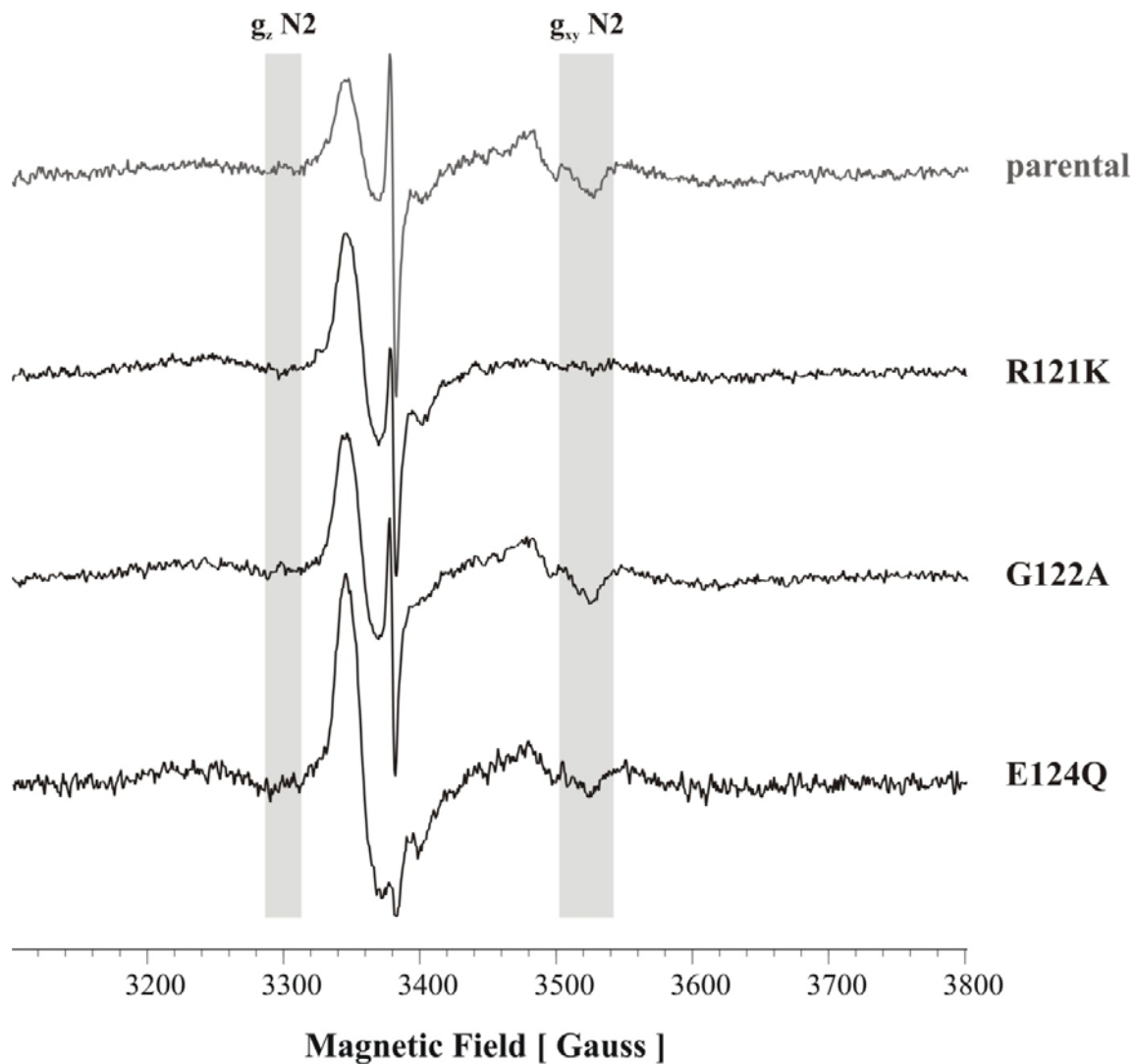


**Figure 3.23: EPR spectra of mitochondrial membranes from the HRGXE-motif mutants at 12 K and 1 mW microwave power.** Field regions where signals mainly from iron-sulfur cluster N2 arise are highlighted in gray. The spectrum of mutant G122A was not significantly different from the spectrum of the parental strain. Spectra of mutants R121K and E124Q show no or markedly reduced signal intensities of iron-sulfur cluster N2, respectively. The higher signal/noise ratio in mutant E124Q was due to lower complex I content. Mitochondrial membranes (~25 mg protein per ml) were reduced with 2 mM NADH. Spectra were recorded by Dr. Klaus Zwicker.

Similar observations were made when EPR spectra were recorded at 40 K for individual analysis of binuclear clusters (data not shown). Likewise the addition of the stronger reductant dithionite did not result in any complex I specific changes in EPR spectra (data not shown). As shown earlier (Kashani-Poor et al., 2001b), the EPR spectrum of complex I from mutant H120A is unchanged.

### 3.4.5 Apparent $K_m$ and $I_{50}$ values for mutants of the HRGXE-motif

For mutants which had at least 25 % of complex I activity, also *apparent*  $K_m$  values for DBQ and  $I_{50}$  values for DQA and rotenone were determined (Table 3.16). Values for mutant G122A were not different from the values for the parental strain. However, mutants H120A and E124Q displayed slight effects on the *apparent*  $K_m$  value for DBQ and on the  $I_{50}$  value for DQA, which might indicate that the ubiquinone and inhibitor binding pocket was distorted in these mutants, since histidine 120 and glutamate 124 are not located at the proposed ubiquinone and inhibitor binding pocket (see Figure 3.22).

**Table 3.16: Effects on inhibitor sensitivity and ubiquinone affinity of mutations introduced into the HRGXE-motif of the 49-kDa subunit in mitochondrial membranes from *Y. lipolytica*.**

Strain	<i>app. K<sub>m</sub></i> for DBQ	$I_{50}$	
		DQA	Rotenone
	$\mu\text{M}$	nM	
parental	15	16	530
H120A <sup>a</sup>	9 <sup>b</sup>	24 <sup>a</sup>	580 <sup>a</sup>
G122A	12	17	600
E124Q	6	12	500

<sup>a</sup> data from (Kashani-Poor et al., 2001b)

<sup>b</sup> data from (Kashani-Poor, Ph.D. Thesis, University Frankfurt, 2000)

## 3.5 Mutagenesis of the 24-kDa subunit close to iron-sulfur cluster N1a

### 3.5.1 Selection of targeted residues

Iron-sulfur cluster N1a ligated by the 24-kDa subunit is considered to be EPR silent in complex I from *Y. lipolytica* due to its very low redox midpoint potential, which does not allow its reduction by NADH or dithionite (see chapter 1.2.6). As reviewed by (Stephens et al., 1996), the redox midpoint potential of iron-sulfur clusters depends on the surrounding protein matrix.

In order to make iron-sulfur cluster N1a reducible and hence EPR detectable, point mutations were introduced which should increase the redox midpoint potential of iron-sulfur cluster N1a. Therefore valine166, alanine 175 and methionine 177 located next to the C-terminal part of the N1a binding motif (see Figure 3.24) in the 24-kDa subunit were exchanged for polar or even positive amino acid residues.

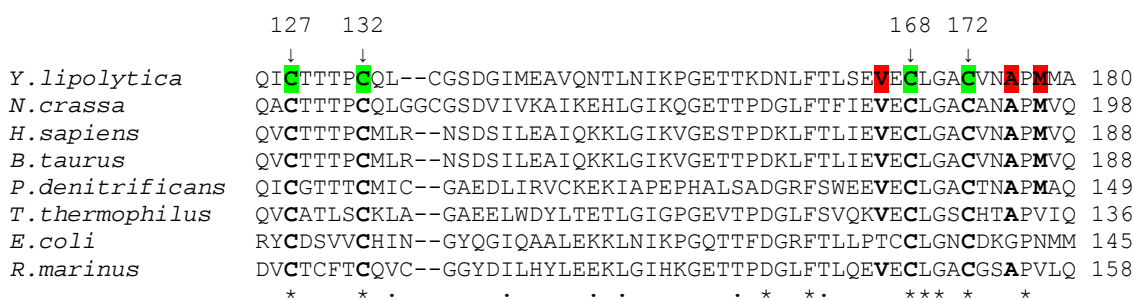


**Figure 3.24: Sequence alignment of the binding motif of iron-sulfur cluster N1a within the 24-kDa subunit.** Cysteine ligands of iron-sulfur cluster N1a are highlighted in green and are labeled according to *Y. lipolytica* numbering. Amino acid residues which were exchanged to increase the redox midpoint potential of iron-sulfur cluster N1a are highlighted in red. Sequences were aligned by the multiple sequence alignment program ClustalW. Invariant (\*), highly (:) and weakly similar (.) positions are labeled. For the complete alignment see Figure 8.4.

In Figure 3.25, the spatial arrangement of the targeted amino acid residues relative to iron-sulfur cluster N1a and its cysteine ligands in the X-ray structure from *T. thermophilus* is shown. Since the ligation and coordination of an iron-sulfur cluster is expected to be highly conserved, a similar arrangement in the 24-kDa subunit from *Y. lipolytica* can be inferred. Therefore, the hydrophobic residues valine 166 and alanine 175 reside most probably at a distance of 8-9 Å from iron-sulfur cluster N1a. Methionine 177 is expected to be located only few Ångströms from iron-sulfur cluster N1a.

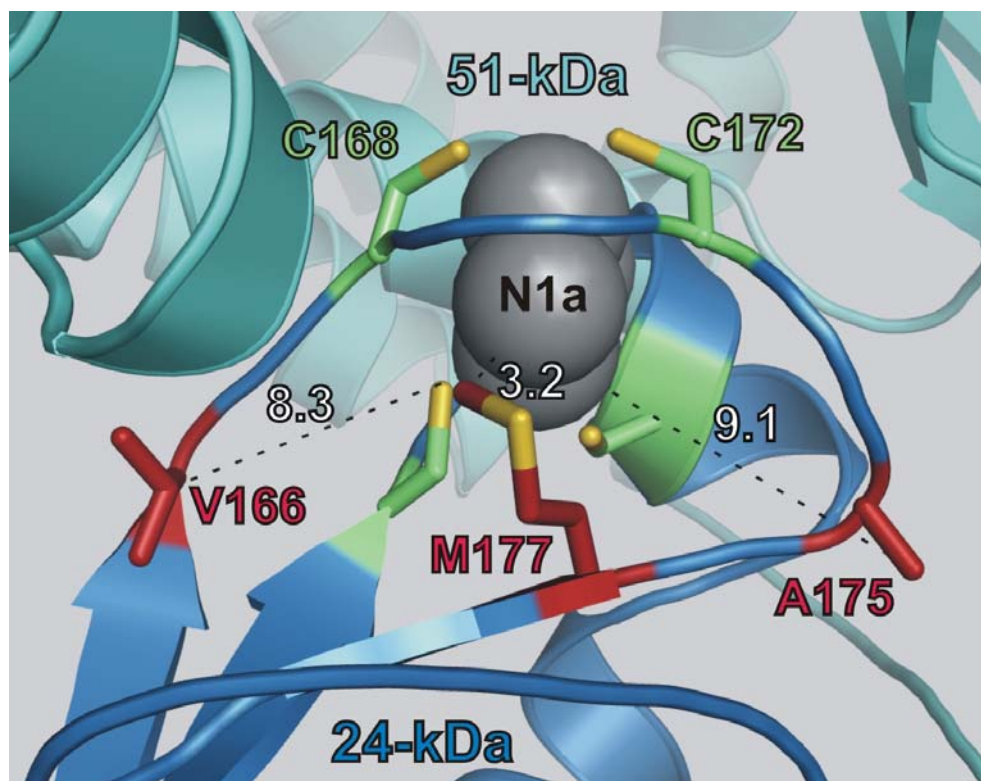


**Figure 3.25: Ligation and coordination of iron-sulfur cluster N1a within the 24-kDa subunit.** Iron-sulfur cluster N1a is located at the interface between the 24-kDa and the 51-kDa subunit, shown in blue and cyan schematic representation, respectively. Ligating cysteines and amino acids residues which were exchanged in order to increase the redox midpoint potential of iron-sulfur cluster N1a are shown in stick representation and are colored in green and red, respectively. Sulfur atoms of the amino acid residues are colored in yellow. Numbers indicate the distance between atoms in Ångströms. The figure was generated from the crystal structure of the hydrophilic domain of complex I from *T. thermophilus* (PDB ID: 2FUG) using the PyMOL program. The mutagenesis wizard from the PyMOL package was used to exchange valine 133 of *T. thermophilus* to methionine 177 of *Y. lipolytica*. Based on steric constraints, the most likely methionine conformation was chosen.

### 3.5.2 Assembly and activity of complex I mutants

The impact of the point mutations on the content and activity of complex I as well as on the EPR spectrum at 40 K, where binuclear iron-sulfur clusters show signals, are summarized in Table 3.17. Exchanging the conserved valine 166 to the similar sized, however polar threonine, had no effect on complex I content and activity. Surprisingly, this was also true when this valine was exchanged with the more spacious and charged lysine. When the conserved alanine 175 was exchanged with the polar serine, this had no effect on content and activity of complex I. An exchange to lysine dramatically

reduced complex I content. Exchange of methionine 177 to histidine was well tolerated by complex I with respect to content and activity. However, introducing lysine resulted in a dramatic decrease of complex I content.

**Table 3.17: Effects of mutations introduced next to iron-sulfur cluster N1a in the 24-kDa subunit on mitochondrial membranes from *Y. lipolytica*.**

Strain	Complex I content <sup>a</sup>	Complex I activity <sup>b</sup>	EPR signals at 40 K (Figure 3.26)
	%	%	
parental	100±2	100±6	reference
V166T	123±2	89±4	not altered
V166K	105±4	107±7	not altered
A175S	101±2	115±3	not altered
A175K	20±1	n.d.	n.d.
M177H	90±3	90±5	not altered
M177K	19±1	n.d.	n.d.

Mean values ± SEM are given.

n.d., not determinable

<sup>a</sup> 100 % of complex I content corresponds to 1.3  $\mu\text{mol}\cdot\text{min}^{-1}\cdot\text{mg}^{-1}$  NADH:HAR oxidoreductase activity determined for the parental strain.

<sup>b</sup> DQA sensitive complex I specific dNADH:DBQ oxidoreductase activity ( $0.64 \mu\text{mol}\cdot\text{min}^{-1}\cdot\text{mg}^{-1}$  was measured for the parental strain) was normalized to complex I content. The ratio of 0.64/1.3 for the parental strain was set as 100 % complex I activity.

The flavoprotein part of complex I, which is composed of the 24-kDa and the 51-kDa subunits, and especially the FMN molecule in the 51-kDa subunit are essential for NADH:HAR oxidoreductase activity (Gavrikova et al., 1995).

Since a mutagenesis of the 24-kDa subunit could have an impact on the adjacent 51-kDa subunit, the values for complex I content given in Table 3.17 might not be reliable. Therefore, complex I content was also assessed by 2D gels (Tricine-SDS-PAGE after blue-native PAGE) following silver staining. 2D gels verified that in

contrast to mutants V166T, V166K, A175S and M177H, there was no assembled complex I in mitochondrial membranes from mutants A175K and M177K (data not shown). Moreover, 2D gels also revealed that the 24-kDa subunit mutations did not result in a subcomplex of complex I, which lacks the flavoprotein part.

### 3.5.3 EPR spectra of the N1 signal

Mitochondrial membranes from mutant strains which had a complex I content of at least 30 % were analyzed by EPR. No changes in the line shape of the N1 signal were visible and no additional EPR signal appeared when mitochondrial membranes were reduced with 2 mM NADH and spectra were recorded at 40 K and 5 mW microwave power (see Figure 3.26).

Just the spectrum from mutant V166T distinctly differed from the parental strain spectrum in signal intensities. However, this difference most probably originated from the higher complex I content in mitochondrial membranes from this mutant (see Table 3.17).

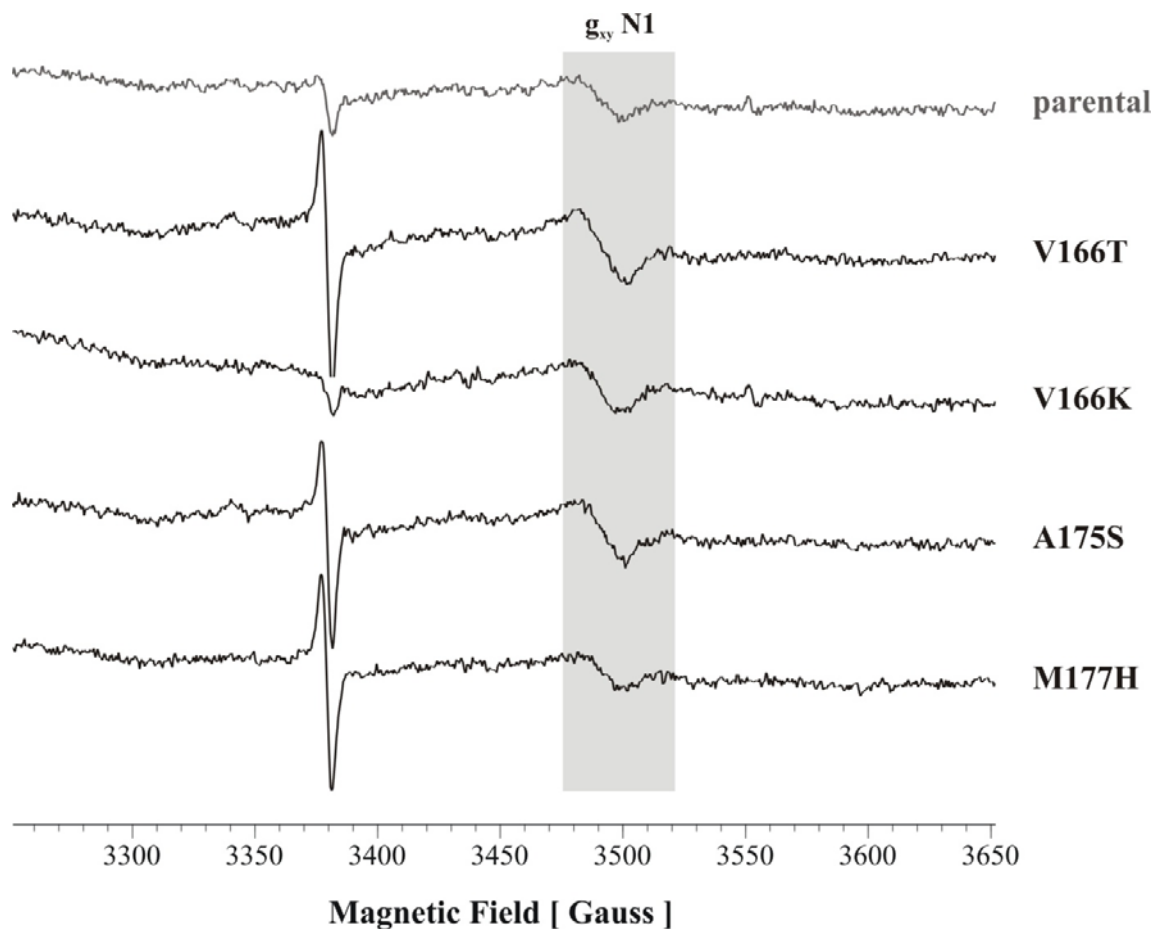


**Figure 3.26: EPR spectra of mitochondrial membranes from point mutants close to iron-sulfur cluster N1a recorded at 40 K and 5 mW microwave power.** Signals arising from iron-sulfur cluster N1 are shaded in gray. The mutant spectra were not significantly different from the parental strain spectrum. Mitochondrial membranes (~20 mg protein per ml for mutant V166K, ~25 mg protein per ml for all other strains) were reduced with 2 mM NADH. EPR spectra were recorded by Dr. Klaus Zwicker.

The finding that there were no significant changes in the EPR spectra indicates that the redox midpoint potential of iron-sulfur cluster N1a was not sufficiently increased by the point mutations to allow reduction of iron-sulfur cluster N1a with NADH to any considerable extent.

Therefore, also the stronger reductant dithionite was used to reduce mitochondrial membranes. Dithionite has a lower redox potential ( $E^{o'}$  ~ -420 mV) than NADH ( $E^{o'}$  ~ -320 mV) and could possibly have reduced iron-sulfur cluster N1a when the mutation only moderately elevated the redox midpoint potential. However, EPR spectra of mutants recorded at 40 K and 5 mW microwave power were unchanged (data not shown). This was also true when EPR spectra from mitochondrial membranes reduced



with NADH alone or with NADH and dithionite were recorded at different settings (12K and 5 mW microwave power; data not shown). These results indicate that the shift in the redox midpoint potential of iron-sulfur cluster N1a, if any, was not sufficient to make iron-sulfur cluster N1a reducible and hence EPR detectable. Alternatively, low redox midpoint potential of iron-sulfur cluster N1a is not the reason for its EPR silence.

### 3.5.4 Mutagenesis of iron-sulfur cluster N1a ligands

It is possible that the N1 EPR signal is composed of the EPR signal of iron-sulfur cluster N1b and some minor contributions from iron-sulfur cluster N1a. Under this assumption, changes in the N1 EPR signal could become detectable when iron-sulfur cluster N1a was lost completely. To selectively eliminate iron-sulfur cluster N1a, two of the four cysteine ligands were individually exchanged to alanines.

The exchange of cysteine 168 or cysteine 172 in the 24-kDa subunit to alanine resulted in strongly decreased complex I content (see Table 3.18). Therefore, it was not possible to record EPR spectra from the cysteine mutants.

**Table 3.18: Effects of mutations introduced into the cysteine ligands of iron-sulfur cluster N1a in mitochondrial membranes from *Y. lipolytica*.**

Strain	Complex I content <sup>a</sup>	Complex I activity <sup>b</sup>
	%	%
parental	100±2	100±6
C168A	13±1	n.d.
C172A	24±1	n.d.

Mean values ± SEM are given.

n.d., not determinable

<sup>a</sup> 100 % of complex I content corresponds to 1.3  $\mu\text{mol}\cdot\text{min}^{-1}\cdot\text{mg}^{-1}$  NADH:HAR oxidoreductase activity determined for the parental strain.

<sup>b</sup> DQA sensitive complex I specific dNADH:DBQ oxidoreductase activity (0.64  $\mu\text{mol}\cdot\text{min}^{-1}\cdot\text{mg}^{-1}$  was measured for the parental strain) was normalized to complex I

content. The ratio of 0.64/1.3 for the parental strain was set as 100 % complex I activity.

Since complex I content was assessed as NADH:HAR oxidoreductase activity, which requires the 51-kDa subunit, a decrease in NADH:HAR oxidoreductase activity in the 24-kDa subunit mutants could be due to a disordered 51-kDa subunit without an effect on complex I assembly, or might have resulted in a subcomplex of complex I lacking the flavoprotein part only. However, silver stained 2D gels excluded both possibilities, showing that there was neither an assembled complex I, nor a subcomplex of complex I in mitochondrial membranes from mutant C168A and C172A (data not shown).

## 4 Discussion

### 4.1 Exploring the proposed ubiquinone and inhibitor binding cavity

Based on the crystal structure of the hydrophilic domain of complex I from *T. thermophilus* (Sazanov and Hinchliffe, 2006), a large number of point mutations were introduced in order to systematically explore the entire surface of the proposed quinone and inhibitor binding pocket of complex I.

#### 4.1.1 Mapping of mutation effects into the structure

Only very few mutations interfered with complex I assembly; however, many mutants decreased complex I activity to various extents (see Table 3.1). Clearly, the effects of the mutations should be discussed in the context of their location within the large putative quinone binding pocket. However, a valid interpretation of the data rests on the assumptions that the used structure adequately represents the putative quinone binding pocket of *Y. lipolytica* and that each point mutation primarily has a local impact. Since the crystal structure of complex I from *Y. lipolytica* or any other eukaryote has not been solved yet, only the structure of the hydrophilic domain from *T. thermophilus* is available (Sazanov and Hinchliffe, 2006). In Figure 4.1, the degree of conservation of the proposed quinone binding pocket between *Y. lipolytica* and *T. thermophilus* is illustrated. Invariant residues are highlighted in red, highly similar and weakly similar residues are colored in orange and yellow, respectively (see the corresponding multiple sequence alignment in Figure 8.1 and Figure 8.2). Indeed, it seems that especially amino acid residues within the proposed quinone and inhibitor binding cavity are highly conserved. Minor differences may reflect the fact that complex I from *T. thermophilus* uses menaquinone as a substrate (Yano et al., 1997).

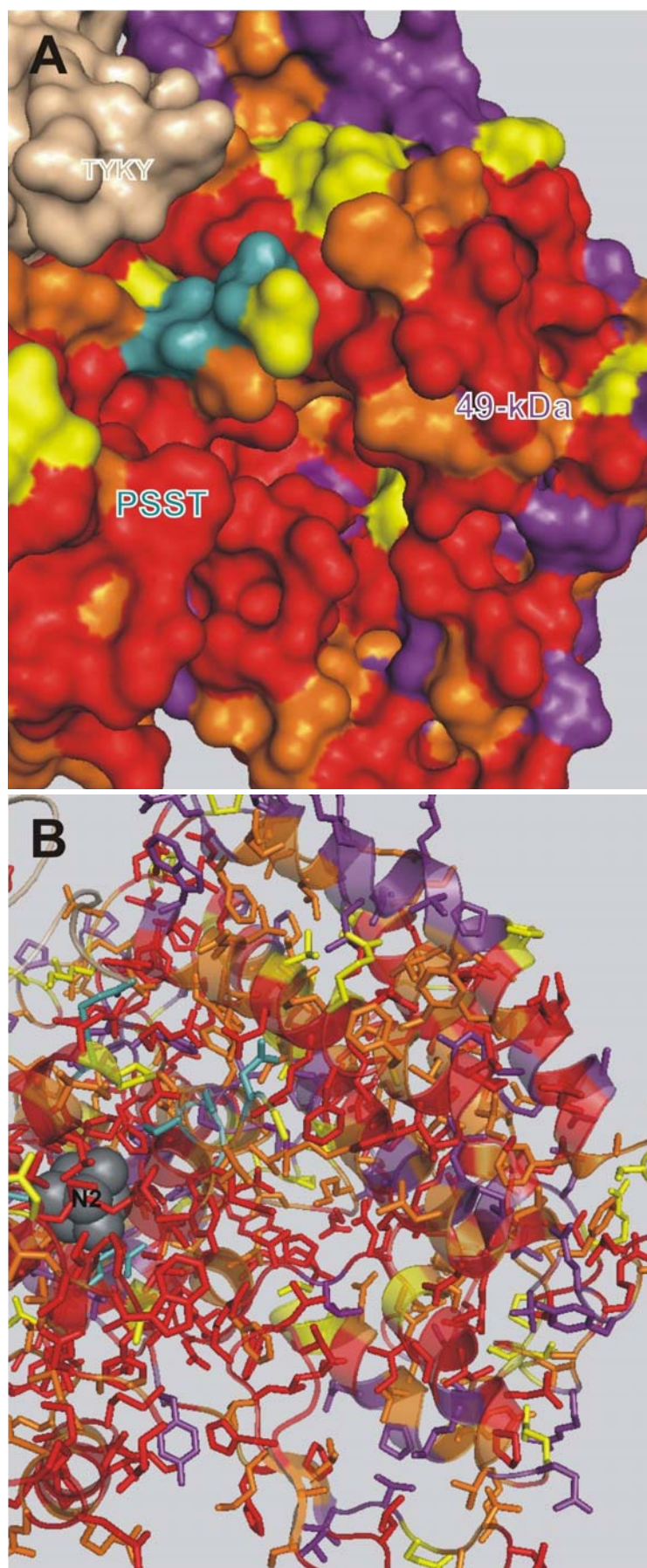


**Figure 4.1: Conserved regions within the quinone and inhibitor binding cavity.** Same view as in Figure 3.3. A, surface representation. B, schematic representation, amino acid residues are shown in stick representation, iron-sulfur cluster N2 is shown in gray as space-filled model. Amino acid residues are colored according to their conservation between *Y. lipolytica* and *T. thermophilus*: red, invariant residues; orange, highly similar; yellow, weakly similar residues. Amino acid residues from the PSST subunit which are not conserved are colored in cyan. Not conserved residues from the 49-kDa subunit are colored in purple (see Figure 8.1 for the corresponding multiple sequence alignment). Especially amino acid residues from the proposed quinone binding cavity are highly conserved between *Y. lipolytica* and *T. thermophilus*. However, phenylalanine 132, alanine 398 and proline 402 from the 49-kDa subunit of *T. thermophilus* located in the left part of the pocket, distal to iron-sulfur cluster N2, are changed to serine 189 (in purple, hidden in A), glycine 445 (in yellow) and leucine 459 (in purple) in *Y. lipolytica*, respectively – possibly owing to the fact that complex I from *T. thermophilus* uses menaquinone as a substrate (Yano et al., 1997). Amino acid residues from the TYKY subunit (beige) were not analyzed. The figure was generated from the crystal structure of the hydrophilic domain of complex I from *T. thermophilus* (PDB ID: 2FUG) by using the PyMOL program. The mutagenesis wizard of the PyMOL package was used to match the *Y. lipolytica* sequence when a residue was not conserved between *T. thermophilus* and *Y. lipolytica*.

Several observations indicate that the effects of the introduced point mutations are rather local. (i) When mitochondrial membranes carrying the most drastic changes at almost all positions were analyzed by EPR, the spectra of iron-sulfur cluster N2 were unchanged in almost all cases (see Figure 3.1 and Figure 3.2), indicating that no long range rearrangements were induced by the mutations. The only exceptions were some drastic exchanges of tyrosine 144 (see Figure 3.10). However, this observation most likely rather reflects the close proximity of tyrosine 144 to iron-sulfur cluster N2 than global structural changes of the quinone and inhibitor binding pocket. (ii) Only 8 out of 94 mutations interfered with complex I assembly (see Table 3.1). (iii) According to the structure from *T. thermophilus*, the exchanged amino acid residues are all located at the surface of the proposed quinone and inhibitor binding cavity (see Figure 3.3); therefore, the integration of very different side chains without changing the overall structure seems feasible.

Since the proposed quinone and inhibitor binding cavity is quite conserved and the effects of the point mutations are probably rather local, it seems valid to map the effects of the mutations into the structure of the proposed quinone and inhibitor binding cavity of the hydrophilic domain from *T. thermophilus*.

### 4.1.2 Identification of functional domains

Not individual mutations but the careful analysis of a large number of systematically chosen mutations allows the identification of domains which are critical, less critical and not critical for complex I activity. As illustrated in Figure 3.3, most residues that are critical for complex I activity form a path reaching from a loop in the N-terminal three stranded  $\beta$ -sheet into the cavity to tyrosine 144 located next to iron-sulfur cluster N2 (colored in red). Residues located around this area are less critical for complex I activity (colored in yellow and green). Interestingly, residues located deeper in the cavity, where the PSST and the 49-kDa subunits form a narrow crevice, can be exchanged without a major effect on complex I activity (colored in blue). However, they still must have an important function, since some of them like glutamate 218 and arginine 224, are highly conserved (see Figure 8.1). One can speculate that they are involved in regulating complex I activity or might help to prevent ROS production at the putative quinone binding site.

Amino acid residues which are critical for complex I activity and are located close to iron-sulfur cluster N2, like tyrosine 144 and valine 460 in the 49-kDa subunit, are probably involved in quinone binding and reduction. Especially the highly conserved tyrosine 144 is very critical. This residue is located only 6-8 Å away from iron-sulfur cluster N2 and all exchanges introduced at this position resulted in almost complete loss of dNADH:DBQ activity (see Table 3.10). This was even the case for the very conservative exchange Y144F by which only the hydroxyl group was removed. Moreover, it was not possible to reactivate complex I activity in this mutant with a variety of salts (see Figure 3.15 and Figure 3.16). EPR spectra from mitochondrial membranes of the drastic mutants Y144R, Y144S and Y144I showed that the N2 signal was severely affected, as expected from the close proximity of this residue to iron-sulfur cluster N2 (see Figure 3.10). Consistently, the more conservative exchanges Y144H and Y144W exerted only minor effects on the EPR signal of iron-sulfur cluster N2 (see Figure 3.10, Figure 3.11, Figure 3.12 and (Kashani-Poor et al., 2001b)). Importantly, an unchanged N2-signal was recorded from mitochondrial membranes as well as from the purified enzyme with the most conservative exchange Y144F (see Figure 3.12). This indicated that loss of activity in the Y144F mutant resulted from perturbation of quinone binding and/or reduction, rather than interference with iron-sulfur cluster N2.

Histidine 95 in the 49-kDa subunit is also critical for complex I activity (see Table 3.1). However, this histidine is located at least 16 Å (edge-to-edge distance) away from iron-sulfur cluster N2, too far away for efficient electron tunneling at catalytic sites (Page et al., 1999; Moser et al., 2006b). Therefore it seems that histidine 95 and other critical residues located at some distance to iron-sulfur cluster N2 form an access path for the substrate quinone. The same could apply for histidine 91 (Grgic et al., 2004), aspartate 99, aspartate 115, aspartate 136 and glutamate 140 in the PSST subunit (Garofano et al., 2003; Ahlers et al., 2000). As an alternative explanation, currently it cannot be excluded that this part of the enzyme is so critical because it is involved in the tight coupling of the redox reaction to the conformational changes leading to proton translocation across the inner mitochondrial membrane. Similarly, exchanges of conserved amino acid residues located in the hydrophobic subunits ND1 (Zickermann et al., 1998; Kurki et al., 2000; Kervinen et al., 2006), ND2 (Amarneh and Vik, 2003), ND3 (Kao et al., 2004a), ND4 (Majander et al., 1996; Torres-Bacete et al., 2007; Euro et al., 2008a), ND4L (Kervinen et al., 2004; Kao et al., 2005b), ND5 (Majander et al., 1996) and ND6 (Kao et al., 2005a; Pätsi et al., 2008) not only interfered with proton translocation but also with NADH:Q oxidoreductase activity of complex I. Since residues from these subunits are not located next to the proposed quinone binding pocket close to iron-sulfur cluster N2 (Sazanov and Hinchliffe, 2006), it seems that they are involved in the tight coupling of the redox reaction to proton pumping and that it is not possible to generate an “ideally uncoupled phenotype” in complex I per se (Euro et al., 2008a; Zickermann et al., 2008; Zickermann et al., 2009).

### 4.1.3 Role of tyrosine 144

Mutations which affect the proposed quinone binding site should change the affinity of the enzyme to the substrate. Interestingly, no mutant with considerable activity displayed a significantly altered *apparent*  $K_m$  value for DBQ (see Table 3.1). However, drastically increased *apparent*  $K_m$  values for Q<sub>1</sub> along with moderately decreased dNADH:Q<sub>1</sub> oxidoreductase activities were found in some tyrosine 144 mutants (see Table 3.12). Moreover, in mutants Y144F and Y144W significantly increased *apparent*  $K_m$  values for Q<sub>2</sub> along with normal  $V_{max}$  values for the dNADH:Q<sub>2</sub> oxidoreductase

activity were measured (see Table 3.13), indicating that the quinone binding site was indeed targeted in this study.

Proton pumping experiments with complex I from mutants Y144F and Y144W clearly showed that the dNADH:Q<sub>1</sub> oxidoreductase activity was coupled to proton pumping (see Figure 3.19 and Figure 3.20), hence Q<sub>1</sub> reduction must take place at the physiological site. These data also demonstrated that the tyrosine was not absolutely essential for proton pumping. However, it would be interesting to determine whether the tyrosine mutants pump protons at the same stoichiometry as the parental strain.

There are several possibilities concerning the precise role of tyrosine 144 in the catalysis of quinone reduction: (i) Tyrosine 144 might be involved in governing conformational and/or electrostatic changes necessary for quinone binding and release. However, it seems unlikely that the absence of one hydroxyl group in mutant Y144F would lead to such a dramatic effect on activity (see Table 3.10), which in addition would depend on the quinone side chain (see Table 3.10, Table 3.12 and Table 3.13). (ii) Tyrosine 144 might be involved in protonating the semiquinone by its hydroxyl group. The results of reactivation attempts (see chapter 3.3.5) and the finding that the pH dependence of the residual activity of the Y144F mutant was unchanged (see Figure 3.14 and Table 3.11) provide no support for this assumption; however it cannot be excluded that the active site is not accessible from the bulk phase during critical catalytical steps. Also, it is hard to envision how protonation of the semiquinone by the hydroxyl group would depend on the quinone side chain. (iii) Tyrosine 144 might be involved in electron transfer from iron-sulfur cluster N2 to the quinone. This seems unlikely, since the distance between donor and acceptor is much more critical for electron transfer than the protein matrix (Page et al., 1999; Moser et al., 2006b) and a tyrosine radical was never observed in complex I. Alternatively, tyrosine 144 might have an indirect effect on the electron transfer from iron-sulfur cluster N2. However, a direct or indirect effect again would not explain the difference observed with different quinone side chains. (iv) Tyrosine 144 might be involved in stabilization of the transition state, but this seems rather unlikely, since this should slow down the enzymatic reaction for all quinone substrates irrespective of the quinone side chain. (v) Tyrosine 144 might be involved in making sure that the quinone binds in a proper orientation at the active site. Formation of a hydrogen bond between the hydroxyl group



and the quinone head group could explain why an increased *apparent*  $K_m$  value for Q<sub>1</sub> and Q<sub>2</sub> was observed in the Y144F mutant. However, the aromatic feature of tyrosine 144 seems to be critical as well, since considerable dNADH:Q<sub>1</sub> oxidoreductase activity was found only in the Y144F, Y144W and Y144H mutants. Therefore, tyrosine 144 might help orientating the quinone substrate via stacking of the aromatic moieties.

Taken together, it seems that tyrosine 144 is important for quinone binding and orientation at the quinone binding site by both hydrogen bonding and aromatic interactions.

#### 4.1.4 Properties of different quinone substrates

Interestingly, for mitochondrial membranes from the parental strain the *apparent*  $K_m$  value for Q<sub>2</sub> was found to be smaller than that for Q<sub>1</sub>, which in turn was smaller than that for DBQ (see Table 3.1, Table 3.12 and Table 3.13). With partition coefficients (log  $P$  cyclohexane/water) of 5.1, 2.65 and 7.2, respectively (Degli Esposti et al., 1996; Lenaz, 1998), these quinones are all very hydrophobic, which means that almost all the substrate distributes to the membrane bilayer and only a small negligible fraction is dissolved in the aqueous phase. Thus, taking the differences in the partition coefficients into account would not change the general outcome that the highest affinity was observed for the quinone with two isoprene units whereas the lowest affinity was observed for the quinone with the decyl side chain. This result is consistent with what was found for complex I from *B. taurus* (Fato et al., 1996; Lenaz, 1998; Hano et al., 2003) and *P. denitrificans* (Zickermann et al., 1998; Kurki et al., 2000) and further supports the finding that the structure of the quinone side chain is specifically recognized by complex I, as demonstrated earlier (Sakamoto et al., 1998). An important consequence of these results is that in future assays Q<sub>1</sub> or Q<sub>2</sub> should be used to determine *apparent*  $K_m$  values for the quinone substrate. DBQ seems to be unsuitable for this purpose, since mutations could further decrease the already low affinity of DBQ to the binding site, which could result in loss of activity, as seems to be the case for the Y144F, Y144W and Y144H mutants. However, DBQ is the substrate of choice to assay maximal NADH:Q oxidoreductase activity of complex I, since it gives higher rates than Q<sub>1</sub> or Q<sub>2</sub>, which are almost fully sensitive to complex I inhibitors. Moreover, the

dNADH:DBQ oxidoreductase activity reflects complex I activity with endogenous Q<sub>9</sub> better than the dNADH:Q<sub>1</sub> oxidoreductase activity (see Table 3.3 and Table 3.4).

#### 4.1.5 The inhibitor binding sites

Some photoaffinity labeling studies identified the PSST (Schuler et al., 1999; Schuler and Casida, 2001b; Nakamaru-Ogiso et al., 2003a) and the 49-kDa subunits (Nakamaru-Ogiso et al., 2003a; Ichimaru et al., 2008; Murai et al., 2009) to comprise the binding site of specific complex I inhibitors. Consistently, several exchanges at the proposed quinone binding pocket described here displayed drastic effects on the sensitivity of complex I towards specific inhibitors (see Table 3.5 and Table 3.6), further confirming the concept that hydrophobic complex I inhibitors act on the putative quinone binding pocket located at the interface of the 49-kDa and PSST subunit (Darrouzet et al., 1998; Kashani-Poor et al., 2001b; Prieur et al., 2001; Kerscher et al., 2001c; Brandt et al., 2003; Kerscher et al., 2005).

Furthermore, the results presented here show that different types of inhibitors apparently bind to distinct and well defined regions within the large quinone binding cavity (see Figure 3.4). Exchanges which affected inhibition by the type A inhibitor DQA and the type B inhibitor rotenone clustered in a subdomain of the quinone binding pocket corresponding to the former [NiFe] site in homologous hydrogenases. Thus, DQA seems to penetrate deeper into this subdomain. Exchanges which affected inhibition by the type C inhibitor C<sub>12</sub>E<sub>8</sub> were found in a different region, where the 49-kDa and the PSST subunits form a narrow crevice. This is consistent with the classification of complex I inhibitors (Friedrich et al., 1994; Degli Esposti and Ghelli, 1994; Degli Esposti, 1998) which was rightly criticized as rather arbitrary (Okun et al., 1999a). Not surprisingly, changing more exposed residues located inbetween the putative binding sites of type A, B and C inhibitors affected inhibition by all three inhibitors. These results confirmed the earlier concept that different types of complex I inhibitors bind to different but partially overlapping binding sites within a large quinone binding pocket as revealed by direct competition binding assays (Okun et al., 1999a). However, the interpretation of the competition binding assays results was questioned. It was suggested that apparent competitive behavior of inhibitors may be caused by

negative allosteric effects, i.e. that the binding of one inhibitor to one binding site induces structural changes which prevent the binding of another inhibitor to a remote binding site (Schuler and Casida, 2001a; Ino et al., 2003; Yagi and Matsuno-Yagi, 2003; Duval et al., 2006; Ichimaru et al., 2008). Alternatively, it was speculated that different inhibitors might inhibit different steps in the catalytic cycle and therefore compete functionally, not spatially (Hirst, 2005a). However, the data presented here clearly indicate that the binding sites of different types of complex I inhibitors indeed overlap spatially within one large binding cavity. Moreover, since these results for the first time allowed the localization of the binding sites of the three inhibitor types within the structure of the quinone binding cavity, they added some new insights: (i) It seems that the binding sites for type A and type C inhibitors overlap, a result which was not observed before (Okun et al., 1999a). (ii) Residues located in the region corresponding to the [NiFe] site in homologous hydrogenases are not essential for complex I activity but are rather responsible for inhibitor binding. However, it should be mentioned that the experimental setup used here does not allow for the identification of residues that are important for inhibitor binding and essential for catalytic activity.

Amiloride is a known inhibitor of  $\text{Na}^+/\text{H}^+$  antiporters (Mochizuki and Oosawa, 1985; Kleyman and Cragoe, 1988; Counillon et al., 1993; Kuroda et al., 1994; Masereel et al., 2003) and the amiloride derivative EIPA was shown to inhibit complex I (Nakamaru-Ogiso et al., 2003a; Nakamaru-Ogiso et al., 2003b; Stolpe and Friedrich, 2004). Since the ND5 subunit shares some sequence similarity with  $\text{Na}^+/\text{H}^+$  antiporters (Hamamoto et al., 1994; Hiramatsu et al., 1998; Mathiesen and Hägerhäll, 2002; Mathiesen and Hägerhäll, 2003) and EIPA was shown to decrease the photoaffinity labeling with a fenpyroximate analogue of a subunit tentatively assigned as ND5 (Nakamaru-Ogiso et al., 2003a), it was suggested that the binding site of EIPA is located in the ND5 subunit of complex I.

In *Y. lipolytica*, deletion of the NB8M subunit leads to the formation of a subcomplex of complex I lacking the ND5 subunit (S. Krack and L. Sokolova, personal communication). Surprisingly, this subcomplex was found to be sensitive to EIPA inhibition (Dr. Stefan Dröse, personal communication). Moreover, with mitochondrial membranes from the *nb8m* $\Delta$  strain an  $I_{50}$  value of 23  $\mu\text{M}$  was determined for EIPA (see Table 3.7), which is not different from what was found for mitochondrial membranes

from the 49-kDa and PSST subunits parental strains (21  $\mu$ M and 23  $\mu$ M, respectively, see Table 3.8 and Table 3.9). If no holocomplex is present in mitochondrial membranes from the *nb8m* $\Delta$  strain, this result would clearly demonstrate that the inhibitor binding site for EIPA is not located in the ND5 subunit.

Since most complex I inhibitors are anticipated to act at the quinone binding site, the  $I_{50}$  value for EIPA was determined for some mutants of the proposed quinone binding pocket. Indeed, some exchanges changed the  $I_{50}$  value of EIPA (see Table 3.8 and Table 3.9). Interestingly, these exchanges clustered in a region where effects on type A, B and C inhibitors were found (see Figure 3.4 and Figure 3.5), indicating that EIPA is a typical complex I inhibitor acting at the quinone binding site. But the observed effects on the  $I_{50}$  value for EIPA were either relatively small or indicated increased sensitivity. However, only mutations that cause pronounced resistance would provide positive evidence that EIPA acts at the quinone binding site.

#### 4.1.6 Comparison to results obtained with other model organisms

It would be interesting to compare the results described here to results obtained in mutagenesis studies with other model organisms. However, only few mutants were made in complex I from other species, and only nine were introduced at the proposed quinone binding pocket assembled by the PSST and 49-kDa subunit (see Table 4.1 and Table 4.2).

Two exchanges were introduced into the 49-kDa subunit of *R. capsulatus* (Prieur et al., 2001). Similar to what was found in *Y. lipolytica*, they did not decrease complex I content; however, mutation D405E decreased complex I activity more strongly, whereas mutation V407M did not decrease complex I activity to the same extent when compared to the corresponding mutations in *Y. lipolytica* (see Table 4.1). Both exchanges were introduced in a region of the proposed quinone and inhibitor binding cavity where effects on the  $I_{50}$  values for DQA and rotenone were identified in *Y. lipolytica*. Consistently, mutant V407M displayed a drastic effect on the  $I_{50}$  value for rotenone.

Two spontaneous mutations affecting the 49-kDa subunit from *Helicobacter pylori* conferred hypersensitivity towards rotenone (Mills et al., 2004). Although the corresponding mutation in *Y. lipolytica* did not significantly change the  $I_{50}$  value for

rotenone, both residues are located right in the region, where drastic effects on the  $I_{50}$  values for rotenone and DQA were observed in *Y. lipolytica*.

In complex I from *E. coli*, two exchanges were introduced in the 49-kDa subunit at the proposed quinone and inhibitor binding cavity (Belevich et al., 2007). The results from mutants H228A and R274A largely corroborated the results found in *Y. lipolytica* (see Table 4.1). However, mutant R274A decreased complex I content in *E. coli*, whereas mutant H228A showed some residual complex I activity.

**Table 4.1: Mutations affecting the 49-kDa subunit at the quinone and inhibitor binding cavity in other model organisms.**

Mutant in <i>Y. lipolytica</i>	Equivalent in other species	Complex I content		Complex I activity		$I_{50}$ for CI inhibitors	
		%		%		nM	
		<i>Y. l.</i>	Other	<i>Y. l.</i>	other	<i>Y. l.</i>	other
<i>E. coli</i>		Type A <sup>a</sup>					
parental <sup>b, c</sup>	parental <sup>d</sup>	100	100	100	100	13-17	~2
H95A <sup>b</sup>	H228A <sup>d</sup>	130	96	<5	33	n.d.	~2
R141A <sup>c</sup>	R274A <sup>d</sup>	130	49	17	<5	n.d.	~2
<i>R. capsulatus</i>		Rotenone					
parental	parental <sup>e</sup>	100±3	100	100±5	100	530	~100
D458E <sup>f</sup>	D405E <sup>e</sup>	83±1	~100	89±3	~50	2200	~140
V460M	V407M <sup>e</sup>	100±2	~200	16±2	~50	760 <sup>c</sup>	~600
<i>H. pylori</i>		Rotenone					
parental	parental <sup>g</sup>	100±3	-	100±5	-	530	ref.
G455S <sup>h</sup>	G398S <sup>g</sup>	98±1	-	72±4	-	700	hyper.
-	F404S <sup>g</sup>	-	-	-	-	-	hyper.

n.d., not determinable

ref., reference; hyper., hypersensitivity

<sup>a</sup> DQA was used for *Y. lipolytica* and rolliniastatin was used for *E. coli*

<sup>b</sup> data from (Grgic et al., 2004)

<sup>c</sup> data from (Kashani-Poor et al., 2001b)

<sup>d</sup> data from (Belevich et al., 2007)

<sup>e</sup> data from (Priour et al., 2001)

<sup>f</sup> data from (Fendel et al., 2008)

<sup>g</sup> data from (Mills et al., 2004)

<sup>h</sup> point mutations were generated by U. Fendel

Three amino acid changes were introduced into the PSST subunit from *E. coli* (Flemming et al., 2006). Mutant E87Q strongly decreased complex I activity, whereas mutant E163Q only slightly interfered with complex I activity in *E. coli* (see Table 4.2). Interestingly, the opposite effects were found in complex I from *Y. lipolytica*.

**Table 4.2: Mutations affecting the PSST subunit at the quinone and inhibitor binding cavity in other model organisms.**

Mutant in <i>Y. lipolytica</i>	Equivalent in <i>E. coli</i>	Complex I content		Complex I activity		$I_{50}$ for CI inhibitors	
		%		%		effect	
		<i>Y. l.</i>	<i>E. c.</i>	<i>Y. l.</i>	<i>E. c.</i>	<i>Y. l.</i>	<i>E. c.</i>
parental <sup>b,c</sup>	parental <sup>a</sup>	100	100	100	100	ref.	s.
E89Q <sup>b</sup>	E67Q <sup>a</sup>	100	~75	88	10	n.a.	n.s.
-	E67D <sup>a</sup>	-	~88	-	78	-	s.
E185Q <sup>c</sup>	E163Q <sup>a</sup>	110	~63	35	76	n.a.	s.

ref., reference

n.a., not altered

s., complex I activity sensitive to piericidin A

n.s., residual complex I activity not sensitive to piericidin A

<sup>a</sup> data (Flemming et al., 2006)

<sup>b</sup> data from (Ahlers et al., 2000),

<sup>c</sup> data from (Garofano et al., 2003)

Taken together, the effects of the few exchanges introduced at the putative quinone and inhibitor binding pocket of other model organisms overall correspond well to those observed with complex I from *Y. lipolytica*. Larger variations may be due to different protocols for sample preparation and kinetic measurements used in different laboratories. However, in order to exclude fundamental differences between the eukaryotic and the prokaryotic enzyme broader mutagenesis studies in prokaryotes will be needed.

#### 4.1.7 Location of the quinone binding site(s)

Clearly, the active site for quinone reduction must be located within electron tunnelling distance to its immediate electron donor. Iron-sulfur cluster N2, ligated by the PSST

subunit, is presumably the electron donor to quinone, since it was found to undergo spin-spin interactions to the semiquinone species  $SQ_{NF}$  and a distance of 8-12 Å between the two paramagnetic species was calculated (Vinogradov et al., 1995; Yano et al., 2005). Together with the structure of the hydrophilic domain of complex I from *T. thermophilus* (Sazanov and Hinchliffe, 2006), this finding reveals that the enzymatically relevant quinone binding site(s) must be located at the interface of the PSST and the 49-kDa subunit. This is consistent with the results presented here and earlier results from mutagenesis (Darrouzet et al., 1998; Kashani-Poor et al., 2001b; Prieur et al., 2001; Grgic et al., 2004; Mills et al., 2004) and photoaffinity labeling studies (Schuler et al., 1999; Schuler and Casida, 2001b; Nakamaru-Ogiso et al., 2003a; Nakamaru-Ogiso et al., 2003a; Ichimaru et al., 2008).

It should be mentioned that other studies gave indications for quinone binding sites in other subunits. Sequence comparison suggested that the ND4 and the ND5 subunits harbour a conserved putative quinone binding motif (aliphatic-(X)<sub>3</sub>-H-(X)<sub>2/3</sub>-(L/T/S) (Fisher and Rich, 2000). However, this suggestion is difficult to reconcile with the finding that the ND4 and ND5 subunits are located in the distal part of the membrane domain (Sazanov and Walker, 2000; Cardol et al., 2002; Holt et al., 2003; Baranova et al., 2007b) and therefore around 100 Å away from iron-sulfur cluster N2, the immediate electron donor to quinone. In addition, exchanging conserved histidines in the ND4 subunit which were predicted to be central to this motif had no significant effects on quinone or inhibitor binding (Torres-Bacete et al., 2007).

Various other mutagenesis studies suggested that the quinone and inhibitor binding pocket of complex I was located in the ND1 (Ghelli et al., 1997; Majander et al., 1996; Zickermann et al., 1998; Kurki et al., 2000), ND4 (Degli Esposti et al., 1994; Ghelli et al., 1997) and/or the ND6 subunit (Jun et al., 1996; Carelli et al., 1999; Pätssi et al., 2008). However, it cannot be excluded that these mutations might have caused long range effects on the quinone binding pocket at the interface between the PSST and the 49-kDa subunit, especially since a tight and reversible coupling between the quinone reduction site near iron-sulfur cluster N2 and subunits of the membrane domain is assumed to be fundamental for proton translocation (Euro et al., 2008a; Zickermann et al., 2008; Zickermann et al., 2009).

In addition, photoaffinity labeling studies with different complex I inhibitors and a ubiquinone derivative suggest that the ND1 (Earley and Ragan, 1984; Earley et al., 1987; Yagi, 1987; Yagi and Hatefi, 1988; Hassinen and Vuokila, 1993; Schuler and Casida, 2001a; Murai et al., 2007; Murai et al., 2009), the ND4 (Gong et al., 2003), the ND5 (Nakamaru-Ogiso et al., 2003a) and/or even the mammal-specific B9 subunit (Heinrich and Werner, 1992; Heinrich et al., 1992) may comprise inhibitor and thus quinone binding sites. However, these studies are prone to generate false positive results, since hydrophobic inhibitors have a preference to associate with and thus predominantly label hydrophobic subunits. In addition, in some studies the photolabile group was attached at a large distance to the toxophoric moiety and therefore on rather flexible parts of the inhibitor. While this design can avoid a decrease in affinity, it also makes the labeling of protein parts not involved in inhibitor binding more likely, as criticized by Miyoshi and coworkers (Ichimaru et al., 2008; Murai et al., 2009).

Nevertheless, it is remarkable that many mutagenesis as well as photoaffinity labeling studies identified the ND1 subunit to harbour the quinone and inhibitor binding site. From these results it may be inferred that the large extramembraneous domains of the ND1 subunit may form a quinone ramp or channel to the proposed quinone binding pocket at the interface between the PSST and the 49-kDa subunits, as proposed by (Zickermann et al., 2009). This interpretation is consistent with other results which suggested that the ND1 subunit is in close proximity to subunits from the hydrophilic domain (Darrouzet et al., 1998; Sazanov et al., 2000; Dupuis et al., 2001; Di Bernardo and Yagi, 2001; Schuler and Casida, 2001a; Yagi and Matsuno-Yagi, 2003; Holt et al., 2003; Kao et al., 2004b; Baranova et al., 2007a; Sinha et al., 2009).

The identification of two (Suzuki and King, 1983; Burbaev et al., 1989; Vinogradov et al., 1995; Ohnishi et al., 2005) (temporarily even three (Magnitsky et al., 2002)) distinct ubisemiquinone species stimulated the proposal of different and spatially separated quinone binding site in complex I (Vinogradov, 1993; Vinogradov et al., 1995; Dutton et al., 1998; Ohnishi, 1998; Ohnishi and Salerno, 2005). However, the sum of the spin concentrations was never found to exceed 1 per complex I (van Belzen et al., 1997)(Dr. Klaus Zwicker, personal communication). In addition, fully active complex I from *Y. lipolytica* and *E. coli* was shown to contain 0.2-1 quinone molecules per complex I (Dröse et al., 2002; Verkhovskaya et al., 2008; Euro et al., 2008a). Therefore it seems



more likely that the spectroscopically different semiquinone species represent the same molecule in different states rather than two quinone molecules simultaneously bound at two spatially separated quinone binding sites.

The presence of only one large binding pocket for the substrate quinone was also deduced from the finding that all tested inhibitors, which are assumed to act at the quinone binding pocket, were shown to bind to overlapping binding sites (Okun et al., 1999a).

Taken together, there is no compelling evidence that in addition to the PSST and the 49-kDa subunits other subunits of complex I also harbor catalytically relevant quinone binding site(s). As a consequence, since the PSST and the 49-kDa subunits were shown to be located far up in the peripheral arm of complex I (Zickermann et al., 2003; Clason et al., 2007; Zickermann et al., 2008), all suggested coupling mechanisms which postulate quinone reduction in the membrane domain of complex I (Brandt, 1997; Dutton et al., 1998; Ohnishi and Salerno, 2005) can be ruled out.

#### 4.1.8 Properties of the quinone binding site

Several observations suggest that the specificity of the quinone binding site of complex I is not very high. (i) Structurally very different quinone analogs like DBQ, Q<sub>0</sub>, Q<sub>1</sub>, Q<sub>2</sub> and even duroquinone can serve as electron acceptors to assay the NADH:Q oxidoreductase activity (Di Virgilio and Azzone, 1982; Estornell et al., 1993; Hano et al., 2003) and all seem to accept electrons at the physiological site (Lenaz, 1998). In addition, studies with systematically modified quinone analogs showed that many structural alterations at the quinone head or tail are tolerated by the quinone binding site (Sakamoto et al., 1996; Ohshima et al., 1998; Sakamoto et al., 1998). Moreover, menaquinone is the natural substrate of complex I from *T. thermophilus* (Yano et al., 1997) and *E. coli* (Tran et al., 1997), although the proposed quinone binding pocket in *T. thermophilus* seems to be very similar to those which bind ubiquinone as a substrate (see Figure 4.1). (ii) In complex I from *Y. lipolytica* the apparent  $K_m$  values for DBQ, Q<sub>1</sub> and Q<sub>2</sub> are in the range of 8-15  $\mu$ M (see Table 3.1, Table 3.12 and Table 3.13). Since these quinones are very hydrophobic (log *P* cyclohexane/water 2.65-7.2 (Degli Esposti et al., 1996; Lenaz, 1998)), they almost completely distribute to the hydrophobic

membrane phase. Assuming that the concentration in the membrane phase is the relevant one and that the hydrophobic membrane phase comprises 0.1-1 % of the total volume under the assay conditions, a very high real  $K_m$  in molar range can be expected. Similar values were determined for complex I from *B. taurus* (Fato et al., 1996; Lenaz, 1998; Hano et al., 2003) and *P. denitrificans* (Zickermann et al., 1998; Kurki et al., 2000). (iii) A plethora of structurally very different inhibitors are thought to bind at the quinone binding site (Degli Esposti, 1998; Miyoshi, 1998; Lümmer, 1998; Okun et al., 1999b; Ushakova et al., 1999; Okun et al., 1999a; Okun et al., 2000). Therefore, it seems that the quinone binding site has been optimized for tight and efficient coupling of quinone reduction to conformational changes which lead to proton pumping rather than to specifically recognize the substrate.

## 4.2 The HRGXE-motif

It had been suggested that amino acid residues from the conserved HRGXE-motif form part of the quinone binding site (Prieur et al., 2001), since the HRGXE-motif shows some similarity to a proposed common sequence motif of quinone binding sites (Fisher and Rich, 2000). However, amino acid residues from the HRGXE-motif are not located within the putative quinone binding pocket, as revealed by the crystal structure of the hydrophilic domain of complex I from *T. thermophilus* (Sazanov and Hinchliffe, 2006) (see also Figure 3.22). Instead, it seems that the HRGXE-motif plays an important structural role, since most exchanges described here interfered with complex I assembly. This was even true for the very conservative exchanges R121K and E124D. Arginine 121 is highly conserved in *Y. lipolytica*, *N. crassa*, *B. taurus*, *H. sapiens*, and also in bacteria like *P. denitrificans*, *R. capsulatus* and *E. coli*. However, a threonine is found at this position in the *T. thermophilus* sequence (see Figure 3.21). The structure of the hydrophilic domain of complex I from *T. thermophilus* reveals that this threonine (64 in *T. thermophilus*) forms a hydrogen bond to an arginine residue from the PSST subunit (83 in *T. thermophilus*) (see Figure 4.2). Interestingly, this arginine is located in close proximity to iron-sulfur cluster N2 and forms a hydrogen bond to a sulfur atom of iron-sulfur cluster N2 through a backbone nitrogen.

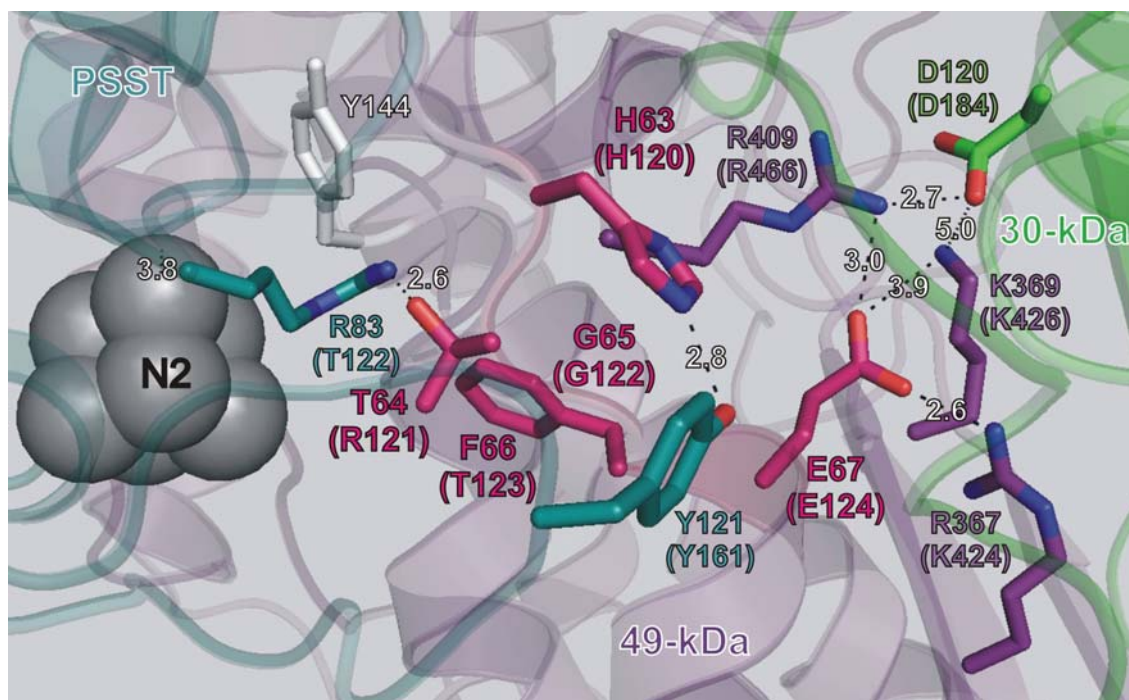


**Figure 4.2: Spatial arrangement of the HRGXE-motif which reaches from iron-sulfur cluster N2 to the 30-kDa subunit.** Amino acid residues from the motif are highlighted in pink and are shown in stick representation. Additional amino acid residues which interact with those of the motif are also shown in stick representation. Numbers indicate the distances between atoms in Ångströms. Amino acid residues are labeled according to *T. thermophilus* numbering, *Y. lipolytica* numbering is given in brackets. For a rough orientation tyrosine 144 is highlighted in white stick representation. Iron-sulfur cluster N2 is shown as a space fill model, the PSST, 49-kDa and 30-kDa subunits are shown in schematic representation. The figure was generated from the crystal structure of the hydrophilic domain of complex I from *T. thermophilus* (PDB ID: 2FUG) by using the PyMOL program.

However, at the position of this arginine a conserved threonine is found in the amino acid sequence of *Y. lipolytica*, *N. crassa*, *B. taurus*, *H. sapiens*, *P. denitrificans*, *R. capsulatus* and *E. coli* (see Figure 4.3). This might explain why the conserved HRGXE-motif is changed to HTGXE-motif in *T. thermophilus*. The concomitant exchange of arginine to threonine in the 49-kDa subunit and threonine to arginine in the PSST subunit in *T. thermophilus* allows the formation of a hydrogen bond with reversed polarity, preserving the overall structure. The R121K mutation in the 49-kDa subunit from *Y. lipolytica* may disrupt the hydrogen bond and thereby destabilize complex I.

```

Y. lipolytica      RASPRQSDIMIVAGTLTNKMAPVLRQVYDQMPEPRWVISMGSCANGGGYYHFSYSVV 164
N. crassa        RASPRQSDVMIVAGTLTNKMAPALRQVYDQMPDRWVISMGSCANGGGYYHYSYSVV 180
P. denitrificans RASPRQSDLMIVAGTLTNKMAPALRKVYDQMPEPRYVISMGSCANGGGYYHYSYSVV 132
R. capsulatus    RASPRQSDVMIVAGTLTNKMAPALRKVYDQMPEPRYVISMGSCANGGGYYHYSYSVV 135
B. taurus       RASPRQSDVMIVAGTLTNKMAPALRKVYDQMPEPRYVISMGSCANGGGYYHYSYSVV 170
H. sapiens      RASPRQSDVMIVAGTLTNKMAPALRKVYDQMPEPRYVISMGSCANGGGYYHYSYSVV 167
T. thermophilus RASPRQADVMIVAGRLSKKMAPVMRRVWEQMPDPKWVISMGACASSGGMFN-NYAIV 124
E. coli         RASPRQADLMVVAGTCFTKMAPVIQRLYDQMLEPKWVISMGACANSGGMYD-IYSVV 142
*****:*:*:*** .*****:::*** :***:***:***:***.***.*** .: *::*

```

**Figure 4.3: Multiple sequence alignment of a highly conserved part of the PSST subunit.** The highly conserved threonine 122 and tyrosine 161 are highlighted in cyan. Threonine 122 is replaced by an arginine in the sequence of *T. thermophilus*. Tyrosine 161 forms a hydrogen bond to histidine 120 from the HRGXE-motif. The third cysteine ligand of iron-sulfur cluster N2 is highlighted in bold. Sequences of *Y. lipolytica*, *N. crassa*, *P. denitrificans*, *R. capsulatus*, *B. taurus*, *H. sapiens*, *T. thermophilus* and *E. coli* were aligned by the multiple sequence alignment program ClustalW. Invariant (\*), highly (:) and weakly similar (.) positions are labeled. For the complete multiple sequence alignment see Figure 8.2.

The highly conserved histidine 120 is hydrogen bonded to tyrosine 161 from the PSST subunit (see Figure 4.2). Interestingly, the H120A mutation decreased complex I activity; however, it did not interfere with complex I assembly (Kashani-Poor et al., 2001b). In contrast, mutations H120R and H120W prevented complex I assembly. This indicates that a spacious arginine or tryptophan at this position disrupts the overall structure, while a histidine at this position is important for normal complex I activity.

A closer look into the structure might also explain why complex I is not assembled in mutant E124D. Glutamate 124 is located adjacent to three positively charged and highly conserved residues (lysine 424, lysine 426 and arginine 466, see Figure 4.4) and therefore potentially forms essential salt bridges (see Figure 4.2).

```

Y. lipolytica      MGVYVVSDGSERPYKKIRAPGFAHLGAFDHIARGHFLPDAVAIIGTMDLVFGEVDR 466
N. crassa        MGVYVVSDGSERPYRVHIRAPGFAHLGGFDHLSRGHMLADAVAVIIGTMDLVFGEVDR 478
B. taurus       FGVYLVSDGSSRPYRCKIKAPGFAHLGLDKMSKGHMLADVVAVIIGTQDIVFGEVDR 430
H. sapiens      FGVYLVSDGSSRPYRCKIKAPGFAHLGLDKMSKGHMLADVVAVIIGTQDIVFGEVDR 463
P. denitrificans FGVYLVADGTNKPRAKLRAPGFAHLQSIDWMSRGHMLADVPAAIIATLDIVFGEVDR 412
R. capsulatus    FGVYLVADGTNKPRAKIRAPGYAHLQSIDAVAKGHQLADVSAIIGTMDVVFGEIDR 413
T. thermophilus LGYYIVSDGGSMPYRVKVRAPSFVNLQSLPYACKGEQVPDMVAIIASLDPVMGDVDR 409
E. coli         NSYYLTSDGSTMSYRTRVRTPSFAHLQQIPAAIRGSLVSDLVYLGSIDFVMSDVDR 407
. *:::** .:: ::::*:::** : : * :.* . :. : * *:::**

```

**Figure 4.4: C-terminal highly conserved part of the multiple sequence alignment from the 49-kDa subunit.** Lysine 424, lysine 426 and arginine 466 are highlighted. Sequences of *Y. lipolytica*, *N. crassa*, *B. taurus*, *H. sapiens*, *P. denitrificans*, *R. capsulatus*, *T. thermophilus* and *E. coli* were aligned by the multiple sequence alignment program ClustalW. Invariant (\*), highly (:) and weakly similar (.) positions are labeled. See Figure 8.1 for the complete multiple sequence alignment.

In turn, lysine 426 and arginine 466 may form salt bridges to a nearby aspartate from the 30-kDa subunit. This aspartate (184, *Y. lipolytica* numbering) seems to have an important function as well, since it is highly conserved and is located in a remarkably conserved region of the 30-kDa subunit (see Figure 4.5).

```

Y. lipolytica      P-VPSITCLYEGANWFEREAYDMYGVFFEGHPDLRRIMTDYGFEGHPLRKDFPLTGY 219
N. crassa        P-VPSITPLYDGANWYEREVYDLFGVFFTGHPDLRRIMTDYGFDDGHPLRKDFPMTGY 221
H. sapiens       P-IESAVSVFKAANWYEREIWDMFGVFFANHPDLRRILTGYGFEGHPFRKDFPLSGY 207
B. taurus        P-IESSVPVYKAANWYEREIWDMFGVFFANHPDLRRILTGYGFEGHPFRKDFPLSGY 209
R. capsulatus    M-CPSIVEVYPAANWYEREVDFMFGILFSGHPDLRRLTGYGFRGHPLRKDFPTTGY 153
T. thermophilus PRLPTVTDLWGSANFLEREVYDLFGIVFEGHPDLRKILTPEDLEGHPLRKDYPLGET 155
P. denitrificans PRLPTVTDLWGSANFLEREVYDLFGIVFEGHPDLRKILTPEDLEGHPLRKDYPLGET 155
E. coli          LHVPTFTKLFNPANWYERETWDLFGITFDGHPNLRRIMMPQTWKGHPLRKDYPARAT 175
      : . : : ** : ** : * : * : * : * : * : * : * : * : * : * : * : *

```

**Figure 4.5: Highly conserved part of the of the amino acid sequence of the 30-kDa subunit.** The invariant aspartate 184 is highlighted in green. Sequences of *Y. lipolytica*, *N. crassa*, *H. sapiens*, *B. taurus*, *R. capsulatus*, *T. thermophilus*, *P. denitrificans* and *E. coli* were aligned by the multiple sequence alignment program ClustalW. Invariant (\*), highly (: ) and weakly similar (.) positions are labeled. The complete multiple sequence alignment is shown in Figure 8.3.

This extensive network of electrostatic interactions may explain the effects observed when glutamate 124 was exchanged. Mutant E124D shows no complex I assembly, indicating that the carboxyl group of the aspartate cannot be placed in sufficient proximity to form essential interactions with lysine 424, lysine 426 and/or arginine 466. Interestingly, mutant E124Q displayed about 55 % of assembled complex I compared to the parental strain; however, complex I activity was rather normal. This seems to indicate that the amide from the glutamine is able to support the electrostatic interactions in the mutant upon some rearrangements which do not interfere with complex I activity. Since glutamate 124 is not located immediately within the quinone binding pocket, the slight changes in the *apparent*  $K_m$  value for DBQ and the  $I_{50}$  value for DQA that were observed in mutant E124Q (see Table 3.16) suggest that these rearrangements also reach into the quinone and inhibitor binding pocket.

Based on the structure of the [NiFe] hydrogenase from *D. fructosovorans* (PDB 1FRF) (Rousset et al., 1998), it had been noticed before that glutamate 124 and arginine 466 might form a salt bridge; therefore a double mutant E124R/R466E was generated (L. Grgic, unpublished data). However, similar to what was found for mutant E124R, no assembled complex I was found in this double mutant. This result further indicates that

glutamate 124 is an essential part of a larger network of electrostatic interactions critical for proper complex I assembly.

Arginine 466 is not as important for complex I assembly as arginine 121 or glutamate 124, since even drastic exchanges did not prevent complex I assembly (Grgic et al., 2004). However, some mutants displayed slight changes in the *apparent*  $K_m$  value for DBQ and in the  $I_{50}$  values for DQA and rotenone. Consistently, a slightly changed sensitivity towards rotenone and piericidin was observed when this arginine was mutated to lysine in complex I from *R. capsulatus* (Prieur et al., 2001). Therefore, similar to what was found for glutamate 124, exchanges of arginine 466 seem to induce structural rearrangements which reach into the quinone and inhibitor binding pocket.

Taken together, it seems that the HRGXE-motif and especially glutamate 124 play an essential structural role in complex I. It is tempting to speculate that this conserved motif, which reaches from iron-sulfur cluster N2 to the 30-kDa subunit and also affects the quinone binding pocket, is involved in transferring conformational changes which finally result in proton translocation across the inner mitochondrial membrane.

### 4.3 Iron-sulfur cluster N1a

Iron-sulfur cluster N1a in complex I from *Y. lipolytica* is not detectable by EPR. However, it must be present, since its ligation motif is highly conserved in the 24-kDa subunit from *Y. lipolytica* as in its homologues (see Figure 3.24). Only reduced binuclear and tetranuclear iron-sulfur clusters are paramagnetic, and therefore a very low redox midpoint potential could explain why this cluster is EPR silent.

By mutating valine 166, alanine 175 and methionine 177 located close to iron-sulfur cluster N1a (see Figure 3.25) to polar and positively charged residues, it might be possible to shift the redox midpoint potential of this cluster to more positive values.

The drastic exchanges A175K and M177K as well as the exchange of the cysteine ligands to alanine in mutants C168A and C172A prevented complex I assembly. This is often observed when iron-sulfur cluster ligands or residues in close proximity to an iron-sulfur cluster are mutated (Aurelio Garofano, unpublished data; Antje Waletko, unpublished data; see also mutant A84V in the PSST subunit in chapter 3.1.1), further

supporting the premise that the 24-kDa subunit from *Y. lipolytica* ligates iron-sulfur cluster N1a.

The rather conservative exchanges V166T, V166K, A175S and M177H displayed normal complex I assembly and activity. However, the EPR spectra from mitochondrial membranes of these mutants were not significantly different from the parental strain. The same was found when mitochondrial membranes were reduced with dithionite, which has a lower redox potential ( $E^{o'} \sim -420$  mV) than NADH ( $E^{o'} \sim -320$  mV).

These results indicated that the introduced mutations did not or not sufficiently increase the redox midpoint potential of iron-sulfur cluster N1a to make it EPR detectable. However, in addition to the signals from complex I, EPR spectra from mitochondrial membranes also display signals from other respiratory chain complexes (see Figure 1.6). Therefore, purification of complex I from the mutants would be necessary to exclude small changes in the complex I spectrum.

Possibly, further exchanges at additional positions (threonine 129, threonine 130, glutamine 133, glutamate 167, leucine 169 and alanine 171) next to iron-sulfur cluster N1a or a combination of several exchanges which did not interfere with complex I assembly could be suited to sufficiently increase the redox midpoint potential of this cluster.

Alternatively, stronger reductants like deazaflavin ( $E^{o'} = -650$  mV) (Blankenhorn, 1976) or  $\text{Eu}^{\text{II}}$ -DTPA (approaching -1 V) (Vincent et al., 2003) could be tested.

Although quite unlikely, it cannot be excluded that the EPR signal from iron-sulfur cluster N1a is not detectable due to other reasons than a very low redox midpoint potential. The EPR signal of iron-sulfur cluster N1a might be hidden by the signal from iron-sulfur cluster N1b. The observation that a stoichiometry of 1.3:1 of the N1 signal to the N2 signal is determined when complex I is reduced with dithionite in redox titrations (Klaus Zwicker, personal communication) points into this direction. Alternatively, iron-sulfur cluster N1a could have an unusual ground state, as proposed for iron-sulfur cluster N5 (Yano et al., 2003) and for iron-sulfur clusters of ferredoxins (Conover et al., 1990; Duderstadt et al., 1999), which might be difficult to detect. Similarly, a very fast relaxation rate or a spin coupling to another paramagnetic species could prevent

detection of the EPR signal. In addition, it was speculated that cluster N1a may not be reducible for kinetic reasons (Reda et al., 2008).

Further studies will be necessary to answer these questions and to gain insight to the function of iron-sulfur cluster N1a.

#### 4.4 *In vivo* screen for complex I deficiency

Due to the redirection of the alternative NADH dehydrogenase (NDH2) to the matrix side of the inner mitochondrial membrane, complex I deficient *Y. lipolytica* strains are viable (Kerscher et al., 2001b). Moreover, these strains do not have any phenotypic growth disadvantages (see upper panel in Figure 3.7). Therefore, in an earlier attempt to develop a screening assay for complex I deficiency and resistance towards complex I specific inhibitors, the expression of the internal alternative NADH dehydrogenase was controlled by inducible promoters (Garofano et al., 2006). However, this assay has several disadvantages. Firstly, *Y. lipolytica* strains have to be grown on minimal media. Secondly, the expression of the internal alternative NADH dehydrogenase could not be controlled stringently enough. Thirdly, this assay inherently would not identify strains in which only proton pumping of complex I is affected. Finally, the screen is not compatible with the preferred mutagenesis strategy.

Therefore, a new *in vivo* plate assay was developed. By growing *Y. lipolytica* on antimycin A or azide containing full medium agar plates, complex III and complex IV were inhibited; thus, oxidative phosphorylation in this obligate aerobic yeast relied on the proton pumping activity of complex I (see Figure 3.6). Indeed, slower growth of the complex I deficient Y144F mutant compared to the parental strain was observed (see Figure 3.7), proving the general concept. With regard to the growth difference between mutant Y144F and the parental strain, best results were obtained at concentrations of 0.3  $\mu$ M antimycin A or 0.5 mM azide, whereby antimycin A always worked better than azide. In order to shut down complex III and complex IV more tightly and/or to decrease the concentrations of inhibitors to avoid side effects, combinations of both inhibitors with varying concentrations were tested. However, the combination of antimycin A and azide on the same plate did not enhance the growth difference between the mutant and the parental strain. Therefore, it seems sufficient to solely use antimycin



A, especially since no resistant colonies appeared. Interestingly, it was important though that the strains reached the late exponential phase in the liquid culture before they were spotted on plates. This might indicate that expression and/or activity levels of complex I and/or the alternative oxidase are upregulated in the late exponential phase of growth.

Some exchanges of highly conserved amino acid residues located at the proposed quinone binding cavity unexpectedly displayed normal complex I content and activity (see chapter 3.1.1 and chapter 3.1.2); therefore, one could speculate that these residues are important for the coupling of the redox reaction to proton pumping. Since the aforementioned screen identifies strains with defects in complex I assembly, stability, oxidoreductase activity as well as proton pumping, these strains were examined on antimycin A-containing plates. Interestingly, none of the mutants displayed any growth deficiency (see Figure 3.8), confirming that complex I assembly and activity are not affected by these mutations. Furthermore, these results also indicate that proton pumping by complex I was unaffected as well, consistent with the emerging concept that the redox reaction is strictly coupled to proton translocation in complex I (Euro et al., 2008a; Zickermann et al., 2008; Zickermann et al., 2009). However, the function of these highly conserved amino acid residues is still elusive.

It should be mentioned that slight impairment of complex I is difficult to determine with this plate assay. Since it was proven here that the basic principle of this assay is valid, one could think of recording growth curves in liquid medium in the presence and absence of antimycin A. Thus, differences in growth i.e. doubling time of different strains could be quantified and evaluated statistically.



## 5 Summary and Outlook

### 5.1 Summary

The NADH:ubiquinone oxidoreductase (complex I) is a large membrane bound protein complex coupling the redox reaction of NADH oxidation and quinone reduction to vectorial proton translocation across bioenergetic membranes (Brandt, 2006). Despite extensive research, the mechanism of proton pumping is still unknown; it seems however that the reduction of quinone induces conformational changes which drive proton uptake from one side and release at the other side of the membrane (Euro et al., 2008a; Zickermann et al., 2009).

In this study the proposed quinone and inhibitor binding pocket located at the interface of the 49-kDa and PSST subunits was explored by a large number of point mutations introduced into complex I from our model organism, the strictly aerobic yeast *Yarrowia lipolytica*. Point mutations were systematically chosen based on the 3.3 Å crystal structure of the hydrophilic domain of complex I from *Thermus thermophilus* (Sazanov and Hinchliffe, 2006). In total, the properties of 94 mutants at 39 positions which completely cover the lining of the large putative quinone and inhibitor binding cavity seen in the partial structure of complex I are described and discussed here.

It turned out that most mutations did not interfere with complex I assembly or stability, but many of them drastically decreased complex I activity. A structure/function analysis allowed the identification of functional domains within the large putative quinone binding cavity. A possible quinone access path ranging from the N-terminal  $\beta$ -sheet of the 49-kDa subunit into the pocket to tyrosine 144 could be defined, since all exchanges introduced here, including the most conservative ones, caused an almost complete loss of dNADH:DBQ oxidoreductase activity of complex I. A region located deeper in the proposed quinone binding pocket is apparently not important for complex I activity, despite the fact that highly conserved amino acid residues are found here. Tyrosine 144 located next to iron-sulfur cluster N2 (the immediate electron donor to quinone) was found to be especially interesting. All exchanges of this tyrosine, even the very conservative mutant Y144F, essentially abolished dNADH:DBQ oxidoreductase

activity of complex I. However, with higher concentrations of Q<sub>1</sub> or Q<sub>2</sub> the dNADH:Q oxidoreductase activity of complex I was largely restored in the mutants with the more conservative exchanges. Proton pumping experiments showed that this activity was also coupled to proton translocation, indicating that these quinones were reduced at the physiological site. However, the *apparent*  $K_m$  values for Q<sub>1</sub> or Q<sub>2</sub> were drastically increased, clearly demonstrating that tyrosine 144 is central for quinone binding and reduction. These results further prove that the enzymatically relevant quinone binding site of complex I is located at the interface of the 49-kDa and PSST subunits.

Kinetic measurements with different ubiquinone derivatives suggested that DBQ is the substrate of choice when the oxidoreductase activity of complex I is to be assayed, since it gave the highest catalytic rates that were also almost completely sensitive towards specific complex I inhibitors. However, if changes in the *apparent*  $K_m$  values of complex I mutants are to be identified, Q<sub>1</sub> or Q<sub>2</sub> were better suited because of their higher affinity to complex I.

The quinone binding pocket is thought to comprise the binding sites for a plethora of specific complex I inhibitors that are usually grouped into three classes (Degli Esposti, 1998). The large array of mutants targeting the quinone binding cavity was examined with a representative of each inhibitor class. Many mutants conferring resistance were identified which, depending on the inhibitor tested, clustered in well defined and partially overlapping regions of the large putative quinone and inhibitor binding cavity. Mutants with effects on type A (DQA) and type B (rotenone) inhibitors were found in a subdomain corresponding to the former [NiFe] site in homologous hydrogenases, whereby the type A inhibitor DQA seems to bind deeper in this domain. Mutants with effects on the type C inhibitor (C<sub>12</sub>E<sub>8</sub>) exclusively were found in a narrow crevice which seems not to be important for complex I activity. Exchanging more exposed amino acid residues at the border of these well defined domains affected all three inhibitor types. Therefore, the results as a whole provide further support for the concept that different inhibitor classes bind to different but partially overlapping binding sites within a single large quinone binding pocket (Okun et al., 1999a). In addition, they also indicate the approximate location of the binding sites of different complex I inhibitor classes within the structure of the large quinone and inhibitor binding cavity at the interface of the 49-kDa and the PSST subunit.

The main results from the mutagenesis study of the quinone and inhibitor binding cavity are illustrated in Figure 5.1.

EIPA, an amiloride derivative and a complex I inhibitor, was suggested to bind to the ND5 subunit of complex I (Nakamaru-Ogiso et al., 2003a). However, a subcomplex of complex I which lacks the ND5 subunit can still be inhibited by EIPA (Dr. Stefan Dröse, personal communication). Moreover, the  $I_{50}$  value of EIPA determined with mitochondrial membranes from the strain containing the subcomplex was found to be unchanged. However, exchanging more exposed amino acid residues within the quinone binding pocket not only altered the  $I_{50}$  value for all three types of complex I inhibitors but also affected the  $I_{50}$  value of EIPA. Therefore, it seems that EIPA, similar to classical complex I inhibitors, acts on the quinone binding pocket of complex I.

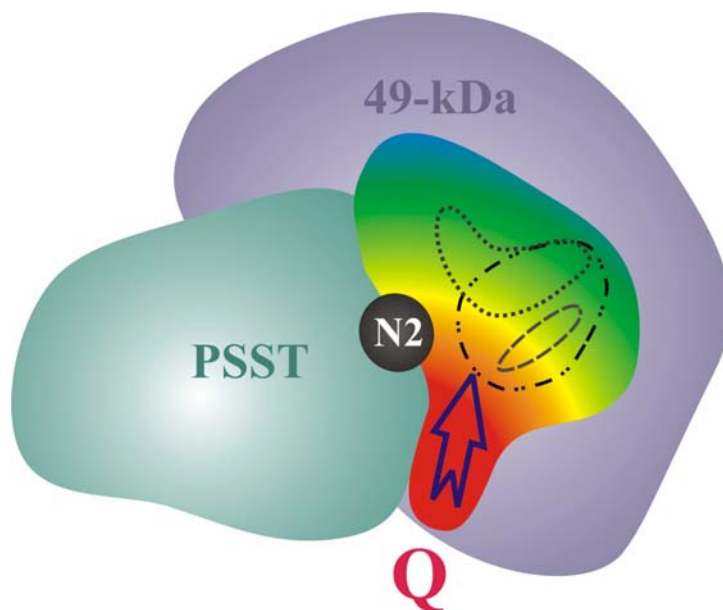


**Figure 5.1: Schematic representation of the quinone and inhibitor binding cavity.** The cavity is located next to iron-sulfur cluster N2 (in black) at the interface of the 49-kDa (in violet) and the PSST subunits (in cyan). The color gradient indicates the position of amino acid residues which are critical (red), less critical (yellow and green) and not critical (blue) for complex I activity. A possible access path for the quinone substrate (Q) is indicated by an arrow. Approximate binding sites of the three types of complex I inhibitors are depicted: --- type A only; - - - type A and B; ··· type C. Figure was adapted from (Zickermann et al., 2009).

It has been proposed earlier that the highly conserved HRGXE-motif in the 49-kDa subunit forms a part of the quinone binding site of complex I (Prieur et al., 2001). Mutagenesis of the HRGXE-motif, revealed that these residues and especially glutamate 124 are rather critical for complex I assembly and seem to have an important structural role. They may also be involved in transferring large conformational changes, consistent with the finding that these residues are not located at the quinone binding pocket but structurally connect iron-sulfur cluster N2 located in the PSST via the 49-kDa subunit to the 30-kDa subunit, as revealed by the crystal structure from *T. thermophilus* (Sazanov and Hinchliffe, 2006).

The question why iron-sulfur cluster N1a is not detectable by EPR in complex I from *Y. lipolytica* and many other model organisms is not solved yet. Introducing polar and positively charged amino acid residues close to this cluster in order to increase its midpoint potential did not result in the appearance of the cluster N1a EPR signal in mitochondrial membranes from the mutants. Clearly, further research will be necessary to gain insights to the function of this iron-sulfur cluster in complex I.

In an additional project, a new and simple *in vivo* screen for complex I deficiency in our model organism *Y. lipolytica* was developed and optimized. This assay probes for defects in complex I assembly and stability, oxidoreductase activity and also proton pumping activity by complex I. Most importantly, this assay is applicable to all *Y. lipolytica* strains and could be used to identify loss-of-function mutants, gain-of-function mutants (i.e. resistance towards complex I inhibitors) and revertants due to mutations in both nuclear and mitochondrially encoded genes of complex I subunits.

## 5.2 Outlook

### 5.2.1 Mutagenesis of the proposed quinone and inhibitor binding cavity

The results obtained with a large array of quinone binding pocket mutants suggest that the binding site for the quinone head group is located next to tyrosine 144 and that the quinone access path is partially formed by the N-terminal part of the 49-kDa subunit. Focusing the same approach more on the PSST subunit could help to identify further

amino acid residues which extend this access path further down towards the membrane plane. In addition, testing ubiquinone analogues with different side chains in combination with structure-based mutagenesis could result in the identification of amino acid residues which are involved in the specific binding of the quinone side chain and hence in substrate recognition by complex I.

Based on steady state kinetics it has been proposed earlier that  $\Delta$ lac-acetogenins form a new type of complex I inhibitors (Hamada et al., 2004; Ichimaru et al., 2005; Murai et al., 2006; Murai et al., 2007) and it has been speculated that the binding site of these inhibitors is very different from the binding sites of classical complex I inhibitors. However, to date it was not possible to identify the amino acid residues or even the subunit(s) which are involved in binding of  $\Delta$ lac-acetogenins by photoaffinity labeling. This hypothesis could be tested by measuring the inhibitory action of  $\Delta$ lac-acetogenins on mutants which displayed marked effects on classical complex I inhibitors.

More importantly, the results presented here together with a crystal structure of holo-complex I and modeling studies could provide clues on how quinone reduction is coupled to proton pumping and how different inhibitors interfere with this machinery.

### 5.2.2 Iron-sulfur cluster N1a

Iron-sulfur cluster N1a is not detectable by EPR in complex I from *Y. lipolytica* and this peculiarity was not altered by changing nearby amino acid residues. However, it has been shown earlier with the 24-kDa subunit from other species that an EPR signal from iron-sulfur cluster N1a was detectable in the overexpressed and purified subunit. (Yano et al., 1994b; Crouse et al., 1994; Yano et al., 1994a; Zu et al., 2002).

In cooperation with the group of Dr. Judy Hirst (MRC, Dunn Human Nutrition Unit, Cambridge, U.K.) the mutants generated and described in this work as well as the unchanged version of the 24-kDa subunit from *Y. lipolytica* will be overexpressed and analyzed by EPR and protein-film voltammetry in order to gain more insights into the function of iron-sulfur cluster N1a.

### 5.2.3 *In vivo* screen for complex I deficiency

On antimycin A or azide containing plates, complex I deficient *Y. lipolytica* strains grow significantly slower than the parental strains. This phenotypic difference could be used to screen for loss-of-function mutations induced by random mutagenesis with mismatch primers in nuclear encoded complex I subunits or loss-of-function mutations in mitochondrially encoded subunits upon induction by the  $MnCl_2$  method (Putramen et al., 1973; Tzagoloff et al., 1975; Meunier et al., 1993) or by acriflavine (Duby and Matagne, 1999). In addition, second site revertants or gain-of-functions mutations which confer resistance towards complex I specific inhibitors could be identified.

The general principle of this screen should also apply to *Y. lipolytica* strains grown in liquid culture in microtiter plates. With such a setup one could directly record growth curves of different strains in parallel and statistically evaluate growth differences.



## 6 Zusammenfassung

Komplex I (NADH:Ubichinon Oxidoreduktase) ist Teil der mitochondrialen Atmungskette, die den schrittweisen Elektronentransfer, überwiegend von NADH, auf den gemeinsamen terminalen Akzeptor Sauerstoff katalysiert (Hatefi, 1985). Die einzelnen Redoxreaktionen zwischen NADH und Sauerstoff werden durch drei membranständige Atmungskettenkomplexe (Komplex I, Komplex III und Komplex IV) bewerkstelligt, die diese exergone Reaktion an die endergone Protonentranslokation über die innere Mitochondrienmembran koppeln. Der so aufgebaute elektrochemische Gradient dient dann zur ATP-Synthese durch die ATP-Synthase (Nakamoto et al., 1999). Dieses grundlegende Prinzip wurde von Peter Mitchell vorgeschlagen (Mitchell, 1961) und wird als die chemiosmotische Theorie bezeichnet.

Mit einer Masse von ~1 MDa ist Komplex I der größte und gleichzeitig auch der am wenigsten verstandene Atmungskettenkomplex (Brandt, 2006). Das membranständige Enzym katalysiert den Elektronentransfer von NADH auf Ubichinon und pumpt dabei vier Protonen über die Mitochondrienmembran (Wikström, 1984; Galkin et al., 1999). Interessanterweise sind alle bekannten Redox-Kofaktoren, ein Flavinmononucleotid (FMN) und 8 bis 9 Eisen-Schwefel-Zentren im hydrophilen Arm des L-förmigen Proteinkomplexes lokalisiert (Carroll et al., 2006b), während die Protonentranslokation über den membranständigen hydrophoben Arm erfolgen muss. Der Mechanismus, der die Redoxreaktion an die räumlich getrennte Protonentranslokation koppelt, ist noch völlig unbekannt. Jedoch deuten neuere Ergebnisse darauf hin, dass die Reduktion des Substrates Ubichinon Konformationsänderungen hervorruft, die letztlich in der Protonenaufnahme auf der einen Seite der Membran und Protonenabgabe auf der anderen Seite der Membran resultieren (Zickermann et al., 2009). Aus der Kristallstruktur des hydrophilen Arms von Komplex I von *Thermus thermophilus* (Sazanov and Hinchliffe, 2006) ist bekannt, dass die Eisen-Schwefel-Zentren eine Elektronentransportkette bilden, die das FMN mit einer großen Proteintasche verbindet. Diese Tasche wird durch die 49-kDa- und die PSST-Untereinheiten aufgebaut und liegt neben dem Eisen-Schwefel-Zentrum N2, dem direkten Elektronendonator für das Chinon.

Es ist daher anzunehmen, dass die Bindestelle für das Ubichinon sich in dieser Proteintasche befindet.

In der vorliegenden Arbeit wurde die putative Ubichinonbindetasche von Komplex I mittels Mutagenese charakterisiert. Als Modellorganismus für zielgerichtete Mutagenese von Komplex I diente die zuvor im Labor von Prof. Brandt etablierte obligat aerobe Hefe *Yarrowia lipolytica* (Kerscher et al., 2001), da die Bäckerhefe *Saccharomyces cerevisiae* keinen Komplex I besitzt (Büschges et al., 1994). Basierend auf der Kristallstruktur des hydrophilen Arms von Komplex I von *T. thermophilus* (Sazanov and Hinchliffe, 2006) wurden Punktmutationen so eingeführt, dass jeder Aminosäurerest in der Ubichinonbindetasche in der Regel gegen eine strukturell ähnliche und eine strukturell andersartige Aminosäure ausgetauscht wurde. Insgesamt werden hier die Ergebnisse von 34 Aminosäureaustauschen an 15 Positionen vorgestellt und mit den Ergebnissen aus früheren Mutagenesestudien an Komplex I von *Y. lipolytica* diskutiert. Somit basieren die Schlussfolgerungen dieser Arbeit auf der Auswertung von insgesamt 94 Mutanten an 39 Aminosäurepositionen.

Mittels Elektronenspinresonanz-Spektroskopie, Blau-nativer Elektrophorese mit anschließender Komplex I Färbung sowie Aktivitätstests (NADH:HAR Oxidoreduktaseaktivität) an mitochondrialen Membranen aus Mutantenstämmen wurde gezeigt, dass die meisten Aminosäureaustausche die Assemblierung und Stabilität von Komplex I nicht störten. Jedoch beeinträchtigten viele die Aktivität von Komplex I (dNADH:DBQ Oxidoreduktaseaktivität). Wie zu erwarten war, hatten konservative Austausche in der Regel geringere Effekte auf die Komplex I Aktivität zur Folge als nicht konservative Austausche. An einigen Positionen führten allerdings selbst sehr konservative Austausche zum fast vollständigen Aktivitätsverlust. Betrachtet man die Lage dieser essenziellen Reste in der Struktur der Chinonbindetasche, dann fällt auf, dass alle in einem bestimmten Bereich der Tasche liegen. Dieser Bereich beginnt an einem N-terminalen  $\beta$ -Faltblatt in der 49-kDa Untereinheit, führt dann in die Tasche und endet am Tyrosin 144 der 49-kDa Untereinheit. Es ist daher anzunehmen, dass Aminosäuren, die essenziell für die Komplex I Aktivität sind aber nicht im Elektrontransferabstand

zum Eisen-Schwefel-Zentrum N2 liegen, einen Zugang für das Chinon in die Tasche bilden.

Jedoch scheint das streng konservierte Tyrosin 144, das nur 6 bis 8 Ångström vom Eisen-Schwefel-Zentrum N2 entfernt ist, eine andere Funktion zu haben. Alle Austausche des Tyrosins, selbst der sehr konservative von Tyrosin nach Phenylalanin, bei dem nur eine Hydroxylgruppe entfernt wird, eliminierten fast vollständig die dNADH:DBQ Oxidoreduktaseaktivität von Komplex I. Wurden als Ubichinonderivate jedoch Q<sub>1</sub> oder Q<sub>2</sub> statt DBQ zur Ermittlung der dNADH:Q Oxidoreduktaseaktivität von Komplex I verwendet, so zeigten alle Mutanten, bei denen das Tyrosin durch einen ebenfalls aromatischen Rest ersetzt wurde, beinahe normale Komplex I Aktivität. Protonenpumpmessungen haben gezeigt, dass diese Aktivität auch tatsächlich zur vektorialen Protonentranslokation führte. Dies bedeutet, dass diese Chinone an der physiologischen Substratbindestelle reduziert werden. Die *apparente*  $K_m$  für Q<sub>2</sub> und insbesondere Q<sub>1</sub> waren jedoch drastisch erhöht. Offenbar ist das Tyrosin 144 von zentraler Bedeutung, aber nicht in jedem Fall essentiell für die Bindung und Reduktion von Ubichinonen am katalytischen Zentrum.

Andere Austausche an Positionen, die tiefer in der Proteintasche liegen (an der Stelle, wo sich die Tasche zur einer Furche verengt), hatten so gut wie gar kein Einfluss auf die Komplex I Aktivität – und dies, obwohl hier auch einige streng konservierte Reste wie Glutamat 218 und Arginin 224 der 49-kDa Untereinheit zu finden sind. Weitere Experimente haben gezeigt, dass diese Reste auch für die Protonentranslokation nicht essenziell sind.

Aktivitätsmessungen mit verschiedenen Ubichinonderivaten an mitochondrialen Membranen zeigten, dass DBQ am geeignetsten ist, um die Aktivität von Komplex I zu bestimmen, da es deutlich höhere Aktivitätsraten ermöglichte als Q<sub>1</sub> oder Q<sub>2</sub> und diese zudem fast vollständig inhibitorsensitiv waren. Des Weiteren entsprachen die Aktivitätsraten mit DBQ eher den relativen Raten, die mit dem endogenen Ubichinon bestimmt wurden, als den Raten mit Q<sub>1</sub>. Für die Bestimmung der *apparenten*  $K_m$  scheinen jedoch Q<sub>1</sub> und Q<sub>2</sub> aufgrund der höheren Affinität besser geeignet zu sein, da eine starke Erhöhung der *apparenten*  $K_m$  nicht zum Aktivitätsverlust führt, wie dies beim DBQ der Fall zu sein scheint.

Es wird allgemein angenommen, dass die Chinonbindetasche auch gleichzeitig die Bindestellen für eine große Anzahl spezifischer Komplex I Inhibitoren beherbergt, die aufgrund von kinetischen Messungen für gewöhnlich in drei Klassen unterteilt werden (Degli Esposti, 1998). Mit je einem Inhibitor aus jeder Klasse wurde getestet, welche Aminosäureaustausche einen Effekt auf welche Inhibitorklasse hatten. Dabei zeigte sich, dass einige Austausche in einer Region, an der in homologen Hydrogenasen das [NiFe]-Zentrum zu finden ist, zu Resistenzen gegenüber DQA (einem Typ A Inhibitor) und Rotenon (einem Typ B Inhibitor) führten. Tiefer in diesem Bereich wurden Reste identifiziert, die beim Austausch ausschließlich Effekte auf DQA zeigten; dies könnte bedeuten, dass DQA tiefer in diesen Bereich eintaucht als Rotenon. Effekte auf den Typ C Inhibitor C<sub>12</sub>E<sub>8</sub> wurden in einer anderen Region der Chinonbindetasche gefunden, und zwar in der Furche, in der Aminosäurereste zu finden sind, die nicht essenziell für die Komplex I Aktivität waren. Austausche von exponierten Aminosäureresten, die sich zwischen dieser Furche und dem Bereich des ehemaligen [NiFe]-Zentrums (hier gab es Effekte auf DQA und Rotenon) befinden, beeinflussten die Inhibition mit allen drei Inhibitoren. Diese Ergebnisse bestätigen die Hypothese, dass die drei Inhibitorklassen an verschiedene, jedoch teilweise überlappende Bindestellen innerhalb einer großen Ubichinonbindetasche binden (Okun et al., 1999). Darüber hinaus zeigen die hier diskutierten Ergebnisse die annähernde Lage der Bindestellen der unterschiedlichen Inhibitoren innerhalb der Struktur der Chinonbindetasche auf.

Amilorid und das Amiloridderivat EIPA sind bekannte Inhibitoren von Na<sup>+</sup>/H<sup>+</sup> Antiportern (Masereel et al., 2003). Da die ND5 Untereinheit von Komplex I Sequenzähnlichkeit zu Na<sup>+</sup>/H<sup>+</sup> Antiportern aufweist (Mathiesen and Hägerhäll, 2002; Mathiesen and Hägerhäll, 2003) und zudem gezeigt wurde, dass EIPA nicht nur Komplex I hemmt (Nakamaru-Ogiso et al., 2003b), sondern auch mit der Photoaffinitätsmarkierung von vermutlich der ND5 Untereinheit durch Inhibitoren interferiert, wurde vorgeschlagen, dass EIPA Komplex I durch die Bindung an die ND5 Untereinheit inhibiert (Nakamaru-Ogiso et al., 2003a). Jedoch ist ein Subkomplex von Komplex I, bei dem die ND5 Untereinheit fehlt, immer noch mit EIPA hemmbar (Dr. Stefan Dröse, persönliche Kommunikation). Zudem war in mitochondrialen Membranen aus dem Subkomplex-generierenden *Y. lipolytica* Stamm *nb8mΔ* die *I*<sub>50</sub> von EIPA unverändert. Des Weiteren hat sich herausgestellt, dass Aminosäureaustausche in der Ubichinonbindetasche die

EIPA Hemmung beeinflussten. Diese Ergebnisse deuten darauf hin, dass EIPA wie die klassischen Komplex I Inhibitoren an die Ubichinonbindetasche und nicht an die ND5 Untereinheit bindet.

Aufgrund von Sequenzvergleichsstudien wurde vermutet, dass das streng konservierte HRGXE-Motiv der 49-kDa Untereinheit Teil eines konservierten Chinonbindemotivs ist (Prieur et al., 2001). Aminosäureaustausche in diesem Motiv interferierten jedoch mit der Komplex I Assemblierung bzw. Stabilität. Wie aus der Kristallstruktur des hydrophilen Arms von Komplex I von *T. thermophilus* hervorgeht (Sazanov and Hinchliffe, 2006), befinden sich die Aminosäurereste des HRGXE-Motivs nicht in der Chinonbindetasche, sondern formen eher eine Verbindung zwischen dem Eisen-Schwefel-Zentrum N2 in der PSST Untereinheit, der 49-kDa Untereinheit und der 30-kDa Untereinheit. Dabei bildet das Histidin 120 und vermutlich auch das Arginin 121 des Motivs Wasserstoffbrücken zu benachbarten Resten aus, während das Glutamat 124 an einem Netzwerk aus ionischen Wechselwirkungen beteiligt ist. Offenbar hat das HRGXE-Motiv eine strukturelle Funktion in Komplex I.

Das Eisen-Schwefel-Zentrum N1a der 24-kDa Untereinheit moduliert möglicherweise die ROS-Produktion von Komplex I (Esterhazy et al., 2008). Leider ist dieses Eisen-Schwefel-Zentrum im Komplex I von *Y. lipolytica* und einigen anderen Organismen nicht mit Elektronenspinresonanz-Spektroskopie detektierbar. Als möglicher Grund hierfür wird ein sehr niedriges Mittelpunktspotential erwogen, sodass dieses Eisen-Schwefel-Zentrum meist im oxidiertem, nicht paramagnetischem Zustand vorliegt (Reda et al., 2008). Das Einführen von polaren oder positiv geladenen Aminosäureresten in die Nähe des Eisen-Schwefel-Zentrums N1a interferierte jedoch entweder mit der Komplex I Assemblierung oder hatte kein Einfluss auf die Elektronenspinresonanz-Spektren von mitochondrialen Membranen der Mutanten. Es ist daher ungeklärt, ob und im welchem Ausmaß diese Mutationen das Mittelpunktspotential von Eisen-Schwefel-Zentrum N1a heraufsetzen konnten und auch, ob ein zu niedriges Mittelpunktspotential tatsächlich der Grund für die Nichtdetektierbarkeit von Eisen-Schwefel-Zentrum N1a ist. Zur Beantwortung dieser Fragen sollen die mutagenisierten Versionen der 24-kDa

Untereinheit in Kooperation mit der Arbeitsgruppe von Dr. Judy Hirst (MRC, Dunn Human Nutrition Unit, Cambridge, England) überexprimiert und mit der Proteinfilmvoltammetrie analysiert werden.

In einem weiteren Teilprojekt der vorliegenden Arbeit wurde ein neuer und einfacher *in vivo* Screen zur Identifizierung von Komplex I defizienten *Y. lipolytica* Stämmen entwickelt. Auf Antimycin A oder Azid-haltigen Vollmediumplatten ist die Oxidative Phosphorylierung von *Y. lipolytica* gänzlich auf einen funktionsfähigen Komplex I angewiesen. *Y. lipolytica* Stämme mit Komplex I Defekten haben auf solchen Platten einen Wachstumsnachteil. Daher könnten Stämme isoliert werden, die eine Störung in der Assemblierung, Oxidoreduktaseaktivität oder Protonenpumpaktivität von Komplex I aufweisen. Neben diesen Funktionsverlustmutanten könnten auch Revertanten oder, mit Hilfe von Komplex I spezifischen Inhibitoren, auch Funktionsgewinnmutanten aufgrund von Resistenzen identifiziert werden. Nach einer induzierten Zufallsmutagenese könnte dieser *in vivo* Screen eine schnelle und einfache Identifizierung von essenziellen Aminosäureresten sowohl in kernkodierten als auch in mitochondrial-kodierten Komplex I Untereinheiten ermöglichen.

## 7 References

1. Abrahams, J.P., A.G.W.Leslie, R.Lutter, and J.E.Walker. 1994. Structure at 2.8 Å resolution of F<sub>1</sub>-ATPase from bovine heart mitochondria. *Nature* 370:621-628.
2. Ahlers, P., K.Zwicker, S.Kerscher, and U.Brandt. 2000. Function of conserved acidic residues in the PSST-homologue of complex I (NADH:ubiquinone oxidoreductase) from *Yarrowia lipolytica*. *J. Biol. Chem.* 275:23577-23582.
3. Albracht, S.P.J. 1993. Intimate relationships of the large and the small subunits of all nickel hydrogenases with two nuclear-encoded subunits of mitochondrial NADH:ubiquinone oxidoreductase. *Biochim. Biophys. Acta* 1144:221-224.
4. Amarneh, B. and S.B.Vik. 2003. Mutagenesis of subunit N of the *Escherichia coli* complex I. Identification of the initiation codon and the sensitivity of mutants to decylubiquinone. *Biochem.* 42:4800-4808.
5. Anderson, S., M.H.L.de Bruijn, A.R.Coulson, I.C.Eperon, F.Sanger, and I.G.Young. 1982. Complete sequence of bovine mitochondrial DNA - conserved features of the mammalian mitochondrial genome. *J. Mol. Biol.* 156:683-717.
6. Baranova, E.A., P.J.Holt, and L.A.Sazanov. 2007a. Projection structure of the membrane domain of *Escherichia coli* respiratory complex I at 8 Å resolution. *J. Mol. Biol.* 366:140-154.
7. Baranova, E.A., D.J.Morgan, and L.A.Sazanov. 2007b. Single particle analysis confirms distal location of subunits NuoL and NuoM in *Escherichia coli* complex I. *J. Struct. Biol.* 159:238-242.
8. Barker, C.D., T.Redda, and J.Hirst. 2007. The flavoprotein subcomplex of complex I (NADH:ubiquinone oxidoreductase) from bovine heart mitochondria: Insights into the mechanisms of NADH oxidation and NAD<sup>+</sup> reduction from protein film voltammetry. *Biochem.* 46:3454-3464.
9. Barth, G. and C.Gaillardin. 1996. *Yarrowia lipolytica*. In Non-conventional yeasts in biotechnology. K.Wolf, editor. Springer, Berlin-Heidelberg. 313-388.
10. Barth, G. and C.Gaillardin. 1997. Physiology and genetics of the dimorphic fungus *Yarrowia lipolytica*. *FEMS Microbiol. Rev.* 19:219-237.

11. Beinert, H. and S.P.J.Albracht. 1982. New insights, ideas and unanswered questions concerning iron-sulfur clusters in mitochondria. *Biochim. Biophys. Acta* 683:245-277.
12. Belevich, G., L.Euro, M.Wikström, and M.Verkhovskaya. 2007. Role of the conserved arginine 274 and histidine 224 and 228 residues in the NuoCD subunit of complex I from *Escherichia coli*. *Biochem.* 46:526-533.
13. Bell, E.L., T.A.Klimova, J.Eisenbart, C.T.Moraes, M.P.Murphy, G.R.S.Budinger, and N.S.Chandel. 2007. The Q<sub>o</sub> site of the mitochondrial complex III is required for the transduction of hypoxic signaling via reactive oxygen species production. *J. Cell Biol.* 177:1029-1036.
14. Benzi, G. and A.Moretti. 1995. Are reactive oxygen species involved in Alzheimer's disease? *Neurobiol. Aging* 16:661-674.
15. Blankenhorn, G. 1976. Nicotinamide-dependent one-electron and 2-electron (flavin) oxidoreduction - thermodynamics, kinetics, and mechanism. *Eur. J. Biochem.* 67:67-80.
16. Böhm, R., M.Sauter, and A.Böck. 1990. Nucleotide sequence and expression of an operon in *Escherichia coli* coding for formate hydrogenlyase components. *Mol. Microbiol.* 4:231-243.
17. Borek, A., M.Sarewicz, and A.Osyczka. 2008. Movement of the iron-sulfur head domain of cytochrome bc<sub>1</sub> transiently opens the catalytic Q<sub>o</sub> site for reaction with oxygen. *Biochem.* 47:12365-12370.
18. Boveris, A., E.Cadenas, and A.O.Stoppani. 1976. Role of ubiquinone in the mitochondrial generation of hydrogen peroxide. *Biochem J.* 156:435-444.
19. Boyer, P.D. 1997. The ATP synthase – a splendid molecular machine. *Annu. Rev. Biochem.* 66:717-749.
20. Brand, M.D., C.Affourtit, T.C.Esteves, K.Green, A.J.Lambert, S.Miwa, J.L.Pakay, and N.Parker. 2004. Mitochondrial superoxide: Production, biological effects, and activation of uncoupling proteins. *Free Radical Biology and Medicine* 37:755-767.
21. Brandt, U. 1996. Energy conservation by bifurcated electron-transfer in the cytochrome bc<sub>1</sub> complex. *Biochim. Biophys. Acta* 1275:41-46.



22. Brandt, U. 1997. Proton-translocation by membrane-bound NADH:ubiquinone-oxidoreductase (complex I) through redox-gated ligand conduction. *Biochim. Biophys. Acta* 1318:79-91.
23. Brandt, U. 1999. Proton translocation in the respiratory chain involving ubiquinone - a hypothetical semiquinone switch mechanism for complex I. *BioFactors* 9:95-101.
24. Brandt, U. 2006. Energy converting NADH:quinone oxidoreductase (complex I). *Annu. Rev. Biochem.* 75:69-92.
25. Brandt, U., S.Kerscher, S.Dröse, K.Zwicker, and V.Zickermann. 2003. Proton pumping by NADH:ubiquinone oxidoreductase. A redox driven conformational change mechanism? *FEBS Lett.* 545:9-17.
26. Brandt, U. and J.G.Okun. 1997. Role of deprotonation events in ubi-hydroquinone:cytochrome *c* oxidoreductase from bovine heart and yeast mitochondria. *Biochem.* 36:11234-11240.
27. Burbaev, D.S., I.A.Moroz, A.B.Kotlyar, V.D.Sled, and A.D.Vinogradov. 1989. Ubisemiquinone in the NADH-ubiquinone reductase region of the mitochondrial respiratory chain. *FEBS Lett.* 254:47-51.
28. Büschges, R., G.Bahrenberg, M.Zimmermann, and K.Wolf. 1994. NADH: ubiquinone oxidoreductase in obligate aerobic yeasts. *Yeast* 10:475-479.
29. Cadenas, E., A.Boveris, C.I.Ragan, and A.O.Stoppani. 1977. Production of superoxide radicals and hydrogen peroxide by NADH-ubiquinone reductase and ubiquinol-cytochrome *c* reductase from beef-heart mitochondria. *Arch. Biochem Biophys.* 180:248-257.
30. Cardol, P., R.F.Matagne, and C.Remacle. 2002. Impact of mutations affecting ND mitochondria-encoded Subunits on the activity and assembly of complex I in chlamydomonas. Implication for the structural organization of the enzyme. *J. Mol. Biol.* 319:1211-1221.
31. Carelli, V., A.Ghelli, L.Bucchi, P.Montagna, A.De Negri, V.Leuzzi, C.Carducci, G.Lenaz, E.Lugaresi, and M.Degli Esposti. 1999. Biochemical features of mtDNA 14484 (ND6/M64V) point mutation associated with Leber's hereditary optic neuropathy. *Ann. Neurol.* 45:320-328.

32. Carroll, J., I.M.Fearnley, R.J.Shannon, J.Hirst, and J.E.Walker. 2003. Analysis of the subunit composition of complex I from bovine heart mitochondria. *Mol. Cell. Proteomics* 2:117-126.
33. Carroll, J., I.M.Fearnley, J.M.Skehel, R.J.Shannon, J.Hirst, and J.E.Walker. 2006a. Bovine complex I is a complex of 45 different subunits. *J. Biol. Chem.* 281:32724-32727.
34. Carroll, J., I.M.Fearnley, and J.E.Walker. 2006b. Definition of the mitochondrial proteome by measurement of molecular masses of membrane proteins. *Proc. Natl. Acad. Sci. USA* 103:16170-16175.
35. Chen, D.-C., J.-M.Beckerich, and C.Gaillardin. 1997. One-step transformation of the dimorphic yeast *Yarrowia lipolytica*. *Appl. Biochem. Biotechnol.* 48:232-235.
36. Chomyn, A., M.W.J.Cleeter, C.I.Ragan, M.Riley, R.F.Doolittle, and G.Attardi. 1986. URF6, last unidentified open reading frame of human mtDNA, codes for an NADH dehydrogenase component. *Science* 234:614-618.
37. Chomyn, A., P.Mariottini, M.W.J.Cleeter, C.I.Ragan, A.Matsuno-Yagi, Y.Hatefi, R.F.Doolittle, and G.Attardi. 1985. Six unidentified reading frames of human mitochondrial DNA encode components of the respiratory-chain NADH dehydrogenase. *Nature* 314:592-597.
38. Clason, T., V.Zickermann, T.Ruiz, U.Brandt, and M.Radermacher. 2007. Direct localization of the 51 and 24 kDa subunits of mitochondrial complex I by three-dimensional difference imaging. *J. Struct. Biol.* 159:433-442.
39. Conover, R.C., A.T.Kowal, W.G.Fu, J.B.Park, S.Aono, M.W.Adams, and M.K.Johnson. 1990. Spectroscopic characterization of the novel iron-sulfur cluster in *Pyrococcus furiosus* ferredoxin. *J. Biol. Chem.* 265:8533-8541.
40. Counillon, L., A.Franchi, and J.Pouyssegur. 1993. A point mutation of the Na<sup>+</sup>/H<sup>+</sup> exchanger gene (Nhe1) and amplification of the mutated allele confer amiloride resistance upon chronic acidosis. *Proc. Natl. Acad. Sci. USA* 90:4508-4512.
41. Crouse, B.R., T.Yano, M.G.Finnegan, T.Yagi, and M.K.Johnson. 1994. Properties of the iron-sulfur center in the 25-kilodalton subunit of the proton-translocating NADH-quinone oxidoreductase of *Paracoccus denitrificans*. *J. Biol. Chem.* 269:21030-21036.

42. Darrouzet, E. and A.Dupuis. 1997. Genetic evidence for the existence of two quinone related inhibitor binding sites in NADH-CoQ reductase. *Biochim. Biophys. Acta* 1319:1-4.
43. Darrouzet, E., J.P.Issartel, J.Lunardi, and A.Dupuis. 1998. The 49-kDa subunit of NADH-ubiquinone oxidoreductase (complex I) is involved in the binding of piericidin and rotenone, two quinone-related inhibitors. *FEBS Lett.* 431:34-38.
44. de Troostembergh, J.-C. and E.-J.Nyns. 1978. Non electrogenic function of the mitochondrial, alternative, cyanide-insensitive respiration in the yeast *Saccharomyces lipolytica*. *Arch. Microbiol.*297-302.
45. de Vries, S. and C.A.M.Marres. 1987. The mitochondrial respiratory chain of yeast. Structure and biosynthesis and the role in cellular metabolism. *Biochim. Biophys. Acta* 895:205-239.
46. Degli Esposti, M. 1998. Inhibitors of NADH-ubiquinone reductase: An overview. *Biochim. Biophys. Acta - Bioenerg.* 1364:222-235.
47. Degli Esposti, M., V.Carelli, M.Crimi, S.Sangiorgi, P.Montagna, G.Lenaz, E.X.Lugaresi, and P.Cortelli. 1994. Functional alterations of the mitochondrially encoded ND4 subunit associated with Leber's hereditary optic neuropathy. *FEBS Lett.* 352:375-379.
48. Degli Esposti, M. and A.X.Ghelli. 1994. The mechanism of proton and electron transport in mitochondrial complex I. *Biochim. Biophys. Acta* 1187:116-120.
49. Degli Esposti, M., A.Ngo, G.L.X.McMullen, A.X.Ghelli, F.Sparla, B.Benelli, M.X.Ratta, and A.W.Linnane. 1996. The specificity of mitochondrial complex I for ubiquinones. *Biochem. J.* 313:327-334.
50. Denke, E., T.Merbitz-Zahradnik, O.M.Hatzfeld, C.Snyder, T.A.Link, and B.L.Trumpower. 1998. Alteration of the midpoint potential and catalytic activity of the Rieske iron-sulfur protein by site directed mutational changes of amino acids forming hydrogen bonds to the iron-sulfur cluster. *J. Biol. Chem.* 273:9085-9093.
51. Di Bernardo, S. and T.Yagi. 2001. Direct interaction between a membrane domain subunit and a connector subunit in the H<sup>+</sup>-translocating NADH-quinone oxidoreductase. *FEBS Lett.* 508:385-388.

52. Di Virgilio, F. and G.F.Azzone. 1982. Activation of site I redox-driven H<sup>+</sup> pump by exogenous quinones in intact mitochondria. *J Biol Chem* 257:4106-4113.
53. Djafarzadeh, R., S.Kerscher, K.Zwicker, M.Radermacher, M.Lindahl, H.Schägger, and U.Brandt. 2000. Biophysical and structural characterization of proton-translocating NADH-dehydrogenase (complex I) from the strictly aerobic yeast *Yarrowia lipolytica*. *Biochim. Biophys. Acta* 1459:230-238.
54. Dröse, S. and U.Brandt. 2008. The mechanism of mitochondrial superoxide production by the cytochrome bc1 complex. *J. Biol. Chem.* 283:21649-21654.
55. Dröse, S., A.Galkin, and U.Brandt. 2009. Measurement of superoxide formation by mitochondrial complex I of *Yarrowia lipolytica*. *Methods Enzymol.* 456.
56. Dröse, S., A.Galkin, and U.Brandt. 2005. Proton pumping by complex I (NADH:ubiquinone oxidoreductase) from *Yarrowia lipolytica* reconstituted into proteoliposomes. *Biochim. Biophys. Acta - Bioenerg.* 1710:87-95.
57. Dröse, S., K.Zwicker, and U.Brandt. 2002. Full recovery of the NADH:ubiquinone activity of complex I (NADH:ubiquinone oxidoreductase) from *Yarrowia lipolytica* by the addition of phospholipids. *Biochim. Biophys. Acta - Bioenerg.* 1556:65-72.
58. Duarte, M., H.Populo, A.Videira, T.Friedrich, and U.Schulte. 2002. Disruption of iron-sulphur cluster N2 from NADH:ubiquinone oxidoreductase by site-directed mutagenesis. *Biochem. J.* 364:833-839.
59. Duby, F. and R.F.Matagne. 1999. Alteration of dark respiration and reduction of phototrophic growth in a mitochondrial DNA deletion mutant of *Chlamydomonas* lacking cob, nd4, and the 3' end of nd5. *Plant Cell* 11:115-125.
60. Duderstadt, R.E., P.S.Brereton, M.W.Adams, and M.K.Johnson. 1999. A pure S = 3/2 [Fe<sub>4</sub>S<sub>4</sub>]<sup>+</sup> cluster in the A33Y variant of *Pyrococcus furiosus* ferredoxin. *FEBS Lett.* 454:21-26.
61. Dujon, B., D.Sherman, G.Fischer, P.Durrens, S.Casaregola, I.Lafontaine, J.de Montigny, C.Marck, C.Neuveglise, E.Talla, N.Goffard, L.Frangeul, M.Aigle, V.Anthouard, A.Babour, V.Barbe, S.Barnay, S.Blanchin, J.M.Beckerich, E.Beyne, C.Bleykasten, A.Boisrame, J.Boyer, L.Cattolico, F.Confanioleri, A.De Daruvar, L.Despons, E.Fabre, C.Fairhead, H.Ferry-Dumazet, A.Groppi, F.Hantraye, C.Hennequin, N.Jauniaux, P.Joyet, R.Kachouri, A.Kerrest, R.Koszul, M.Lemaire, I.Lesur, L.Ma, H.Muller, J.M.Nicaud, M.Nikolski,

- S.Oztas, O.Ozier-Kalegeropoulos, S.Pellenz, S.Potier, G.F.Richard, M.L.Straub, A.Suleau, D.Swennen, F.Tekaia, M.Wesolowski-Louvel, E.Westhof, B.Wirth, M.Zeniou-Meyer, I.Zivanovic, M.Bolotin-Fukuhara, A.Thierry, C.Bouchier, B.Caudron, C.Scarpelli, C.Gaillardin, J.Weissenbach, P.Wincker, and J.L.Souciet. 2004. Genome evolution in yeasts. *Nature* 430 :35-44.
62. Dupuis, A., M.Chevallet, E.Darrouzet, H.Duborjal, J.Lunardi, and J.P.Issartel. 1998. The complex I from *Rhodobacter capsulatus*. *Biochim. Biophys. Acta* 1364:147-165.
63. Dupuis, A., I.Prieur, and J.Lunardi. 2001. Toward a characterization of the connecting module of complex I. *J. Bioenerg. Biomembr.* 33:168.
64. Dutton, P.L., C.C.Moser, V.D.Sled, F.Daldal, and T.Ohnishi. 1998. A reductant-induced oxidation mechanism for complex I. *Biochim. Biophys. Acta* 1364:245-257.
65. Duval, R.A., G.Lewin, E.Peris, N.Chahboune, A.Garofano, S.Dröse, D.Cortes, U.Brandt, and R.Hocquemiller. 2006. Heterocyclic analogues of squamocin as inhibitors of mitochondrial complex I. On the role of the terminal lactone of annonaceous acetogenins. *Biochem.*
66. Earley, F.G., S.D.Patel, C.I.Ragan, and G.Attardi. 1987. Photolabelling of a mitochondrially encoded subunit of NADH dehydrogenase with [3H]dihydrorotenone. *FEBS Lett.* 219:108-112.
67. Earley, F.G. and C.I.Ragan. 1984. Photoaffinity labelling of mitochondrial NADH dehydrogenase with arylazidoamorphigenin, an analogue of rotenone. *Biochem J.* 224:525-534.
68. Emerit, J., M.Edeas, and F.Bricaire. 2004. Neurodegenerative diseases and oxidative stress. *Biomed. Pharmacother.* 58:39-46.
69. Eschemann, A., A.Galkin, W.Oettmeier, U.Brandt, and S.Kerscher. 2005. HDQ (1-Hydroxy-2-dodecyl-4(1H)quinolone), a high affinity inhibitor for mitochondrial alternative NADH dehydrogenase. *J. Biol. Chem.* 280:3138-3142.
70. Esterhazy, D., M.S.King, G.Yakovlev, and J.Hirst. 2008. Production of reactive oxygen species by complex I (NADH:ubiquinone oxidoreductase) from *Escherichia coli* and comparison to the enzyme from mitochondria. *Biochem.* 47:3964-3971.

71. Estornell, E. 2000. Mitochondrial complex I: New insights from inhibitor assays. *Protoplasma* 213:11-17.
72. Estornell, E., R.Fato, F.Pallotti, and G.Lenaz. 1993. Assay conditions for the mitochondrial NADH:coenzyme Q oxidoreductase. *FEBS Lett.* 332:127-131.
73. Euro, L., G.Belevich, M.I.Verkhovsky, M.Wikström, and M.Verkhovskaya. 2008a. Conserved lysine residues of the membrane subunit NuoM are involved in energy conversion by the proton-pumping NADH:ubiquinone oxidoreductase (complex I). *Biochim. Biophys. Acta* 1777:1166-1172.
74. Euro, L., D.A.Bloch, M.Wikström, M.I.Verkhovsky, and M.Verkhovskaya. 2008b. Electrostatic interactions between FeS clusters in NADH:ubiquinone oxidoreductase (complex I) from *Escherichia coli*. *Biochem.* 47:3185-3193.
75. Fato, R., E.Estornell, S.Di Bernardo, F.Pallotti, G.P.Castelli, and G.Lenaz. 1996. Steady-state kinetics of the reduction of coenzyme Q analogs by complex I (NADH:ubiquinone oxidoreductase) in bovine heart mitochondria and sub-mitochondrial particles. *Biochem.* 35:2705-2716.
76. Fearnley, I.M. and J.E.Walker. 1992. Conservation of sequences of subunits of mitochondrial complex I and their relationships with other proteins. *Biochim. Biophys. Acta* 1140:105-134.
77. Fendel, U., M.A.Tocilescu, S.Kerscher, and U.Brandt. 2008. Exploring the inhibitor binding pocket of respiratory complex I. *Biochim. Biophys. Acta - Bioenerg.* 1777:660-665.
78. Fernandes, A.S., M.M.Pereira, and M.Teixeira. 2002. Purification and characterization of the complex I from the respiratory chain of *Rhodothermus marinus*. *J. Bioenerg. Biomembr.* 34:413-421.
79. Fernandes, A.S., F.L.Sousa, M.Teixeira, and M.M.Pereira. 2006. Electron paramagnetic resonance studies of the iron-sulfur centers from complex I of *Rhodothermus marinus*. *Biochem.* 45:1002-1008.
80. Finel, M., J.M.Skehel, S.P.J.Albracht, I.M.Fearnley, and J.E.Walker. 1992. Resolution of NADH:ubiquinone oxidoreductase from bovine heart mitochondria into two subcomplexes, one of which contains the redox centers of the enzyme. *Biochem.* 31:11425-11434.

81. Finkel, T. and N.J.Holbrook. 2000. Oxidants, oxidative stress and the biology of ageing. *Nature* 408:239-247.
82. Fisher, N. and P.R.Rich. 2000. A motif for quinone binding sites in respiratory and photosynthetic systems. *J. Mol. Biol.* 296:1153-1162.
83. Flemming, D., P.Hellwig, S.Lepper, D.P.Kloer, and T.Friedrich. 2006. Catalytic importance of acidic amino acids on subunit NuoB of the *Escherichia coli* NADH:ubiquinone oxidoreductase (complex I). *J. Biol. Chem.* 281:24781-24789.
84. Flemming, D., A.Schlitt, V.Spehr, T.Bischof, and T.Friedrich. 2003. Iron-sulfur cluster N2 of the *Escherichia coli* NADH:ubiquinone oxidoreductase (complex I) is located on subunit NuoB. *J. Biol. Chem.* 278:47602-47609.
85. Flemming, D., S.Stolpe, D.Schneider, P.Hellwig, and T.Friedrich. 2005. A possible role for iron-sulfur cluster N2 in proton translocation by the NADH:ubiquinone oxidoreductase (complex I). *J. Mol. Microbiol. Biotechnol.* 10:222.
86. Fridovich, I. 1978. The biology of oxygen radicals. *Science* 201:875-880.
87. Friedrich, T. 1998. The NADH:ubiquinone oxidoreductase (complex I) from *Escherichia coli*. *Biochim. Biophys. Acta* 1364:134-146.
88. Friedrich, T. 2001. Complex I: A chimaera of a redox and conformation-driven proton pump? *J. Bioenerg. Biomembr.* 33:169-177.
89. Friedrich, T., B.Brors, P.Hellwig, L.Kintscher, T.Rasmussen, D.Scheide, U.Schulte, W.Mäntele, and H.Weiss. 2000. Characterization of two novel redox groups in the respiratory NADH:ubiquinone oxidoreductase (complex I). *Biochim. Biophys. Acta* 1459:305-309.
90. Friedrich, T., P.van Heek, H.Leif, T.Ohnishi, E.Forche, B.Kunze, R.Jansen, W.Trowitzsch-Kienast, G.Höfle, H.X.Reichenbach, and H.Weiss. 1994. Two binding sites of inhibitors in NADH:ubiquinone oxidoreductase (complex I). Relationship of one site with the ubiquinone-binding site of bacterial glucose:ubiquinone oxidoreductase. *Eur. J. Biochem.* 219:691-698.

91. Friedrich, T. and H.Weiss. 1997. Modular evolution of the respiratory NADH:ubiquinone oxidoreductase and the origin of its modules. *J. theor. Biol.* 187:529-540.
92. Galkin, A. and U.Brandt. 2005. Superoxide radical formation by pure complex I (NADH:ubiquinone oxidoreductase) from *Yarrowia lipolytica*. *J. Biol. Chem.* 280:30129-30135.
93. Galkin, A.S., V.G.Grivennikova, and A.D.Vinogradov. 1999.  $\rightarrow$  H<sup>+</sup>/2e<sup>-</sup> stoichiometry in NADH-quinone reductase reactions catalyzed by bovine heart submitochondrial particles. *FEBS Lett.* 451:157-161.
94. Garofano, A., A.Eschemann, U.Brandt, and S.Kerscher. 2006. Substrate-inducible versions of internal alternative NADH:ubiquinone oxidoreductase from *Yarrowia lipolytica*. *Yeast* 23:1129-1136.
95. Garofano, A., K.Zwicker, S.Kerscher, P.Okun, and U.Brandt. 2003. Two aspartic acid residues in the PSST-homologous NUKM subunit of complex I from *Yarrowia lipolytica* are essential for catalytic activity. *J. Biol. Chem.* 278:42435-42440.
96. Gavrikova, E.V., V.G.Grivennikova, V.D.Sled, T.Ohnishi, and A.D.Vinogradov. 1995. Kinetics of the mitochondrial three-subunit NADH dehydrogenase interaction with hexammineruthenium(III). *Biochim. Biophys. Acta* 1230:23-30.
97. Ghelli, A.X., M.Degli Esposti, V.Carelli, and G.Lenaz. 1997. Changes in mitochondrial complex I activity and coenzyme Q binding site in Leber's hereditary optic neuropathy (LHON). *Molec. Aspects Med.* 18 (Supplement):s263-s267.
98. Gong, X., T.Xie, L.Yu, M.Hesterberg, D.Scheide, T.Friedrich, and C.-A.Yu. 2003. The ubiquinone-binding site in NADH:ubiquinone oxidoreductase from *Escherichia coli*. *J. Biol. Chem.* 278:25731-25737.
99. Grgic, L., K.Zwicker, N.Kashani-Poor, S.Kerscher, and U.Brandt. 2004. Functional significance of conserved histidines and arginines in the 49 kDa subunit of mitochondrial complex I. *J. Biol. Chem.* 279:21193-21199.
100. Grigorieff, N. 1998. Three-dimensional structure of bovine NADH:ubiquinone oxidoreductase (complex I) at 22 Å in ice. *J. Mol. Biol.* 277:1033-1046.



101. Guenebaut, V., A.Schlitt, H.Weiss, K.Leonard, and T.Friedrich. 1998. Consistent structure between bacterial and mitochondrial NADH:ubiquinone oxidoreductase (complex I). *J. Mol. Biol.* 276:105-112.
102. Guenebaut, V., R.Vincentelli, D.Mills, H.Weiss, and K.Leonard. 1997. Three-dimensional structure of NADH-dehydrogenase from *Neurospora crassa* by electron microscopy and conical tilt reconstruction. *J. Mol. Biol.* 265:409-418.
103. Hamada, T., N.Ichimar, M.Abe, D.Fujita, A.Kenmochi, T.Nishioka, K.Zwicker, U.Brandt, and H.Miyoshi. 2004. Synthesis and inhibitory action of novel acetogenin mimics with bovine heart mitochondrial complex I. *Biochem.* 43:3651-3658.
104. Hamamoto, T., M.Hashimoto, M.Hino, M.Kitada, Y.Seto, T.Kudo, and K.Horikoshi. 1994. Characterization of a gene responsible for the Na<sup>+</sup>/H<sup>+</sup> antiporter system of alkalophilic *Bacillus* species strain C-125. *Mol. Microbiol.* 14:939-946.
105. Hano, N., Y.Nakashima, K.Shinzawa-Itoh, and S.Yoshikawa. 2003. Effect of the side chain structure of coenzyme Q on the steady state kinetics of bovine heart NADH:coenzyme Q oxidoreductase. *J. Bioenerg. Biomembr.* 35:257-265.
106. Hassinen, I.E. and P.T.Vuokila. 1993. reaction of dicyclohexylcarbodiimide with mitochondrial proteins. *Biochim. Biophys. Acta* 1144:107-124.
107. Hatefi, Y. 1985. The mitochondrial electron transport and oxidative phosphorylation system. *Annu. Rev. Biochem.* 54:1015-1069.
108. Heinrich, H., J.E.Azeveda, and S.Werner. 1992. Characterization of the 9.5-kDa ubiquinone-binding protein of NADH:ubiquinone oxidoreductase (complex I) from *Neurospora crassa*. *Biochem.* 31:11420-11424.
109. Heinrich, H. and S.Werner. 1992. Identification of the ubiquinone-binding site of NADH:ubiquinone oxidoreductase (complex I) from *Neurospora crassa*. *Biochem.* 31:11413-11419.
110. Helenius, A., D.R.McCaslin, E.Fries, and C.Tanford. 1979. Properties of detergents. *Methods Enzymol.* LVI:734-749.
111. Helenius, A. and K.Simons. 1972. The binding of detergents to lipophilic and hydrophilic proteins. *J. Biol. Chem.* 247:3656-3661.

112. Henry, M.-F. and E.-J.Nyns. 1975. Cyanide-insensitive respiration. An alternative mitochondrial pathway. *Sub-Cell. Biochem.* 4:1-65.
113. Hinchliffe, P. and L.A.Sazanov. 2005. Organization of iron-sulfur clusters in respiratory complex I. *Science* 309:771-774.
114. Hiramatsu, T., K.Kodama, T.Kuroda, T.Mizushima, and T.Tsuchiya. 1998. A putative multisubunit  $\text{Na}^+/\text{H}^+$  antiporter from *Staphylococcus aureus*. *J. Bacteriol.* 180:6642-6648.
115. Hirst, J. 2005a. Current knowledge about the mechanism of energy transduction by respiratory complex I. In *Biophysical and Structural Aspects of Bioenergetics*. M.Wikström, editor. RSC Publishing, Cambridge. 185-200.
116. Hirst, J. 2005b. Energy transduction by respiratory complex I - an evaluation of current knowledge. *Biochem. Soc. Trans.* 33:525-529.
117. Hirst, J., J.Carroll, I.M.Fearnley, R.J.Shannon, and J.E.Walker. 2003. The nuclear encoded subunits of complex I from bovine heart mitochondria. *Biochim. Biophys. Acta* 1604:135-150.
118. Hoffman, C.S. 1997. Rapid isolation of yeast chromosomal DNA. In *Current Protocols in Molecular Biology*. F.M.Ausubel, R.Brent, R.E.Kingston, D.D.Moore, J.G.Seidman, J.A.Smith, and K.Struhl, editors. John Wiley & Sons, Inc.
119. Hofhaus, G., H.Weiss, and K.Leonard. 1991. Electron microscopic analysis of the peripheral and membrane parts of mitochondrial NADH dehydrogenase (complex I). *J. Mol. Biol.* 221:1027-1043.
120. Hollingworth, R.M., K.I.Ahmmadsahib, G.Gadelhak, and J.L.McLaughlin. 1994. New inhibitors of complex I of the mitochondrial electron transport chain with activity as pesticides. *Biochem. Soc. Trans.* 22:230-233.
121. Holt, P.J., D.J.Morgan, and L.A.Sazanov. 2003. The location of NuoL and NuoM subunits in the membrane domain of the *Escherichia coli* complex I - implications for the mechanism of proton pumping. *J. Biol. Chem.* 278:43114-43120.
122. Horgan, D.J., T.P.Singer, and J.E.Casida. 1968. Studies on the respiratory chain-linked reduced nicotinamide adenine dinucleotide dehydrogenase. XIII. Binding

- sites of rotenone, piericidin A and amytal in the respiratory chain. *J. Biol. Chem.* 243:834-843.
123. Ichimaru, N., M.Murai, M.Abe, T.Hamada, Y.Yamada, S.Makino, T.Nishioka, H.Makabe, A.Makino, T.Kobayashi, and H.Miyoshi. 2005. Synthesis and inhibition mechanism of  $\Delta$ lac-acetogenins, a novel type of inhibitor of bovine heart mitochondrial complex I. *Biochem.* 44:816-825.
  124. Ichimaru, N., M.Murai, N.Kakutani, J.Kako, A.Ishihara, Y.Nakagawa, T.Nishioka, T.Yagi, and H.Miyoshi. 2008. Synthesis and characterization of new piperazine-type inhibitors for mitochondrial NADH-ubiquinone oxidoreductase (complex I). *Biochem.* 47:10816-10826.
  125. Ino, T., T.Nishioka, and H.Miyoshi. 2003. Characterization of inhibitor binding sites of mitochondrial complex I using fluorescent inhibitor. *Biochim. Biophys. Acta - Bioenerg.* 1605:15-20.
  126. Joseph-Horne, T., D.W.Hollomon, and P.M.Wood. 2001. Fungal respiration: a fusion of standard and alternative components. *Biochim. Biophys. Acta - Bioenerg.* 1504:179-195.
  127. Jun, A.S., I.A.Trounce, M.D.Brown, J.M.Shoffner, and D.C.Wallace. 1996. Use of transmitochondrial cybrids to assign a complex I defect to the mitochondrial DNA-encoded NADH dehydrogenase subunit 6 gene mutation at nucleotide pair 14459 that causes Leber hereditary optic neuropathy and dystonia. *Mol. Cell. Biol.* 16:771-777.
  128. Kao, M.C., S.Di Bernardo, E.Nakamaru-Ogiso, H.Miyoshi, A.Matsuno-Yagi, and T.Yagi. 2005a. Characterization of the membrane domain subunit NuoJ (ND6) of the NADH-quinone oxidoreductase from *Escherichia coli* by chromosomal DNA manipulation. *Biochem.* 44:3562-3571.
  129. Kao, M.C., S.Di Bernardo, M.Perego, E.Nakamaru-Ogiso, A.Matsuno-Yagi, and T.Yagi. 2004a. Functional roles of four conserved charged residues in the membrane domain subunit NuoA of the proton-translocating NADH-quinone oxidoreductase from *Escherichia coli*. *J. Biol. Chem.* 279:32360-32366.
  130. Kao, M.C., A.Matsuno-Yagi, and T.Yagi. 2004b. Subunit proximity in the H<sup>+</sup>-translocating NADH-quinone oxidoreductase probed by zero-length cross-linking. *Biochem.* 43:3750-3755.

131. Kao, M.C., E.Nakamaru-Ogiso, A.Matsuno-Yagi, and T.Yagi. 2005b. Characterization of the membrane domain subunit NuoK (ND4L) of the NADH:quinone oxidoreductase from *Escherichia coli*. *Biochem.* 44:9545-9554.
132. Kashani-Poor, N., S.Kerscher, V.Zickermann, and U.Brandt. 2001a. Efficient large scale purification of his-tagged proton translocating NADH:ubiquinone oxidoreductase (complex I) from the strictly aerobic yeast *Yarrowia lipolytica*. *Biochim. Biophys. Acta - Bioenerg.* 1504:363-370.
133. Kashani-Poor, N., K.Zwicker, S.Kerscher, and U.Brandt. 2001b. A central functional role for the 49-kDa subunit within the catalytic core of mitochondrial complex I. *J. Biol. Chem.* 276:24082-24087.
134. Kerscher, S. 2000. Diversity and origin of alternative NADH:ubiquinone oxidoreductases. *Biochim. Biophys. Acta* 1459:274-283.
135. Kerscher, S., S.Dröse, K.Zwicker, V.Zickermann, and U.Brandt. 2002. *Yarrowia lipolytica*, a yeast genetic system to study mitochondrial complex I. *Biochim. Biophys. Acta - Bioenerg.* 1555:83-91.
136. Kerscher, S., G.Durstewitz, S.Casaregola, C.Gaillardin, and U.Brandt. 2001a. The complete mitochondrial genome of *Yarrowia lipolytica*. *Comp. Funct. Genom.* 2:80-90.
137. Kerscher, S., A.Eschemann, P.M.Okun, and U.Brandt. 2001b. External alternative NADH:ubiquinone oxidoreductase redirected to the internal face of the mitochondrial inner membrane rescues complex I deficiency in *Yarrowia lipolytica*. *J. Cell Sci.* 114:3915-3921.
138. Kerscher, S., N.Kashani-Poor, K.Zwicker, V.Zickermann, and U.Brandt. 2001c. Exploring the catalytic core of complex I by *Yarrowia lipolytica* yeast genetics. *J. Bioenerg. Biomembr.* 33:187-196.
139. Kerscher, S., J.G.Okun, and U.Brandt. 1999. A single external enzyme confers alternative NADH:ubiquinone oxidoreductase activity in *Yarrowia lipolytica*. *J. Cell Sci.* 112:2347-2354.
140. Kerscher, S., V.Zickermann, K.Zwicker, and U.Brandt. 2005. Insights into the mechanism of mitochondrial complex I from its distant relatives, the [NiFe] hydrogenases. In *Biophysical and Structural Aspects of Bioenergetics*. M.Wikström, editor. RSC Publishing, Cambridge. 156-184.

141. Kervinen, M., R.Hinttala, H.M.Helander, S.Kurki, J.Uusimaa, M.Finel, K.Majamaa, and I.E.Hassinen. 2006. The MELAS mutations 3946 and 3949 perturb the critical structure in a conserved loop of the ND1 subunit of mitochondrial complex I. *Human Molecular Genetics* 15:2543-2552.
142. Kervinen, M., J.Patsi, M.Finel, and I.E.Hassinen. 2004. A pair of membrane-embedded acidic residues in the NuoK subunit of *Escherichia coli* NDH-1, a counterpart of the ND4L subunit of the mitochondrial complex I, are required for high ubiquinone reductase activity. *Biochem.* 43:773-781.
143. Kleyman, T.R. and E.J.Cragoe. 1988. Amiloride and its analogs as tools in the study of ion-transport. *J. Membr. Biol.* 105:1-21.
144. Kohlstadt, M., K.Dorner, R.Labatzke, C.Koc, R.Hielscher, E.Schiltz, O.Einsle, P.Hellwig, and T.Friedrich. 2008. Heterologous production, isolation, characterization and crystallization of a soluble fragment of the NADH:ubiquinone oxidoreductase (complex I) from *Aquifex aeolicus*. *Biochem.* 47:13036-13045.
145. Kurki, S., V.Zickermann, M.Kervinen, I.E.Hassinen, and M.Finel. 2000. Mutagenesis of three conserved Glu residues in a bacterial homologue of the ND1 subunit of complex I affects ubiquinone reduction kinetics but not inhibition by dicyclohexylcarbodiimide. *Biochem.* 39:13496-13502.
146. Kuroda, T., T.Shimamoto, K.Inaba, T.Kayahara, M.Tsuda, and T.Tsuchiya. 1994. Properties of the Na<sup>+</sup>/H<sup>+</sup> antiporter in *Vibrio parahaemolyticus*. *J. Biochem.* 115:1162-1165.
147. Kushnareva, Y., A.N.Murphy, and A.Andreyev. 2002. Complex I-mediated reactive oxygen species generation: modulation by cytochrome c and NAD(P)<sup>+</sup> oxidation-reduction state. *Biochem J* 368:545-553.
148. Kussmaul, L. and J.Hirst. 2006. The mechanism of superoxide production by NADH:ubiquinone oxidoreductase (complex I) from bovine heart mitochondria. *Proc. Natl. Acad. Sci. USA* 103:7607-7612.
149. Leif, H., V.D.Sled, T.Ohnishi, H.Weiss, and T.Friedrich. 1995. Isolation and characterization of the proton-translocating NADH:ubiquinone oxidoreductase from *Escherichia coli*. *Eur. J. Biochem.* 230:538-548.
150. Lenaz, G. 1998. Quinone specificity of complex I. *Biochim. Biophys. Acta* 1364:207-221.

151. Lin, M.T. and M.F.Beal. 2006. Mitochondrial dysfunction and oxidative stress in neurodegenerative diseases. *Nature* 443:787-795.
152. Loeffen, J., O.Elpeleg, J.Smeitink, R.Smeets, S.Stöckler-Ipsiroglu, H.Mandel, R.Sengers, F.Trijbels, and L.Van den Heuvel. 2001. Mutations in the complex I *NDUFS2* gene of patients with cardiomyopathy and encephalomyopathy. *Ann. Neurol.* 49:195-201.
153. Lümnen, P. 1998. Complex I inhibitors as insecticides and acaricides. *Biochim. Biophys. Acta* 1364:287-296.
154. Magnitsky, S., L.Toulokhonova, T.Yano, V.D.Sled, C.Hägerhäll, V.G.Grivennikova, D.S.Burbaev, A.D.Vinogradov, and T.Ohnishi. 2002. EPR characterization of ubisemiquinones and iron-sulfur cluster N2, central components of the energy coupling in the NADH-ubiquinone oxidoreductase (complex I) *in situ*. *J. Bioenerg. Biomembr.* 34:193-208.
155. Majander, A., M.Finel, M.L.Savontaus, E.Nikoskelainen, and M.K.F.Wikström. 1996. Catalytic activity of complex I in cell lines that possess replacement mutations in the ND genes in Leber's hereditary optic neuropathy. *Eur. J. Biochem.* 239:201-207.
156. Marques, I., M.Duarte, J.Assuncao, A.V.Ushakova, and A.Videira. 2005. Composition of complex I from *Neurospora crassa* and disruption of two "accessory" subunits. *Biochim. Biophys. Acta* 1707:211-220.
157. Masereel, B., L.Pochet, and D.Laeckmann. 2003. An overview of inhibitors of Na<sup>+</sup>/H<sup>+</sup> exchanger. *European Journal of Medicinal Chemistry* 38:547-554.
158. Mathiesen, C. and C.Hägerhäll. 2002. Transmembrane topology of the NuoL, M and N subunits of NADH:quinone oxidoreductase and their homologues among membrane-bound hydrogenases and bona fide antiporters. *Biochimica et Biophysica Acta - Bioenerg.* 1556:121-132.
159. Mathiesen, C. and C.Hägerhäll. 2002. Transmembrane topology of the NuoL, M and N subunits of NADH:quinone oxidoreductase and their homologues among membrane-bound hydrogenases and bona fide antiporters. *Biochim. Biophys. Acta* 1556:121-132.
160. Mathiesen, C. and C.Hägerhäll. 2003. The 'antiporter module' of respiratory chain complex I includes the MrpC/NuoK subunit - a revision of the modular evolution scheme. *FEBS Lett.* 549:7-13.

161. Matsushita, K., T. Ohnishi, and H.R. Kaback. 1987. NADH-ubiquinone oxidoreductases of the *Escherichia coli* aerobic respiratory chain. *Biochem.* 26:7732-7737.
162. Medentsev, A.G. and V.K. Akimenko. 1999. Development and activation of cyanide-resistant respiration in the yeast *Yarrowia lipolytica*. *Biochem.* 64:945-951.
163. Meunier, B., P. Lemarre, and A.-M. Colson. 1993. Genetic screening in *Saccharomyces cerevisiae* for large numbers of mitochondrial point mutations which affect structure and function of catalytic subunits of cytochrome-c oxidase. *Eur. J. Biochem.* 213:129-135.
164. Michel, H. 1998. The mechanism of proton pumping by cytochrome c oxidase. *Proc. Natl. Acad. Sci. USA* 95:12819-12824.
165. Mills, S.D., W. Yang, and K. McCormack. 2004. Molecular characterization of benzimidazole resistance in *Helicobacter pylori*. *Antimicrob Agents Chemother.* 48:2524-2530.
166. Mitchell, P. 1961. Coupling of phosphorylation to electron and hydrogen transfer by a chemi-osmotic type of mechanism. *Nature* 191:144-148.
167. Miyoshi, H. 1998. Structure-activity relationships of some complex I inhibitors. *Biochim. Biophys. Acta* 1364:236-244.
168. Mochizuki, N. and F. Oosawa. 1985. Amiloride-sensitive Na<sup>+</sup>-H<sup>+</sup> antiporter in *Escherichia coli*. *J. Bacteriol.* 163:395-397.
169. Morgan, D.J. and L.A. Sazanov. 2008. Three-dimensional structure of respiratory complex I from *Escherichia coli* in ice in the presence of nucleotides. *Biochim. Biophys. Acta - Bioenerg.* 1777:711-718.
170. Morgner, N., V. Zickermann, S. Kerscher, I. Wittig, A. Abdrakhmanova, H.D. Barth, B. Brutschy, and U. Brandt. 2008. Subunit mass fingerprinting of mitochondrial complex I. *Biochim. Biophys. Acta - Bioenerg.* 1777:1384-1391.
171. Moser, C.C., T.A. Farid, S.E. Chobot, and P.L. Dutton. 2006a. Electron tunneling chains of mitochondria. *Biochim. Biophys. Acta - Bioenerg.* 1757:1096-1109.

172. Moser, C.C., C.C. Page, and P.L. Dutton. 2006b. Darwin at the molecular scale: Selection and variance in electron tunnelling proteins including cytochrome c oxidase. *Philos. Trans. R. Soc. Lond. B. Biol. Sci.* 361:1295-1305.
173. Murai, M., N. Ichimaru, M. Abe, T. Nishioka, and H. Miyoshi. 2006. Mode of inhibitory action of  $\Delta$ lac-acetogenins, a new class of inhibitors of bovine heart mitochondrial complex I. *Biochem.* 45:9778-9787.
174. Murai, M., A. Ishihara, T. Nishioka, T. Yagi, and H. Miyoshi. 2007. The ND1 subunit constructs the inhibitor binding domain in bovine heart mitochondrial complex I. *Biochem.* 46:6409-6416.
175. Murai, M., K. Sekiguchi, T. Nishioka, and H. Miyoshi. 2009. Characterization of the inhibitor binding site in mitochondrial NADH-ubiquinone oxidoreductase by photoaffinity labeling using a quinazoline-type inhibitor. *Biochem.* 48:688-698.
176. Nakamaru-Ogiso, E., A. Matsuno-Yagi, S. Yoshikawa, T. Yagi, and T. Ohnishi. 2008. Iron-sulfur cluster N5 is coordinated by an HXXXCXXCXXXXXC motif in the NuoG subunit of *Escherichia coli* NADH:quinone oxidoreductase (complex I). *J Biol Chem* 283:25979-25987.
177. Nakamaru-Ogiso, E., K. Sakamoto, A. Matsuno-Yagi, H. Miyoshi, and T. Yagi. 2003a. The ND5 subunit was labeled by a photoaffinity analogue of fenpyroximate in bovine mitochondrial complex I. *Biochem.* 42:746-754.
178. Nakamaru-Ogiso, E., B.B. Seo, T. Yagi, and A. Matsuno-Yagi. 2003b. Amiloride inhibition of the proton-translocating NDH-quinone oxidoreductase of mammals and bacteria. *FEBS Lett.* 14:43-46.
179. Nakamaru-Ogiso, E., T. Yano, and T. Ohnishi. 2005. Characterization of the iron-sulfur cluster N7 (N1c) in the subunit NuoG of the proton-translocating NADH-quinone oxidoreductase from *Escherichia coli*. *J. Biol. Chem.* 280:301-307.
180. Nakamoto, R.K., C.J. Ketchum, and M.K. al-Shawi. 1999. Rotational coupling in the F<sub>0</sub>F<sub>1</sub> ATP synthase. *Annu. Rev. Biophys. Biomol. Struct.* 28:205-234.
181. Neugebauer, J.M. 1990. Detergents: An overview. *Methods Enzymol.* 182:239-282.
182. Neugebauer, J.M. 1992. A guide to the properties and uses of detergents in biology and biochemistry. Calbiochem-Novabiochem Corporation.



183. Ohnishi, T. 1998. Iron-sulfur clusters semiquinones in complex I. *Biochim. Biophys. Acta* 1364:186-206.
184. Ohnishi, T., H.Blum, Y.M.Galante, and Y.Hatefi. 1981. Iron-sulfur N-1 clusters studied in NADH-ubiquinone oxidoreductase and in soluble NADH dehydrogenase. *J. Biol. Chem.* 256:9216-9220.
185. Ohnishi, T., J.E.Johnson, T.Yano, R.LoBrutto, and W.R.Widger. 2005. Thermodynamic and EPR studies of slowly relaxing ubisemiquinone species in the isolated bovine heart complex I. *FEBS Lett.* 579:500-506.
186. Ohnishi, T. and E.Nakamaru-Ogiso. 2008. Were there any "misassignments" among iron-sulfur clusters N4, N5 and N6b in NADH-quinone oxidoreductase (complex I)? *Biochim. Biophys. Acta - Bioenerg.* 1777:703-710.
187. Ohnishi, T. and J.C.Salerno. 2005. Conformation-driven and semiquinone-gated proton-pump mechanism in the NADH-ubiquinone oxidoreductase (complex I). *FEBS Lett.* 579:4555-4561.
188. Ohshima, M., H.Miyoshi, K.Sakamoto, K.Takegami, J.Iwata, K.Kuwabara, H.Iwamura, and T.Yagi. 1998. Characterization of the ubiquinone reduction site of mitochondrial complex I using bulky synthetic ubiquinones. *Biochem.* 37:6436-6445.
189. Okun, J.G., P.Lümmen, and U.Brandt. 1999a. Three classes of inhibitors share a common binding domain in mitochondrial complex I (NADH:ubiquinone oxidoreductase). *J. Biol. Chem.* 274:2625-2630.
190. Okun, J.G., V.Zickermann, and U.Brandt. 1999b. Properties of the common inhibitor binding domain in mitochondrial NADH-dehydrogenase (complex I). *Biochem. Soc. Trans.* 27:596-601.
191. Okun, J.G., V.Zickermann, K.Zwicker, H.Schägger, and U.Brandt. 2000. Binding of detergents and inhibitors to bovine complex I - A novel purification procedure of bovine complex I retaining full inhibitor sensitivity. *Biochim. Biophys. Acta* 1459:77-87.
192. Page, C.C., C.C.Moser, X.Chen, and P.L.Dutton. 1999. Natural engineering principles of electron tunnelling in biological oxidation-reduction. *Nature* 402:47-52.

193. Pätsi, J., M.Kervinen, M.Finel, and I.E.Hassinen. 2008. Leber hereditary optic neuropathy mutations in the ND6 subunit of mitochondrial complex I affect ubiquinone reduction kinetics in a bacterial model of the enzyme. *Biochem. J.* 409:129-137.
194. Peng, G., G.Fritsch, V.Zickermann, H.Schägger, R.Mentele, F.Lottspeich, M.Bostina, M.Radermacher, R.Huber, K.O.Stetter, and H.Michel. 2003. Isolation, characterization and electron microscopic single particle analysis of the NADH:ubiquinone oxidoreductase (complex I) from the hyperthermophilic eubacterium *Aquifex aeolicus*. *Biochem.* 42:3032-3039.
195. Pohl, T., T.Bauer, K.Dorner, S.Stolpe, P.Sell, G.Zocher, and T.Friedrich. 2007. Iron-sulfur cluster N7 of the NADH:ubiquinone oxidoreductase (Complex I) is essential for stability but not involved in electron transfer. *Biochem.* 46:6588-6596.
196. Prieur, I., J.Lunardi, and A.Dupuis. 2001. Evidence for a quinone binding site close to the interface between NUOD and NUOB subunits of complex I. *Biochim. Biophys. Acta - Bioenerg.* 1504:173-178.
197. Putramen, A., H.Baranows, and W.Prazmo. 1973. Induction by manganese of mitochondrial antibiotic-resistance mutations in yeast. *Mol. Gen. Genet.* 126:357-366.
198. Radermacher, M., T.Ruiz, T.Clason, S.Benjamin, U.Brandt, and V.Zickermann. 2006. The three-dimensional structure of complex I from *Yarrowia lipolytica*: A highly dynamic enzyme. *J. Struct. Biol.* 154:269-279.
199. Rais, I., M.Karas, and H.Schägger. 2004. Two-dimensional electrophoresis for the isolation of integral membrane proteins and mass spectrometric identification. *Proteomics* 4:2567-2571.
200. Rasmussen, T., D.Scheide, B.Brors, L.Kintscher, H.Weiss, and T.Friedrich. 2001. Identification of two tetranuclear FeS clusters on the ferredoxin-type subunit of NADH:ubiquinone oxidoreductase (complex I). *Biochem.* 40:6124-6131.
201. Reda, T., C.D.Barker, and J.Hirst. 2008. Reduction of the iron-sulfur clusters in mitochondrial NADH:ubiquinone oxidoreductase (complex I) by  $\text{Eu}^{\text{II}}$ -DTPA, a very low potential reductant. *Biochem.* 47:8885-8893.

202. Rousset, M., Y.Montet, B.Guigliarelli, N.Forget, M.Asso, P.Bertrand, J.C.Fontecilla-Camps, and E.C.Hatchikian. 1998. [3Fe-4S] to [4Fe-4S] cluster conversion in *Desulfovibrio fructosovorans* [NiFe] hydrogenase by site-directed mutagenesis. *Proc. Natl. Acad. Sci. USA* 95:11625-11630.
203. Sakamoto, K., H.Miyoshi, K.Matsushita, M.Nakagawa, J.Ikeda, M.Ohshima, O.Adachi, T.Akagi, and H.Iwamura. 1996. Comparison of the structural features of ubiquinone reduction sites between glucose dehydrogenase in *Escherichia coli* and bovine heart mitochondrial complex I. *Eur. J. Biochem.* 237:128-135.
204. Sakamoto, K., H.Miyoshi, M.Ohshima, K.Kuwabara, K.Kano, T.Akagi, T.Mogi, and H.Iwamura. 1998. Role of the isoprenyl tail of ubiquinone in reaction with respiratory enzymes: Studies with bovine heart mitochondrial complex I and *Escherichia coli* bo-type ubiquinol oxidase. *Biochem.* 37:15106-15113.
205. Sambrook, J., E.F.Fritsch, and T.Maniatis. 1989. Molecular cloning. A Laboratory Manual. Cold Spring Harbor Laboratory Press, Cold Spring Harbor, NY.
206. Satoh, T., H.Miyoshi, K.Sakamoto, and H.Iwamura. 1996. Comparison of the inhibitory action of synthetic capsaicin analogues with various NADH-ubiquinone oxidoreductases. *Biochim. Biophys. Acta* 1273:21-30.
207. Sazanov, L.A. and P.Hinchliffe. 2006. Structure of the hydrophilic domain of respiratory complex I from *Thermus thermophilus*. *Science* 311:1430-1436.
208. Sazanov, L.A., S.Y.Peak-Chew, I.M.Fearnley, and J.E.Walker. 2000. Resolution of the membrane domain of bovine complex I into subcomplexes: Implications for the structural organization of the enzyme. *Biochem.* 39:7229-7235.
209. Sazanov, L.A. and J.E.Walker. 2000. Cryo-electron crystallography of two sub-complexes of bovine complex I reveals the relationship between the membrane and peripheral arms. *J. Mol. Biol.* 392:455-464.
210. Schägger, H. 2002. Respiratory chain supercomplexes of mitochondria and bacteria. *Biochim. Biophys. Acta - Bioenerg.* 1555:154-159.
211. Schägger, H. 2003. Blue Native Electrophoresis. In Membrane Protein Purification and Crystallization: A Practical Guide. C.Hunte, G.von Jagow, and H.Schägger, editors. Academic Press, San Diego. 105-130.

212. Schägger, H., R.de Coo, M.F.Bauer, S.Hofmann, C.Godinot, and U.Brandt. 2004. Significance of respirasomes for the assembly/stability of human respiratory chain complex I. *J. Biol. Chem.* 279:36349-36353.
213. Schägger, H. and K.Pfeiffer. 2000. Supercomplexes in the respiratory chains of yeast and mammalian mitochondria. *EMBO J.* 19:1777-1783.
214. Schröter, T., O.M.Hatzfeld, S.Gemeinhardt, M.Korn, T.Friedrich, B.Ludwig, and T.A.Link. 1998. Mutational analysis of residues forming hydrogen bonds in the Rieske [2Fe-2S] cluster of the cytochrome *bc<sub>1</sub>* complex in *Paracoccus denitrificans*. *Eur. J. Biochem.* 255:100-106.
215. Schuler, F. and J.E.Casida. 2001a. Functional coupling of PSST and ND1 subunits in NADH:ubiquinone oxidoreductase established by photoaffinity labeling. *Biochim. Biophys. Acta - Bioenerg.* 1506:79-87.
216. Schuler, F. and J.E.Casida. 2001b. The insecticide target in the PSST subunit of complex I. *Pest Management Science* 57:932-940.
217. Schuler, F., T.Yano, S.Di Bernardo, T.Yagi, V.Yankovskaya, T.P.Singer, and J.E.Casida. 1999. NADH-quinone oxidoreductase: PSST subunit couples electron transfer from iron-sulfur cluster N2 to quinone. *Proc. Natl. Acad. Sci. USA* 96:4149-4153.
218. Schulte, U. and H.Weiss. 1995. Generation and characterization of NADH:ubiquinone oxidoreductase mutants in *Neurospora crassa*. *Methods Enzymol.* 260:3-14.
219. Seidman, C.E., K.Struhl, J.Sheen, and T.Jessen. 1997. Introduction of Plasmid DNA into Cells. In *Current Protocols in Molecular Biology*. F.M.Ausubel, R.Brent, R.E.Kingston, D.D.Moore, J.G.Seidman, J.A.Smith, and K.Struhl, editors. John Wiley & Sons, Inc.
220. Sherwood, S. and J.Hirst. 2006. Investigation of the mechanism of proton translocation by NADH:ubiquinone oxidoreductase (complex I) from bovine heart mitochondria: Does the enzyme operate by a Q-cycle mechanism? *Biochem. J.* 400:541-550.
221. Sinha, P.K., J.Torres-Bacete, E.Nakamaru-Ogiso, N.Castro-Guerrero, A.Matsuno-Yagi, and T.Yagi. 2009. Critical roles of subunit NuoH (ND1) in the assembly of peripheral subunits with the membrane domain of *Escherichia coli* NDH-1. *J. Biol. Chem.* in press.

222. Sled, V.D., T.Friedrich, H.Leif, H.Weiss, Y.Fukumori, M.W.Calhoun, R.B.Gennis, T.Ohnishi, and S.W.Meinhardt. 1993. Bacterial NADH-quinone oxidoreductases: Iron-sulfur clusters and related problems. *J. Bioenerg. Biomembr.* 25:347-356.
223. Sled, V.D. and A.D.Vinogradov. 1993. Kinetics of the mitochondrial NADH-ubiquinone oxidoreductase interaction with hexammineruthenium(III). *Biochim. Biophys. Acta* 1141:262-268.
224. Starkov, A.A. 2008. The role of mitochondria in reactive oxygen species metabolism and signaling. *Ann. N. Y. Acad. Sci.* 1147:37-52.
225. Stephens, P.J., D.R.Jollie, and A.Warshel. 1996. Protein control of redox potentials of iron-sulfur proteins. *Chem. Rev.* 96:2491-2513.
226. Stolpe, S. and T.Friedrich. 2004. The *Escherichia coli* NADH:ubiquinone oxidoreductase (complex I) is a primary proton pump but may be capable of secondary sodium antiport. *J. Biol. Chem.* 279:18377-18383.
227. Stroh, A., O.Anderka, K.Pfeiffer, T.Yagi, M.Finel, B.Ludwig, and H.Schägger. 2004. Assembly of respiratory complexes I, III, and IV into NADH oxidase supercomplex stabilizes complex I in *Paracoccus denitrificans*. *J. Biol. Chem.* 279:5000-5007.
228. Suthammarak, W., Y.Y.Yang, P.G.Morgan, and M.M.Sedensky. 2009. Complex I function is defective in complex IV-deficient *Caenorhabditis elegans*. *J. Biol. Chem.* 284:6425-6435.
229. Suzuki, H. and T.E.King. 1983. Evidence of an ubisemiquinone radical(s) from the NADH-ubiquinone reductase of the mitochondrial respiratory chain. *J. Biol. Chem.* 258:352-358.
230. Tabor, S. 1987. Phosphatases and Kinases. *In* Current Protocols in Molecular Biology. F.M.Ausubel, R.Brent, R.E.Kingston, D.D.Moore, J.G.Seidman, J.A.Smith, and K.Struhl, editors. John Wiley & Sons, Inc.
231. Tocilescu, M.A., U.Fendel, K.Zwicker, S.Kerscher, and U.Brandt. 2007. Exploring the ubiquinone binding cavity of respiratory complex I. *J. Biol. Chem.* 282:29514-29520.

232. Torres-Bacete, J., E.Nakamaru-Ogiso, A.Matsuno-Yagi, and T.Yagi. 2007. Characterization of the NuoM (ND4) subunit in *Escherichia coli* NDH-1 - conserved charged residues essential for energy-coupled activities. *J. Biol. Chem.* 282:36914-36922.
233. Tran, Q.H., J.Bongaerts, D.Vlad, and G.Unden. 1997. Requirement for the proton-pumping NADH dehydrogenase I of *Escherichia coli* in respiration of NADH to fumarate and its bioenergetic implications. *Eur. J. Biochem.* 244:155-160.
234. Turrens, J.F. and A.Boveris. 1980. Generation of superoxide anion by the NADH dehydrogenase of bovine heart-mitochondria. *Biochem. J.* 191:421-427.
235. Tzagoloff, A., A.Akai, and R.B.Needleman. 1975. Assembly of mitochondrial-membrane system - isolation of nuclear and cytoplasmic mutants of *Saccharomyces cerevisiae* with specific defects in mitochondrial functions. *J. Bacteriol.* 122:826-831.
236. Ueno, H., H.Miyoshi, M.Inoue, Y.Niidome, and H.Iwamura. 1996. Structural factors of rotenone required for inhibition of various NADH-ubiquinone oxidoreductases. *Biochim. Biophys. Acta* 1276:195-202.
237. Uhlmann, M. and T.Friedrich. 2005. EPR signals assigned to Fe/S cluster N1c of the *Escherichia coli* NADH:ubiquinone oxidoreductase (complex I) derive from cluster N1a. *Biochem.* 44:1653-1658.
238. Ushakova, A.V., V.G.Grivennikova, T.Ohnishi, and A.D.Vinogradov. 1999. Triton X-100 as a specific inhibitor of the mammalian NADH-ubiquinone oxidoreductase (complex I). *Biochim. Biophys. Acta* 1409:143-153.
239. van Belzen, R., A.B.Kotlyar, N.Moon, W.R.Dunham, and S.P.J.Albracht. 1997. The iron-sulfur cluster 2 and ubisemiquinone radicals of NADH:ubiquinone oxidoreductase are involved in energy coupling in submitochondrial particles. *Biochem.* 36:886-893.
240. Vanlerberghe, G.C. and L.McIntosh. 1997. Alternative oxidase: From gene to function. *Annu. Rev. Plant Physiol.* 48:703-734.
241. Verkhovskaya, M.L., N.Belevich, L.Euro, M.Wikström, and M.I.Verkhovsky. 2008. Real-time electron transfer in respiratory complex I. *Proc. Natl. Acad. Sci. USA* 105:3763-3767.

242. Videira, A. 1998. Complex I from the fungus *Neurospora crassa*. *Biochim. Biophys. Acta* 1364:89-100.
243. Vincent, K.A., G.J.Tilley, N.C.Quammie, I.Streeter, B.K.Burgess, M.R.Cheesman, and F.A.Armstrong. 2003. Instantaneous, stoichiometric generation of powerfully reducing states of protein active sites using Eu(II) and polyaminocarboxylate ligands. *Chem. Commun. (Camb.)* 2590-2591.
244. Vinogradov, A.D. 1993. Kinetics, control, and mechanism of ubiquinone reduction by the mammalian respiratory chain-linked NADH-ubiquinone reductase. *J. Bioenerg. Biomembr.* 25:367-374.
245. Vinogradov, A.D. 1998. Catalytic properties of the mitochondrial NADH-ubiquinone oxidoreductase (complex I) and the pseudo-reversible active/inactive enzyme transition. *Biochim. Biophys. Acta* 1364:169-185.
246. Vinogradov, A.D. 2001. Respiratory complex I: Structure, redox components, and possible mechanisms of energy transduction. *Biochemistry-Moscow* 66:1086-1097.
247. Vinogradov, A.D., V.D.Sled, D.S.Burbaev, V.G.X.Grivennikova, I.A.Moroz, and T.Ohnishi. 1995. Energy-dependent complex I-associated ubisemiquinones in submitochondrial particles. *FEBS Lett.* 370:83-87.
248. Voet, D. and J.G.Voet. 1992. Elektronentransport und oxidative Phosphorylierung. In *Biochemie*. A.Maelicke and W.Müller-Esterl, editors. VCH Verlagsgesellschaft mbH, Weinheim, New York, Basel, Cambridge. 527-560.
249. Waletko, A., K.Zwicker, A.Abdrakhmanova, V.Zickermann, U.Brandt, and S.Kerscher. 2005. Histidine 129 in the 75-kDa subunit of mitochondrial complex I from *Yarrowia lipolytica* is not a ligand for [Fe<sub>4</sub>S<sub>4</sub>] cluster N5 but is required for catalytic activity. *J. Biol. Chem.* 280:5622-5625.
250. Wang, D.-C., S.W.Meinhardt, U.Sackmann, H.Weiss, and T.Ohnishi. 1991. The iron-sulfur clusters in the two related forms of mitochondrial NADH:ubiquinone oxidoreductase made by *Neurospora crassa*. *Eur. J. Biochem.* 197:257-264.
251. Weidner, U., S.Geier, A.Ptock, T.Friedrich, H.Leif, and H.Weiss. 1993. The gene locus of the proton-translocating NADH:ubiquinone oxidoreductase in *Escherichia coli*. Organization of the 14 genes and relationship between the

- derived proteins and subunits of mitochondrial complex I. *J. Mol. Biol.* 233:109-122.
252. Wikström, M.K.F. 1984. Two protons are pumped from the mitochondrial matrix per electron transferred between NADH and ubiquinone. *FEBS Lett.* 169:300-304.
253. Wikström, M.K.F., K.Krab, and M.Saraste. 1981. Proton-translocating cytochrome complexes. *Annu. Rev. Biochem.* 50:623-655.
254. Wittig, I., M.Karas, and H.Schägger. 2007. High resolution clear native electrophoresis for in-gel functional assays and fluorescence studies of membrane protein complexes. *Mol. Cell Proteomics* 6:1215-1225.
255. Yagi, T. 1987. Inhibition of NADH-ubiquinone reductase activity by N,N'-dicyclohexylcarbodiimide and correlation of this inhibition with the occurrence of energy-coupling site 1 in various organisms. *Biochem.* 26:2822-2828.
256. Yagi, T. and Y.Hatefi. 1988. Identification of the dicyclohexylcarbodiimide-binding subunit of NADH-ubiquinone oxidoreductase (complex I). *J. Biol. Chem.* 263:16150-16155.
257. Yagi, T. and A.Matsuno-Yagi. 2003. The proton-translocating NADH-quinone oxidoreductase in the respiratory chain: The secret unlocked. *Biochem.* 42:2266-2274.
258. Yagi, T., T.Yano, S.Di Bernardo, and A.Matsuno-Yagi. 1998. Prokaryotic complex I (NDH-1), an overview. *Biochim. Biophys. Acta* 1364:125-133.
259. Yakovlev, G., T.Redda, and J.Hirst. 2007. Reevaluating the relationship between EPR spectra and enzyme structure for the iron-sulfur clusters in NADH:quinone oxidoreductase. *Proc. Natl. Acad. Sci. USA* 104:12720-12725.
260. Yano, T., S.S.Chu, V.D.Sled, T.Ohnishi, and T.Yagi. 1997. The proton-translocating NADH-quinone oxidoreductase (NDH-1) of thermophilic bacterium *Thermus thermophilus* HB-8. *J. Biol. Chem.* 272:4201-4211.
261. Yano, T., W.R.Dunham, and T.Ohnishi. 2005. Characterization of the  $\Delta\mu_{\text{H}^+}$ -sensitive ubisemiquinone species ( $\text{SQ}_{\text{Nf}}$ ) and the interaction with cluster N2: New insight into the energy-coupled electron transfer in complex I. *Biochem.* 44:1744-1754.



262. Yano, T., J.Sklar, E.Nakamaru-Ogiso, T.Yagi, and T.Ohnishi. 2003. Characterization of cluster N5 as a fast-relaxing [4Fe-4S] cluster in the Nqo3 subunit of the proton-translocating NADH-ubiquinone oxidoreductase from *Paracoccus denitrificans*. *J. Biol. Chem.* 278:15514-15522.
263. Yano, T., V.D.Sled, T.Ohnishi, and T.Yagi. 1994a. Identification of amino acid residues associated with the [2Fe- 2S] cluster of the 25 kDa (NQO2) subunit of the proton- translocating NADH-quinone oxidoreductase of *Paracoccus denitrificans*. *FEBS Lett.* 354:160-164.
264. Yano, T., V.D.Sled, T.Ohnishi, and T.Yagi. 1994b. Expression of the 25-kilodalton iron-sulfur subunit of the energy-transducing NADH-ubiquinone oxidoreductase of *Paracoccus denitrificans*. *Biochem.* 33:494-499.
265. Yano, T., V.D.Sled, T.Ohnishi, and T.Yagi. 1996. Expression and characterization of the flavoprotein subcomplex composed of 50-kDa (NQO1) and 5-kDa (NQO2) subunits of the proton-translocating NADH-quinone oxidoreductase of *Pracoccus denitrificans*. *J. Biol. Chem.* 271:5907-5913.
266. Yano, T. and T.Yagi. 1999. H<sup>+</sup>-translocating NADH-quinone oxidoreductase (NDH-1) of *Paracoccus denitrificans*. *J. Biol. Chem.* 274:28606-28611.
267. Yano, T., T.Yagi, V.D.Sled, and T.Ohnishi. 1995. Expression and characterization of the 66-kilodalton (NQO3) iron- sulfur subunit of the proton-translocating NADH-quinone oxidoreductase of *Paracoccus denitrificans*. *J. Biol. Chem.* 270:18264-18270.
268. Zerbetto, E., L.Vergani, and F.DabbeniSala. 1997. Quantification of muscle mitochondrial oxidative phosphorylation enzymes via histochemical staining of blue native polyacrylamide gels. *Electrophoresis* 18:2059-2064.
269. Zhou, C., Y.Huang, and S.Przedborski. 2008. Oxidative stress in Parkinson's disease: A mechanism of pathogenic and therapeutic significance. *Ann. N. Y. Acad. Sci.* 1147:93-104.
270. Zickermann, V., B.Barquera, M.K.F.Wikström, and M.Finel. 1998. Analysis of the pathogenic human mitochondrial mutation ND1/3460, and mutations of strictly conserved residues in its vicinity, using the bacterium *Paracoccus denitrificans*. *Biochem.* 37:11792-11796.

271. Zickermann, V., M.Bostina, C.Hunte, T.Ruiz, M.Radermacher, and U.Brandt. 2003. Functional implications from an unexpected position of the 49 kDa subunit of complex I. *J. Biol. Chem.* 278:29072-29078.
272. Zickermann, V., S.Dröse, M.A.Tocilescu, K.Zwicker, S.Kerscher, and U.Brandt. 2008. Challenges in elucidating structure and mechanism of proton pumping NADH:ubiquinone oxidoreductase (complex I). *J Bioenerg Biomembr.* 40:475-483.
273. Zickermann, V., S.Kerscher, K.Zwicker, M.A.Tocilescu, M.Radermacher, and U.Brandt. 2009. Architecture of complex I and its implications for electron transfer and proton pumping. *Biochim. Biophys. Acta - Bioenerg.* in press.
274. Zickermann, V., K.Zwicker, M.A.Tocilescu, S.Kerscher, and U.Brandt. 2007. Characterization of a subcomplex of mitochondrial NADH:ubiquinone oxidoreductase (complex I) lacking the flavoprotein part of the N-module. *Biochim. Biophys. Acta* 1767:393-400.
275. Zu, Y., S.Di Bernardo, T.Yagi, and J.Hirst. 2002. Redox properties of the [2Fe-2S] center in the 24 kDa (NQO2) subunit of NADH:ubiquinone oxidoreductase (complex I). *Biochem.* 41:10056-10069.
276. Zwicker, K., A.Galkin, S.Dröse, L.Grgic, S.Kerscher, and U.Brandt. 2006. The redox-Bohr group associated with iron-sulfur cluster N2 of complex I. *J. Biol. Chem.* 281:23013-23017.

## 8 Appendix

### 8.1 Genes and primers

#### 8.1.1 NUCM gene (ACCESSION AJ249783)

TCTAGAATGTGGTTGGTCGTTTCCTTTTTTGGCGT	35
TTTTGAAGGGTTAATCTTGCATCTCATTACAAAATATGGTGGATTCTGAAGGAGAGAGA	95
TGTAGGTTCAAATTTGGGGGAAATATAAGCCGAAACCGTAGTAGGGGTGAAGTTGAGGGG	155
GAGGTCGTTGGGACGCCATAATATACTGTGTTGTAGGATATTCTGTGCTAAAATCAACAC	215
AAATTAATGGAATAGAGTCCTTTAGAAGTAAATATTCGCAAATTGCGTCCAAAAATACA	275
CCCCTACAGAGCCCGCTCACAGTCACCTGAATCAACTCATTAACGTTGCTAACCACTT	335
TATCCACTACTTGGAAATAAAACAAAGCAGTCTTCAAACCTCCCCAAAAGATCACTTATTG	395
AAACTATGAAACTTGCATTACAATAACCGTCCCTTTTTTATCCCCTTTTGTATCTTTATAT	455
CTTCTGTAAACCTCTCAAACCTCGCAAACCGTGATTCCTTTGAGCTTGGGAAGTTTGGC	515
Primer n49knc1	
←	
TGGTCAGACTTCCACACATAAACCTCCACCCAATGAAAGCCGAGCTATTGAAAGAGGGAG	575
ATGGTAGAACGATGCAATTGGGCTTTTTCCACGGGACAAGTCGTGAATTATATAGCTACG	635
GGCCAATTGTCTTAATCTACTGACTTCTTACCACCACAACCACCCCAACCTATATAC	695
ACTCCTTCAACCTAACCCCGTTTGGCGCAATCAGCGTTCTCGGAATACTCCCATCTGG	755
ACTAAACTCTTCACAGCGACCGAACCTCTGTTACACACCAAAGCACAAACCCCTCACACA	815
Primer 49-1	
→	
ATGCTGCGATCTGCTGCTGCCCCGAGCCGTCAGGGCTGTGCGCCCCGGCTGTCTGCTCGA	875
MetLeuArgSerAlaAlaAlaArgAlaValArgAlaValArgProArgLeuSerAlaArg	20
TACATGGCCACCACCGCTCTGCCCCAGGACCCCATCCCCTCCGGAGCTCTGGGCCAGAAG	935
TyrMetAlaThrThrAlaLeuProGlnAspProIleProSerGlyAlaLeuGlyGlnLys	40
Primer n49nc2	
←	
GTGCCTCACGTCGATGAGAGCCACCAGGACCTGCTGTTCCGAACCTCTCACATGGTGGAG	995
ValProHisValAspGluSerHisGlnAspLeuLeuPheArgThrSerHisMetValGlu	60
GATCTCGAGACCTACGACGAGGACTCCCCTATCAACACGTCGGACGCCAACACCCGAATC	1055
AspLeuGluThrTyrAspGluAspSerProIleAsnThrSerAspAlaAsnThrArgIle	80
Primer 49-4	
→	
CGAGCCTTACCATCAACTTTGGTCCCCAGCATCCCGCTGCCACGGTGTGCTGCGTCTG	1115
ArgAlaPheThrIleAsnPheGlyProGlnHisProAlaAlaHisGlyValLeuArgLeu	100
ATTCTGGAGCTGTCTGGAGAGGAAATCATTCGATCGGACCCCAACGTCGGTCTGCTGCAC	1175
IleLeuGluLeuSerGlyGluGluIleIleArgSerAspProHisValGlyLeuLeuHis	120

	Primer 49-2 →	
CGAGGAACCGAGAAGCTCATTGAGTACAAGACTTACATGCAGGCGCTGCCATACTTTGAT		1235
ArgGlyThrGluLysLeuIleGluTyrLysThrTyrMetGlnAlaLeuProTyrPheAsp		140
CGTCTGGATTACGTGTCCATGATGACCAACGAGCAGGTTTTCTCTCTGGCTGTCGAGAAG		1295
ArgLeuAspTyrValSerMetMetThrAsnGluGlnValPheSerLeuAlaValGluLys		160
CTGCTCAACGTGGAGGTGCCCCTGCGAGGCAAGTACATCCGAACCATGTTCCGAGAGATC		1355
LeuLeuAsnValGluValProLeuArgGlyLysTyrIleArgThrMetPheGlyGluIle		180
ACCCGAGTGCTCAACCATCTCATGTCCGTGTGTTACACGCCATGGATGTCGGTGCTCTG		1415
ThrArgValLeuAsnHisLeuMetSerValCysSerHisAlaMetAspValGlyAlaLeu		200
ACCCCTTCCTTTGGGGTTTTGAGGAGCGAGAAAAGCTTATGGAGTTCTACGAGCGAGTC		1475
ThrProPheLeuTrpGlyPheGluGluArgGluLysLeuMetGluPheTyrGluArgVal		220
	Primer 49i2 →	
TCTGGAGCCCGTCTGCACGCCGCGTACGTGCGACCTGGAGGAGTCTCCCAGGACCTGCC		1535
SerGlyAlaArgLeuHisAlaAlaTyrValArgProGlyGlyValSerGlnAspLeuPro		240
GCCGGCCTGCTGGACGATATTTACATGTGGGCTACACAGTTCCGGTGACCGTCTGGACGAA		1595
AlaGlyLeuLeuAspAspIleTyrMetTrpAlaThrGlnPheGlyAspArgLeuAspGlu		260
	Primer 49-3 →	
ATCGAGGAGCTGCTGACCGATAACCGAATTTGGAAGCTACGAACCGTCAACATTGGAACC		1655
IleGluGluLeuLeuThrAspAsnArgIleTrpLysLeuArgThrValAsnIleGlyThr		280
GTGACCGCCCAGGACGCCTTGAACCTTGGTCTTTCCGGCCCCATGCTGCGAGGATCCGGT		1715
ValThrAlaGlnAspAlaLeuAsnLeuGlyLeuSerGlyProMetLeuArgGlySerGly		300
ATCCCTTTGACATTCGAAAGAACGCCCCCTACGACGCATACGACAAGGTTCGACTTCGAC		1775
IleProPheAspIleArgLysAsnAlaProTyrAspAlaTyrAspLysValAspPheAsp		320
GTCCCCGTCGGCATGAACGGAGATTGTTACGACCGATACCTGATTCGAATGGCCGAGTTC		1835
ValProValGlyMetAsnGlyAspCysTyrAspArgTyrLeuIleArgMetAlaGluPhe		340
CGACAGTCGCTGCGAATCATCGAGCAGTGCTGCAACGACATGCCGCGCGCCGTTAAG		1895
ArgGlnSerLeuArgIleIleGluGlnCysCysAsnAspMetProAlaGlyAlaValLys		360
	Primer n49i1 ←	
GTGGAGGACTTCAAGATTAACCTCGCCTCCTAGAAACCTCATGAAGGAGGATATGGAGGCC		1955
ValGluAspPheLysIleAsnSerProProArgAsnLeuMetLysGluAspMetGluAla		380
CTGATCCACCACTTCCTGCTCTACACAAAGGGATACTCTGTTCTCCCGGAGAGACCTAC		2015
LeuIleHisHisPheLeuLeuTyrThrLysGlyTyrSerValProProGlyGluThrTyr		400
	Primer 49-2.5 →	
ACCGCCATCGAGGCCCCCAAGGGAGAGATGGGTGTCTACGTCGTCTCCGACGGTAGTGAG		2075
ThrAlaIleGluAlaProLysGlyGluMetGlyValTyrValValSerAspGlySerGlu		420
CGACCATAACAAGTGCAAGATCCGAGCCCCGGATTTGCCCATCTCGGAGCCTTTGATCAC		2135

ArgProTyrLysCysLysIleArgAlaProGlyPheAlaHisLeuGlyAlaPheAspHis	440
Primer n49kc2	
→	
ATTGCCCCGAGGACATTTTCCTTCCCCACGCCGTGGCCATTATTGGTACCATGGATCTTGTG	2195
IleAlaArgGlyHisPheLeuProAspAlaValAlaIleIleGlyThrMetAspLeuVal	460
TTTGGAGAGGTTGATCGATAGTCATAGAATACATACTAAGCAGAGTCGCATATGCGTGTG	2255
PheGlyGluValAspArg***	466
CTCGTGGAATGTACTGTAGAGGGTTGTACACTGTATGTGAGAGCAGAGTTGCTATAAGGA	2315
GAGGTGGTGGATGCGTGACTGTTAGTTGGACTGTGAGTCAGAATGGTCCGTTGAGAGCAA	2375
TGTGGGTCATGCTAAATCTCTTAATGCTTTCTCTTCTACTATGGTGATGTTACCTCACAG	2435
ATACAACAATCGAGATACGGGTCGCGAGACGAGTAGATGTGAGACTACAAATACTGTACA	2495
CTTGTATAACTAATCTACAGGACAGGTGAATGCGAAAGTAAAATGCGATCATCTCTCGGC	2555
CGTAGATGGTCATATTAGTCACATATAATCTGATGCCGGTAAATTTACATGTCAAGCAT	2615
Primer n49kc3	
→	
GTCCATATGGATCTGTCATCAAGCGAGACAGCCACCAAGACTGGAACCAATGCCGCTGGT	2675
AGTAATGGACCTTCTGGTACCAGAGCTGTCATCATTTGCTTGAACCACCTCCTTCATATG	2735
CTCACAAAATCACATGGCTGTGGTTCATCTCACACCAATCCTTTGAGCATATGTCATTCA	2795
TGTAGCATGCATAAACATGTCATCAAAGAAACATATTGGGGCGATGGGAACCTGATAAGGG	2855
GGTGGATGAACATCTGATCTATTGGATGAACTCGATATAAATGATCGTTAATTGAACTAC	2915
TTGTAGTTATTACAAACACTTTTGC AAGTCTAGATCATGATTACTTGTGTACACCTACT	2975
GATGCGTGATCAATAGGTAAACCATGATCTGGTGAATACCATTACCTGTCCCCTGGTGTA	3035
CATAAGCATACTACGGGACAACCTTCTGCACAGAGAGAGATC	3076

**Table 8.1: Sequencing primers for the NUCM gene.**

Name	Sequence
n49knc1 (reverse)	5'-ATGTGTGGAAGTCTGACC-3'
49-1	5'-TCACACAATGCTGCGATC-3'
n49nc2 (reverse)	5'-CCTGGTGGCTCTCATCGACG-3'
49-4	5'-TCCGAGCCTTCACCATCAAC-3'
49-2	5'-ACATGCAGGCGCTGCCATAC-3'
49i2	5'-GCGTACGTGCGACCTGGA-3'
49-3	5'-AGGAGCTGCTGACCGATAAC-3'
n49i1 (reverse)	5'-GCCTCCATATCCTCC-3'
49-2.5	5'-GAGACCTACACCGCCATCGAG-3'
n49kc2	5'-ACGCCGTGGCCATTATTG-3'
n49kc3	5'-GATCTGTCATCAAGCGAG-3'

**Table 8.2: Mutagenesis primers for the NUCM gene.**

<b>Mutant</b>	<b>Name</b>	<b>Sequence</b>
V97G	NUCM V97Gf	5'-GGGCTGCGTCTGATTCTGGAGC-3'
	NUCM V97r (reverse)	5'-ACCGTGGGCAGCGGGATGCTG-3'
V97I	NUCM V97If	5'-ATACTGCGTCTGATTCTGGAGC-3'
	NUCM V97r (reverse)	5'-ACCGTGGGCAGCGGGATGCTG-3'
V97W	NUCM V97Wf	5'-TGGCTGCGTCTGATTCTGGAGC-3'
	NUCM V97r (reverse)	5'-ACCGTGGGCAGCGGGATGCTG-3'
R99D	NUCM R99Df	5'-GATCTGATTCTGGAGCTGTCTG-3'
	NUCM R99r (reverse)	5'-CAGCACACCGTGGGCAGCGGGATG-3'
R99T	NUCM R99Tf	5'-ATCCTGATTCTGGAGCTGTCTG-3'
	NUCM R99r (reverse)	5'-CAGCACACCGTGGGCAGCGGGATG-3'
H120R	NUCM H120Rf	5'-CGCCGAGGAACCGAGAAGCTCATTG-3'
	NUCM H120r (reverse)	5'-CAGCAGACCGACGTGGGGGTC-3'
H120W	NUCM H120Wf	5'-TGGCGAGGAACCGAGAAGCTCATTG-3'
	NUCM H120r (reverse)	5'-CAGCAGACCGACGTGGGGGTC-3'
R121K	NUCM R121Kf	5'-AAAGGAACCGAGAAGCTCATTG-3'
	NUCM H120Hr (reverse)	5'-GTGCAGCAGACCGACGTGG-3'
G122A	NUCM G122Af	5'-GCAACCGAGAAGCTCATTGAGTAC-3'
	NUCM R121Rr (reverse)	5'-TCGGTGCAGCAGACCGACG-3'
G122V	NUCM G122Vf	5'-GTAACCGAGAAGCTCATTGAGTAC-3'
	NUCM R121Rr (reverse)	5'-TCGGTGCAGCAGACCGACG-3'
E124D	NUCM E124Df	5'-GACAAGCTCATTGAGTACAAGAC-3'
	NUCM T123Tr (reverse)	5'-GGTTCCTCGGTGCAGCAGACC-3'
E124Q	NUCM E124Qf	5'-CAGAAGCTCATTGAGTACAAGAC-3'
	NUCM T123Tr (reverse)	5'-GGTTCCTCGGTGCAGCAGACC-3'
Y144F	NUCM Y144Ff	5'-TTCGTGTCCATGATGACCAACG-3'
	NUCM Y144r (reverse)	5'-ATCCAGACGATCAAAGTATGG-3'
Y144H	NUCM Y144Hf	5'-CACGTGTCCATGATGACCAACG-3'
	NUCM Y144r (reverse)	5'-ATCCAGACGATCAAAGTATGG-3'
Y144I	occurred by chance when mutant Y144F was generated	
Y144W	NUCM Y144Wf	5'-TGGGTGTCCATGATGACCAACG-3'
	NUCM Y144r (reverse)	5'-ATCCAGACGATCAAAGTATGG-3'
V145F	NUCM V145Ff	5'-TTCTCCATGATGACCAACGAGCAG-3'
	NUCM V145r (reverse)	5'-GTAATCCAGACGATCAAAGTATG-3'

<b>Mutant</b>	<b>Name</b>	<b>Sequence</b>
V145T	NUCM V145Tf	5'-ACGTCCATGATGACCAACGAGCAG-3'
	NUCM V145r (reverse)	5'-GTAATCCAGACGATCAAAGTATG-3'
M188C	NUCM M188Cf	5'-TGCTCCGTGTGTTACACGCC-3'
	NUCM M188r (reverse)	5'-GAGATGGTTGAGCACTCGGGTG-3'
M188L	NUCM M188Lf	5'-CTGTCCGTGTGTTACACGCC-3'
	NUCM M188r (reverse)	5'-GAGATGGTTGAGCACTCGGGTG-3'
M188Y	NUCM M188Yf	5'-TATTCCGTGTGTTACACGCCATG-3'
	NUCM M188r (reverse)	5'-GAGATGGTTGAGCACTCGGGTG-3'
S192Y	NUCM S192Yf	5'-TACCACGCCATGGATGTCGGTGC-3'
	NUCM S192r (reverse)	5'-ACACACGGACATGAGATGGTTG-3'
F207W	NUCM F207Wf	5'-TGGGAGGAGCGAGAAAAGCTTATG-3'
	NUCM F207r (reverse)	5'-ACCCCAAAGGAAGGGGGTCAG-3'
R210I	NUCM R210If	5'-ATAGAAAAGCTTATGGAGTTCTAC-3'
	NUCM R210r (reverse)	5'-CTCCTCAAACCCCAAAGGAAG-3'
E211Q	NUCM E211Qf	5'-CAAAGCTTATGGAGTTCTACG-3'
	NUCM E211r (reverse)	5'-TCGCTCCTCAAACCCCAAAG-3'
E218Q	NUCM E218Qf	5'-CAGCGAGTCTCTGGAGCCCGTC-3'
	NUCM E218r (reverse)	5'-GTAGAACTCCATAAGCTTTTCTC-3'
R224D	occurred by chance when mutant R224N was generated	
R224I	NUCM R224If	5'-ATTCTGCACGCCGCTACGTGC-3'
	NUCM R224r (reverse)	5'-GGCTCCAGAGACTCGCTCG-3'
R224K	NUCM R224Kf	5'-AAGCTGCACGCCGCTACGTGC-3'
	NUCM R224r (reverse)	5'-GGCTCCAGAGACTCGCTCG-3'
R224N	NUCM R224Nf	5'-AATCTGCACGCCGCTACGTGC-3'
	NUCM R224r (reverse)	5'-GGCTCCAGAGACTCGCTCG-3'
L225A	NUCM L225Af	5'-GCGCACGCCGCTACGTGCGACC-3'
	NUCM L225r (reverse)	5'-ACGGGCTCCAGAGACTCGCTC-3'
L225F	NUCM L225Ff	5'-TTCCACGCCGCTACGTGCGACC-3'
	NUCM L225r (reverse)	5'-ACGGGCTCCAGAGACTCGCTC-3'
L225H	NUCM L225Hf	5'-CACCACGCCGCTACGTGCGACC-3'
	NUCM L225r (reverse)	5'-ACGGGCTCCAGAGACTCGCTC-3'
L225V	NUCM L225Vf	5'-GTCCACGCCGCTACGTGCGACC-3'
	NUCM L225r (reverse)	5'-ACGGGCTCCAGAGACTCGCTC-3'
K407H	NUCM K407Hf	5'-CACGGAGAGATGGGTGTCTACG-3'

Mutant	Name	Sequence
	NUCM K407r (reverse)	5'-GGGGGCCTCGATGGCGGTGTAG-3'
K407R	NUCM K407Rf	5'-CGAGGAGAGATGGGTGTCTACG-3'
	NUCM K407r (reverse)	5'-GGGGGCCTCGATGGCGGTGTAG-3'
K407W	NUCM K407Wf	5'-TGGGGAGAGATGGGTGTCTACG-3'
	NUCM K407r (reverse)	5'-GGGGGCCTCGATGGCGGTGTAG-3'

### 8.1.2 NUKM gene (ACCESSION AJ250340)

GAATTC<sup>3</sup>CCAGAGA 13

CAGTTCTTCTCTGCGAAAAC<sup>3</sup>TGATATCCGAGCTGGGCTTTCTGCGGGCTCTGGACACGAG 73

AAACAACCCCGAGACGGAGGAGTTCTATCCGGATCTCATGTCTGTTATGGGCACTCAGGC 133

CGTGAACGGCAAGAGCATCTCGATCCAGTACACCAACACTCAGACGGCCGAGTTTGAGCG 193

GGCATGGCAGGGTACAGACACCAAGTTTGTGCGCAACCTCAAGGCACACAATCGAGAGAC 253

GTACGAGGACAGAATCCTGTACCAGACTCAGGCCATGCTTCGAGTGCATAACAAGGGCGG 313

TCTGCTGTATTGGATGGACGGTGTGTTGCTTGGTAAGGACCCCAAGTACATTGAGTCGTA 373

CAAGAAGCACGCTGCCAAGTGTGCTGGGCTGCTCGGGAGAAGCGACGCAAGCAGCAAGATGC 433

TGAGGAGAGAGTTGCAGGGCTGTGCAAGGATGTTAACGATAACCGCTATGGCTAGTGGAGA 493

AGAGGCTTATGGATTCAATTTAATGCTATATTTATTGTATTTTTACCCAAACGAATGAGAG 553

AGCTGAGCTCGAAATGAAAATGAGAATACTGGTACGAGTAACTACAATTACTCGTACCGG 613

TACTTGTGTGTAATTGGAATACTGAGCCAGTGGAGAGTGCATTCTCCCGTTTTTTGTACA 673

TTATCTAGTGGATATAACTAACATTCGAATCAAAAAGCTATCTTGGTTCTGATTTTATAC 733

TGTTTGACACCCCTGTCCATAGTAATATCTTAAGCAGTGGATGGAATCATGATCACTGTA 793

TACTGTATACACCTTCATGATGTTTACAAGCGCTATACTGGTGATGTTGTCCCAACAGGT 853

TAGGGTTTTGATCCCTCCTCAGTGTGTTTGCACGTGATCTGGCGTCCAGCCAATAACAGCA 913


ATCACAAGTGGTATTACCAAGAAGCGTGATTTTCGCGCGGTGGCGTTTTTCCCTCGTTGT 973

TGCCGTCGGTTGGCAGTCTCGTTCTCTTCACACCAGGCCAACATTTCTTCAATTGCAACA 1033

TTTTTCTACACTTGTAGGTGCATGTTTGGTGTGTTGTCTGAGACGAGGGAGTGAGTCGGAG 1093

ATGTGTTTTTTTTTAGCGAGGAGTGCTCGGAATTGGATATTTAAACACACAAAAACGGTA 1153

Primer SAPA/ORF/c



ATTTCCGGTGGCTGGTGCGATTAAACACGTCGTCCTGTACCAGCTTGTCTCGTACGCC 1213

CTTATATCTCTTCTTACCCCAAACCACTCCTCCATTAAGCTTCTGCATTGGCCAATCA 1273

GGGCTTCCCATATTTGGGTAACGAAATTATGGTTGGAGGCTTCCACTATCGTATATTTGC 1333

ACCAGCCAGCAGAGCACCTCACGCTTGTGTATCGTCAAAAACCACACATCCCTACAGC 1393

ATGCTCAGATCACAGATTGGCCGACTGGCTCTGCGACCGACGCTGGTCCCGCCACTGTC 1453

MetLeuArgSerGlnIleGlyArgLeuAlaLeuArgProThrLeuValProAlaThrVal 20

ATCCCCAGACCCGAGCATACTCCGCTCCCGCTGGAACCCCGAGTGTCTGCTCCTCCTCC 1513

IleProGlnThrArgAlaTyrSerAlaProAlaGlyThrProArgValSerSerSerSer 40

ATGCCACCGACTTCCCTCTCCCTCACAGCAGAAGCCCAACAGCGCCGTCGACTACACC 1573

MetProThrAspPheProLeuProSerGlnGlnLysProAsnSerAlaValAspTyrThr 60



Primer SAPA/seq		
CTGACCACTCTGGATGC	CGTGGCCAACTGGGCTCGACAGGGCTCTTTCTGGCCCCGTGACC	1633
LeuThrThrLeuAspAlaValAlaAsnTrpAlaArgGlnGlySerPheTrpProValThr		80
TTCGGTCTGGCGTGCTGTGCCGTCGAAATGATGCACGTGTCTGCCCCCGGTACGATCAG		1693
PheGlyLeuAlaCysCysAlaValGluMetMetHisValSerAlaProArgTyrAspGln		100
GATCGTCTGGGTATCATTTTCCGAGCCTCCCCTCGACAGTCCGATATCATGATTGTGGCC		1753
AspArgLeuGlyIleIlePheArgAlaSerProArgGlnSerAspIleMetIleValAla		120
GGAACCCTCACAAACAAAATGGCCCCCGTGCTGCGTCAGGTGTACGACCAGATGCCCGAG		1813
GlyThrLeuThrAsnLysMetAlaProValLeuArgGlnValTyrAspGlnMetProGlu		140
CCCCGATGGGTTCATCTCCATGGGCTCCTGCGCTAACGGTGGTGGATACTACCACTTCTCC		1873
ProArgTrpValIleSerMetGlySerCysAlaAsnGlyGlyGlyTyrTyrHisPheSer		160
TACTCGGTGGTGCAGGCTGCGACCGAATCGTGCCTGTGGACGTCTACGTTCCCGGATGT		1933
TyrSerValValArgGlyCysAspArgIleValProValAspValTyrValProGlyCys		180
CCCCCACCTCCGAGGCCCTCATGTACGGCGTCTTCCAGCTCCAGCGAAAGATGCGAAAC		1993
ProProThrSerGluAlaLeuMetTyrGlyValPheGlnLeuGlnArgLysMetArgAsn		200
ACAAAGATTACCCGAATGTGGTACCGAAAGTAAGCATAATAAACGTTTAGATAGTGAGTC		2053
ThrLysIleThrArgMetTrpTyrArgLys***		210
GGCTGTGTGTAGCCAAAGCTCATCAACGCAGGTCCATTGGTCCGTGTGAGGTACATGTAG		2113
ATCTTTTTTACCATGCACCAGGTAGGTCTACGCACCCTCAATTCTGGATGGAGTGATGGTT		2173
ATTGGTACTTCAAGACGCAGTATATTAGCTGTTGATGTTTCGTTGTGTTATTCAATCACCT		2233
GTCTACTAGTATCAAATACCGTACTTGTAGTAGAGGAATTC		2274

**Table 8.3: Sequencing primers for the NUKM gene.**

Name	Sequence
SAPA/ORF/c	5'-CTGTCACCAGCTTGTCTCG-3'
SAPA/seq	5'-CCCTGACCACTCTGGATGC-3'

**Table 8.4: Mutagenesis primers for the NUKM gene.**

Mutant	Name	Sequence
A84V	NUKM A84Vf	5'-GTGTGCTGTGCCGTCGAAATGATG-3'
	NUKM A84r (reverse)	5'-CAGACCGAAGGTCACGGGCCAG-3'
V88F	NUKM V88Ff	5'-TTCGAAATGATGCACGTGTCTG-3'
	NUKM V88r (reverse)	5'-GGCACAGCACGCCAGACCGAAG-3'
V88L	NUKM V88Lf	5'-CTCGAAATGATGCACGTGTCTG-3'
	NUKM V88r (reverse)	5'-GGCACAGCACGCCAGACCGAAG-3'

Mutant	Name	Sequence
V88M	NUKM V88Mf	5'-ATGGAAATGATGCACGTGTCTG-3'
	NUKM V88r (reverse)	5'-GGCACAGCACGCCAGACCGAAG-3'

### 8.1.3 NUHM gene (ACCESSION AJ250338)

	ATCCCAATCAGATGTACTTGTAATTTAGTT	30	
TGCCATTGAACACATATGTCCGATTAGTAAGCAAGAAACCCAGAGTGAATACACGTCCAA		90	
AATATAATGAAGCTCAAATCGTGTGTCTGGCGACATCAATCGCACAAGGGTGATCCGTTA		150	
ATCCGTATTTTCATCCCCTCCTCCCTCCAGCCAATATCCTCCCTCCCAATTACTCAACCTT		210	
AATTCAGGTCATCAACCAATAGGCGTGGCCCAATTTCTGAAAACTAACTCTGGAGCGTT		270	
	Primer 24k PB Seq1 →		
	← Primer 24 PB3		
TGGGTCAAGG	GCACGAACATCTCCATCACCACAGCTTCAGCTC	GACCTTCACACACAAAA	330
	← Primer 24 PB1		
ATGCTCCGACTGATCCGACCCCGTTTGGCAGCTCTCGCCCGGCCACC	ACTCGGGCCCC		390
MetLeuArgLeuIleArgProArgLeuAlaAlaLeuAlaArgProThrThrArgAlaPro			20
		Primer 24k PB2 →	
CAGGCTCTCAATGCCCGAACTCACATTGTCTCTGTACACCGAAACACTGAGAACAACAAC			450
GlnAlaLeuAsnAlaArgThrHisIleValSerValHisArgAsnThrGluAsnAsnAsn			40
CCCAGCATTCCCTTTGAGTTCTCCCCGAGAACATGAAGCGAGCTGAGGAGGTGATTGCC			510
ProSerIleProPheGluPheSerProGluAsnMetLysArgAlaGluGluValIleAla			60
AAGTACCCCTCAGTACAAGAAGGCTGCTGTTATGCCTCTTCTCGACATTGGCCAGCGA			570
LysTyrProProGlnTyrLysLysAlaAlaValMetProLeuLeuAspIleGlyGlnArg			80
CAGCTCGGTTATACCTCCATCTCCGTCATGAACTACGTGGCCAAGCTGCTGGAAATGCC			630
GlnLeuGlyTyrThrSerIleSerValMetAsnTyrValAlaLysLeuLeuGluMetPro			100
CCCATGCGAGTCTATGAGGTGGCCACCTTCTACACAATGTACAACCGAACCCCTATGGGC			690
ProMetArgValTyrGluValAlaThrPheTyrThrMetTyrAsnArgThrProMetGly			120
CGGTACCATCTGCAGATCTGTACCACCACCCCTGTGCTGCTGTGGCTCCGACGGTATC			750
ArgTyrHisLeuGlnIleCysThrThrThrProCysGlnLeuCysGlySerAspGlyIle			140
ATGGAGGCTGTCCAGAACACCCTTAACATCAAGCCCGGTGAGACCACCAAGGACAACCTC			810
MetGluAlaValGlnAsnThrLeuAsnIleLysProGlyGluThrThrLysAspAsnLeu			160
TTCACTCTCTGAGGTTGAGTGTCTCGGAGCCTGTGTCAACGCCCCATGATGGCCATC			870
PheThrLeuSerGluValGluCysLeuGlyAlaCysValAsnAlaProMetMetAlaIle			180
AACGACGACTACTACGAGGATCTCACTCCCGAGGGAACCGTCAAGCTTCTGGAGGACTGC			930
AsnAspAspTyrTyrGluAspLeuThrProGluGlyThrValLysLeuLeuGluAspCys			200

AAGGCCGGCAAGATGCCCACTCCCGGCCCGAGAACCACGTTTCGACGAGACTGCGAGCCC	990
LysAlaGlyLysMetProThrProGlyProGluAsnHisValArgArgAspCysGluPro	220
GCCTCCGGCCAGAAGGTGCTGCTCAGCAAGGAGCCTCATAACGTGGCCGATTTCTCCAG	1050
AlaSerGlyGlnLysValLeuLeuSerLysGluProHisAsnValAlaAspPheLeuGln	240
Primer 24k GB2	
GAGGGTATTTAAGGGAAGGAGACTCATCACACAAGAGAAAGTCAAAAATGCCATGGCTGA	1110
GluGlyIle***	243
TATGGCTGATATAGCATAACATTAGATTCGGAACGAGGGCGGCTGGGGGCAACGCCTCTT	1170
TACAAGTTGGAGCGTAGTCTCAAAGTAGAAATGACACATGACAGAGATTATGTATTTATG	1230
TACTTACACTGTCGTAGTTTCTTGTACTCG	1260

**Table 8.5: Sequencing primers for the NUHM gene.**

Name	Sequence
24k PB Seq	5'-GCACGAACATCTCCATCACC-3'
24 PB3 (reverse)	5'-CATTTTTGTGTGTGAAGGTC-3'
24 PB1 (reverse)	5'-GGTGGGCCGGGCGAGAGCTGC-3'
24 PB2	5'-CACCGAAACACTGAGAACAAC-3'
24k GB2	5'-GGAAGGAGACTCATCACAC-3'

**Table 8.6: Mutagenesis primers for the NUHM gene.**

Mutant	Name	Sequence
V166T	NUHM V166Tf	5'-ACTGAGTGTCTCGGAGCCTGTG-3'
	NUHM E165Er (reverse)	5'-CTCAGAGAGAGTGAAGAGG-3'
V166K	NUHM V166Kf	5'-AAGGAGTGTCTCGGAGCCTGTG-3'
	NUHM E165Er (reverse)	5'-CTCAGAGAGAGTGAAGAGG-3'
C168A	NUHM C168Af	5'-GCTCTCGGAGCCTGTGTCAACG-3'
	NUHM E167Er (reverse)	5'-CTCAACCTCAGAGAGAGTG-3'
C172A	NUHM C172Af	5'-GCTGTCAACGCCCCATGATGG-3'
	NUHM A171Ar (reverse)	5'-GGCTCCGAGACTCAACC-3'
A175S	NUHM A175Sf	5'-TCCCCCATGATGGCCATCAACG-3'
	NUHM N174Nr (reverse)	5'-GTTGACACAGGCTCCGAGAC-3'
A175K	NUHM A175Kf	5'-AAGCCCATGATGGCCATCAACG-3'
	NUHM N174Nr (reverse)	5'-GTTGACACAGGCTCCGAGAC-3'
M177H	NUHM M177Hf	5'-CACATGGCCATCAACGACTAC-3'



<i>Y. lipolytica</i>	NLGLSGPMLRGSIGIPFDIRKNAPYDAYDKVDFDVPVGM-NGDCYDRYLIRMAEFRQSLRI	346
<i>N. crassa</i>	NLSFTGVMLRGSIGVPWDIRKSQPYDAYDQVEFDVPIGI-NGDCYDRYLCRMEEFRQSLRI	358
<i>B. taurus</i>	NYGFSGVMLRGSIGIWDLRKTQPYDVYDQVEFDVPIGS-RGDCYDRYLCRVEEMRQSIRI	310
<i>H. sapiens</i>	NYGFSGVMLRGSIGIWDLRKTQPYDVYDQVEFDVPIGS-RGDCYDRYLCRVEEMRQSLRI	343
<i>P. denitrificans</i>	DWGYTGVMVRGSGLAWDLRRSQPYECYDEFDFQIPVGR-NGDCYDRYLCRMAEMRESCKI	290
<i>R. capsulatus</i>	KWGYSGVMVRGSGLAWDLRRSQPYECYDEFDFKVAVGK-NGDCYDRYLVRMAEMRESTKI	290
<i>T. thermophilus</i>	DLGLTGGSRLRAGSVNYDVRKAYPYSGYETYTFDVPVLS-EGDVFDRMLVRIEMRESVKI	289
<i>E. coli</i>	EWGTTGAGLRATGIDFVDRKARPYSGYENDFEIPVGGVSDCYTRVMLKVEELRQSLRI	287
	. . :* :*:*:*:*:*:* * . * : * . : : * : * : *	
<i>Y. lipolytica</i>	IEQCCNDMPAGA---VKVEDFKINSPPRNLMKEDMEALIHFFLLYTKGYSVPPGETYTAI	403
<i>N. crassa</i>	IHQCLNKMPAGP---VRVEDYKISPPPRSAMKENMEALIHFFLLYTKGYAVPPGDYTAI	415
<i>B. taurus</i>	ISQCLNKMPAGE---IKVDDAKVSPPKRAEMKTSMESLIHFFKLYTEGYQVPPGATYTAI	367
<i>H. sapiens</i>	IAQCLNKMPAGE---IKVDDAKVSPPKRAEMKTSMESLIHFFKLYTEGYQVPPGATYTAI	400
<i>P. denitrificans</i>	MQQAVQKLRAPF-AGDVLARGKLTTPPRAEMKRDMSLIHFFKLYTEGFKVPAGEVYAAV	349
<i>R. capsulatus</i>	ILQACAKLRAPDGQGDILARGKLTTPKRAEMKTSMEALIHFFKLYTEGFKVPAGEVYAAV	350
<i>T. thermophilus</i>	IKQALERLEPGP---VRDPNPQITPPPRHLLTSMEAVIYHFKHYTEGFHPPKGEVYVPT	346
<i>E. coli</i>	LEQCLNNMPEGP---FKRDHPLTTPPKERTLQHIETLITHFLQVSWGVPMPANESFQMI	344
	: * . : . . * : : * : * * : * * . :	
<i>Y. lipolytica</i>	EA <b>PK</b> GEMGVYVSDGSERPYKCKIRAPGFAHLGAFDHIARGHF <b>LPDAV</b> AI <b>IG</b> TM <b>LR</b> FG <b>Q</b>	463
<i>N. crassa</i>	EGPKGEMGVYVSDGSERPYRVHIRAPGFAHLGGFDHLSRGHMLADAVAVIGTMDLVFGE	475
<i>B. taurus</i>	EAPKGEFGVYLVSDGSSRPYRCKIKAPGFAHLGAGLDKMSKGHMLADVVAIIGTQDIVFGE	427
<i>H. sapiens</i>	EAPKGEFGVYLVSDGSSRPYRCKIKAPGFAHLGAGLDKMSKGHMLADVVAIIGTQDIVFGE	460
<i>P. denitrificans</i>	EGPKGEFGVYLVADGTNKPWRAKLRAPGFAHLQSIDWMSRGHMLADVPAIATLDIVFGE	409
<i>R. capsulatus</i>	EAPKGEFGVYLVADGTNKPYRAKIRAPGYAHLQSIDAVAKGHQLADVSAIIGTMDVVFGE	410
<i>T. thermophilus</i>	ESARGELGYIYVSDGSGMPYRVKVRAPSFVNLQSLPYACKGEQVPMVAIIASLDPVMGD	406
<i>E. coli</i>	EATKGINSYLLTSDGSTMYSYRTRVTPSFAHLQQIPAAIRGSLVSLIVYLVGSLDFVMSD	404
	* . . : * . : * * . : : : : * . : : * : * . : : * * . : :	
<i>Y. lipolytica</i>	VDR	466
<i>N. crassa</i>	VDR	478
<i>B. taurus</i>	VDR	430
<i>H. sapiens</i>	VDR	463
<i>P. denitrificans</i>	VDR	412
<i>R. capsulatus</i>	IDR	413
<i>T. thermophilus</i>	VDR	409
<i>E. coli</i>	VDR	407
	: **	

**Figure 8.1: Amino acid sequence alignment of the 49-kDa subunit from various organisms.** Exchanged amino acid residues are highlighted as in Figure 3.3 – according to their importance for complex I activity: Blue, all exchanges resulted in complex I activity comparable to the parental strain (>75%); green, complex I activity was reduced (25-75%); yellow, at least one exchange resulted in strongly reduced complex I activity (<25%); red, several exchanges strongly reduced complex I activity (<25%). Residues which change the  $I_{50}$  value for DQA, rotenone or  $C_{12}E_8$  are colored in orange. The HRGXE-motif is highlighted in pink. The NCBI sequences of *Y. lipolytica* (ACCESSION CAG78336), *N. crassa* (ACCESSION CAA38368), *B. taurus* (ACCESSION P17694), *H. sapiens* (ACCESSION AAC27453), *P. denitrificans* (ACCESSION P29916), *R. capsulatus* (ACCESSION AAC24988), *T. thermophilus* (ACCESSION AAA97941) and *E. coli* (ACCESSION CAA48363) were aligned by the multiple sequence alignment program ClustalW. Invariant (\*), highly (:) and weakly similar (.) positions are labeled.

## 8.2.2 The PSST subunit

<i>Y. lipolytica</i>	MLRSQIG--RLALRP----TLVP--ATVIPQTRAYS-----APAGTPRVSSSSMPTD	44
<i>N. crassa</i>	MMSSVRTGASMALRARPTAQIVPFRAAAVASISSSSRKDATGAVAPAGAQHGIARRERRE	60
<i>P. denitrificans</i>	-----MTGLNTAG-----ADRLATAELN-----	19
<i>R. capsulatus</i>	-----MGVMTGSNTAA-----VMDVAAAALN-----	22
<i>B. taurus</i>	-----MAALALRLL-HPILAVRSGVGAALQVRG-----VHSSMAADSPSSTQPA	44
<i>H. sapiens</i>	-----MAVLSAPGLRGFRILGLRSVGLAVQARG-----VHQSVATDGPSTQPA	45
<i>T. thermophilus</i>	-----MALKDLFERD-----	10
<i>E. coli</i>	-----MDYTLTRIDPNG-----ENDRYPLQKQEIIVT	26
<i>Y. lipolytica</i>	FPLPSQQKPN-----SAVDYTLTTLDAVANWARQGSFWPVTFGLACCAVEMMHVSAPRY	98
<i>N. crassa</i>	VPLPSQEGTK-----GAVQYALTTLDSIVNWARQSSSLWPMTFGLACCAVEMMHLSTPRY	114
<i>P. denitrificans</i>	----RELQDK-----GFLLTTEDEDIINWARNGSLHWMTFGLACCAVEMMQTSMTRY	66
<i>R. capsulatus</i>	----RDLQDK-----GFLLTTEAEDIINWARNGSLHWMTFGLACCAVEMMHTAMTRY	69
<i>B. taurus</i>	VSQARAVVPKPAALPSSRGEYVVAKLDDLINWARRSSSLWPMTFGLACCAVEMMHAAPRY	104
<i>H. sapiens</i>	LPKARAVAPK----PSSRGEYVVAKLDDLINWARRSSSLWPMTFGLACCAVEMMHAAPRY	101
<i>T. thermophilus</i>	---VQELERE-----GILFTTLEKLVAVGGRSLSLWPATFGLACCAIEMMASTDARN	58
<i>E. coli</i>	DPLEQEVNKN-----VFMGKLNMDVNWGRKNSIWPYNFGLSCCYVEMVTSFTAVH	76
	: . . : : * . * . * : . * * * : * * : * : .	
<i>Y. lipolytica</i>	DQDRLG-IIFRASPRQSDIMIVAGTTLTNKMAPVLRQVYDQMPEPRWVISMGSCANGGGYY	157
<i>N. crassa</i>	DQDRLG-IIFRASPRQSDVMIVAGTTLTNKMAPALRQVYDQMPDPRWVISMGSCANGGGYY	173
<i>P. denitrificans</i>	DLERFG-TAPRASPRQSDLMIIVAGTTLTNKMAPALRKVYDQMPEPRYVISMGSCANGGGYY	125
<i>R. capsulatus</i>	DVERYG-FAPRASPRQSDVMIVAGTTLTNKMAPALRKVYDQMPEPRYVISMGSCANGGGYY	128
<i>B. taurus</i>	DMDRFG-VVFRASPRQSDVMIVAGTTLTNKMAPALRKVYDQMPEPRYVISMGSCANGGGYY	163
<i>H. sapiens</i>	DMDRFG-VVFRASPRQSDVMIVAGTTLTNKMAPALRKVYDQMPEPRYVISMGSCANGGGYY	160
<i>T. thermophilus</i>	DLARFGSEVFRASPRQADVMIVAGRLSKKMAPVMRRVWEQMPDPKWI SMGACASSGGMF	118
<i>E. coli</i>	DVARFGAEVLRASPRQADLMVVAGTCTKMAPVIQRLYDQMLEPKWVISMGACANSGGMY	136
	* * * * * : * : * * * . * * * . : : : * : * : * * * : * * * :	
<i>Y. lipolytica</i>	HFSYSVVRGCDRIVPVDVYVPGCPPTSEALMYGVFQLQRKMRNTKI-----	203
<i>N. crassa</i>	HYSYSVVRGCDRIVPVDIYVPGCPPTSEALMYGIFQLQRKMRNTKI-----	219
<i>P. denitrificans</i>	HYSYSVVRGCDRIVPVDIYVPGCPPTAEALLYGILQLQR--RASGA-----	169
<i>R. capsulatus</i>	HYSYSVVRGCDRIVPVDIYVPGCPPSAEALMYGILQLQRKIRRTGT-----	174
<i>B. taurus</i>	HYSYSVVRGCDRIVPVDIYVPGCPPTAEALLYGILQLQKKIKREKR-----	209
<i>H. sapiens</i>	HYSYSVVRGCDRIVPVDIYIPGCPPTAEALLYGILQLQRKIKRERR-----	206
<i>T. thermophilus</i>	N-NYAIVQNVDSVVPVDVYVPGPPRPEALYAVMQLQKKVGRQAYNERGER-----L	170
<i>E. coli</i>	D-IYSVVQGVDFIPVDVYIPGCPPRPEAYMQALMLLQESIGKERRPLSWVVDGQGVYRA	195
	. * : : * . : * * * : * * * * . * * : : : * * .	
<i>Y. lipolytica</i>	--TRMWYRK-----	210
<i>N. crassa</i>	--TRMWYRK-----	226
<i>P. denitrificans</i>	--PARW-----	173
<i>R. capsulatus</i>	--LVR-----	177
<i>B. taurus</i>	--LRIWYRR-----	216
<i>H. sapiens</i>	--LQIWYRR-----	213
<i>T. thermophilus</i>	PPVAAWKRTRG-----	181
<i>E. coli</i>	NMQSERERKRGERIAVTNLRTPDEI	220

**Figure 8.2: Amino acid sequence alignment of the PSST subunit from various organisms.**

As in Figure 3.3, exchanged amino acid residues are highlighted according to their importance for complex I activity: Green, complex I activity was reduced (25-75%); yellow, at least one exchange resulted in strongly reduced complex I activity (<25%). Residues which change the  $I_{50}$  value for DQA, rotenone or  $C_{12}E_8$  are colored in orange. Cysteine ligands of iron-sulfur cluster N2 are highlighted in yellow in the amino acid sequence from *T. thermophilus*. The NCBI sequences of *Y. lipolytica* (ACCESSION CAB65525), *N. crassa* (ACCESSION CAF06152), *P. denitrificans* (ACCESSION P29918), *R. capsulatus* (ACCESSION AAC24986), *B. taurus* (ACCESSION CAA46154), *H. sapiens* (ACCESSION AAI11518), *T. thermophilus* (ACCESSION AAA97939) and *E. coli* (ACCESSION BAA16121) were aligned by the multiple sequence alignment program ClustalW. Invariant (\*), highly (: ) and weakly similar (.) positions are labeled.



## 8.2.4 The 24-kDa subunit

<i>Y. lipolytica</i>	---MLR--LIRPRLAALAR-----PTTRAPQALNAR--THIVSVHRNTENNNSIP	44
<i>N. crassa</i>	MATKLTFFLMRTAVRAATRLSTKPSITAPVSRACLSISARRPSDTLMVHRNTPDNNPDIP	60
<i>H. sapiens</i>	---MFFSAALRARAAGLTAHWG-----RHVRNLHKTAMQNGAGGALFVHRDTPENNPDP	52
<i>B. taurus</i>	---MFLSAALRARAAGLAAHWG-----KHIRNLHKTAVQNGAGGALFVHRDTPENNPETP	52
<i>P. denitrificans</i>	-----MLRRLSFIQPS	12
<i>T. thermophilus</i>	-----	
<i>E. coli</i>	-----MHENQQPQTEA	11
<i>R. marinus</i>	-----MADFVKKPVVPLPELHPEPQIPADQ	25
<i>Y. lipolytica</i>	FEFSPENMKRAEEVIKYPQYKKAAMVPLLDIGQRQLGYTSSIVMNYVAKLLEMPMRV	104
<i>N. crassa</i>	FKFSADNEKVEEIIKRYPPQYKKAAMVPLLDIGQRQHGFCSSIVMNEVARLLEMPMRV	120
<i>H. sapiens</i>	FDFTPENYKRIEAIKVNYPGHHKAAAVLPVLDLAQRQNGWLPISAMNKVAEVLQVPPMRV	112
<i>B. taurus</i>	FDFTPENYKRIEAIKVNYPGHHKAAAVLPVLDLAQRQNGWLPISAMNKVAEILQVPPMRV	112
<i>P. denitrificans</i>	FEFTPANLEWARAQMTKYPEGROQSAIIPVLWRAQEQEGWLSRPAIEYCADLLGMPYIRA	72
<i>T. thermophilus</i>	MGFFDDKQDFLEETFACYPPGRRRAIMPLLRVQEEGWIRPERIEEIIARLVGTPTPEV	60
<i>E. coli</i>	FELSAAREAAIEHEMHHYED--PRAASIEALKIVQKQRGWVDPGAIHAIADVLGIPASDV	69
<i>R. marinus</i>	LFFTEEEKAKIARFKEQYLE--PAGAVMKTLLWLAQEKFGFLPPEVLQLVADELGIPIYAVQV	83
	: : : . * . * : * * . : * : . . .	
<i>Y. lipolytica</i>	YEVATFYTMYNRTPMG-RYHLQIC <sup>T</sup> TT <sup>P</sup> C <sup>Q</sup> L--CGSDGIMEAVQNTLNKPGETTKDNLF	161
<i>N. crassa</i>	YEVASFYTMYNRTPVG-KFHVQAC <sup>T</sup> TT <sup>P</sup> C <sup>Q</sup> LGGCGSDVIVKAIKEHLGKQGETTPDGLF	179
<i>H. sapiens</i>	YEVATFYTMYNRTPVG-KYHIQVC <sup>T</sup> TT <sup>P</sup> C <sup>M</sup> LR--NSDSILEAIQKKGKIKVGETTPDKLF	169
<i>B. taurus</i>	YEVATFYTMYNRTPVG-KYHIQVC <sup>T</sup> TT <sup>P</sup> C <sup>M</sup> LR--NSDSILEAIQKKGKIKVGETTPDKLF	169
<i>P. denitrificans</i>	LEVATFYFMFQLQPVGSAHIQIC <sup>G</sup> TT <sup>T</sup> C <sup>M</sup> IC--GAEDLIRVCKEKIAPPEPHALSADGRF	130
<i>T. thermophilus</i>	MGVASFYSYQFVPTG-KYHLQV <sup>C</sup> ATL <sup>S</sup> C <sup>K</sup> LA--GAEELWDYLTE <sup>T</sup> LGI <sup>G</sup> PGVE <sup>T</sup> PDGLF	117
<i>E. coli</i>	EGVATFY <sup>S</sup> QIFRQ <sup>P</sup> VG-RHVIRY <sup>C</sup> DSV <sup>V</sup> CHIN--GYQGIQAALKLNKIPGQ <sup>T</sup> TFDGRF	126
<i>R. marinus</i>	YGVATFY <sup>T</sup> QYYKE <sup>K</sup> KG-KVVL <sup>D</sup> VC <sup>T</sup> CF <sup>T</sup> C <sup>Q</sup> VC--GGYDILHYLEEKLG <sup>I</sup> HKGET <sup>T</sup> PDGLF	140
	**.* * * : * * : . : : : : * *	
<i>Y. lipolytica</i>	TLSE <sup>V</sup> E <sup>C</sup> LGAC <sup>V</sup> N <sup>A</sup> P <sup>M</sup> MAIN-DDYYEDLTPEGTVKLLEDCKAG-----KMPTPGPENHVR	215
<i>N. crassa</i>	TFIEVE <sup>C</sup> LGAC <sup>A</sup> N <sup>A</sup> P <sup>M</sup> VQIN-DDYFEDLTPETIKQVLSALKESVTDVSKAPQPGPQ- <sup>S</sup> GR	237
<i>H. sapiens</i>	TLIEVE <sup>C</sup> LGAC <sup>V</sup> N <sup>A</sup> P <sup>M</sup> VQIN-DNYEEDLTAKDIEEIIIDELKAG-----KIPKPGPR- <sup>S</sup> GR	222
<i>B. taurus</i>	TLIEVE <sup>C</sup> LGAC <sup>V</sup> N <sup>A</sup> P <sup>M</sup> VQIN-DNYEEDLTPKDIEEIIIDELKAG-----KIPKPGPR- <sup>S</sup> GR	222
<i>P. denitrificans</i>	SWEVE <sup>C</sup> LGAC <sup>T</sup> N <sup>A</sup> P <sup>M</sup> AQIG-KDFYEDLTVEKLAALIDRFAAGE-----VPVPGPQ- <sup>N</sup> GR	183
<i>T. thermophilus</i>	SVQKVE <sup>C</sup> LGS <sup>C</sup> HTA <sup>P</sup> VIQVNDPEPYVECVTRARLEALLAGLRAG-----	160
<i>E. coli</i>	TL <sup>L</sup> PT <sup>C</sup> CL <sup>G</sup> NC <sup>D</sup> KGP <sup>N</sup> MMIDEDTHAH-LTPEAIPPELLERYK-----	166
<i>R. marinus</i>	TLQVE <sup>C</sup> LGAC <sup>G</sup> S <sup>A</sup> PV <sup>L</sup> QV <sup>S</sup> NGPYV <sup>H</sup> NLTPEKVDQ <sup>L</sup> LEDL <sup>K</sup> Q <sup>G</sup> K-----LPPFVSL <sup>T</sup> LP <sup>Q</sup>	195
	: . *** * ..* :. . . : * : :	
<i>Y. lipolytica</i>	RDCEPASG-----QKVLLSKEPHNVADFLQEGI	243
<i>N. crassa</i>	QTCENAAG-----LTSLTS-EPYG-PEVTRSDL	263
<i>H. sapiens</i>	FSCEPAGG-----LTSLTE-PPKPGFGVQAGL	249
<i>B. taurus</i>	FSCEPAGG-----LTSLTE-PPKPGFGVQAGL	249
<i>P. denitrificans</i>	FSAEALGGPTALADLKGGEAHNASVARALRLGDSIKRIDGTEVPITTPWLATQNGV	239
<i>T. thermophilus</i>	-----KRLEEIE <sup>L</sup> PGKCGHHVHEVEV	181
<i>E. coli</i>	-----	
<i>R. marinus</i>	DEAELGGN-----RRSDAEAVESYRTPPVAHHTR	224

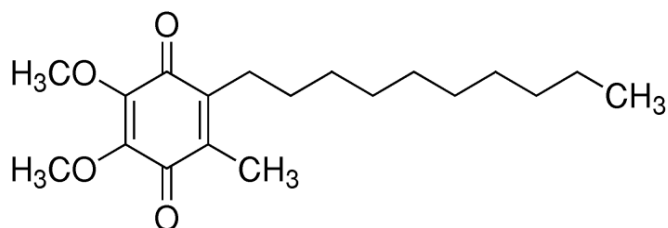
**Figure 8.4: Amino acid sequence alignment of the 24-kDa subunit from various organisms.** Exchanged amino acids are highlighted in red. The cysteine ligands of iron-sulfur-cluster N1a are highlighted in green. The NCBI sequences of *Y. lipolytica* (ACCESSION CAG80440), *N. crassa* (ACCESSION CAA54990), *H. sapiens* (ACCESSION CAG33209), *B. taurus* (ACCESSION P04394), *P. denitrificans* (ACCESSION AAA25588), *T. thermophilus* (ACCESSION AAA979421), *E. coli* (ACCESSION BAA16114) and *R. marinus* (ACCESSION AAY42999) were aligned by the multiple sequence alignment program ClustalW. Invariant (\*), highly (:) and weakly similar (.) positions are labeled.



## 8.3 Structural formulas

### 8.3.1 Ubiquinones

#### 8.3.1.1 DBQ



Molecular Formula: C<sub>19</sub>H<sub>30</sub>O<sub>4</sub>

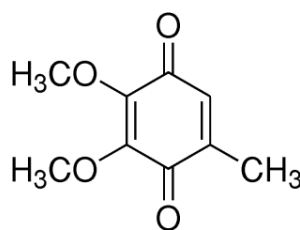
Molar mass: 322.4 g·mol<sup>-1</sup>

log *P*: 7.2 (cyclohexane/water)      4.7 (membrane/water)

Solubility: ethanol and DMSO

E<sub>278-350 nm</sub>      ε = 12.5 mM<sup>-1</sup>cm<sup>-1</sup> (in ethanol)

#### 8.3.1.2 Q<sub>0</sub>

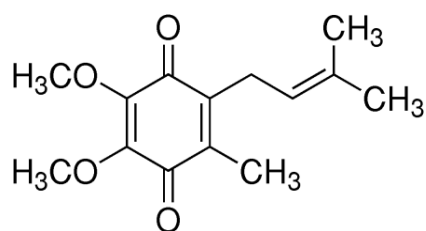


Molecular Formula: C<sub>9</sub>H<sub>10</sub>O<sub>4</sub>

Molar mass: 182.17 g·mol<sup>-1</sup>

log *P*: 0.39 (cyclohexane/water)

Hazards: irritant

8.3.1.3 Q<sub>1</sub>

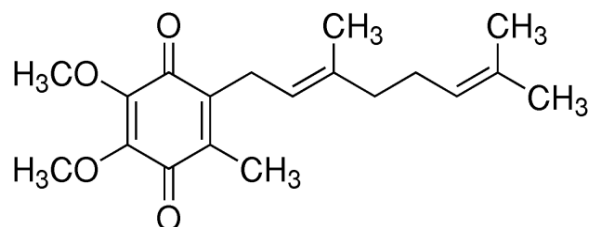
Molecular Formula: C<sub>14</sub>H<sub>18</sub>O<sub>4</sub>

Molar mass: 250.29 g·mol<sup>-1</sup>

log *P*: 2.65 (cyclohexane/water)    2.9 (membrane/water)

Solubility: ethanol and DMSO

E<sub>275 nm</sub>    ε = 14 mM<sup>-1</sup>cm<sup>-1</sup>

8.3.1.4 Q<sub>2</sub>

Molecular Formula: C<sub>19</sub>H<sub>26</sub>O<sub>4</sub>

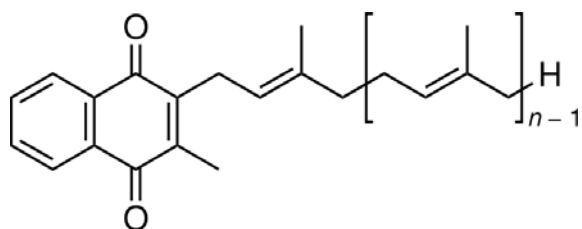
Molar mass: 318.41 g·mol<sup>-1</sup>

log *P*: 5.1 (cyclohexane/water)    4.0 (membrane/water)

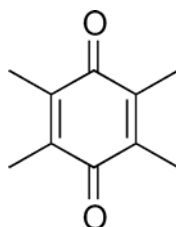
Solubility: ethanol and DMSO

E<sub>275 nm</sub>    ε = 14 mM<sup>-1</sup>cm<sup>-1</sup>

### 8.3.1.5 Menaquinone



### 8.3.1.6 Duroquinone



Molecular Formula:  $C_{10}H_{12}O_2$

Molar mass:  $164.2 \text{ g}\cdot\text{mol}^{-1}$

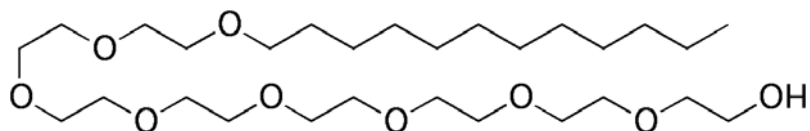
$\log P$ : 2.45 (cyclohexane/water)

Solubility: ethanol and DMSO

Hazards: Irritant

## 8.3.2 Inhibitors

### 8.3.2.1 $C_{12}E_8$

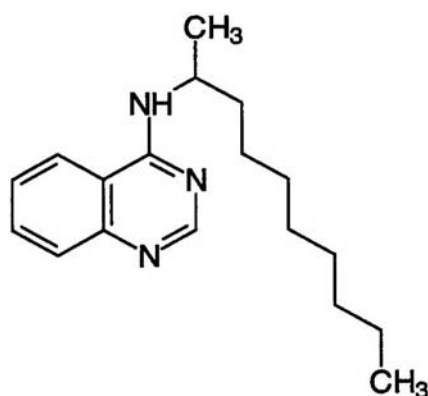


Inhibitor class: Type C

Molecular Formula:  $C_{28}H_{58}O_9$

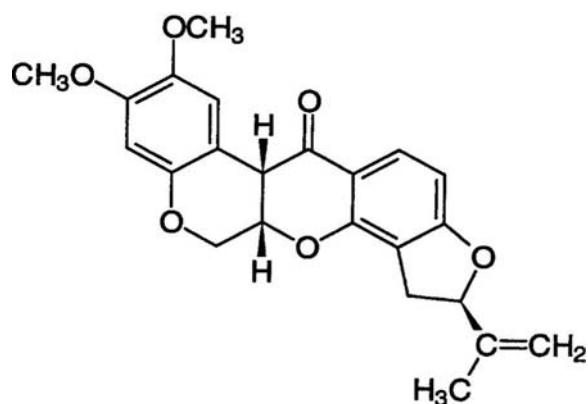
Molar mass:	538.75 g·mol <sup>-1</sup>
Solubility:	water
Literatur:	(Helenius and Simons, 1972; Helenius et al., 1979; Neugebauer, 1990; Neugebauer, 1992)

### 8.3.2.2 DQA



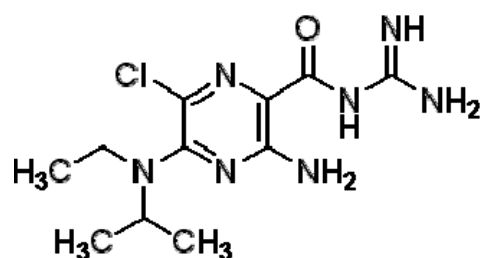
Inhibitor class:	Class I/Type A
Molecular Formula:	C <sub>18</sub> N <sub>2</sub> H <sub>3</sub>
Molar mass:	285.4 g·mol <sup>-1</sup>
Solubility:	ethanol and DMSO
E <sub>291 nm</sub>	ε = 8.14 mM <sup>-1</sup> cm <sup>-1</sup> in ethanol
Literature:	(Hollingworth et al., 1994)

## 8.3.2.3 Rotenone



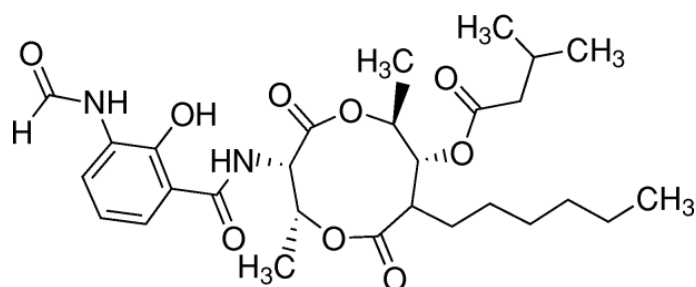
Inhibitor class:	Class II/Type B
Molecular Formula:	$C_{23}H_{22}O_6$
Molar mass:	$394.42 \text{ g}\cdot\text{mol}^{-1}$
Solubility:	ethanol and DMSO
Comment:	light sensitive
Literatur:	(Horgan et al., 1968;Ueno et al., 1996)
Hazards:	toxic, dangerous for the environment

## 8.3.2.4 EIPA



Molecular Formula:	$C_{11}H_{18}ClN_7O$
Molar mass:	$299.76 \text{ g}\cdot\text{mol}^{-1}$
Solubility:	ethanol and DMSO
Hazards:	irritant

### 8.3.2.5 Antimycin A



Molecular Formula:  $C_{28}H_{40}N_2O_9$

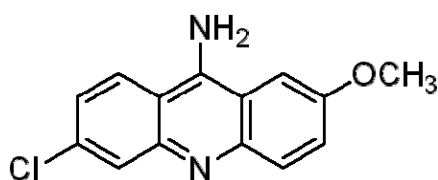
Molar mass:  $548.6252 \text{ g}\cdot\text{mol}^{-1}$

Solubility: ethanol and DMSO

Hazards: toxic

### 8.3.3 Other compounds

#### 8.3.3.1 ACMA



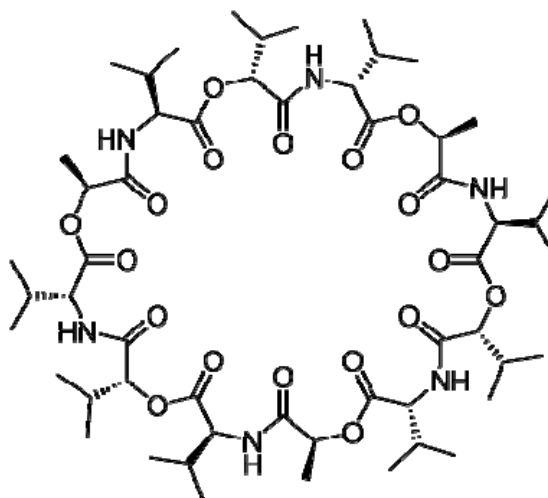
Molecular Formula:  $C_{14}H_{11}ClN_2O$

Molar mass:  $258.70 \text{ g}\cdot\text{mol}^{-1}$

Solubility: ethanol and DMSO

Hazards: harmful

### 8.3.3.2 Valinomycin



Molecular Formula:  $C_{54}H_{90}N_6O_{18}$

Molar mass:  $1111.32 \text{ g}\cdot\text{mol}^{-1}$

Solubility: ethanol and DMSO

Hazards: very toxic

## 8.4 Abbreviations

ACMA 9-amino-6-chloro-2-methoxyacridine

ADP adenosine-5'-diphosphate

APS ammonium-persulfate

ATP adenosine-5'-triphosphate

A.U. arbitrary units

bp base pair

BSA bovine serum albumin

$C_{12}E_8$  n-alkyl-polyoxyethylene-ether

C-terminus carboxyl-terminus

---

DBQ	n-decylubiquinone
DMSO	dimethyl-sulfoxide
dNADH	deamino-nicotinamide-adeninedinucleotide, reduced form
DQA	2-decyl-4-quinazolinyl-amine
ds	double stranded
DTT	dithiothreitol
EDTA	ethylenediaminetetraacetic acid
EIPA	5-(N-ethyl-N-isopropyl)-amiloride
EPR	electron paramagnetic resonance
EtSH	2-mercaptoethanol
Eu <sup>II</sup> -DTPA	Eu <sup>II</sup> diethylenetriamine-N,N,N',N'',N''-pentaacetate
FAD	flavine-adenine-dinucleotide, oxidized form
FADH <sub>2</sub>	flavine-adenine-dinucleotide, reduced form
FCCP	carbonyl-cyanide-p-trifluoromethoxyphenylhydrazone
FeS	iron-sulfur cluster
FMN	flavine-mononucleotide
FPLC	fast protein liquid chromatography
g	acceleration of gravity
GLB	gel loading buffer
GPN	gel buffer native
HAR	hexaammineruthenium(III)-chloride
Hepes	4-(2-hydroxyethyl)-1-piperazineethanesulfonic acid
his-tag	affinity marker composed of six histidines



---

HMW	high molecular weight
Hyg	hygromycin
$I_{50}$	inhibitor concentration, which inhibits an enzymatic reaction rate to 50 %
K	Kelvin
kb	kilobase
kDa	kiloDalton
<i>app. K<sub>m</sub></i>	apparent Michaelis constant
Mes	2-(N-morpholino)ethanesulfonic acid
Mops	3-(N-morpholino)propanesulfonic acid
mtDNA	mitochondrial deoxyribonucleic acid
NAD <sup>+</sup>	nicotinamide-adenine-dinucleotide, oxidized form
NADH	nicotinamide-adenine-dinucleotide, reduced form
NaN <sub>3</sub>	sodium-azide
NaPi	sodium-dihydrogen-phosphate
NDH2i	internal version of the alternative NADH-dehydrogenase
Ni-NTA	Ni <sup>2+</sup> -nitrilotriacetic acid
N-terminus	amino-terminus
OD	optical density
OG	octyl-β-D-glucopyranoside
ORF	open reading frame
OXPHOS	oxidative phosphorylation
PAGE	polyacrylamide gel electrophoresis
PCR	polymerase chain reaction

---

PEG	polyethylene-glycol
P <sub>i</sub>	inorganic phosphate
PIPO strain	<i>Yarrowia lipolytica</i> strain with a hexa histidine-tag at the NUGM subunit (30-kDa subunit) of complex I
PMSF	phenylmethanesulphonylfluoride
Q	ubiquinone
Q <sub>1</sub>	2,3-dimethoxy-5-methyl-6-(3-methyl-2-butenyl)-1,4-benzoquinone
Q <sub>2</sub>	2,3-dimethoxy-5-methyl-6-geranyl-1,4-benzoquinone
QH <sub>2</sub>	ubiquinol
ROS	reactive oxygen species
RT	room temperature
SDS	sodium-dodecyl-sulfate
SEM	standard error of mean
ss	single stranded
TEMED	tetramethylethylenediamine
Tricine	N-(tri(hydroxymethyl)methyl)glycine
Tris	tris(hydroxymethyl)aminomethane
Units	μmol NADH/min
UV	ultraviolet
V <sub>max</sub>	maximum velocity of an enzymatic reaction

## 8.5 List of Figures

<b>Figure 1.1:</b> Semi-schematic representation of the mitochondrial respiratory chain.....	<b>2</b>
<b>Figure 1.2:</b> The crystal structure of the peripheral domain of complex I from <i>T. thermophilus</i> contains 7 out of 14 central subunits of complex I.....	<b>5</b>
<b>Figure 1.3:</b> Schematic representation of the inhibitor binding pocket of complex I.....	<b>8</b>
<b>Figure 1.4:</b> Schematic representation of a binuclear and a tetranuclear iron-sulfur cluster.....	<b>9</b>
<b>Figure 1.5:</b> Comparison of an EPR spectrum recorded at 12 K and 0.1 mW from purified complex I from <i>Y. lipolytica</i> to a simulated spectrum .....	<b>11</b>
<b>Figure 1.6:</b> Example of an EPR spectrum from mitochondrial membranes from <i>Y. lipolytica</i> recorded at 12 K and 1 mW microwave power .....	<b>12</b>
<b>Figure 1.7:</b> The respiratory chain of <i>Y. lipolytica</i> strains used for mutagenesis.....	<b>16</b>
<b>Figure 1.8:</b> Regions which underwent mutagenesis in this study are highlighted in the structure of the peripheral domain of complex I from <i>T. thermophilus</i> .....	<b>18</b>
<b>Figure 2.1:</b> Map of the pUB4 (and pUB26) shuttle vector .....	<b>24</b>
<b>Figure 3.1:</b> EPR spectra of mitochondrial membranes of selected 49-kDa mutants at 12 K and 5 mW microwave power .....	<b>48</b>
<b>Figure 3.2:</b> EPR spectra of mitochondrial membranes of the PSST mutant V88F at 12 K and 5 mW microwave power .....	<b>48</b>
<b>Figure 3.3:</b> Impact of mutations affecting the proposed ubiquinone and inhibitor binding cavity on complex I activity .....	<b>52</b>
<b>Figure 3.4:</b> Impact of mutations affecting the proposed ubiquinone and inhibitor binding cavity on inhibitor binding .....	<b>61</b>
<b>Figure 3.5:</b> Effects of mutants of the quinone and inhibitor binding site on the $I_{50}$ value for EIPA.....	<b>66</b>

<b>Figure 3.6:</b> The respiratory chain of <i>Y. lipolytica</i> strains used for mutagenesis .....	67
<b>Figure 3.7:</b> On antimycin A and azide containing plates mutant Y144F displays diminished growth.....	68
<b>Figure 3.8:</b> Probing of fully redox active mutants for proton pumping defects.....	70
<b>Figure 3.9:</b> Sequence alignment of the 49-kDa subunit harboring the highly conserved tyrosine 144.....	71
<b>Figure 3.10:</b> EPR spectra of mitochondrial membranes of tyrosine 144 mutants at 12 K and 5 mW microwave power.. ..	74
<b>Figure 3.11:</b> EPR spectra of purified complex I from tyrosine mutants Y144F and Y144W at 12 K and 1 mW microwave power .....	75
<b>Figure 3.12:</b> 25 K minus 40 K difference EPR spectra from purified complex I of mutants Y144F and Y144W compared to the parental strain and to a highly concentrated complex I standard.....	77
<b>Figure 3.13:</b> dNADH:DBQ oxidoreductase activity of mutant Y144F at increasing DBQ concentrations .....	79
<b>Figure 3.14:</b> Dependence of complex I activity on pH in mitochondrial membranes from mutant Y144F.....	80
<b>Figure 3.15:</b> Reactivation of DQA sensitive complex I activity by different additives at pH 7.4.....	82
<b>Figure 3.16:</b> Reactivation of total dNADH:DBQ activity by different additives .....	83
<b>Figure 3.17:</b> Reactivation of DQA sensitive complex I activity by acetic acid.....	84
<b>Figure 3.18:</b> Normalized dNADH:Q <sub>1</sub> oxidoreductase activity in mitochondrial membranes of tyrosine 144 mutants at different concentrations of Q <sub>1</sub> .....	86
<b>Figure 3.19:</b> Proton pumping by mutants Y144F and Y144W assayed as quench in ACMA fluorescence.....	90
<b>Figure 3.20:</b> Rotenone resistance of proton pumping by mutants Y144F and Y144W ..	91

<b>Figure 3.21:</b> Sequence alignment of the N-terminal part of the 49-kDa subunit harboring the HRGXE-motif .....	<b>92</b>
<b>Figure 3.22:</b> Location of the HRGXE-motif close to iron-sulfur cluster N2 but at some distance from the ubiquinone and inhibitor binding pocket .....	<b>93</b>
<b>Figure 3.23:</b> EPR spectra of mitochondrial membranes from the HRGXE-motif mutants at 12 K and 1 mW microwave power .....	<b>96</b>
<b>Figure 3.24:</b> Sequence alignment of the binding motif of iron-sulfur cluster N1a within the 24-kDa subunit.....	<b>98</b>
<b>Figure 3.25:</b> Ligation and coordination of iron-sulfur cluster N1a within the 24-kDa subunit.....	<b>99</b>
<b>Figure 3.26:</b> EPR spectra of mitochondrial membranes from point mutants close to iron-sulfur cluster N1a recorded at 40 K and 5 mW microwave power.....	<b>102</b>
<b>Figure 4.1:</b> Conserved regions within the quinone and inhibitor binding cavity .....	<b>107</b>
<b>Figure 4.2:</b> Spatial arrangement of the HRGXE-motif which reaches from iron-sulfur cluster N2 to the 30-kDa subunit .....	<b>121</b>
<b>Figure 4.3:</b> Multiple sequence alignment of a highly conserved part of the PSST subunit.....	<b>122</b>
<b>Figure 4.4:</b> C-terminal highly conserved part of the multiple sequence alignment from the 49-kDa subunit.....	<b>122</b>
<b>Figure 4.5:</b> Highly conserved part of the of the amino acid sequence of the 30-kDa subunit.....	<b>123</b>
<b>Figure 5.1:</b> Schematic representation of the quinone and inhibitor binding cavity.....	<b>131</b>
<b>Figure 8.1:</b> Amino acid sequence alignment of the 49-kDa subunit from various organisms.....	<b>179</b>
<b>Figure 8.2:</b> Amino acid sequence alignment of the PSST subunit from various organisms.....	<b>180</b>

**Figure 8.3:** Amino acid sequence alignment of the 30-kDa subunit from various organisms .....181

**Figure 8.4:** Amino acid sequence alignment of the 24-kDa subunit from various organisms .....182

## 8.6 List of Tables

<b>Table 1.1:</b> Central subunits of complex I .....	3
<b>Table 2.1:</b> Enzymes used.....	23
<b>Table 2.2:</b> Used plasmids .....	23
<b>Table 2.3:</b> <i>Escherichia coli</i> strains used.....	24
<b>Table 2.4:</b> <i>Yarrowia lipolytica</i> strains used.....	25
<b>Table 3.1:</b> Effects of point mutations introduced into the 49-kDa subunit in mitochondrial membranes from <i>Y. lipolytica</i> .....	42
<b>Table 3.2:</b> Effects of point mutations introduced into the PSST subunit in mitochondrial membranes from <i>Y. lipolytica</i> .....	45
<b>Table 3.3:</b> Complex I activity with different ubiquinones in mitochondrial membranes from 49-kDa subunit mutants.....	53
<b>Table 3.4:</b> Complex I activity with different ubiquinones in mitochondrial membranes from PSST subunit mutants.....	55
<b>Table 3.5:</b> Effects of 49-kDa subunit mutations on inhibitor sensitivity in mitochondrial membranes from <i>Y. lipolytica</i> .....	56
<b>Table 3.6:</b> Effects of PSST subunit mutations on inhibitor sensitivity in mitochondrial membranes from <i>Y. lipolytica</i> .....	58
<b>Table 3.7:</b> Characteristics of mitochondrial membranes from the <i>nb8m</i> $\Delta$ strain.....	62
<b>Table 3.8:</b> Effects of point mutations in the 49-kDa subunit on EIPA inhibition in mitochondrial membranes from <i>Y. lipolytica</i> .....	62

<b>Table 3.9:</b> Effects of point mutations in the PSST subunit on EIPA inhibition in mitochondrial membranes from <i>Y. lipolytica</i> .....	<b>63</b>
<b>Table 3.10:</b> Effects of point mutations of Y144 in the 49-kDa subunit on complex I content, activity and N2 EPR signal in mitochondrial membranes from <i>Y. lipolytica</i> ...	<b>72</b>
<b>Table 3.11:</b> Parameters determining pH dependence of complex I activity in mitochondrial membranes from mutant Y144F and the parental strain .....	<b>80</b>
<b>Table 3.12:</b> Apparent $K_m$ values and $V_{max}$ values for tyrosine 144 mutants when Q <sub>1</sub> was used as electron acceptor .....	<b>87</b>
<b>Table 3.13:</b> Apparent $K_m$ values and $V_{max}$ values for the Y144F and Y144W mutants when Q <sub>2</sub> was used as electron acceptor .....	<b>88</b>
<b>Table 3.14:</b> $I_{50}$ values for DQA, rotenone, C <sub>12</sub> E <sub>8</sub> and EIPA determined in mitochondrial membranes from tyrosine mutants in the presence of 150 $\mu$ M Q <sub>1</sub> .....	<b>89</b>
<b>Table 3.15:</b> Effects of mutations introduced into the HRGXE-motif of the 49-kDa subunit on complex I content, activity and N2 EPR signal in mitochondrial membranes from <i>Y. lipolytica</i> .....	<b>94</b>
<b>Table 3.16:</b> Effects on inhibitor sensitivity and ubiquinone affinity of mutations introduced into the HRGXE-motif of the 49-kDa subunit in mitochondrial membranes from <i>Y. lipolytica</i> .....	<b>97</b>
<b>Table 3.17:</b> Effects of mutations introduced next to iron-sulfur cluster N1a in the 24-kDa subunit on mitochondrial membranes from <i>Y. lipolytica</i> .....	<b>100</b>
<b>Table 3.18:</b> Effects of mutations introduced into the cysteine ligands of iron-sulfur cluster N1a in mitochondrial membranes from <i>Y. lipolytica</i> .....	<b>103</b>
<b>Table 4.1:</b> Mutations affecting the 49-kDa subunit at the quinone and inhibitor binding cavity in other model organisms .....	<b>115</b>
<b>Table 4.2:</b> Mutations affecting the PSST subunit at the quinone and inhibitor binding cavity in other model organisms .....	<b>116</b>
<b>Table 8.1:</b> Sequencing primers for the NUCM gene .....	<b>171</b>

---

<b>Table 8.2:</b> Mutagenesis primers for the NUCM gene .....	<b>172</b>
<b>Table 8.3:</b> Sequencing primers for the NUKM gene.....	<b>175</b>
<b>Table 8.4:</b> Mutagenesis primers for the NUKM gene .....	<b>175</b>
<b>Table 8.5:</b> Sequencing primers for the NUHM gene.....	<b>177</b>
<b>Table 8.6:</b> Mutagenesis primers for the NUHM gene .....	<b>177</b>



## **Danksagung**

Mein Dank gilt Prof. Dr. Ulrich Brandt für die Überlassung des Themas, die Bereitstellung aller notwendigen Mittel und die Diskussionsbereitschaft, sowie Prof. Dr. Volker Müller für die Betreuung der Promotion im Fachbereich Biowissenschaften.

Besonderer Dank geht an Dr. Stefan Kerscher für viele interessante Diskussionen, für die Hilfsbereitschaft und für das Korrekturlesen der vorliegenden Arbeit, sowie an Dipl.-Ing. Gudrun Beyer für die Hilfe beim der Erzeugung zahlreicher Mutanten, die stete Hilfsbereitschaft im alltäglichem Laboralltag und die Organisation des Mollilabors in dem wir alle sehr bequem und effizient arbeiten können.

Dr. Klaus Zwicker danke ich für die Aufnahme der EPR-Spektren und die Diskussionsbereitschaft rund um die EPR-Spektroskopie und Eisen-Schwefel-Zentren.

Bei Andrea Duchene, Dr. Volker Zickermann und Karin Siegmund möchte ich mich für ihre Hilfe bei der Komplex I Reinigung und bei Ilka Siebels und Dr. Stefan Dröse für die Hilfe bei der Rekonstitution von Komplex I und bei den Protonenpumpmessungen bedanken.

Für die Unterstützung rund um die Proteinelektrophorese danke ich Prof. Dr. Hermann Schägger, Dr. Ilka Wittig und Christian Bach.

Andrea Böttcher danke ich für die IT- und Netzwerkadministration und Lena Schmidt für das unauffällige Erledigen aller anfallenden Formalitäten.

Für zahlreiche Tipps zur spektroskopischen Bestimmung von Enzymkinetiken und zur Mitochondrienpräparation möchte ich Dr. Ljuban Grgic und Dr. Alexander Galkin danken.

Blanka Wrzesniewska und Krzysztof Dobrynin danke ich für ihre Freundschaft und uneingeschränkte Hilfsbereitschaft.

Bei allen anderen nicht namentlich erwähnten Kollegen möchte ich mich für die stete Hilfe und die angenehme Arbeitsatmosphäre bedanken.

Zum Schluss möchte ich meinen Geschwistern und ganz besonders meinem Ehemann für die verlässliche Unterstützung auch und besonders in schwierigen Zeiten danken.

Diese Arbeit ist meinen lieben Eltern gewidmet.

## Lebenslauf

Name: Maja Aleksandra Tocilescu

Geburtsdatum: 26.05.1979

Geburtsort: Belgard, Polen

Familienstand: verheiratet

Ausbildung: seit August 2005: Promotion im Labor von Prof. Dr. Ulrich Brandt, Arbeitsgruppe Molekulare Bioenergetik am Zentrum der Biologischen Chemie des Fachbereichs Medizin der Johann Wolfgang Goethe-Universität, Frankfurt am Main

September 2004 bis Juni 2005: Diplomarbeit im Labor von Prof. Dr. Ulrich Brandt, Arbeitsgruppe Molekulare Bioenergetik am Zentrum der Biologischen Chemie des Fachbereichs Medizin der Johann Wolfgang Goethe-Universität, Frankfurt am Main (Note 1)

1999-2005: Studium der Biologie mit den Schwerpunktfächern Zell-und Entwicklungsbiologie (Note 1), Genetik (Note 1) und Physik/Biophysik (Note 2) an der Johann Wolfgang Goethe-Universität, Frankfurt am Main

1999: Abitur an der Schillerschule Frankfurt am Main

1996-1999: Schillerschule Frankfurt am Main

1991-1996: Gesamtschule Stierstadt

1990-1991: Ahnatal-Schule in Vellmar

1988-1990: Grundschule Niedervellmar

1986-1988: Grundschule in Karlino, Polen